STIFFNESS OF COUPLING SLABS IN SHEAR WALL BUILDINGS

STIFFNESS OF COUPLING SLABS IN SHEAR WALL BUILDINGS

by

Adel A. Mahmoud, B.Sc.

A Thesis
Submitted to the School of Graduate Studies
in Partial Fulfilment of the Requirements
for the Degree
Master of Engineering

McMaster University
January 1976

To my dear wife Magda whose patience, understanding, and assistance are deeply appreciated.

ACKNOWLEDGEMENTS

The author wishes to express his sincere gratitude to Dr. W. K. Tso for his guidance and interest during the course of this study; and his patience during the correction of this thesis.

I am grateful to Dr. M. A. Dokainish for his guidance and cooperation.

My thanks go to McMaster University for awarding me the scholarship and teaching assistantship.

Sincere appreciation is due to John Meyer, John Wells and Wille for their help in the laboratory work.

Thanks are also due to Miss B. A. Bedell, who typed the manuscript.

Master of Engineering (1976)
(Civil Engineering)

McMaster University
Hamilton, Ontario.

TITLE: Stiffness of Coupling Slabs in Shear Wall Buildings

AUTHOR: Adel A. Mahmoud, B.Sc. (Cairo University)

SUPERVISOR: Dr. W. K. Tso

NUMBER OF PAGES: xvi, 206

SCOPE AND CONTENTS:

In this thesis, a study was made on the coupling effect of floor slabs on the behaviour of shear wall structures. The slab coupled shear walls were analysed by the finite element technique to obtain the bending stiffness. Experimental verification was done on a small scale model of steel walls coupled by a steel slab. Design curves to estimate the stiffness of the various slab coupled wall configurations are presented. In addition, a study was made on the influence of the dimensions and shapes of the walls (plane walls, T-section walls and box core walls), wall openings, and slab dimensions on the effective width and stiffness of the connecting slab.

TABLE OF CONTENTS

LIST OF FIGURES

LIST OF SYMBOLS

Any symbol used is generally defined when introduced. The standard symbols are listed below:

$\bar{a}$	Height of the shear wall model above its point of rotation
a_1	Square of length ij
a_2	Square of length jk
a_3	Square of length ki
d	Length of overhanging part of the slab beyond the walls
$\bar{D}$	Flexural rigidity of the slab
e_x	Distance from the inner edge of the wall to the centriod of its cross-section
E	Modulus of elasticity
F_Z'	External nodal force in Z' direction
$F_{\theta X}'$	External nodal moment about X' axis
$F_{\theta Y}'$	External nodal moment about Y' axis
h	Wall thickness
h_s	Storey height
H	Total height of the structure
I	Moment of inertia of the equivalent beam
I_1	Moment of inertia of the planar wall
I_2	Moment of inertia of the T-section wall
K_b	Bending stiffness of the slab
ℓ	Wall openings
ℓ_1	Distance between point of contraflexure and the inner edge of the planar wall
ℓ_2	Distance between point of contraflexure and the inner edge of the T-section wall

L	Distance between outer edges of walls
ℓ_x, m_x, n_x	Direction cosines of X' axis with X,Y,Z axes
ℓ_y, m_y, n_y	Direction cosines of Y' axis with X,Y,Z axes
L_z, m_z, n_z	Direction cosines of Z' axis with X,Y,Z axes
M'_x, M'_y, M'_{xy}	The internal moments and twisting moment at nodes referred to the local axes
M	Rotational moment at the centriod of the cross-section of the wall
P	The forces acting at the walls and causing relative displacement Δ
$\overline{P}$	Applied horizontal load at the shear wall model
R	Rotational nondimensional stiffness of the slab at the centriod of the cross-section
t	Slab thickness
w	Wall width
W_i	Displacement of node i in Z direction
W'_i	Displacement of node i in Z' direction
Y_e	Effective width of the slab
Y	Width of the slab
X, Y, Z	Set of global axes
X', Y', Z'	Set of local axes
X_i, Y_i	Coordinates of node i referred to the global axes
X_j, Y_j	Coordinates of node j referred to the global axes
X_k, Y_k	Coordinates of node k referred to the global axes
z	Flange width
α_i	Arbitrary constants
γ	Variable connecting e_x to w
θ'_X, θ'_Y	Rotational displacements about X',Y' axes
ν	Poisson's ratio

Δ	Relative displacement between the walls
$\bar{\Delta}$	Horizontal displacement of the shear wall model
ϕ	Angle of rotation of the wall

Matrices

$\{F'_i\}$	Nodal force vector in the direction of local axes
$\{F'_e\}$	Column vector of element nodal forces in the direction of the local axes
$\{F_e\}$	Column vector of element nodal forces in the direction of the global axes
$\{F\}$	Column vector of the nodal forces
$\{F_a\}$	The column vector of known nodal forces
$\{F_b\}$	The column vector of unknown nodal forces
$\{K'_e\}$	Element stiffness matrix referred to the local axes
$\{K_e\}$	Element stiffness matrix referred to the global axes
$\{K\}$	Total stiffness matrix
$\{M'_e\}$	Internal load vector of an element in the local axes
$\{r'\}$	Curvature and twist of the plate referred to the local axes
$\Delta\{r'\}$	Virtual internal curvature and twist
$[T]$	Transformation matrix
$\{\delta'_i\}$	Nodal displacement vector of node i
$\{\delta'_e\}$	Column vector of element nodal displacements in the local axes
$\{\delta_e\}$	Column vector of element nodal displacements in the global axes
$\Delta\{\delta'_e\}$	Virtual external displacements
$\{\delta\}$	Column vector of nodal displacements
$\{\delta_a\}$	The column vector of unknown displacements

$\{\delta_b\}$ The column vector of the known displacements

$\{\lambda\}$ Matrix of direction cosines

Superscripts

' The quantity referred to the local axes (X',Y',Z'). When this superscript if dropped the quantity referred to the global axes (X,Y,Z).

-1 Inverse of matrix

T Transpose of matrix

Subscript

i,j,k Value of the quantity at nodes i,j,k

CHAPTER 1

INTRODUCTION

1.1 High-rise Buildings and the Use of Shear Walls

High-rise buildings have become a common type of structure all over the world. The trend of construction of high-rise buildings for both office and residential purposes is rapidly increasing. The increase in population densities due to urbanization, the growth of population and high cost of land in urban areas are the main reasons for the need of high-rise buildings.

Although the construction of high-rise buildings has solved the problem of usable space in urban areas, it has caused many environmental, psychological and social problems. In addition to these problems, there remain many engineering and technical problems associated with tall building construction. To provide efficient elevating devices for the users, the operation of heating and cooling systems, the supply of water and electricity, to provide telephone and other means of communication through the building, to provide safety against fire hazards, to provide structural safety to withstand wind and earthquake effects, to devise new construction materials and improve construction techniques, are some of these problems. This thesis deals with one aspect of these problems associated with tall buildings, namely, the study of the behaviour of shear wall buildings coupled by flat slabs to resist lateral loading due to wind or earthquakes.

Structural components such as walls, beams, columns and floor slabs form an integrated structural system of a building. The structure and its components support the vertical and lateral loads applied to the building. The vertical loads arise due to the self weight of the components, the occupants and other objects broadly classified as live loads. The lateral loads arise due to the action of wind, earthquakes or blast effect. To design a structurally safe building, it is necessary to find the load taken by each component, so that each component can be designed accordingly. In high-rise buildings, the consideration of deflection due to lateral loads becomes particularly important. For that reason it is necessary to provide adequate lateral stiffness to the structure. This lateral stiffness can be provided by using various specially designed structural systems. Among these systems, the use of reinforced concrete shear walls coupled by floor slabs have become very common. In such a system the high in-plane stiffness of the shear walls is employed to resist the lateral loads. The floor slabs act as horizontal diaphrams to distribute the lateral loads among the walls and also coupled the walls. The complex interaction of the floor slabs with the walls increases the lateral stiffness of the structure. Besides acting as load bearing walls, these shear walls can act as internal partitions, acoustic barriers and provide fire divisions within the building.

The arrangement of shear walls in a typical apartment building is shown in Figure (1.1). The shear walls are mainly located on both sides of the corridor. The elevator shaft and stairwell are also enclosed by shear walls. The present thesis is a study of the coupling effect of the flat slabs on the stiffness of the shear wall structure.

1.2 Review of the Previous Work

One common method of analysing shear wall structures is known as the continuous approach. In this approach the connecting beams or slabs between the walls are replaced by a continuous distributing laminae of equivalent stiffness.

When the shear walls are arranged in a symmetric manner in the plan of the building, wind and seismic loads will cause translational displacements only. The deformation of the building is confined to a plane. The load displacement behaviour of the structure can then be considered by a two-dimensional analysis. Common examples of symmetric buildings are apartment buildings with two-parallel sets of regularly spaced shear walls. In such cases the behaviour of the whole building can be studied from the two-dimensional behaviour of a typical pair of shear walls. The shear wall may be coupled either through the floor slabs or floor beams or both. This class of problems is generally known as the planar coupled shear walls problems. The analysis of uniform

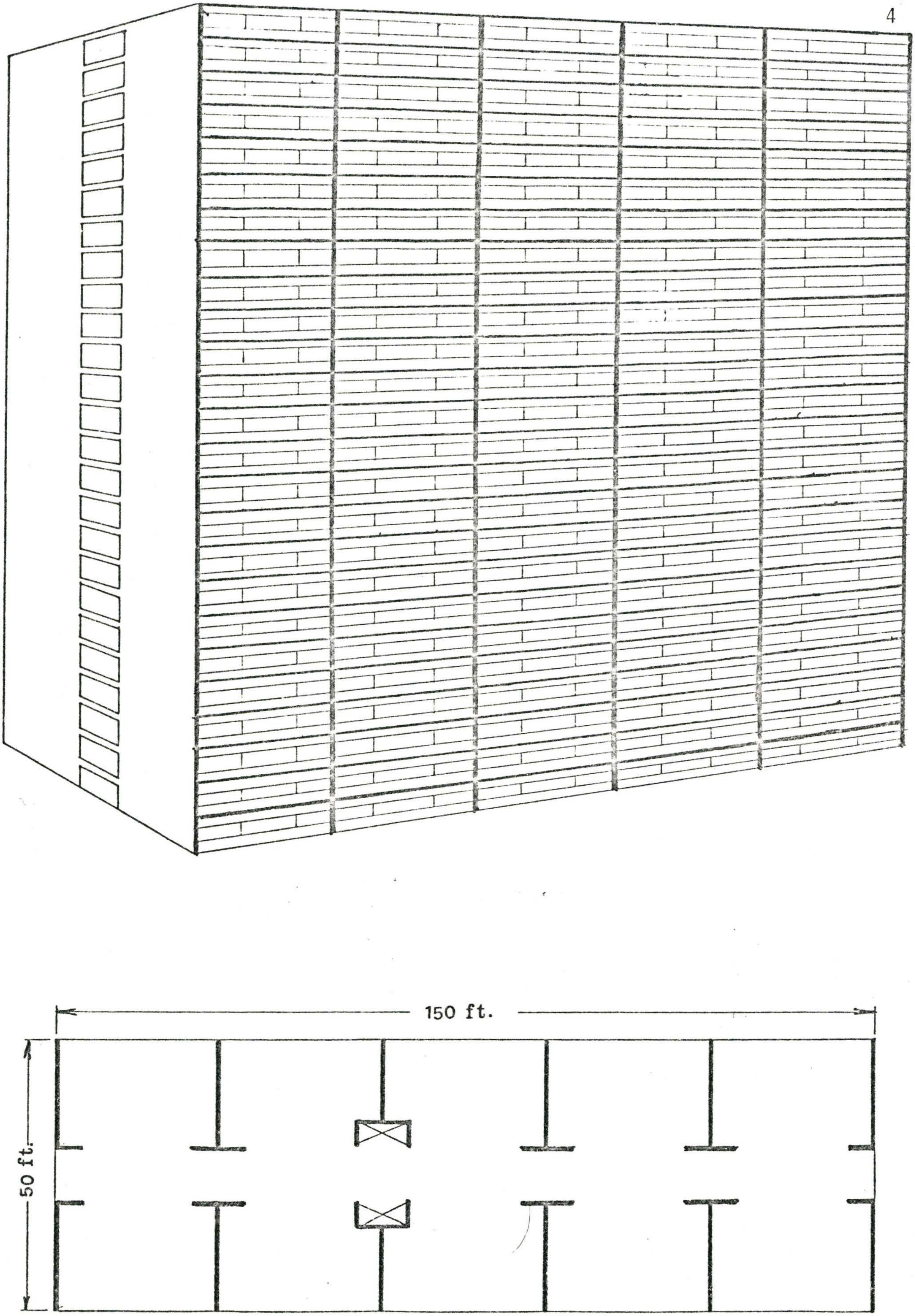

Figure (1.1) Typical Apartment Building.

plane coupled shear walls under lateral loadings has been presented by many researchers. A representative list of publications on the subject is given below.

Beck [1] and Rosman [20] developed the basic differential equation for the analysis of coupled shear walls using the continuous technique. Coull and Chaudhury [4, 5] presented sets of design curves to enable the deflection as well as the stresses in the walls and connecting beams to be calculated under different lateral loading conditions. Coull [7], Tso and Chan [27] presented the analysis of coupled shear walls resting on an elastic foundation. Tso [26] obtained the stresses induced in coupled shear walls due to foundation movements. Also, Tso and Chan [25] studied the dynamic properties of coupled shear walls. Coull and Subedi [8] gave a solution for unsymmetrical walls with two bands of openings and symmetrical walls with three bands of openings. Hussein [14] presented a method of solving the governing simultaneous second order coupled differential equations for multi-bay coupled shear walls resting on rigid foundations. Elkholy and Robinson [12] presented the analysis of coupled shear walls with one or more bands of opening resting on rigid or elastic foundations using the finite difference technique. Schwaighofer and Microys [21] analysed the coupled shear walls as equivalent frames using a standard matrix structural analysis technique.

When symmetry does not exist in the plan of the building, the lateral loads will cause twisting of the building in addition to translation. Out of plane displacement exists in this case and a three-dimensional analysis will be necessary.

Tso and Biswas [28, 29] presented a method to analyse nonplanar coupled shear walls subjected to arbitrary lateral loading and torque. Biswas and Tso [2] presented an approach to study the flexural and torsional deformation of multi-storey shear wall buildings subjected to lateral loadings.

Treating the structure as a collection of rectangular space frames with floor slabs idealized as infinitely rigid diaphrams one can obtain the stiffness matrix of the structure by determining the stiffness of the individual elements and the rigid in-plane diaphram action of the floor slabs. Heidebrecht and Swift [13], using the stiffness matrix approach, presented a method where the coupling action of the floor slab was considered by assuming equivalent beams connecting the shear walls. Taranath [23] used a similar approach with a finite element idealization to obtain the transverse stiffness of the floor slab.

If the coupling action of floor slabs is replaced by equivalent coupling beams, then the flat slab-shear wall problem can be solved by one of the methods mentioned before. However, the problem remains as to how one should replace the slab by equivalent beams. To study the coupling effect of flat slabs, Qadeer and Smith [17] presented the bending stiffness of the slabs for pairs of planar shear walls. A set of charts were given for the equivalent stiffness of slabs coupling planar walls. Coull and El-hag [9] presented some experimental results for the effective stiffness of floor slabs connecting plane walls, T-section walls and rectangular box core walls. The results of Qadeer and Smith, Coull and El-hag will be discussed in later chapters.

1.3 Purpose of Research

The purpose of the research described in this thesis is to develop a method for the analysis of the slab coupled shear walls. The main object is to determine the slab stiffness in the coupled wall configuration and to determine the effective width of an equivalent beam between the walls. This equivalent beam can then replace the slab in the overall analysis of the shear wall building. The finite element technique is used to obtain the stiffness of the slab. A computer program is developed to obtain the stiffness of the slab and its equivalent beam dimensions.

Sets of design curves are obtained to represent the relation between the rotational stiffness of the slab, and the equivalent beam width as a function of the width of the opening between the walls.

An experimental model is designed to simulate the behaviour of a planar shear wall coupled by a floor slab. Experimental tests were carried out and the results were compared with the theoretical results.

Three main parts are included in this thesis. Developing the method and converting it into a computer program is the first part. Comparison between the results obtained from the computer program and the experimental results is the second part. Finally, a set of design curves is presented based on the theoretical finite element analysis. It is hoped that the results developed in this thesis will be useful to designers and researchers studying the behaviour of shear wall multi-storey buildings with coupling floor slabs.

CHAPTER 2

FINITE ELEMENT FORMULATION

2.1 General

In this chapter, we will illustrate the use of the Finite Element Method based on the displacement approach as applied to the study of a plate under bending. The method will then be used to compute the rotational stiffness of the slab connecting two shear walls.

2.2 Basic Assumptions

The analysis of a flat slab coupling two shear walls is based on the following assumptions:

i) The slab is considered homogeneous, isotropic and linearly elastic with Poisson's ratio equal to 0.15.

ii) The slab is considered infinitely stiff in its plane. Hence, the in plane deformation is neglected.

iii) The slab is thin and the deflection is small so that the classical plate theory applies.

iv) The plane sections of the wall remain plane during bending.

2.3 Bending Stiffness Matrix for a Plate Element

The derivation of the bending stiffness matrix for a plate, using the displacement finite element method, necessitates an assumed expression for deflection w' normal to the plane of each element. Various conforming and nonconforming functions can be used. A conforming function satisfies both the displacement and slope continuity along the common edges between the adjacent elements. If a complete slope continuity is required on the interface between various elements, the mathematical and computational difficulties often rise disproportionately fast. It is, however, relatively simple to obtain a shape function which ensures continuity of displacements between the adjacent elements and violates the transverse slope continuity. Such a function is called a non-conforming function. An alternate way is to satisfy the transverse slope continuity along one of the sides of the element, resulting in a displacement function to be partially conforming. This is satisfied by using triangular elements and displacement functions suggested by Rawtani and Dokainish [19]. In the present analysis, a bending stiffness matrix for a partially conforming triangular element is developed and used.

2.3.1 System of Axes and the Nodal Coordinates

The middle surface of the plate is subdivided into triangular elements as shown in Figure (2.1(a)). Let the nodes of a typical element be i, j, k. The nodes will be defined by their coordinates. Two sets of right handed axes are used to describe each element. One set is the set of global axes denoted by X, Y, Z. Assuming the plate lies in the X-Y plane, the coordinates of the nodes in the global axes are denoted by $(X_i, Y_i, 0)$, $(X_j, Y_j, 0)$ and $(X_k, Y_k, 0)$, respectively. The second set of axes is the local axes denoted by X', Y', Z'. In the local axes the element lies in the X'-Y' plane. The two axes X', Y' will be chosen such that the displacement function will be partially conforming. This will be satisfied if the origin is taken to be the vertex i and Y'-axis is along the line ij. The direction of X'-axis is such that X_k is always positive, as shown in Figures (2.1(a)) and (2.1(b)). By this arrangement the local coordinates of the nodes, i, j, k will be

$$(0,0,0), \quad (0, Y_j', 0) \text{ and } (X_k', Y_k', 0) \tag{2.1}$$

From Figure (2.1(c)) the coordinates Y_j', X_k' and Y_k' will be given by

$$Y_j' = \sqrt{a_1} \tag{2.2}$$

$$Y_k' = (a_1 + a_3 - a_2)/2\sqrt{a_1} \tag{2.3}$$

and

$$X_k' = \sqrt{a_3 - Y'^2_k} \tag{2.4}$$

where a_1, a_2 and a_3 are the square of the lengths of the sides ij, jk and ki, respectively.

2.3.2 Displacement Formulation of the Plate Problem

Three displacement components are considered as nodal parameters. The first is the displacement w' in the Z' direction, the second is the rotation about X'-axis (θ_x') and

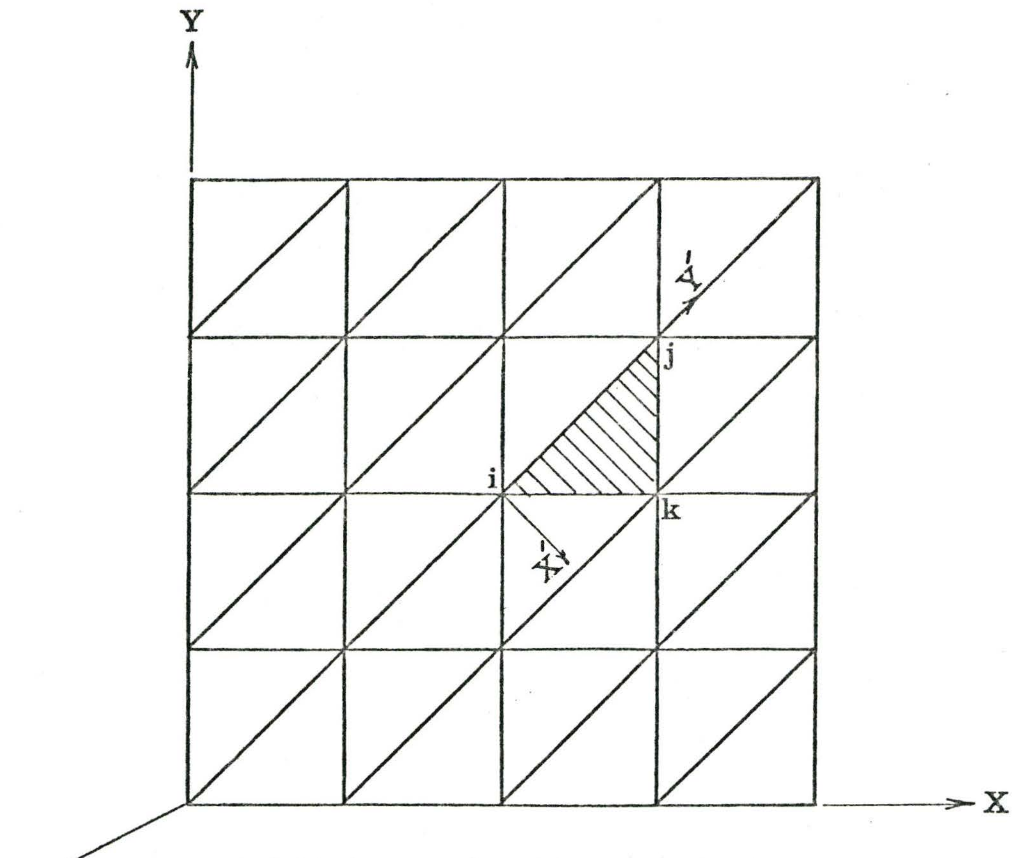

a-Subdivision of a Plate and the Global Axes

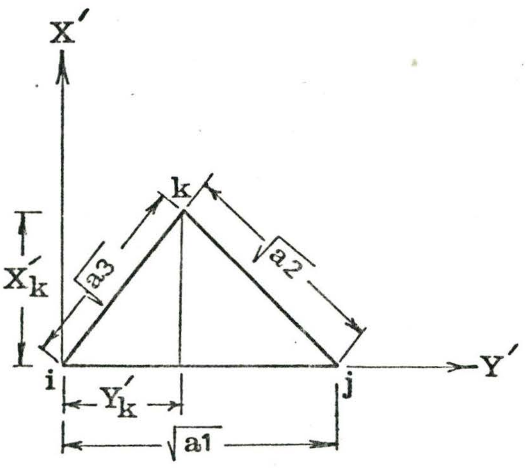

c-Dimensions of the Sides of an Element

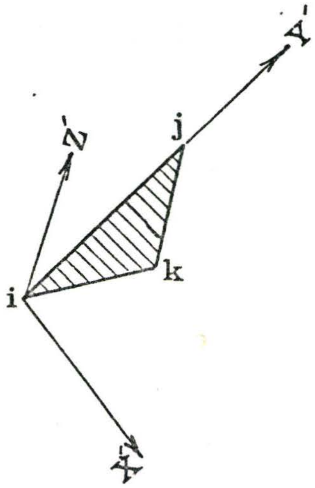

b-Local Coordinate Axes for an Element

Figure (2.1) Systems of Axes and Node Numbers.

the third is the rotation about the Y'-axis (θ'_Y) where

$$\theta'_X = \frac{\partial w'}{\partial Y'} \tag{2.5(a)}$$

and

$$\theta'_Y = -\frac{\partial w'}{\partial X'} \tag{2.5(b)}$$

The partially conforming displacement function as suggested in reference [19] with respect to the local axes is a cubic polynomial in X' and Y', namely,

$$w' = \alpha_1+\alpha_2X'+\alpha_3Y'+\alpha_4X'^2+\alpha_5X'Y'+\alpha_6Y'^2+\alpha_7X'^3+\alpha_8X'^2Y'+\alpha_9Y'^3 \tag{2.6}$$

Where α_i, $i = 1,9$ are arbitrary constants.

Along the line X' equals zero, the transverse slope $\frac{\partial w'}{\partial X'}$ will be $\alpha_2 + \alpha_5 Y'$. Since the value of the slope is specified at the two ends of this line, the expression for the transverse slope is unique along the line $X' = 0$. This makes the displacement function w' partially conforming.

Equation (2.6) can be written in matrix form as

$$w' = [C]\{\alpha\} \tag{2.7}$$

where

$$[C] = [1,X',Y',X'^2,X'Y', Y'^2,X'^3,X'^2Y',Y'^3] \tag{2.8}$$

and $\{\alpha\}$ is the column vector of coefficients α_1 to α_9.
The nodal displacement vector referred to the local axes can be defined as,

$$\{\delta'_i\} = \begin{Bmatrix} w'_i \\ \theta'_{Xi} \\ \theta'_{Yi} \end{Bmatrix} \tag{2.9}$$

From Equations (2.5), (2.6) and (2.9) the nodal displacement vector becomes

$$\{\delta_i'\} = \begin{bmatrix} 1 & X_i' & Y_i' & X_i'^2 & X_i'Y_i' & Y_i'^2 & X_i'^3 & X_i'^2Y_i' & Y_i'^3 \\ 0 & 0 & 1 & 0 & X_i' & 2Y_i' & 0 & X_i'^2 & 3Y_i'^2 \\ 0 & -1 & 0 & -2X_i' & -Y_i' & 0 & -3X_i'^2 & -2X_i'Y_i' & 0 \end{bmatrix} \begin{Bmatrix} \alpha_1 \\ \alpha_2 \\ \alpha_3 \\ \alpha_4 \\ \alpha_5 \\ \alpha_6 \\ \alpha_7 \\ \alpha_8 \\ \alpha_9 \end{Bmatrix} \tag{2.10}$$

The element displacement vector referred to the local axes will be given by the listing of the nodal displacements, now totalling three,

$$\{\delta_e'\} = \begin{Bmatrix} \delta_i' \\ \delta_j' \\ \delta_k' \end{Bmatrix} \tag{2.11}$$

From Equations (2.10) and (2.11) the element displacement vector referred to the local axes becomes

$$\{\delta'_e\}=\begin{bmatrix} 1 & X'_i & Y'_i & X_i'^2 & X'_iY'_i & Y_i'^2 & X_i'^3 & X_i'^2Y'_i & Y_i'^3 \\ 0 & 0 & 1 & 0 & X'_i & 2Y'_i & 0 & X_i'^2 & 3Y_i'^2 \\ 0 & -1 & 0 & -2X'_i & -Y'_i & 0 & -3X_i'^2 & -2X'_iY'_i & 0 \\ 1 & X'_j & Y'_j & X_j'^2 & X'_jY'_j & Y_j'^2 & X_j'^3 & X_j'^2Y'_j & Y_j'^3 \\ 0 & 0 & 1 & 0 & X'_j & 2Y'_j & 0 & X_j'^2 & 3Y_j'^2 \\ 0 & -1 & 0 & -2X'_j & -Y'_j & 0 & -3X_j'^2 & -2Y'_jX'_j & 0 \\ 1 & X'_k & Y'_k & X_k'^2 & X'_kY'_k & Y_k'^2 & X_k'^3 & X_k'^2Y'_k & Y_k'^3 \\ 0 & 0 & 1 & 0 & X'_k & 2Y'_k & 0 & X_k'^2 & 3Y_k'^2 \\ 0 & -1 & 0 & -2X'_k & -Y'_k & 0 & -3X_k'^2 & -2X'_kY'_k & 0 \end{bmatrix} \begin{Bmatrix} \alpha_1 \\ \alpha_2 \\ \alpha_3 \\ \alpha_4 \\ \alpha_5 \\ \alpha_6 \\ \alpha_7 \\ \alpha_8 \\ \alpha_9 \end{Bmatrix} \qquad (2.12$$

Substituting for (X'_i, Y'_i, Z'_i), (X'_j, Y'_j, Z'_j) and (X'_k, Y'_k, Z'_k) from Equation (2.1), Equation (2.12.a) becomes

$$\{\delta'_e\}=\begin{bmatrix} 1 & 0 & 0 & 0 & 0 & 0 & 0 & 0 & 0 \\ 0 & 0 & 1 & 0 & 0 & 0 & 0 & 0 & 0 \\ 0 & -1 & 0 & 0 & 0 & 0 & 0 & 0 & 0 \\ 1 & 0 & Y'_j & 0 & 0 & Y_j'^2 & 0 & 0 & Y_j'^3 \\ 0 & 0 & 1 & 0 & 0 & 2Y'_j & 0 & 0 & 3Y_j'^2 \\ 0 & -1 & 0 & 0 & -Y'_j & 0 & 0 & 0 & 0 \\ 1 & X'_k & Y'_k & X_k'^2 & X'_kY'_k & Y_k'^2 & X_k'^3 & X_k'^2Y'_k & Y_k'^3 \\ 0 & 0 & 1 & 0 & X'_k & 2Y'_k & 0 & X_k'^2 & 3Y_k'^2 \\ 0 & -1 & 0 & -2X'_k & -Y'_k & 0 & -3X_k'^2 & -2X'_kY'_k & 0 \end{bmatrix} \begin{Bmatrix} \alpha_1 \\ \alpha_2 \\ \alpha_3 \\ \alpha_4 \\ \alpha_5 \\ \alpha_6 \\ \alpha_7 \\ \alpha_8 \\ \alpha_9 \end{Bmatrix} \qquad (2.12$$

Equation (2.12b) can be written in matrix form as

$$\{\delta'_e\} = [A]\ \{\alpha\} \qquad (2.13)$$

From Equations (2.7) and (2.13) the displacement function becomes

$$W' = [C][A]^{-1} \{\delta'_e\} \tag{2.14}$$

The element stiffness matrix will be obtained by applying the principle of virtual work. If the external and internal forces are statically equivalent, then the external and internal work done will be equal. Let the external nodal force vector referred to the local axes be

$$\{F'_i\} = \begin{Bmatrix} F'_{Zi} \\ F'_{\theta Xi} \\ F'_{\theta Yi} \end{Bmatrix} \tag{2.15}$$

Where F'_{Zi}, $F'_{\theta Xi}$, and $F'_{\theta Yi}$ are the external force and moments in the Z', X', Y' directions respectively. The element nodal forces $\{F'_e\}$ referred to the local axes will be

$$\{F'_e\} = \begin{Bmatrix} F'_i \\ F'_j \\ F'_k \end{Bmatrix}$$

$$= [F'_{Zi}, F'_{\theta Xi}, F'_{\theta Yi}, F'_{Zj}, F'_{\theta Xj}, F'_{\theta Yj}, F'_{Zk}, F'_{\theta Xk}, F'_{\theta Yk}]^T \tag{2.16}$$

The corresponding internal moments for each element will be

$$\{M'_e\} = [M'_{Xi}, M'_{Yi}, M'_{XYi}, M'_{Xj}, M'_{Yj}, M'_{XYj}, M'_{Xk}, M'_{Yk}, M'_{XYk}]^T \tag{2.17}$$

The curvature $\{r'\}$ at any point in the directions of local axes will be

$$\{r'\} = \begin{Bmatrix} \dfrac{\partial^2 W'}{\partial X'^2} \\ \\ \dfrac{\partial^2 W'}{\partial Y'^2} \\ \\ 2\dfrac{\partial^2 W'}{\partial X' \partial Y'} \end{Bmatrix} \tag{2.18}$$

From Equations (2.6) and (2.18) the curvature vector becomes

$$\{r'\} = \begin{bmatrix} 0 & 0 & 0 & 2 & 0 & 0 & 6X' & 2Y' & 0 \\ 0 & 0 & 0 & 0 & 0 & 2 & 0 & 0 & 6Y' \\ 0 & 0 & 0 & 0 & 2 & 0 & 0 & 4X' & 0 \end{bmatrix} \begin{Bmatrix} \alpha_1 \\ \alpha_2 \\ \alpha_3 \\ \alpha_4 \\ \alpha_5 \\ \alpha_6 \\ \alpha_7 \\ \alpha_8 \\ \alpha_9 \end{Bmatrix} \tag{2.19}$$

Substituting for $\{\alpha\}$ from Equation (2.13), Equation (2.19) becomes

$$\{r'\} = [C_1][A^{-1}]\{\delta'_e\} \tag{2.20}$$

where

$$[C_1] = \begin{bmatrix} 0 & 0 & 0 & 2 & 0 & 0 & 6X' & 2Y' & 0 \\ 0 & 0 & 0 & 0 & 0 & 2 & 0 & 0 & 6Y' \\ 0 & 0 & 0 & 0 & 2 & 0 & 0 & 4X' & 0 \end{bmatrix} \tag{2.21}$$

Let $\Delta\{\delta'_e\}$ be the virtual displacement, and $\Delta\{r'\}$ the corresponding virtual curvature at the nodes. The work done by the external nodal forces is equal to the sum of the products of the individual force components and corresponding displacements,

$$\text{Work Done} = [\Delta\{\delta_e'\}]^T \cdot \{F_e'\} \tag{2.22a}$$

Similarly, the internal work per unit volume done by the internal forces is

$$[\Delta\{r'\}]^T \cdot \{M_e'\} \tag{2.22b}$$

Equating the external work with the total internal work, we have

$$\int_V [\Delta\{r'\}]^T \cdot \{M_e'\} \cdot d(vol) = [\Delta\{\delta_e'\}]^T \cdot \{F_e'\} \tag{2.22}$$

For an isotropic linearly elastic plate, the relation between the curvature and moments is given by

$$\{M_i'\} = \left\{\begin{bmatrix} M_{Xi}' \\ M_{Yi}' \\ M_{XYi}' \end{bmatrix}\right\}$$

$$= \frac{E \cdot t^3}{12(1-\nu^2)} \cdot [D] \cdot \{r'\} \tag{2.23}$$

where E is the modulus of elasticity, t is the thickness and ν is Poisson's ratio of the plate; and

$$[D] = \begin{bmatrix} 1 & \nu & 0 \\ \nu & 1 & 0 \\ 0 & 0 & \frac{1-\nu}{2} \end{bmatrix} \tag{2.24}$$

Substituting Equations (2.17), (2.20) and (2.23) into Equation (2.22), it becomes

$$\frac{E}{12(1-\nu^2)}\iint[\Delta\{\delta_e'\}]^T[A^{-1}]^T[C_1]^T.t^3[D][C_1][A^{-1}]\{\delta_e'\}dx'dy'$$

$$= [\Delta\{\delta_e'\}]^T.\ \{F_e'\} \tag{2.25}$$

Since $\Delta\{\delta_e'\}$ is an arbitrary, the elements of matrix $[A^{-1}]$ are constant and assuming uniform plate thickness, Equation (2.25) becomes,

$$\{F_e'\} = \frac{E\ t^3}{12(1-\nu^2)}\ [A^{-1}]^T[\iint [C_1]^T[D][C_1]\ dx'\ dy'][A]^{-1}\ \{\delta_e'\} \tag{2.26}$$

Comparing the definition of the stiffness matrix

$$\{F_e'\} = [k_e']\ \{\delta_e'\} \tag{2.27}$$

The bending stiffness matrix for the element referred to the local axes is given by

$$[k_e'] = \frac{E\ t^3}{12(1-\nu^2)}\ [A^{-1}]^T[\iint [C_1]^T[D][C_1]dx'dy'][A^{-1}] \tag{2.28}$$

Integrating over the area of the element as will be given in Appendix (a), the element stiffness matrix $[k_e']$ becomes

$$[k_e'] = \frac{E\ t^3}{12(1-\nu^2)}\ [A^{-1}]^T[B][A^{-1}] \tag{2.29}$$

where

$$[B] = \begin{bmatrix} 0 & & & & & & & & \\ 0 & 0 & & & & & & & \\ 0 & 0 & 0 & & & & \text{Symmetric} & & \\ 0 & 0 & 0 & 4\ell_{11} & & & & & \\ 0 & 0 & 0 & 0 & 2(1-\nu)\ell_{11} & & & & \\ 0 & 0 & 0 & 4\nu\ell_{11} & 0 & 4\ell_{11} & & & \\ 0 & 0 & 0 & 12\ell_{21} & 0 & 12\nu\ell_{21} & 36\ell_{31} & & \\ 0 & 0 & 0 & 4\ell_{12} & 4(1-\nu)\ell_{21} & 4\nu\ell_{12} & 12\ell_{22} & 4\ell_{13}+8(1-\nu)\ell_{31} & \\ 0 & 0 & 0 & 12\nu\ell_{12} & 0 & 12\ell_{12} & 36\nu\ell_{22} & 12\nu\ell_{13} & 36\ell_{13} \end{bmatrix} \tag{2.30}$$

and

$$\begin{aligned} \ell_{11} &= \frac{1}{2} X'_k \; Y'_j \\ \ell_{21} &= \frac{1}{6} X'^2_k \; Y'_j \\ \ell_{31} &= \frac{1}{12} X'^3_k \; Y'_j \\ \ell_{12} &= \frac{1}{6} X'_k \; Y'_j \; (Y'_j + Y'_k) \\ \ell_{13} &= \frac{1}{12} X'_k \; Y'_j \; (Y'^2_j + Y'_j \; Y'_k + Y'^2_k) \\ \ell_{22} &= \frac{1}{24} X'^2_k \; Y'^2_j \; (Y'_j + 2Y'_k) \end{aligned} \tag{2.31}$$

2.4 Total Stiffness Matrix for the Plate

2.4.1 Transformation to the Common Global Axes

To assemble the element stiffness matrices into a single total stiffness matrix, all the matrices must be referred to the set of global axes. Each element stiffness matrix must be transformed from the local axes to the global axes.

The element nodal displacements in local axes $\{\delta'_e\}$ are related to the element nodal displacements in the global axes by the relation

$$\{\delta'_e\} = [T]\{\delta_e\} \tag{2.32}$$

where

$\{\delta_e\}$ is the nodal displacement of an element referred to the global axes. $[T]$ is the transformation square matrix of order equal to the number of the element nodal displacements. Similarly the element nodal forces in the local axes $\{F'_e\}$ are related to the element nodal forces in the global axes $\{F_e\}$ by the relation

$$\{F'_e\} = [T]\ \{F_e\} \tag{2.33}$$

Using Equations (2.32), and (2.33), Equation (2.27) becomes

$$[T]\ \{F_e\} = [k'_e][T]\{\delta_e\} \tag{2.34}$$

Each of the two sets of axes are orthogonal, therefore, the transformation matrix $[T]$ is orthogonal, i.e.,

$$[T]^{-1} = [T]^T \tag{2.35}$$

Equation (2.34) becomes

$$\{F_e\} = [T]^T\ [k'_e][T]\{\delta_e\} \tag{2.36}$$

Comparing the definition of the stiffness matrix

$$\{F_e\} = [k_e]\{\delta_e\} \tag{2.37}$$

The bending stiffness matrix $[k_e]$ referred to the global axes will be

$$[k_e] = [T]^T \; [k_e'][T] \tag{2.38}$$

The transformation matrix [T] is given by

$$[T] = \begin{bmatrix} \lambda & 0 & 0 \\ 0 & \lambda & 0 \\ 0 & 0 & \lambda \end{bmatrix} \tag{2.39}$$

$[\lambda]$ is a sub-matrix of direction cosines and defined as follows:

$$[\lambda] = \begin{bmatrix} n_z & l_z & m_z \\ n_x & l_x & m_x \\ n_y & l_y & m_y \end{bmatrix} \tag{2.40}$$

where

l_x, m_x, n_x are the direction cosines of X' with X, Y, Z axes
l_y, m_y, n_y are the direction cosines of Y' with X, Y, Z axes
l_z, m_z, n_z are the direction cosines to Z' with X, Y, Z axes

These direction cosines can be evaluated from the following relations

$$C = X_{ji} \, Y_{ki} - X_{ki} \, Y_{ji} \quad , \text{ where } , \quad Y_{ji} = Y_j - Y_i \quad \text{etc.}$$

$$F = \sqrt{X_{ji}^2 + Y_{ji}^2}$$

$$G = - |C|$$

$$\begin{aligned} l_z &= 0, & m_z &= 0 & n_z &= \frac{C}{G} \\ l_y &= X_{ji}/F & m_y &= Y_{ji}/F & n_y &= 0 \\ l_x &= m_y . n_z & m_x &= -n_z . l_y & n_x &= 0 \end{aligned} \tag{2.41}$$

2.4.2 Assembly of the Element Stiffness Matrix

Having calculated the stiffness matrices $[K_e]$ for the individual elements, the next step is to combine all these matrices, according to the sequence of node numbering employed on the structure to obtain the complete stiffness matrix for that structure. The method of obtaining the assembled matrix [K] for the structure from the element stiffness matrices $[K_e]$ is best illustrated by an example.

Figure (2.2(a)) shows a plate subdivided into twelve triangles. There are three degrees of freedom at each node. Therefore, the 9x9 stiffness matrix for each element can be subdivided into 3x3 submatrices, as shown in Figure (2.2(b)). With the total number of nodes equal to 12 for this structure, the total stiffness matrix [K] will be of size 36 x 36 and it can be subdivided into 3x3 submatrices. As shown in Figure (2.2(c)) the element stiffness submatrices are inserted in their appropriate locations in the total stiffness matrix. Consider, for example, element (e). While deriving the stiffness matrix for this element, the numbers, i, j, k were assigned to the nodes as shown. Thus, i, j, k correspond to node numbers 4, 8, 5 respectively on the plate. Thus the submatrix $[K_e^{ij}]$ of the element will be inserted at the submatrix location (4, 8) in matrix [K], as shown in Figure (2.2(c)). Similarly, all the submatrices of all the other elements can be inserted in the proper location. If more than one submatrix is to be inserted in the same location of [K], all these submatrices are to be added to each other.

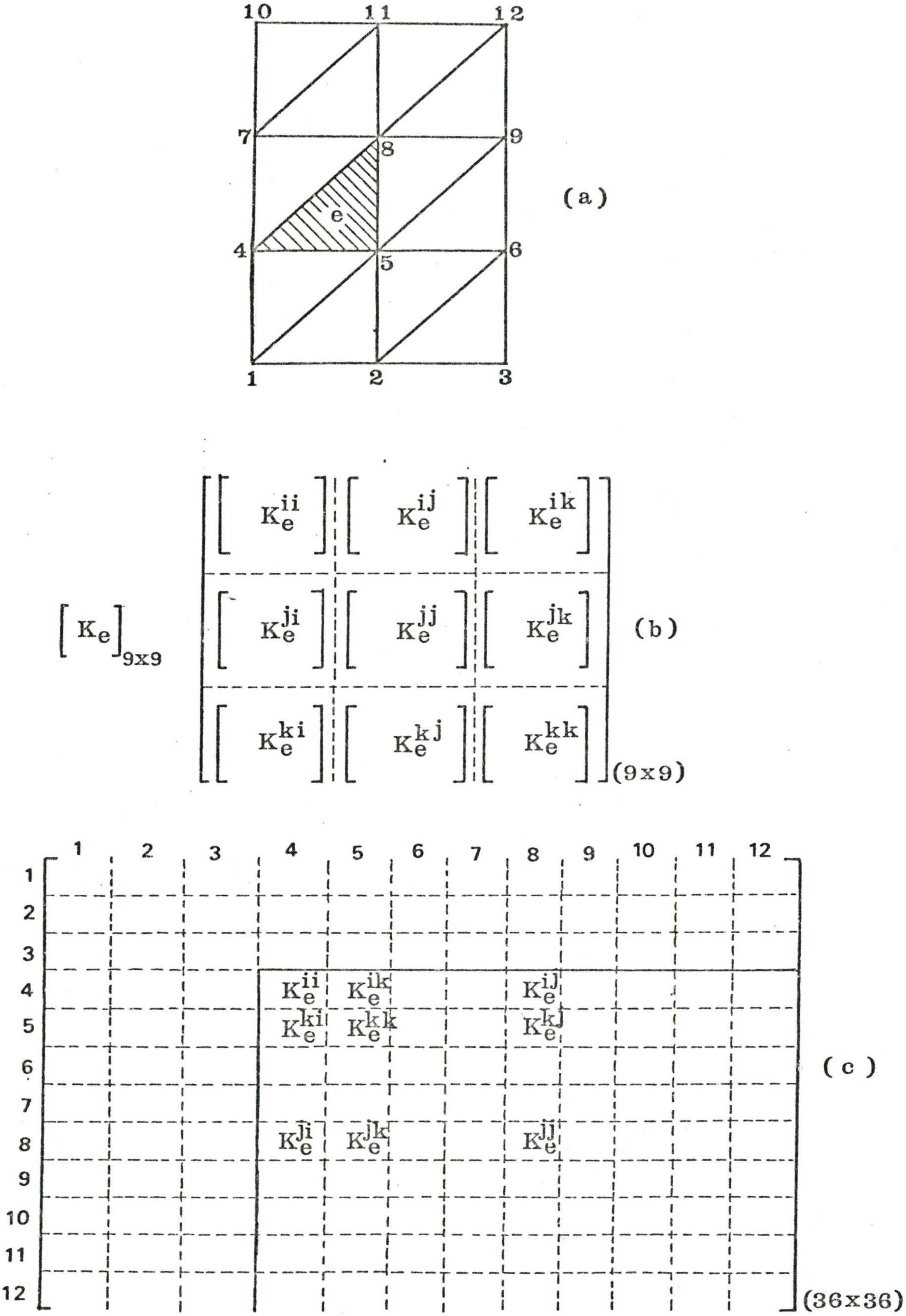

Figure (2.2) Generation of Total Stiffness Matrix.

If the boundary conditions require certain nodal displacements to be zero, the rows and the columns of [K] corresponding to these displacements are deleted to get the final stiffness matrix for the structure. In the problem considered in Figure (2.2(a)), let us assume that the edge containing the nodes 1, 2 and 3 is fixed. Then the displacements of these nodes (i.e., first nine components of $\{\delta\}$) are zero. Thus the first 9 rows and columns of [K] are deleted to get the final stiffness matrix [K] as shown by the solid lines in Figure (2.2(c)). The nodal forces of such an element $\{F_e\}$ will also be assembled to obtain the total force vector {F}. The total displacement vector $\{\delta\}$ will be obtained from the equilibrium equation

$$\{F\} = [K]\{\delta\} \tag{2.42}$$

2.5 Application of the Bending Stiffness Matrix

The nodal displacements can be obtained by solving Equation (2.42). A finite element computer program was developed to solve the plate bending problem that has been previously described. The first check for the accuracy of the computer program and the displacement function used is obtained by solving a square plate and a rectangular plate with all edges fixed as shown in Figures (2.3(a)) and (2.3(b)). The finite element results for the nodal displacements will be compared by the finite difference results. The square plate is of dimension 8' by 8' while the rectangular plate is 4' by 8'. Both the plates are subjected to a central lateral load

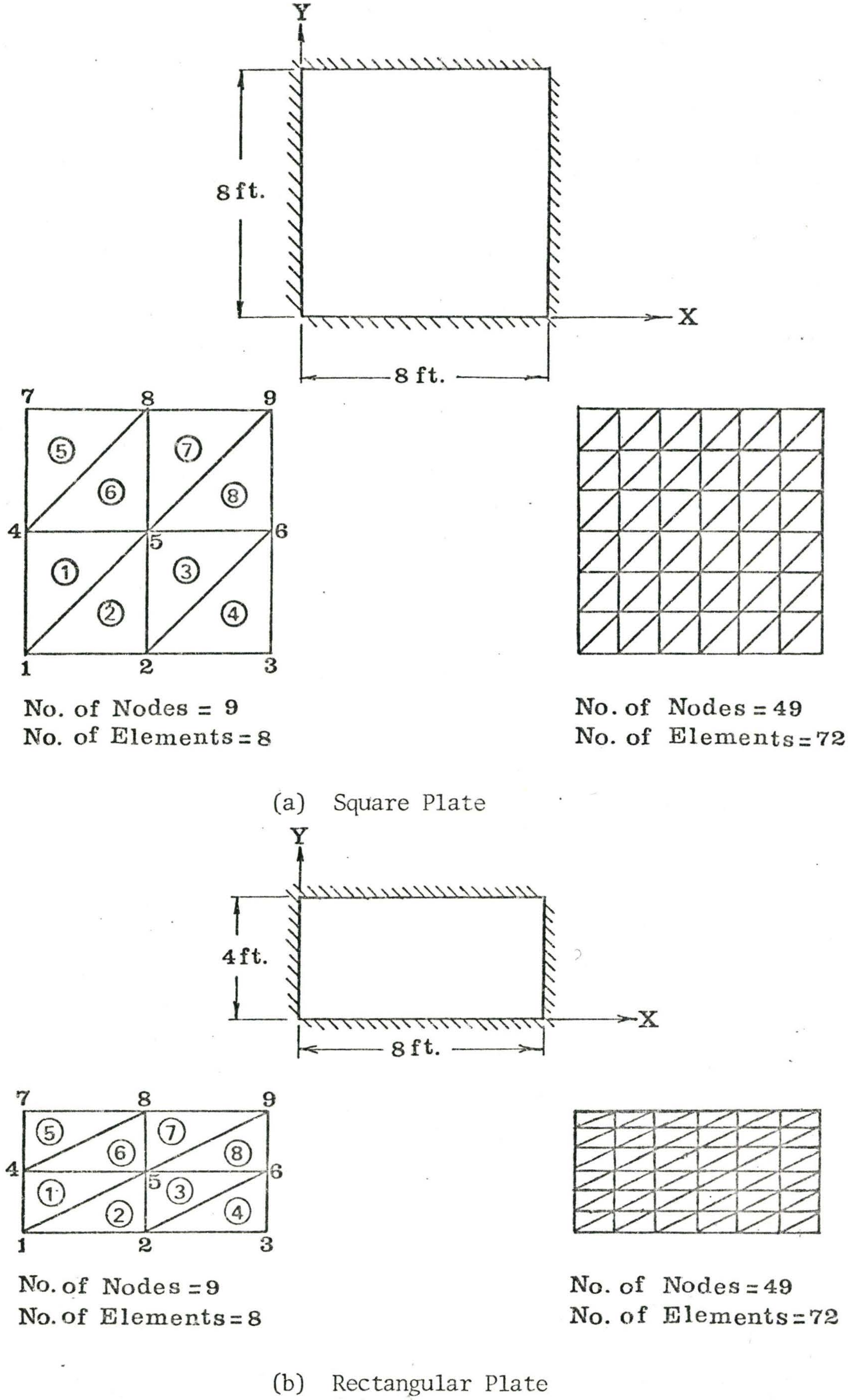

Figure (2.3) Dimensions of Plates and Finite Element Meshes.

of 1000 kip. The thickness of each plate is 0.667 ft., the modulus of elasticity is 4.32×10^5 kip/ft^2 and the Poisson's ratio equals to 0.15. Four finite element meshes of 8, 16, 32 and 72 elements are chosen for the study of both the plates. Plotted in Figure (2.4) is the relation between the number of elements and the central deflection. It is clear from that figure that there is a rapid convergence to the exact solution, an indication that the chosen function is fairly efficient. Table (2.1) shows the computer results for the deflection and the two slopes of the central node. Szilard [22] solved the plate by the finite difference method, the results of which are tabulated for different aspect ratios for the plate. The central deflection is given by the equation

$$W_{max} = C_1 \cdot \frac{q\ a^2}{\bar{D}} \tag{2.43}$$

where

q is the central load, W_{max}, a, $\bar{D}$, are the maximum central deflection, the short length, the flexural rigidity of the plates. C_1 is a factor tabulated based on the finite difference calculations. The value of C_1 for the square plate is 0.0056, and for the rectangular plate is 0.0072. Using Equation (2.43), the value of the central deflection for the square plate is 0.033 feet and for the rectangular plate is .0106 feet. Good agreement can be observed between these results and those given in Table (2.1). The two slopes at the central point are approximately equal to zero. The computed results agree with the physical behaviour of the plate.

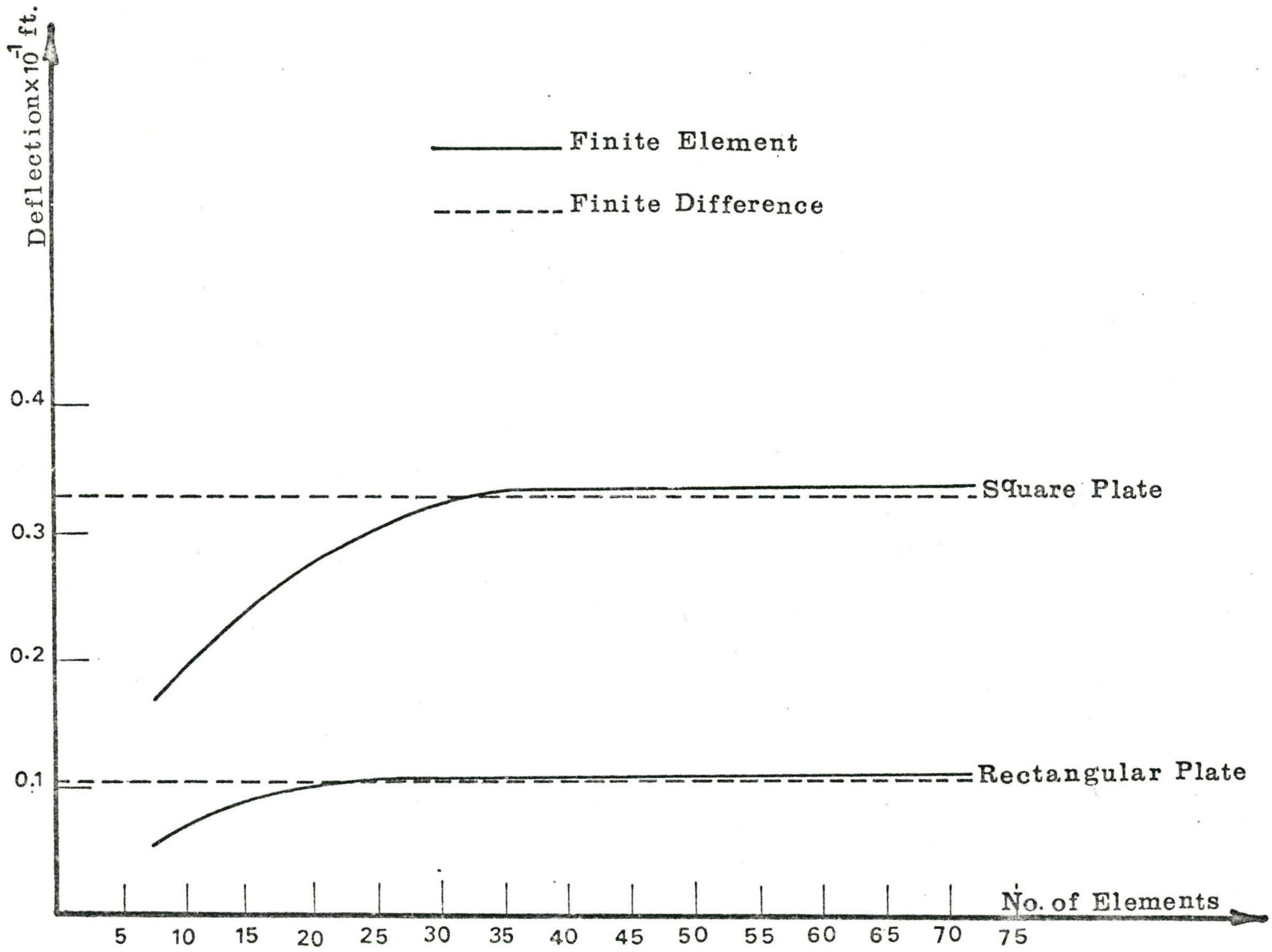

Figure (2.4) Relation Between Number of Elements and Central Deflection.

This serves as a check for the efficiency and accuracy of the proposed finite element scheme.

Square Plate			Rectangular Plate		
W_{max}	θ_X	θ_Y	W_{max}	θ_X	θ_Y
.03355	$.4472 \times 10^{-15}$	$.8809 \times 10^{-16}$	.01085	$.1071 \times 10^{-15}$	$.974 \times 10^{-17}$

Table (2.1) Computer Results for the Slope and Deflection of Central Point.

CHAPTER 3

METHOD OF ANALYSIS

3.1 General

Theoretical and experimental methods have been used to obtain the rotational stiffness and the effective width of the slabs coupling shear walls. The theoretical analysis for the slab stiffness was based on the solution of the plate equation by the finite difference method [17]. The analysis was carried out for the slab coupled planar walls only. The experimental work was carried out with different wall configurations [9]. The experimental results presented covers three ratios of wall openings relative to the full width of the coupled shear walls. For any other ratio of openings, extrapolation of the results becomes necessary. Therefore, it is useful to formulate the coupling slab problem in general terms, so that the stiffness of the coupling slab can be computed for a variety of geometric configurations for design purposes.

In this chapter, a finite element analysis for the slab is employed for finding the bending stiffness of the slab. To facilitate the overall analysis of shear wall buildings, it is convenient to imagine that the slab acts as a connecting beam between the walls. The effective width of this beam will be estimated, and the slab rotational stiffness at the centroidal axes of the wall is obtained in the present analysis. At the end of this chapter, an evaluation for the method of analysis and the computer program will be carried out, by comparing the results obtained using the finite element method with the previous results obtained in references [9], [17].

3.2 Solution of the Finite Element Equation Applied to the Coupled Slab Problem

To consider the form of interaction between the slab and the walls, an idealized structure is chosen. This idealized structure consists of two shear walls with a slab connecting them, as shown in Figure (3·1). The slab is free at all edges and rigidly connected to the walls.

Consider a high-rise building consisting of shear walls supporting flat slab floors as shown in Figure (3·2). Under lateral loads, these shear walls will rotate causing a relative displacement, Δ, between the ends of the slab. Figure (3·3) shows the rotation of the walls and the corresponding relative displacement. In view of the large in-plane stiffness of the slab, it is generally assumed that both walls deflect equally, so that the rotations of the cross-sections are taken to be the same. In this case, the effective stiffness of the floor slab will be defined by the relationship between the relative displacement Δ, (Figure (3·3)) and the forces producing it. If the relative displacement, Δ, is unity, the corresponding force to this displacement will represent the bending stiffness of the slab. It is convenient

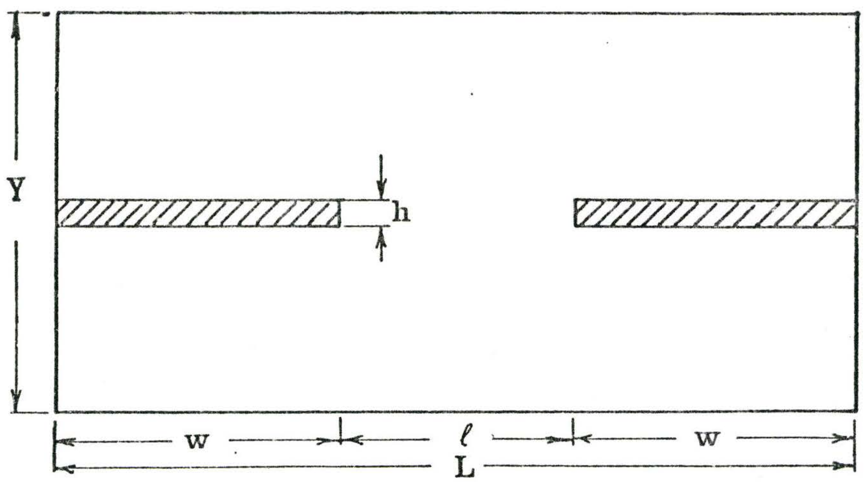

(a) Complete Plan Dimension and Notations.

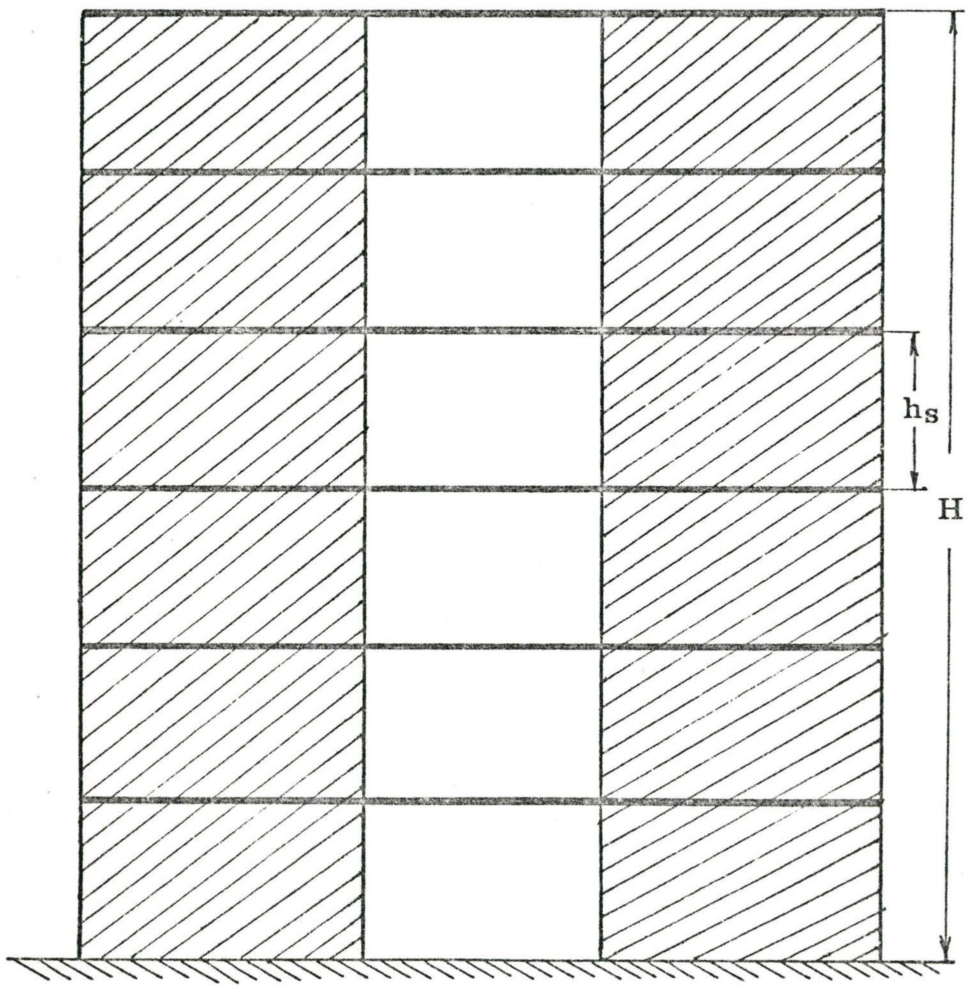

(b) Elevation Showing Flat Slab Type Structure.

Figure (3.1).

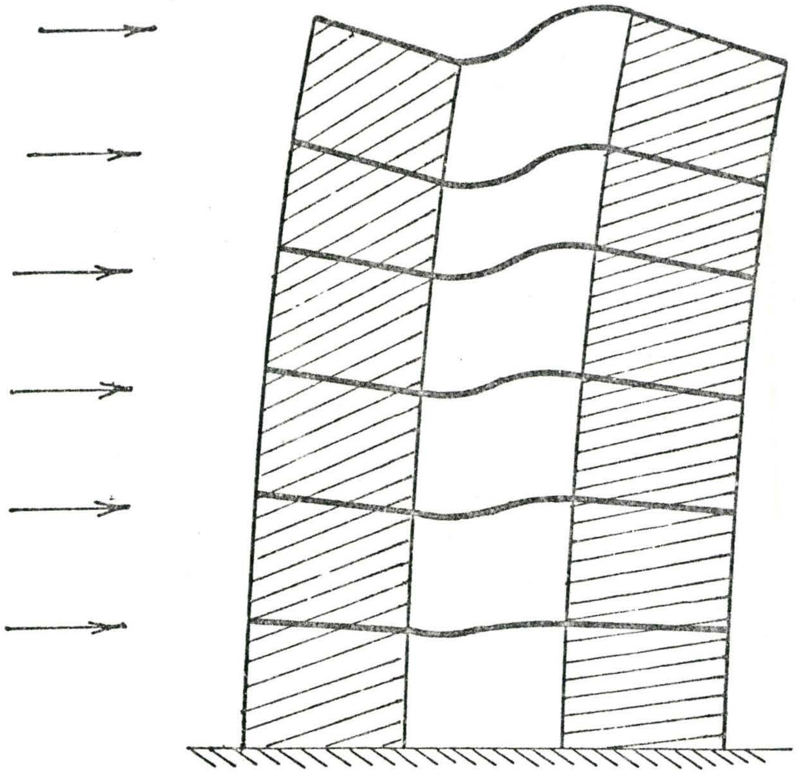

Figure (3.2) Deformation of Cross Wall Structure Under Lateral Loading.

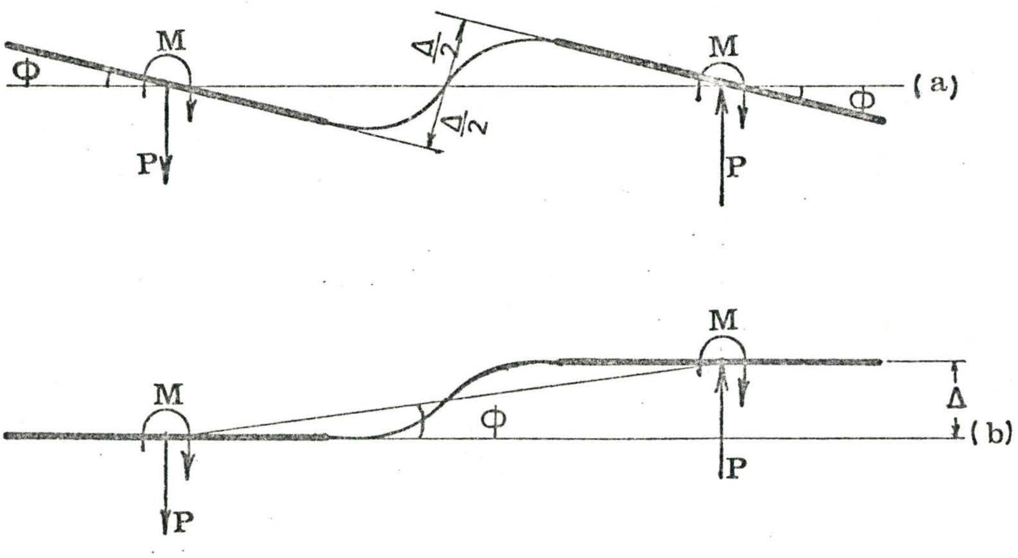

Figure (3.3) Slab Deformation Resulting from Rotation of Walls.

to consider the slab as a lintel beam between the walls. If this beam is assumed to have a depth equal to the thickness of the slab, its effective width, Y_e will be determined such that its bending stiffness becomes the same as that of the slab. Also, the rotational stiffness of that beam calculated at the centroid of the cross-section of the wall is taken as the rotational stiffness of the slab. This rotational stiffness represents the slab effective stiffness on the shear wall.

To calculate the bending stiffness of the slab, the overall stiffness matrix [k] can be obtained as described in the previous chapter. A unit relative vertical displacement with zero slopes will be specified at the nodes on the boundaries between the slab and the walls. The corresponding vertical nodal forces are computed and the summation of these vertical nodal forces on one wall represents the bending stiffness of the slab.

Equation (2.42) represents the force-displacement relationship for the mathematical model shown in Figure (3-4). The displacements at the nodes at the boundaries between the walls and the slab are known while the forces are unknown. On the other hand, the remaining nodes have known zero applied forces but the displacements are unknown. Thus the force and displacement vectors in Equation (2.42) are partially known in the sense that in each vector some elements are known and some are unknown. For example, as shown in Figure (3.4), the nodes numbered from 1 to 69 have zero forces

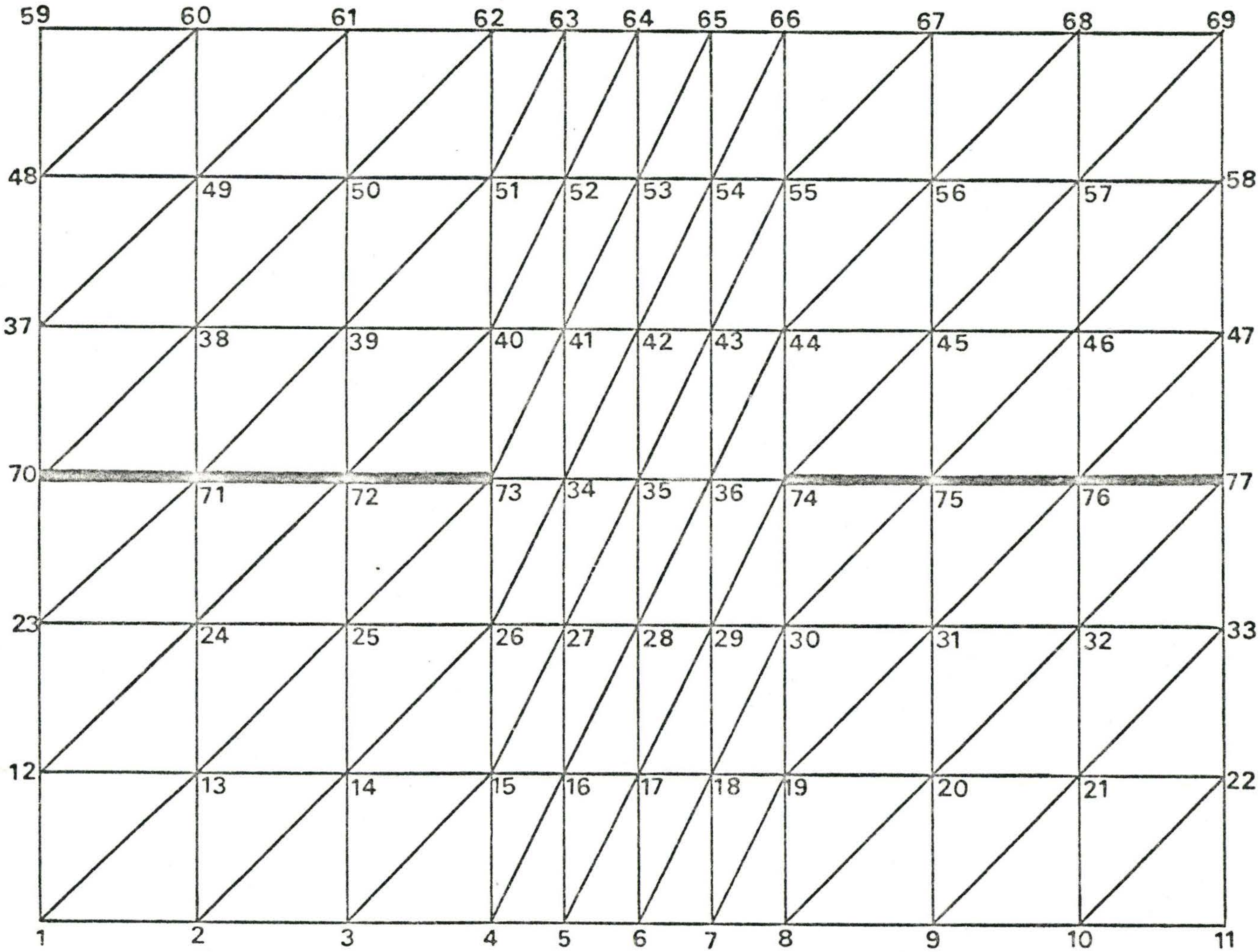

Figure (3.4) Typical Problem with Sequence of Numbering the Nodes.

and unknown displacements. The nodes numbered from 70 to 77 have known displacements and unknown forces and moments. To obtain the solution, Equation (2.42) can be written as

$$\begin{Bmatrix} \{F_a\} \\ --- \\ \{F_b\} \end{Bmatrix} = \left[\begin{array}{c|c} [K_{aa}] & [K_{ab}] \\ \hline [K_{ba}] & [K_{bb}] \end{array}\right] \cdot \begin{Bmatrix} \{\delta_a\} \\ ---- \\ \{\delta_b\} \end{Bmatrix} \tag{3.1}$$

where

$\{F_a\}$ represents the known zero forces

$\{F_b\}$ represents the unknown forces

$\{\delta_a\}$ represents the unknown displacements

$\{\delta_b\}$ represents the known displacements

Expanding Equation (3.1), we obtain

$$\{F_a\} = [K_{aa}]\cdot\{\delta_a\} + [K_{ab}]\cdot\{\delta_b\} \tag{3.2}$$

$$\{F_b\} = [K_{ba}]\cdot\{\delta_a\} + [K_{bb}]\cdot\{\delta_b\} \tag{3.3}$$

Solving Equations (3.2) and (3.3) and noting that $\{F_a\}$ is a zero vector, the solution becomes

$$\{F_b\} = [[K_{bb}] - [K_{ba}][K_{aa}]^{-1}[K_{ab}]]\cdot\{\delta_b\} \tag{3.4}$$

or

$$\{F_b\} = [\bar{K}]\cdot\{\delta_b\} \tag{3.5}$$

The vector $\{\delta_b\}$ represents the known displacements of the nodes at the boundaries between the slab and the walls.

Solving Equation (3.5) for unit relative displacement and zero slope, the nodal forces and moments will be obtained. The summation of the vertical forces at the boundary between the wall and the slab then represent the bending stiffness of the slab.

3.3 Considerations for Symmetry and Anti-Symmetry of Some Slab Configurations

For the purpose of saving computer time and core storage, conditions of symmetry and anti-symmetry are given careful consideration. When circumstances permit, one quarter or one half of the slab is solved to obtain the solution instead of using the complete slab.

3.3.1 Boundary Conditions for One Quarter of the Slab

Figure (3.5(a)) shows a slab configuration in which only one quarter of the slab needs to be considered. Due to the conditions of loading, the X-X axis is an axis of symmetry and the Y-Y axis is an axis of anti-symmetry. Figure (3.5(b)) shows a quarter of the slab with boundary conditions along the two axes X-X and Y-Y. From this figure the boundary conditions along the Y-Y axis are such that at each node, both w_i, and θ_{Xi} are equal to zero and θ_{Yi} is unknown. The corresponding forces F_{zi} and $F_{\theta Xi}$ are unknown and $F_{\theta Yi}$ equals to zero. Nodes along the X-X axis have θ_{Xi} equals to zero and both w_i and θ_{Yi} are unknown. Correspondingly both F_{Zi} and $F_{\theta Yi}$ are equal to zero and $F_{\theta Xi}$ is unknown.

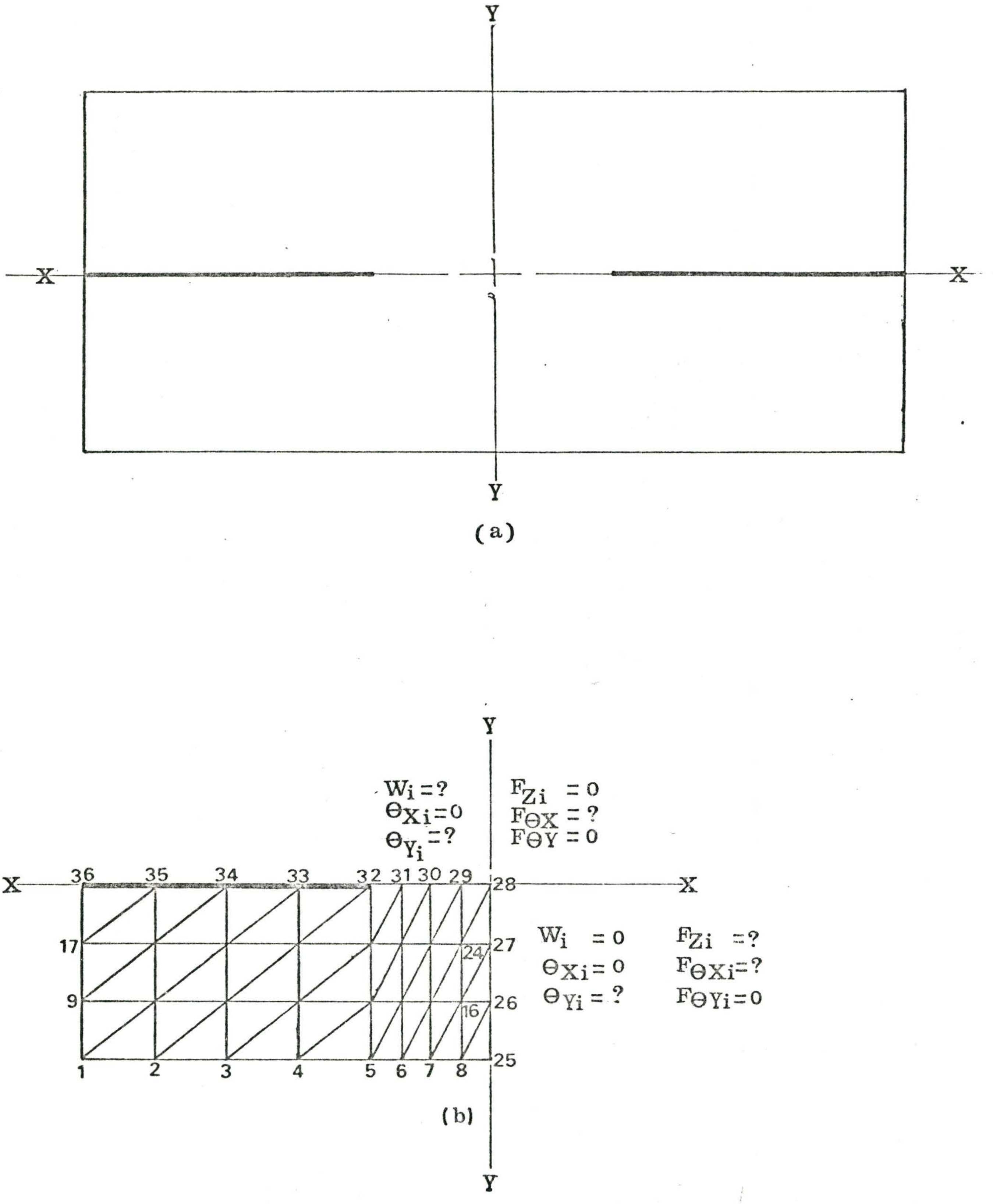

Figure (3.5) Typical Problem and the Boundary Conditions for Quarter of the Slab.

3.3.2 Boundary Conditions for One Half of the Slab

If one axis of symmetry exists, then only one half of the plate needs to be considered. Figure (3.6(a)) shows an example of the case where the first wall is a planar wall, while the other wall is a T-section. The boundary conditions along the axis X-X are shown in Figure (3.6(b)). Along boundary X-X the force F_{Zi}, the moment $F_{\theta Yi}$ and the rotation θ_{Xi} are equal to zero, while the deflection w_i, the rotation θ_{Yi} and the moment $F_{\theta Xi}$ are unknown.

3.3.3 Method of Solution

The plate is divided into two regions. The first region includes the nodes not on the X-X and Y-Y axes. These nodes have zero applied forces on them. These forces are excluded from the analysis as explained in Section 3.1. The second region includes the nodes along the X-X and Y-Y axes. The nodes on the boundary between the wall and the slab are given unit displacements, while the corresponding forces are to be determined. For other nodes on the axes, the boundary conditions are applied as was explained before. The force vector $\{F_b\}$ and consequently the stiffness matrix $[\bar{K}]$ are so arranged that the nodes with zero forces appear first in the force and displacement vector as shown below.

$$\begin{Bmatrix} \{F_{b1}\} \\ \hline \{F_{b2}\} \end{Bmatrix} = \left[\begin{array}{c|c} [K'_{11}] & [K'_{12}] \\ \hline [K'_{21}] & [K'_{22}] \end{array}\right] \begin{Bmatrix} \{\delta_{b1}\} \\ \hline \{\delta_{b2}\} \end{Bmatrix} \qquad (3.6)$$

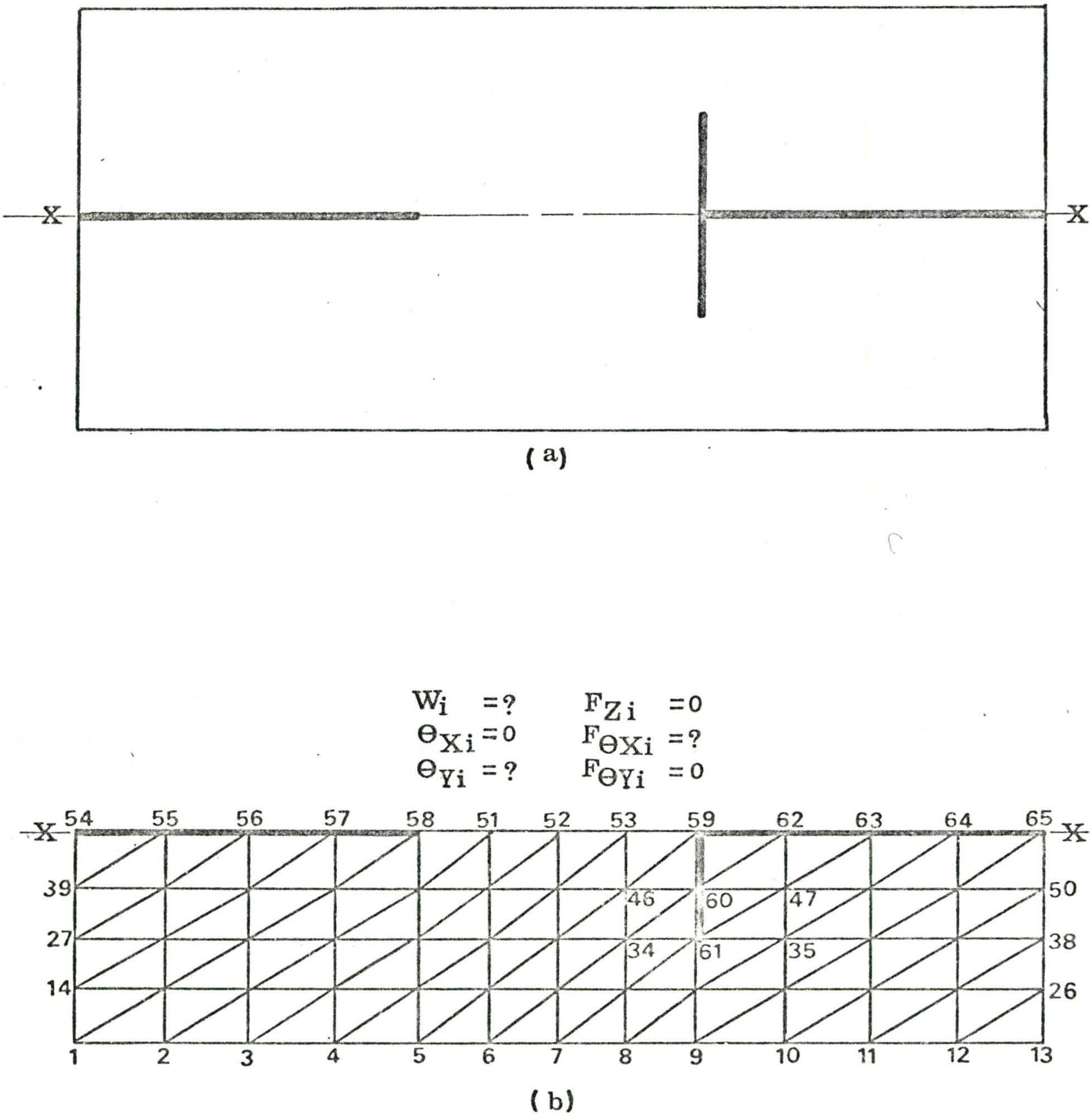

Figure (3.6) Typical Problem and the Boundary for Half of the Slab.

where

$\{F_{b1}\}$ are the zero forces resulting from the arrangement of the force vector.

$\{F_{b2}\}$ are the unknown forces at the nodes along the axes.

$\{\delta_{b1}\}$ are the unknown displacements at the nodes along the axes.

$\{\delta_{b2}\}$ are the known displacements at the nodes along the axes.

Equation (3.6) can be treated in the same way as described in connection with Equation (3.1), and the final solution will be

$$\{F_{b2}\} = [\bar{K}_2]\cdot\{\delta_{b2}\} \tag{3.7}$$

where

$$[\bar{K}_2] = [[K'_{22}] - [K'_{21}][K'_{11}]^{-1}\ [K'_{12}]] \tag{3.8}$$

The displacement vector $\{\delta_{b2}\}$ is given as a known input and Equation (3.7) can be solved to obtain the force vector $\{F_{b2}\}$ which includes the nodal forces at the boundary between the wall and the slab.

3.4 Equivalent Effective Width of the Slab

If the slab is considered as a beam of the same thickness connecting the two walls, the bending stiffness of that beam at its connection to the wall will necessarily be equal to the stiffness of the slab. Let K_b represent the bending stiffness of the slab, then

K_b = sum of all vertical forces at the nodes on the boundary between the wall and the slab due to a relative unit displacement between the walls.

The stiffness of the equivalent beam equals to K_b , thus

$$K_b = \frac{12\ E.I}{\ell^3} \tag{3.9}$$

in which E is the modulus of elasticity, I is the moment of inertia of the equivalent beam and ℓ is the width of the opening between the two walls (connecting beam length). Let Y_e be the effective width of the equivalent beam. Since the equivalent beam has the same thickness and modulus of elasticity as the slab, Equation (3.9) becomes

$$\frac{Y_e . t^3}{12} = \frac{K_b . \ell^3}{12\ E} \tag{3.10}$$

The effective width Y_e can be normalized to the total width of the slab Y, thus

$$\frac{Y_e}{Y} = \frac{K_b . \ell^3}{E . t^3 . Y} \tag{3.11}$$

The width of the slab Y will be the distance centreline to centreline between two consecutive shear walls. The relation between Y_e/Y and the distance ℓ is represented in the form of a set of curves as will be described in Chapter 5. The length ℓ will also be normalized to the total width L as shown in Figure (3.1(a)).

3.5 Rotational Stiffness of the Slab

The rotational stiffness of the slab or its effective stiffness to the shear walls is obtained at the centroid of the wall cross-sections. Three types of wall cross-sections will be studied. The first type consists of the situation where two T-section walls are connected by the slab. The second type consists of two planar walls coupled by the slab and the third type consists of one planar wall and one T-section wall coupled by the slab.

3.5.1 The Rotational Stiffness for the Configuration of a Slab Coupled T-Section Walls or Planar Walls

A general formula for the rotational stiffness will be obtained for the configuration of two T-section walls coupled by a beam. The two planar walls configuration can be taken as a special case of the T-section walls. Figure (3.7) shows two T-section walls connected by the equivalent beam. Let P be the force which causes a relative displacement, Δ, between the two walls coupled by the slab. The same force P will cause a relative displacement, Δ, between the two ends of the equivalent beam. The fixed end moment will then be

$$M_1 = \frac{P\ell}{2} \tag{3.12}$$

Let e_x be the distance from the inner edge of the wall to its centroid. The rotational moment at the centriod of the cross-section of the wall will be M, where

$$M = \frac{P\ell}{2} + P\ e_x \tag{3.13}$$

Let ϕ be the angle of rotation of the wall due to the moment M, from Figure (3.7(b)) we have

$$\phi = \frac{\Delta}{2} \Big/ (\ell/2 + e_x)$$

$$\phi = \frac{\Delta}{\ell + 2\, e_x} \tag{3.14}$$

The rotational stiffness of the slab is then defined as

$$\frac{M}{\phi} = \frac{P}{\Delta} \times \frac{(\ell + 2e_x)^2}{2} \tag{3.15}$$

Since the value of P/Δ represents the bending stiffness K_b , thus Equation (3.15) becomes

$$\frac{M}{\phi} = \frac{K_b}{2} (\ell + 2\, e_x)^2 \tag{3.16}$$

To normalize this rotational stiffness, it will be divided by the flexural rigidity of the slab $\bar{D}$ where

$$\bar{D} = \frac{E \cdot t^3}{12(1-\nu^2)} \tag{3.17}$$

Thus the nondimensional rotational stiffness of the slab at the centroid of the cross-section of the wall becomes

$$R = \frac{M}{\phi \cdot \bar{D}} \tag{3.18}$$

Using Equations (3.16), (3.17) and (3.11), Equation (3.18) becomes

$$R = \frac{6(Y_e/Y)\cdot(Y/\ell)\cdot(1-\nu^2)}{[\ell/(\ell + 2\, e_x)]^2} \tag{3.19}$$

Equation (3.19) relates the rotational stiffness R to the equivalent width Y_e for a T-section wall.

Figure (3.8) shows the configuration of a coupled planar walls. The centroid of the cross-section of the planar wall is at the middle of the wall, thus

$$e_x = \frac{w}{2} \tag{3.20}$$

Substituting Equation (3.20) into Equation (3.19), the non-dimensional rotational stiffness of the slab coupled planar walls, becomes

$$R = \frac{6(Y_e/Y)\cdot(Y/\ell)\cdot(1-\nu^2)}{[\ell/(\ell+w)]^2} \tag{3.21}$$

3.5.2 Rotational Stiffness for the Configuration of a Slab Coupled Planar Wall with T-Section Wall

The rotational stiffness of the slab coupled planar wall with T-section wall is obtained considering the actual position of the point of contraflexure, which is no longer at the midpoint of the connecting beam. This analysis is done to evaluate the assumption of considering the point of contraflexure to be at the middle of the connecting beam. The actual analysis is derived in this section while the discussion is delayed till Chapter 5 where a general discussion of various effects is presented.

The external moment applied to the coupled walls is resisted by the moment carried by each wall and the axial forces in the two walls. Each wall will resist a moment according to its stiffness. Since the two walls have different

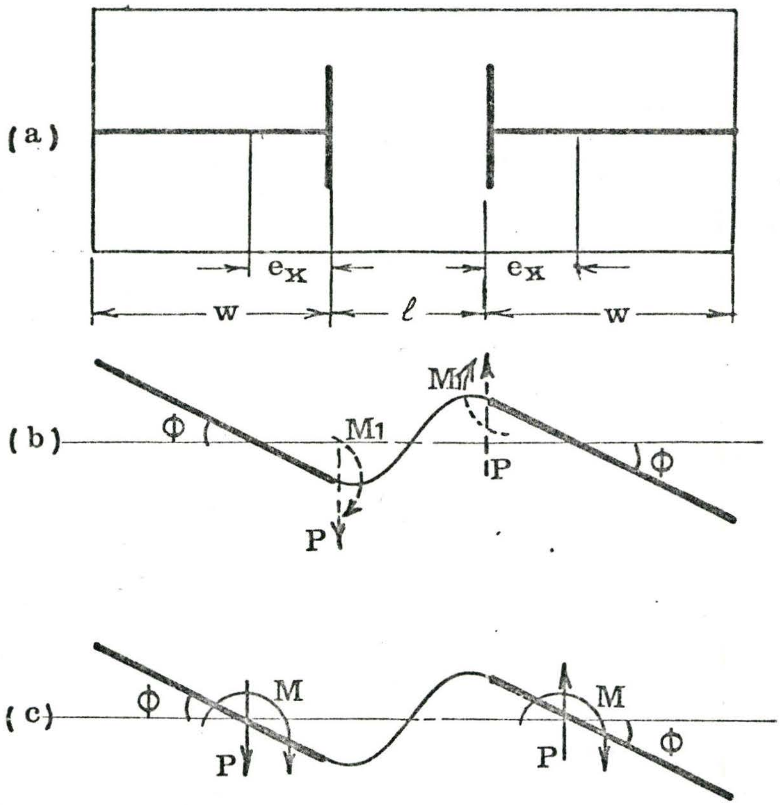

Figure (3.7) Typical Plan and the Rotation of T-Section Walls.

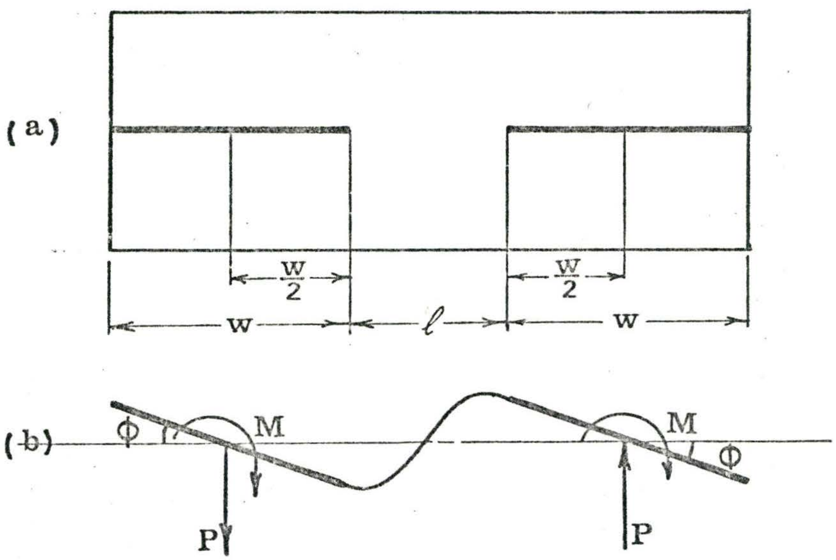

Figure (3.8) Typical Plan and the Rotation of Planar Walls.

stiffnesses, then the moment carried by each wall is different. Thus the point of contraflexure is no longer at the mid-span between the two walls. Let I_1 and I_2 represent the inertias of the planar and T-section walls about axes passing through their respective centroids, then from Figure (3.9)

$$\ell_1/\ell_2 = I_1/I_2 \tag{3.22}$$

where ℓ_1 and ℓ_2 are the distances between the point of contraflexure and the inner edges of the planar wall and the T-section wall, respectively. In terms of wall opening ℓ we have

$$\ell_1 = \frac{\ell}{1+I_2/I_1} \tag{3.23}$$

and

$$\ell_2 = \frac{\ell}{1+I_1/I_2} \tag{3.24}$$

Since the angle of rotation of the two walls will be the same, then

$$\frac{\Delta_1}{\Delta_2} = \frac{\ell_1 + w/2}{\ell_2 + e_x} \tag{3.25}$$

or

$$\Delta_2 = \frac{\ell_2 + e_x}{\ell + \frac{w}{2} + e_x} . \Delta \tag{3.26}$$

Substituting Equation (3.24) into (3.26)

$$\Delta_2 = \frac{[\ell/(1+I_1/I_2)] + e_x}{\ell + \frac{w}{2} + e_x} . \Delta \tag{3.27}$$

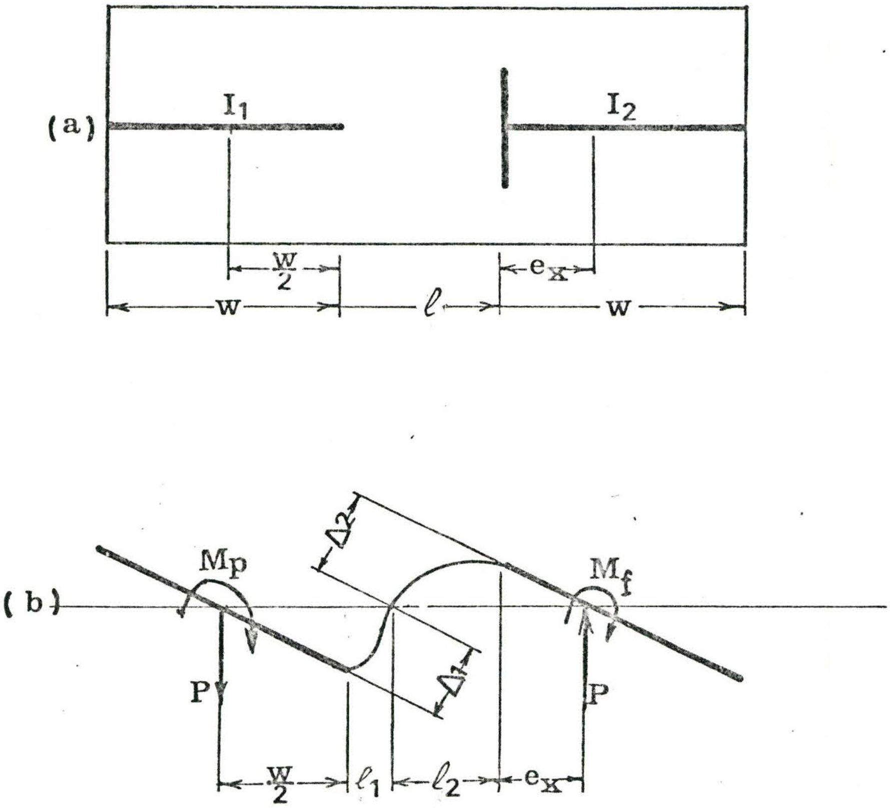

Figure (3.9) Typical Plan and Rotations of Planar Wall with T-Section Wall.

The angle of rotation of the wall ϕ is given by

$$\phi = \frac{\Delta_2}{\ell_2 + e_x} \tag{3.28}$$

From Equations (3.24) and (3.27), Equation (3.28) becomes

$$\phi = \frac{\Delta}{\ell + \frac{W}{2} + e_x} \tag{3.29}$$

Let M_p be the rotational moment acting at the centroid of the planar wall section, then

$$M_p = P\,\ell_1 + P\,\frac{W}{2} \tag{3.30}$$

Using Equations (3.17), (3.23) and (3.29), the nondimensional rotational stiffness of the slab at the centroid of the planar wall section R_p, becomes

$$R_p = \frac{M_p}{\overline{D}\cdot\phi}$$

$$= 6(Y_e/Y)\cdot(Y/\ell)\cdot(1-\nu^2)\cdot\left[\frac{2}{1+I_2/I_1} + \frac{W}{\ell}\right]\cdot\left[1+\frac{W}{2\ell}+\frac{e_x}{\ell}\right] \tag{3.31}$$

In a similar way, the rotational moment M_f calculated at the centroid of the T-section wall will be

$$M_f = \frac{P}{2}\left[\frac{2\,\ell}{1+I_1/I_2} + 2\,e_x\right] \tag{3.32}$$

The nondimensional rotational stiffness of the slab at the centroid of the cross-section of the T-section wall R_f, becomes

$$R_f = 6(Y_e/Y)\cdot(Y/\ell)\cdot(1-\nu^2)\cdot\left[\frac{2}{1+I_1/I_2}+\frac{2\,e_x}{\ell}\right]\cdot\left[1+\frac{W}{2\ell}+\frac{e_x}{\ell}\right] \tag{3.33}$$

We have discussed the various formulae used to obtain the equivalent width of the slab and the rotational stiffness of the slab for a variety of coupled wall configurations. In the remaining sections, we shall outline the flow chart of a computer program developed and calibrate the computer program by comparing some computed results against results that have appeared in the literature.

3.6 Computer Program

A computer program is developed to carry out the computation using the method of analysis described above. Figure (3.10) shows a flow chart for that program. It consists of three parts:

The first part is a group of subroutines to formulate the total stiffness matrix of the slab. These subroutines are:

a) Subroutine LAMDA to obtain the direction cosines of the local axes.

b) Subroutine AINVRS to obtain the inversion of maxtrix [A].

c) Subroutine BENDK to formulate the element stiffness matrix in the local axes.

d) Subroutine TRANS to transform the element stiffness matrix from the local to the global axes.

e) Subroutine ASSEMB to formulate the total stiffness matrix.

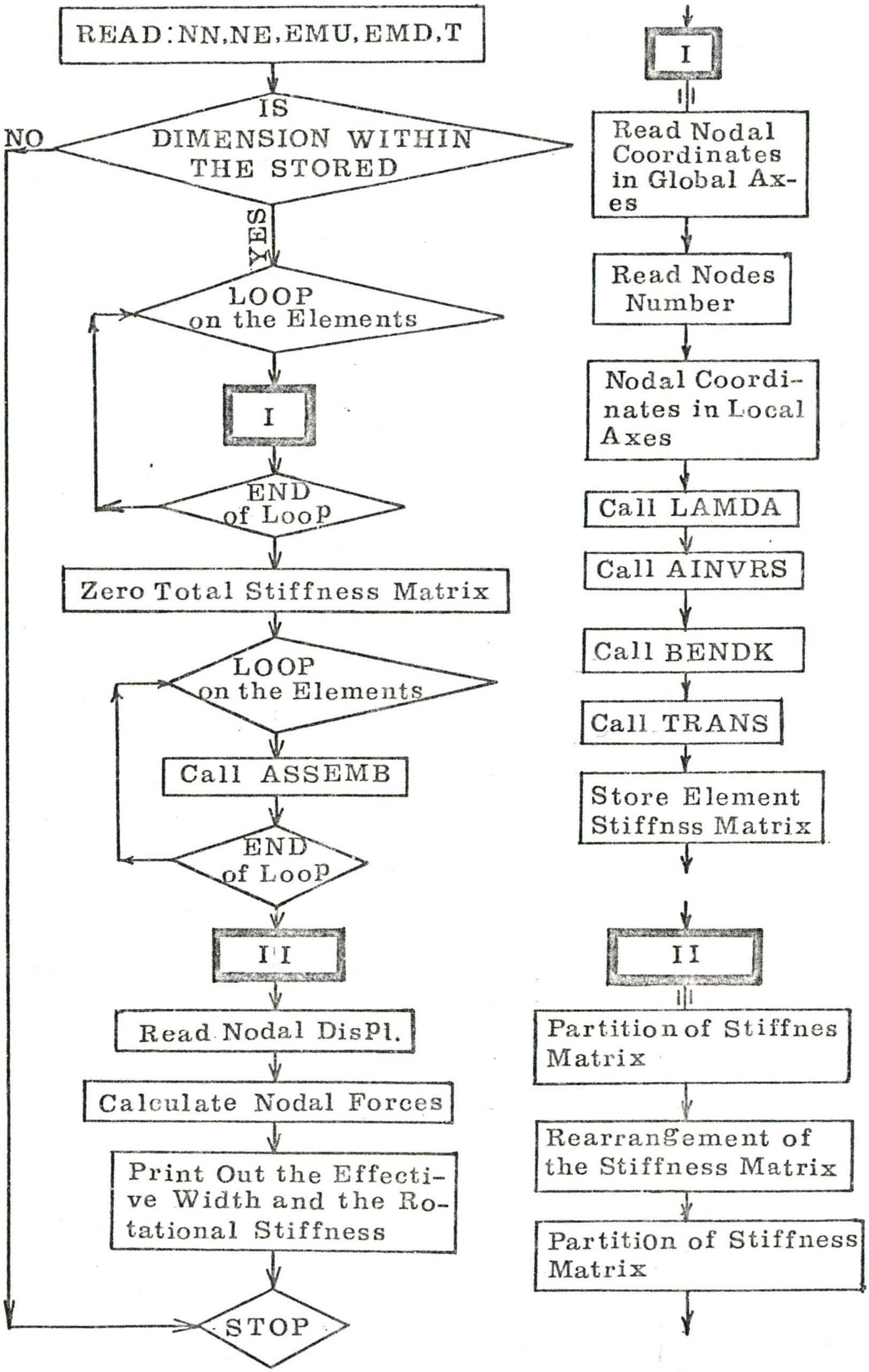

Figure (3.10) Flow Chart for the Computer Program.

The second part is the partition of the stiffness matrix to obtain the matrix $[\bar{K}]$ represented in Equation (3.5). This partition is used to omit the unknown displacements along the nodes not located on the boundary between the wall and the slab, nor on the axis of symmetry and antisymmetry.

The third part includes the boundary conditions for the cases where only a quarter and a half of the slab are solved. This part, together with the first two parts is represented in two programs. One program is for solving the quarter of the slab problem, and the other is for solving the half of the slab problem. A complete listing of the program is given in Appendix B.

3.7 Verification of the Computer Program and the Method of Analysis

In order to check the method of analysis suggested in this thesis and to test the computer program, different slabs are analysed and the results are compared with the previously obtained results given in the literature [9, 17]. In addition, a problem with a known solution is solved by the computer program to verify its accuracy.

3.7.1 Analytical Verification

Consider a slab connecting two shear walls as shown in Figure (3.11(a)). The configuration consists of two planar walls of thickness one foot each with an opening 3.5 feet in between. The slab width is taken to be the same as the thickness of the walls. Figure (3.11(b)) shows a quarter of the slab to be solved and the method of numbering of the nodes. The computer results are shown in Table (3.1). This slab is solved analytically as a beam of a width of one foot and depth 0.667 foot fixed at both ends. Table (3.2) shows the analytical results.

Since the slab is of the same width as the wall thickness, it is expected that its effective width will be the full width. As given in Table (3.1) the ratio of the equivalent width to the total width is 1.005. This means that the equivalent beam width equals the width of the slab with an error of 0.5%. Comparing the stiffness and the fixed end moments, we can conclude that the computer results agree with the analytical values within an acceptable accuracy.

3.7.2 Comparison with Results Given in the Literature

A set of curves has been presented by Qadeer and Smith [17] on the slab coupled planar wall problem. These curves were obtained by using the finite difference method to solve the plate equation. These curves show the relations between the normalized wall openings and both the normalized effective width Y_e/Y and the nondimensional rotational stiffness R. It should be pointed out that in this investigation the continuity between the slabs are considered and the wall thicknesses are taken to be infinitesimal. In addition, Qadeer and Smith [17] carried out two sets of experiments,

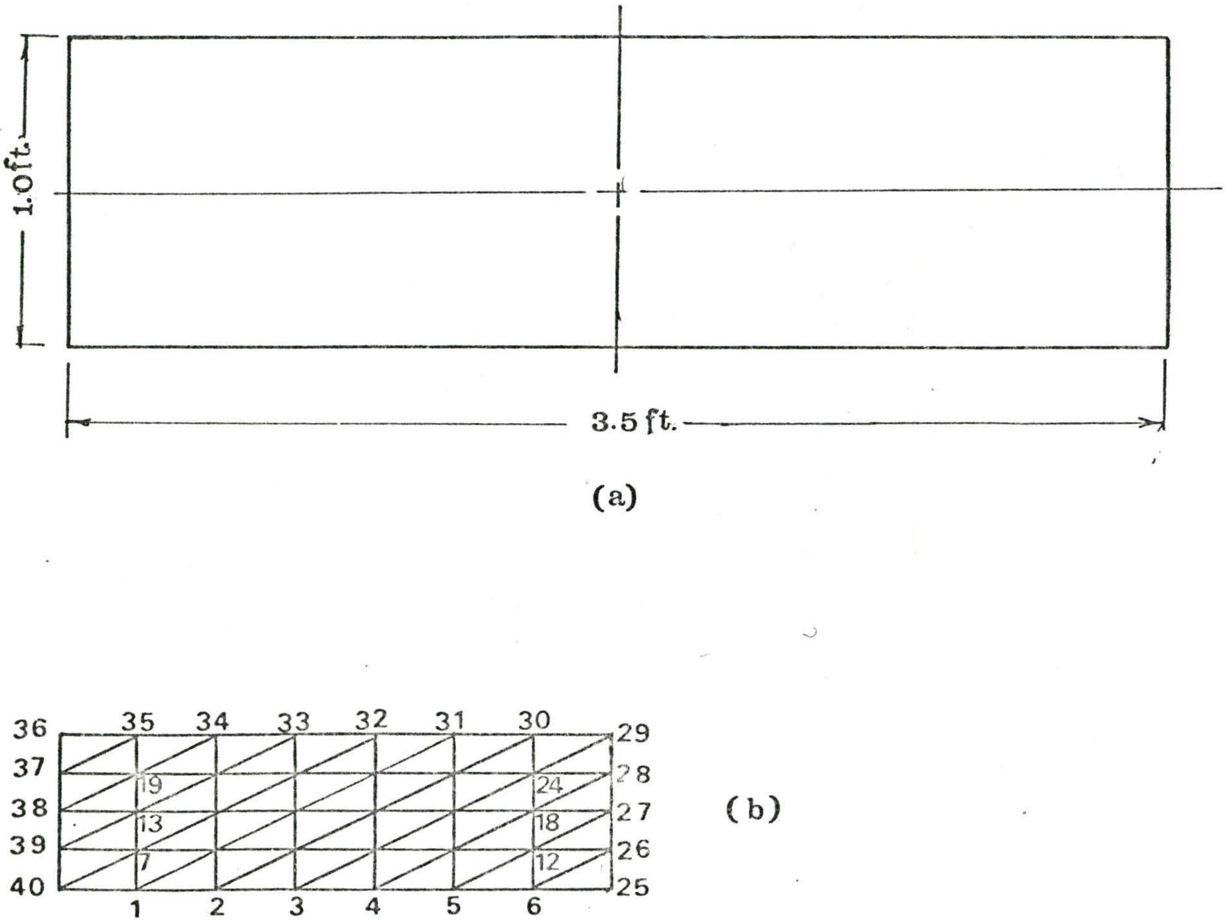

Figure (3.11) Numerical Example - Full Dimensions and the Finite Element Mesh.

Table (3.1) Computer Results

Y ft.	ℓ ft.	Y_e/Y	Stiffness (reaction)	My x 10^2					$2\Sigma My$ x 10^2
				36	37	38	39	40	
1	3.5	1.00577	$3.006\text{x}10^3$	3.237	6.769	6.85	6.066	3.385	52.614

Table (3.2) Analytical Results

Y ft.	ℓ ft.	Stiffness (reaction)	M
1	3.5	$2.99\text{x}10^3$	$52.2\text{x}10^2$

in which the slabs are considered free along the edges.

Figure (3.12) shows the plan dimensions of the problem studied in reference [17] with d as the length of the overhanging part of the slab beyond the walls. Table (3.3) shows the dimensions of the slabs and the wall configuration that were studied experimentally, while Table (3.4) shows the dimensions of the slabs which were solved by the finite difference scheme. The same slabs with all edges free are analysed by the finite element method as presented in this thesis. The results based on the finite difference scheme and the finite element technique are plotted in Figure (3.14). In the same figure, the percentage of difference in the effective width of the slab between the two methods is also plotted. The results based on the finite element technique are also plotted in Figure (3.13) with the experimental results of reference [17].

From Figure (3.13), the finite element results give higher values for the stiffness of the slab. At the same time, the finite element analysis also gives higher values than the finite difference analysis for the stiffness of the slab. However, it should be noted that the computed results based on finite element technique follow similar trend results given by Qadeer and Smith.

Coull and El-hag [9] published sets of curves obtained experimentally for slabs coupled shear walls. These curves show the relation between the ratio ℓ/L and both the nondimensional rotational stiffness and the equivalent beam

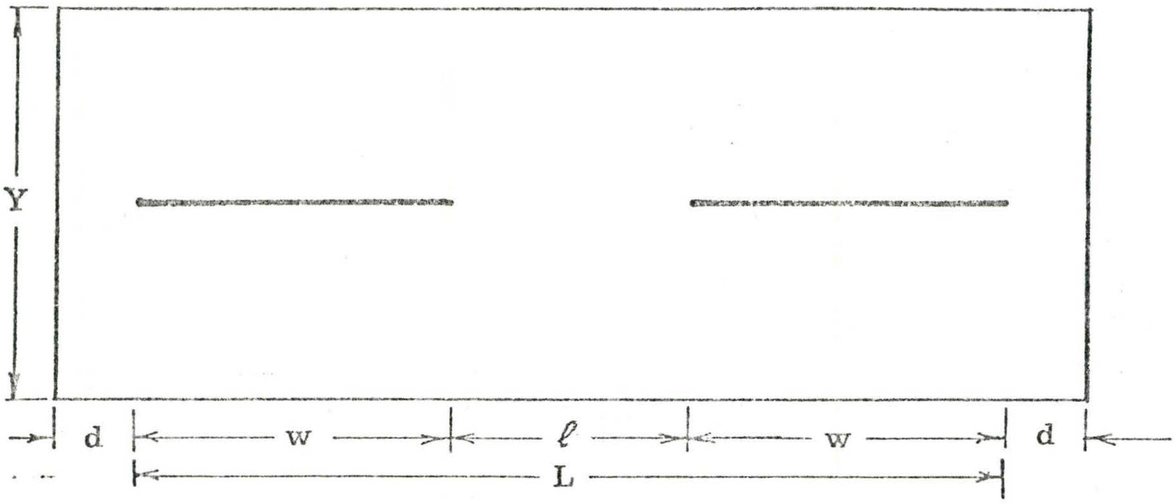

Figure (3.12) Plan Dimension for Slab Solved in Ref. [17].

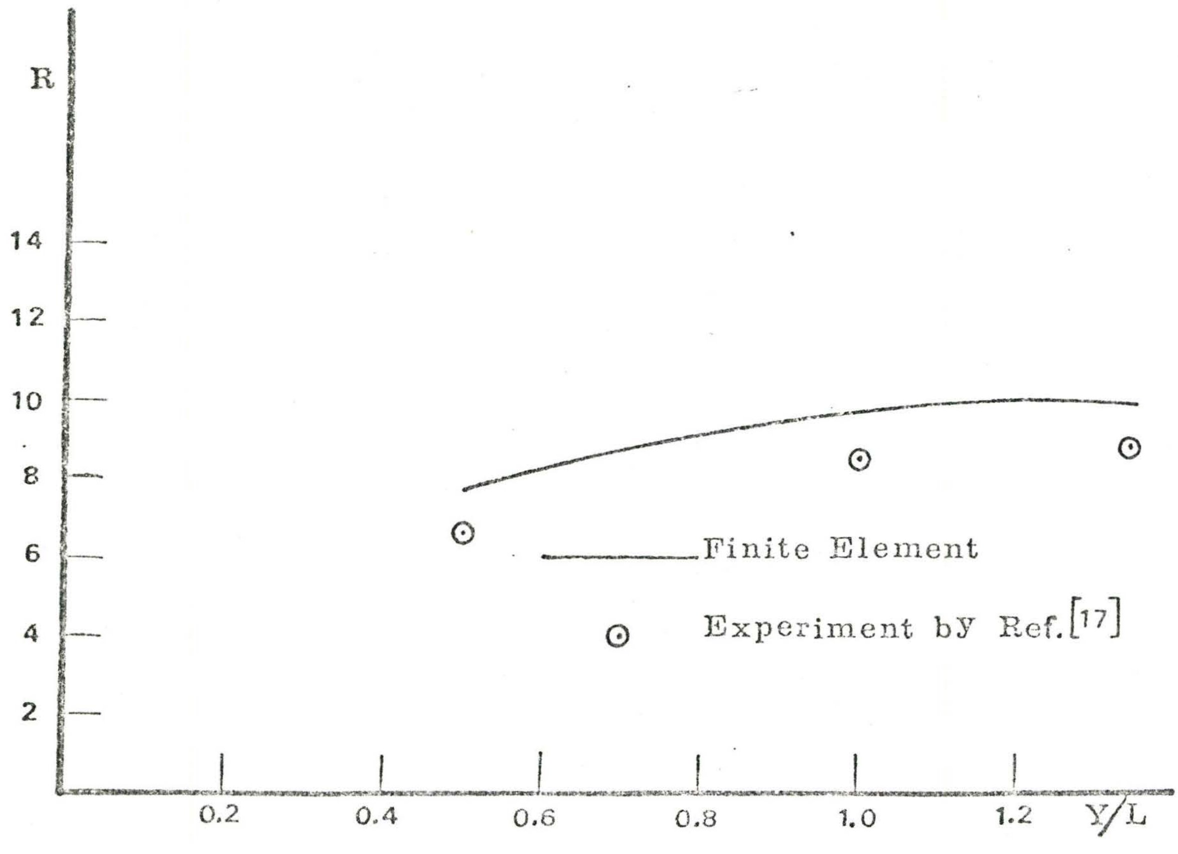

Figure (3.13) Theoretical and Experimental Results (Y/L vs. R.).

Table (3.3) Dimensions of Coupled Wall Configuration to Compare with Experimental Results given in Ref. [17].

ℓ ft.	w ft.	Y ft.	L ft.	ℓ/L	w/L	Y/L
6	3	6	12	.5	.25	.5
6	3	12	12	.5	.25	1
6	3	16.1	12	.5	.25	1.34

Table (3.4) Dimensions of Coupled Wall Configuration to Compare with the Finite Difference Results given in Ref. [17].

L ft.	32	32	32	32	32	32	32	32
Y ft.	8	8	8	8	8	8	8	8
ℓ ft.	1.6	3.2	6.4	9.6	12.8	16	19.2	22.4
w ft.	15.2	14.4	12.8	11.2	9.6	8	6.4	4.8
ℓ/L	.05	0.1	.2	.3	.4	.5	.6	.7
Y/L	.25	.25	.25	.25	.25	.25	.25	.25

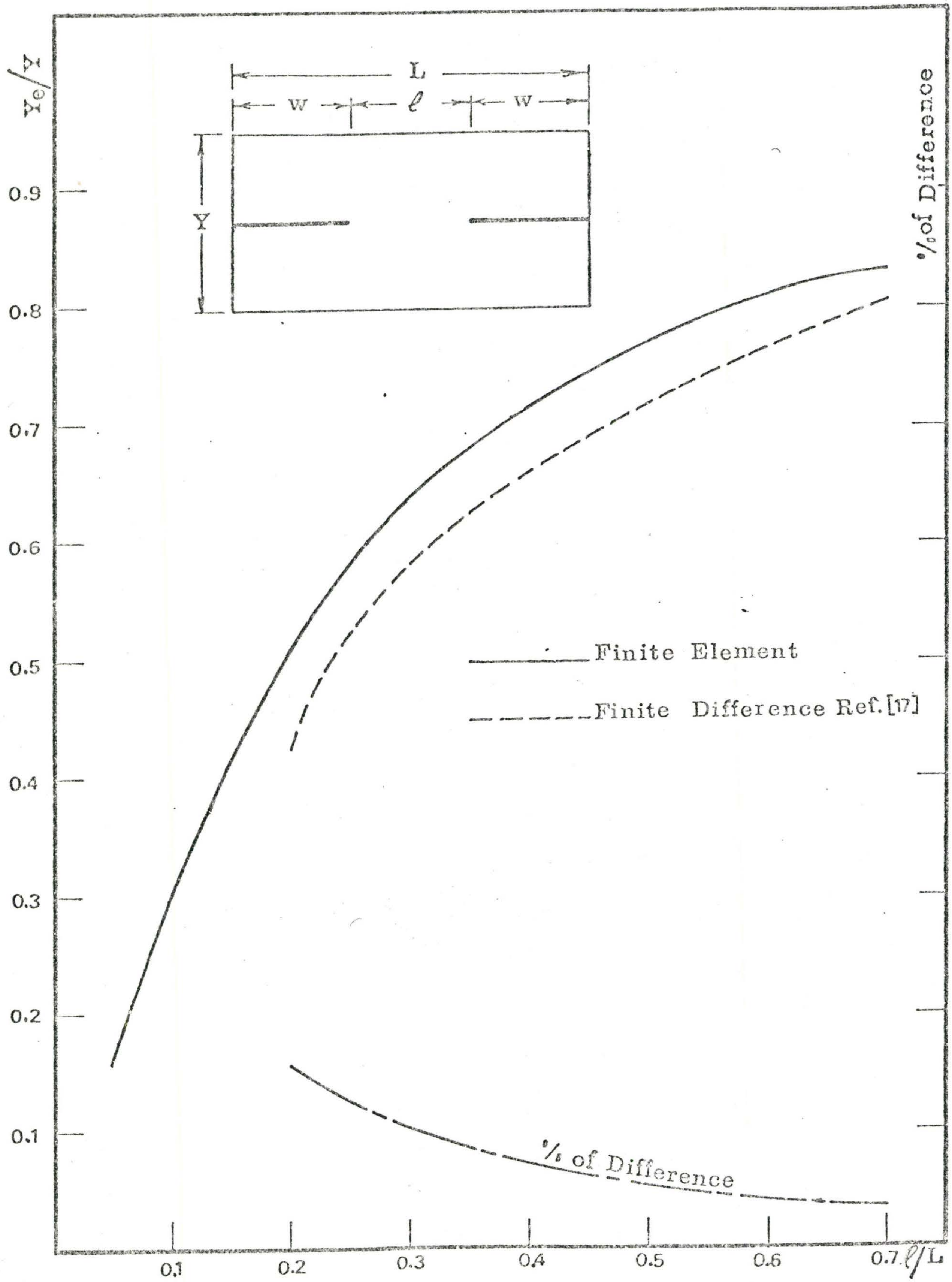

Figure (3.14) Comparison Between the Finite Element and Finite Difference Results (ℓ/L vs. Y_e/Y).

width of the slab. No theoretical investigation was presented in this paper. In the experiment the model consists of two steel walls coupled by a perspex sheet to act as a slab. We shall use these experimental values to provide a check on the proposed finite element scheme of computation.

For the planar wall configuration, four sets of slab sizes are considered. In the first two sets of the slabs, the ratio Y/L is taken as 0.3 and 0.5. The resulting finite element values together with the experimental values given in reference [9], are plotted in Figures (3.15), (3.17) and (3.18), for different values of ℓ/L. In the third set of slabs, the ratio w/Y is chosen as constant, while the ratios Y/L and ℓ/L are taken as variables. Table (3.5) shows the dimensions of these slabs. The lower graph in Figure (3.15) shows the finite element results and the experimental results given in reference [9] for the third set of slabs. Table (3.6) shows the dimensions for the fourth set of slabs in which w/Y is also taken as constant. Plotted in Figure (3.16) is the relationship between Y/L and Y_e/Y, for both the finite element results and the experimental results given in reference [9].

These figures show reasonable agreement between the experimental and the theoretical results, with an exception when the ratio of ℓ/L equals 0.2. This deviation may be due to the difficulty of accurate measurement when the opening between the walls becomes small.

A second comparison is made between the finite element results and the experimental work given in reference [9],

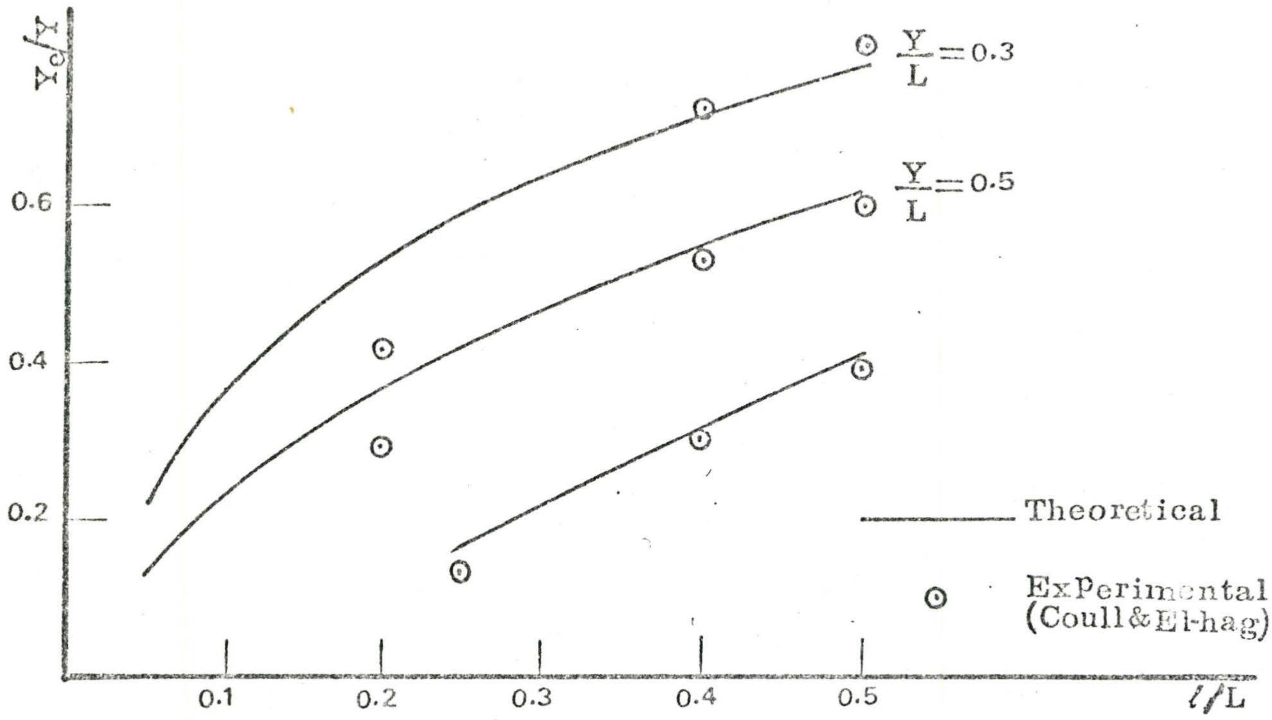

Figure (3.15) Comparison Between the Experimental and the Finite Element Results (ℓ/L vs. Y_e/Y).

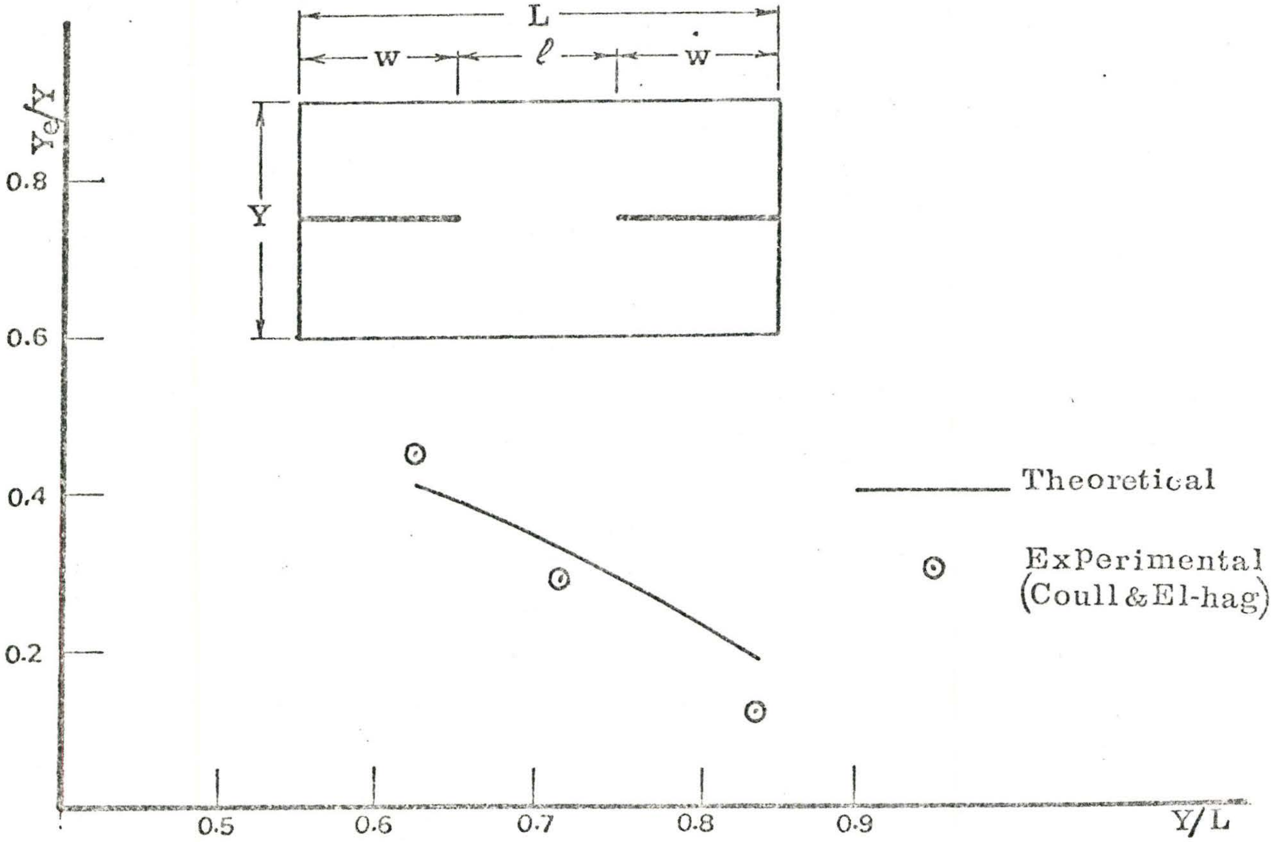

Figure (3.16) Comparison Between the Experimental and the Finite Element Results (Y/L vs. Y_e/Y).

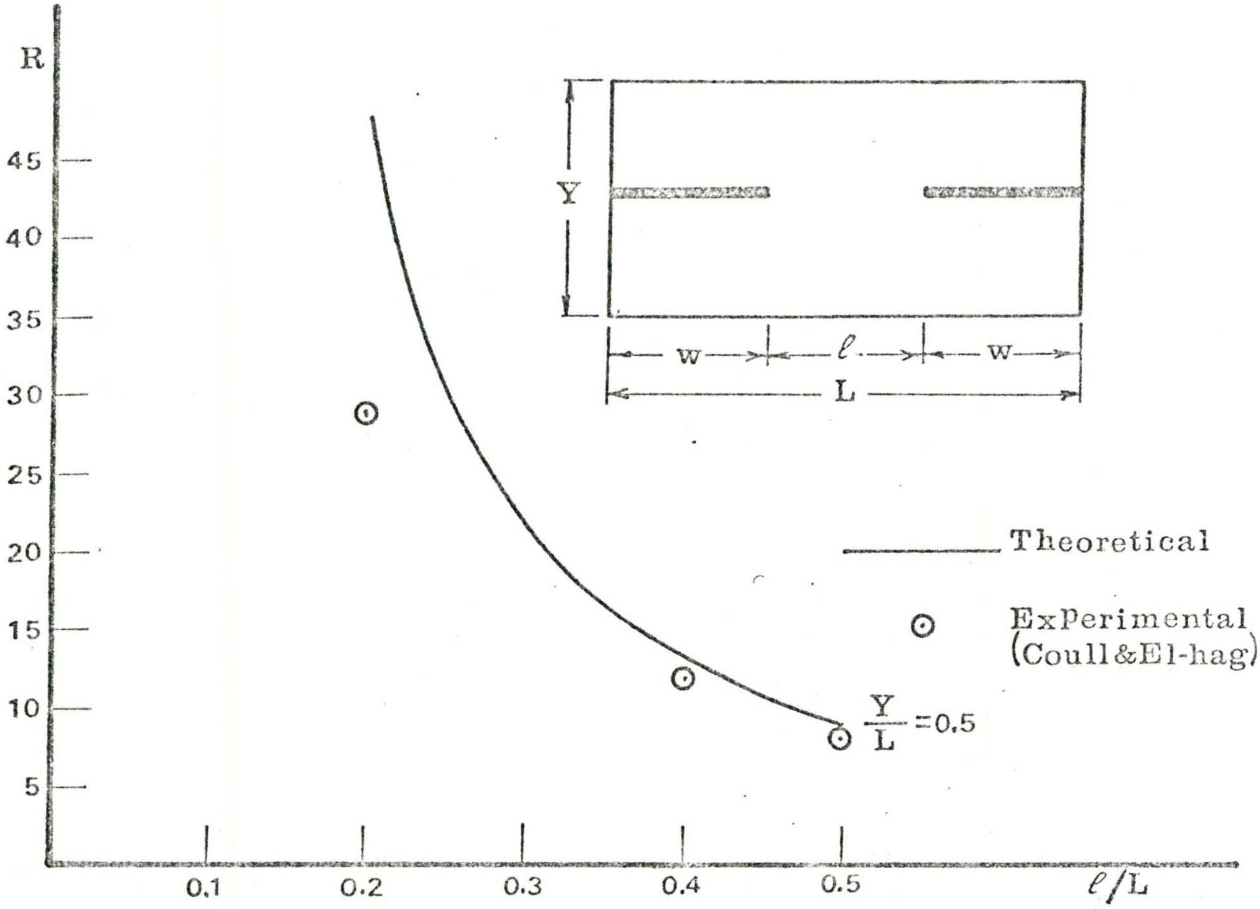

Figure (3.17) Comparison Between the Experimental and the Finite Element Results. (ℓ/L vs. R).

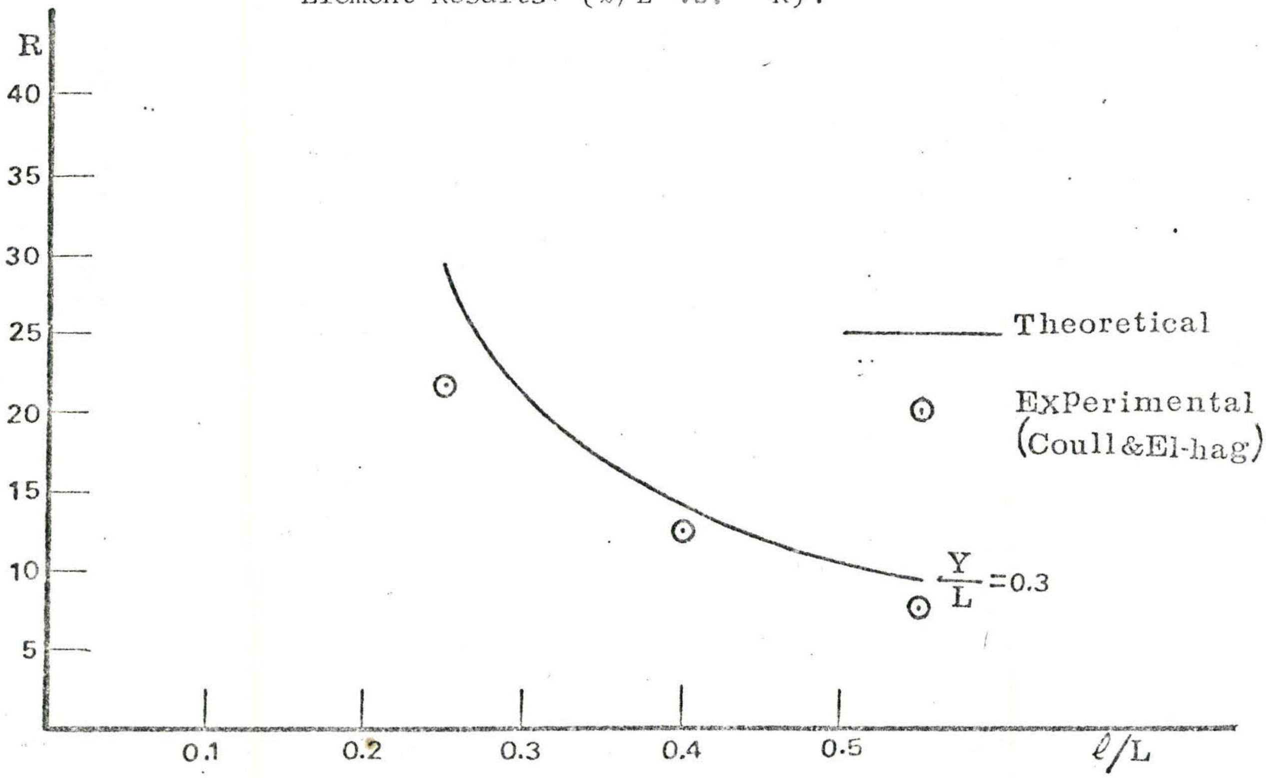

Figure (3.18) Comparison Between the Experimental and the Finite Element Results (ℓ/L vs. R).

for the slabs coupled box core walls. Table (3.7) shows the dimensions of the slabs under study. Plotted in Figure (3.19) is the relations between ℓ/L and Y_e/Y for Z/Y equals 0.3 and 0.5. This figure shows some deviation between the finite element results and the experimental results. This deviation may be due to possible local deformation of the core walls in the experimental set-up.

By comparing the results obtained by the finite element scheme with the experimental results given in reference [9], it is concluded that the computer program is operational. At the same time the method of analysis is sufficiently accurate to represent the coupling slab stiffness.

It should be noted that the theoretical and experimental curves, obtained by Qadeer and Smith [17] and Coull and El-hag [9], respectively, represent the relations between the wall openings and the slab stiffness, for moderate to large wall openings only. No data were given for small values of wall opening (ℓ/L = 0.1 say). In practice, the arrangement of shear walls in high-rise buildings is such that usually, the practical range of ℓ/L is between 0.1 to 0.2. In addition, the curves represented in the previous two references are computed assuming infinitesimal wall thickness. As will be shown later, such an assumption under estimates the stiffness of the slab.

For values of ℓ/L equals 0.2 , the experimental results given in reference [9] do not agree well with the theoretical results given by the finite element scheme.

Table (3.5) Dimensions of Coupled Wall Configuration to Compare with Experimental Results Given in Ref. [9].

ℓ	w	L	Y	ℓ/L	Y/L	w/Y
20	10	40	33.4	.5	.835	.3
16	12	40	40	.4	1	.3
10	15	40	50	.25	1.25	.3

Table (3.6) Dimensions of Coupled Wall Configuration to Compare with Experimental Results Given in Ref. [9].

ℓ	w	L	Y	ℓ/L	Y/L	w/Y
6.55	16.75	40	33.5	.1635	.836	.5
11.5	14.25	40	28.5	.2865	.713	.5
15	12.5	40	25	.375	.625	.5

Table (3.7) Dimensions of Coupled Wall Configuration to Compare with Experimental Results Given in Ref. [19].

W/Y	Z/Y	w	Z	ℓ/L	L	ℓ
.3	.3	3.6	3.6	.25	9.6	2.4
				.4	12	4.8
				.5	14.4	7.2
.5	.5	6	6	.25	16	4
				.4	20	8
				.5	24	12

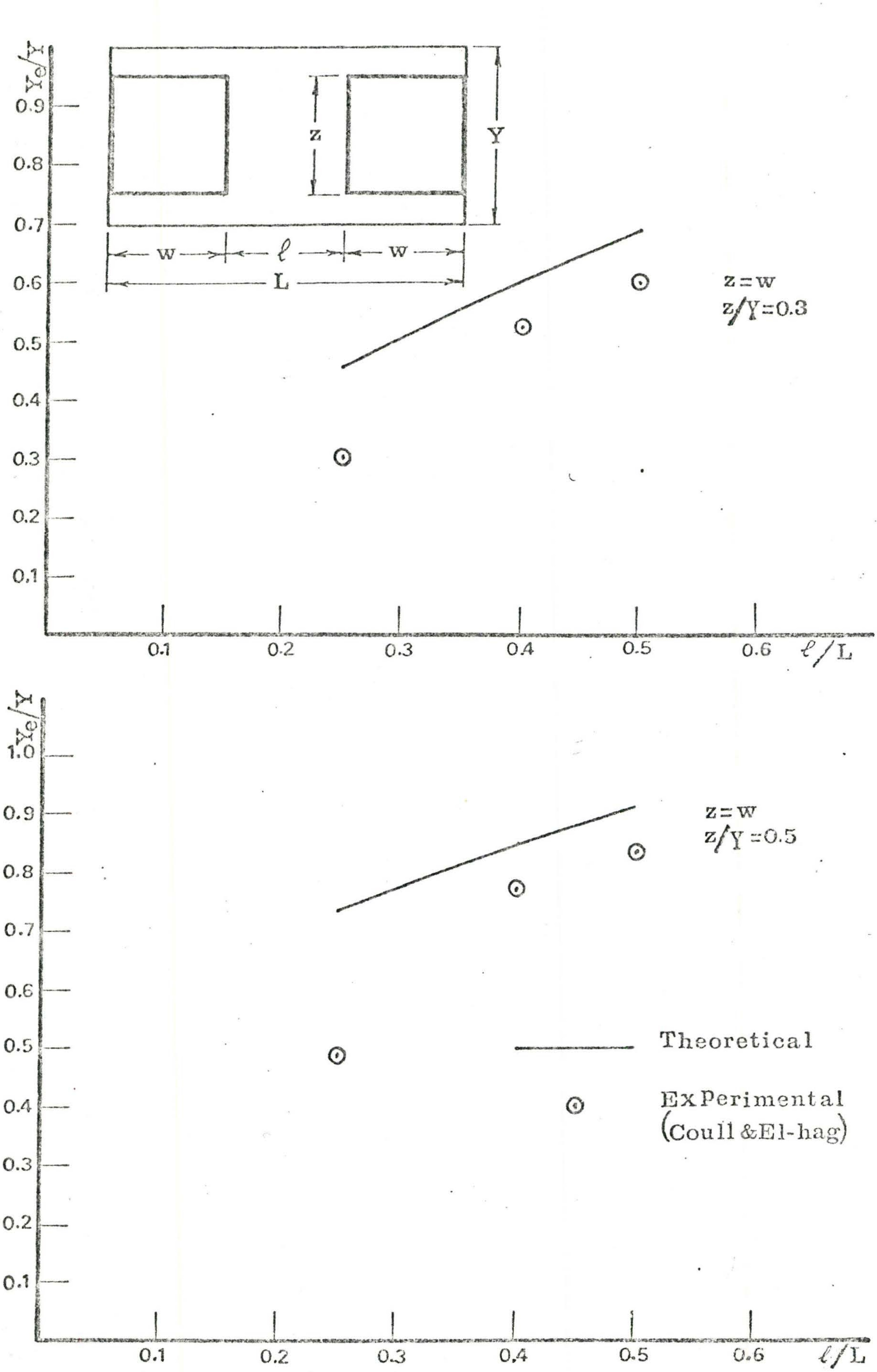

Figure (3.19) Comparison Between the Theoretical and Experimental Results for Slab Coupled Box Core Wall (ℓ/L vs. Y_e/Y).

Since we are interested particularly in small wall openings, it was decided that an experiment would be carried out to obtain data for small wall opening coupled wall configurations. Such experimental work will be described in the next chapter.

CHAPTER 4

EXPERIMENTAL WORK

4.1 General

As discussed in Chapter 3, the critical range of wall opening is where ℓ/L less than 0.2. However, there appears relatively little information on the stiffness of the coupled wall system in this range. Some experimental work has been carried out by Coull and El-hag [9]. Comparison between their experimental results with the finite element computation results shows good agreement for values of ℓ/L greater than 0.25. For smaller values of ℓ/L, some difference exists between the theoretical and experimental values. Therefore, an experiment is carried out to study the stiffness of the slab coupled planar walls. Such experimental investigation will complement the theoretical studies presented, particularly in the range of small wall openings.

4.2 Mathematical Representation for the Experimental Model

When a coupled shear wall is subjected to lateral forces, its deflected shape will be as shown in Figure (3.2). The effective stiffness of floor slab will be defined by the relationship between the relative vertical displacement Δ (Figure (3.3)) and the forces producing it. If the two walls are similar, each wall will move $\Delta/2$, and the line of contraflexure of the slab will be at the mid-span between the walls. Therefore, one can study the behaviour of coupled shear walls by making use of this anti-symmetrical property. In other words, one can use one shear wall connected to a slab and use a roller support to simulate the line of contraflexure condition at the mid-line of the connecting slab.

Figure (4.1) shows the suggested structural system that simulates the behaviour of the coupled shear walls as described by Qadeer and Smith [17], while Figure (4.2) shows the actual model that has been used in the present study. From Figure (4.1), the relative displacement Δ and the rotation ϕ can be expressed as

$$\frac{\Delta}{2} = \frac{M}{EI} \cdot \frac{\ell^3}{12(\ell+w)} \tag{4.1}$$

$$\phi = \frac{\Delta}{\ell+w} \tag{4.2}$$

Therefore,

$$\frac{M}{\phi} = \frac{6\ EI(\ell+w)^2}{\ell^2} \tag{4.3}$$

The nondimensional rotational stiffness R is

$$R = \frac{M}{D\phi} \tag{4.4}$$

and the moment of inertia of the equivalent beam is

$$I = \frac{Y_e \cdot t^3}{12} \tag{4.5}$$

From Equations (4.3), (4.4) and (4.5), we get

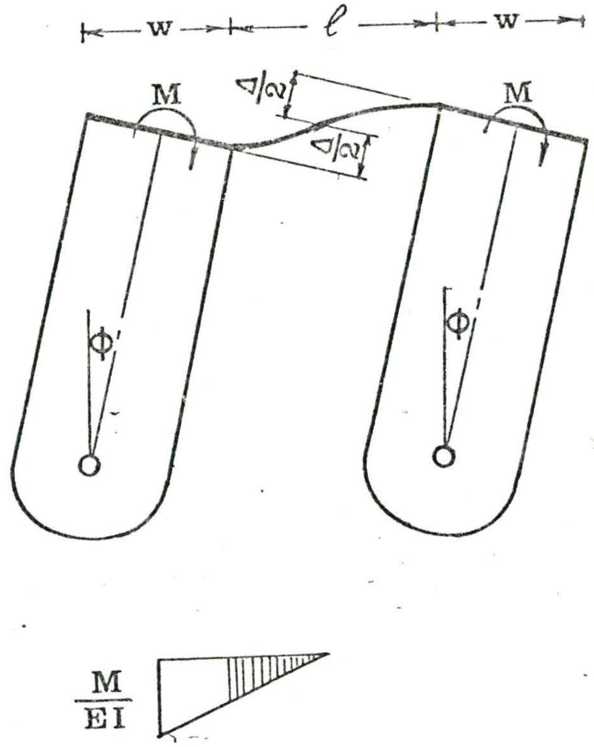

Figure (4.1) Simulation of the Behaviour of the Slab Under Lateral Loading.

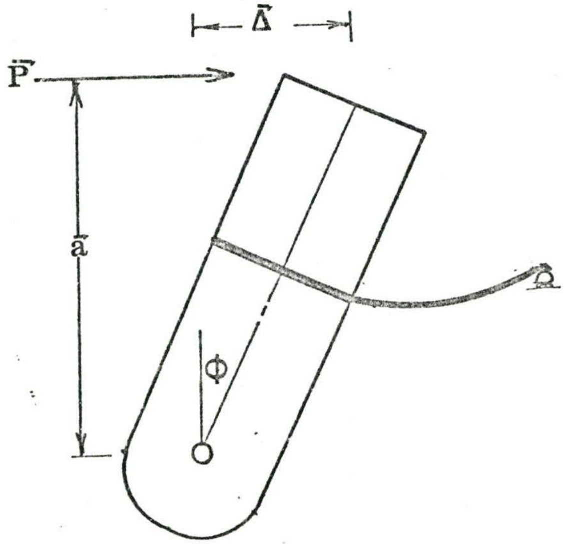

Figure (4.2) Half of the Slab with Roller Support at the Line of Contraflexure.

$$Y_e = R \cdot \frac{\ell^3}{6(\ell+w)^2(1-\nu^2)} \tag{4.6}$$

The ratio Y_e/Y, becomes

$$\frac{Y_e}{Y} = \frac{R}{6(1-\nu^2)} \cdot \frac{1}{(Y/\ell)(1+w/\ell)^2} \tag{4.7}$$

In the experimental investigation shown in Figure (4.2),

$$\phi \simeq \frac{\bar{\Delta}}{\bar{a}} \tag{4.8}$$

$$M = \bar{P} \cdot \bar{a} \tag{4.9}$$

where

$\bar{P}$ represents the lateral load applied to the wall at distance $\bar{a}$ from the supporting point.

$\bar{\Delta}$ represents the horizontal displacement of the wall due to the load $\bar{P}$.

ϕ is the angle of rotation of the wall.

Substituting Equations (4.8) and (4.9) into Equation (4.4) yields

$$R = \frac{12\,\bar{a}^2(1-\nu^2)}{E\,t^3} \cdot \frac{\bar{P}}{\bar{\Delta}} \tag{4.10}$$

Equation (4.7), becomes

$$\frac{Y_e}{Y} = \frac{2\,\bar{a}^2}{E\,t^3} \cdot \frac{1}{(Y/\ell)(1+w/\ell)^2} \cdot \frac{\bar{P}}{\bar{\Delta}} \tag{4.11}$$

The values of $\overline{P}/\overline{\Delta}$ will be obtained experimentally for different slab lengths, from which the values of Y_e/Y and R can be obtained.

4.3 Description of the Model

Figure (4.3) shows the experimental set-up used in the tests. The model consists of:

i One planar steel wall of dimensions 20" x 6" x 3/8".

ii A steel slab of dimensions 36" x 12" x 1/4". The stress-strain relationship for the steel of the slab is shown in Figure (4.4).

iii A heavy steel frame with a 3/4 inch diameter shaft at the top is used as a roller support, as shown in Figure (4.5).

iv A heavy steel block fixed to the floor to act as a rigid foundation for the shear wall, as shown in Figure (4.5).

v Four dial gauges with accuracy $\frac{1}{1000}$ of an inch for measuring the deflections of the wall, the steel frame and the foundation block. Their locations are shown in Figure (4.5).

The behaviour of the coupled shear walls can be simulated by allowing the wall to rotate in its plane. The wall is pivoted freely on ball bearings carried on a 3/4 inch diameter steel rod. The steel rod is supported on another two bearings fixed in the side of a heavy steel angle, as

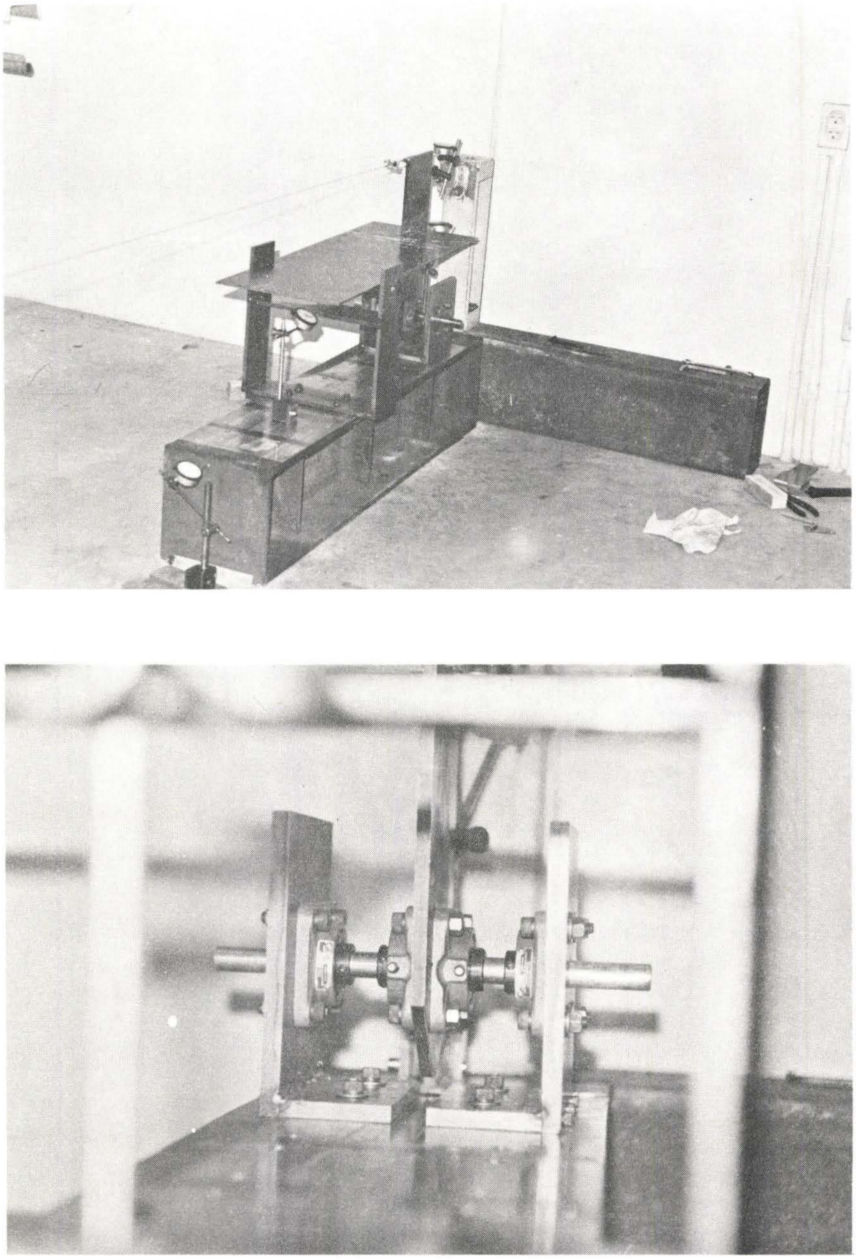

Figure (4.3)

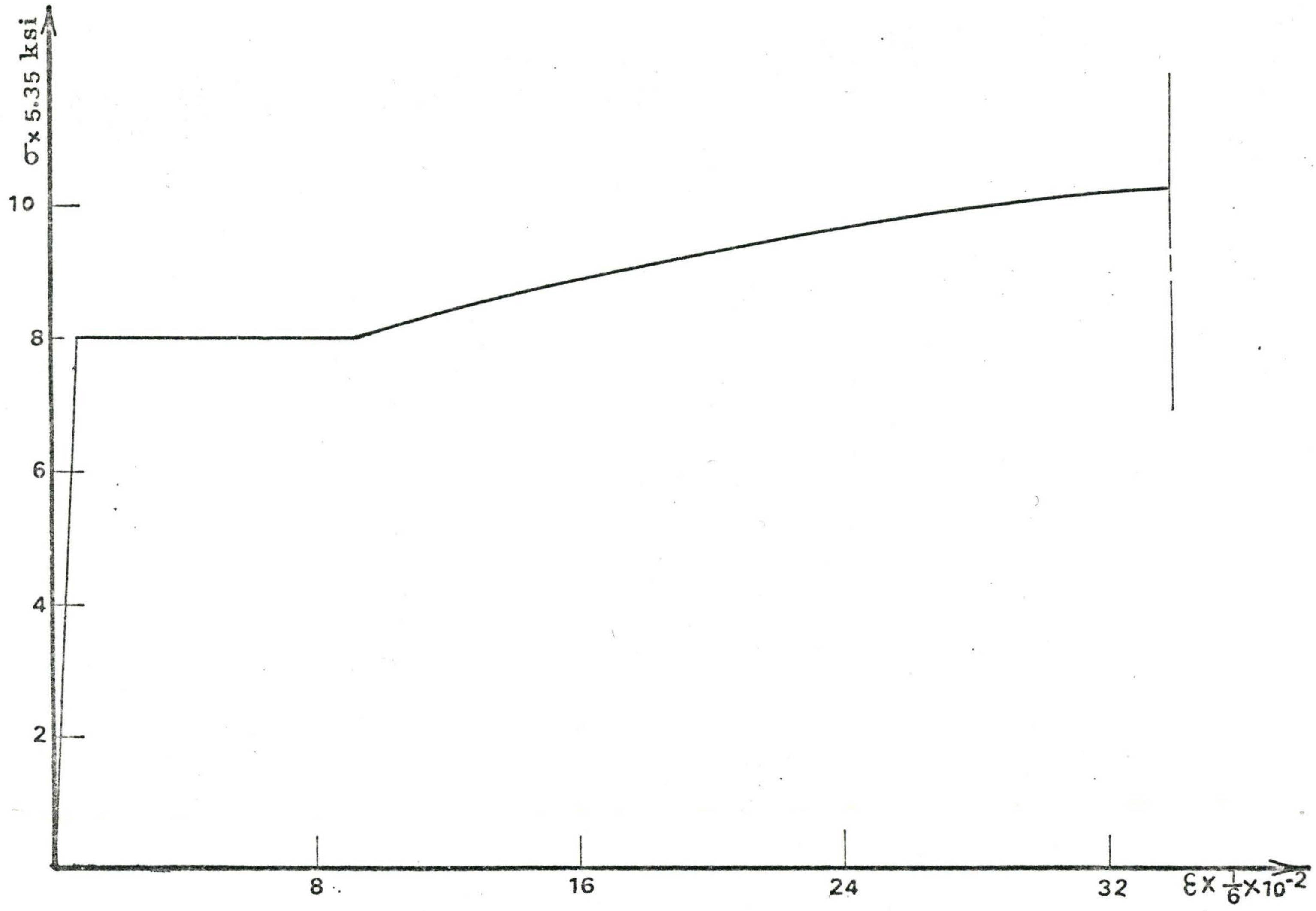

Figure (4.4) Stress-Strain Relationship of the Steel of the Slab.

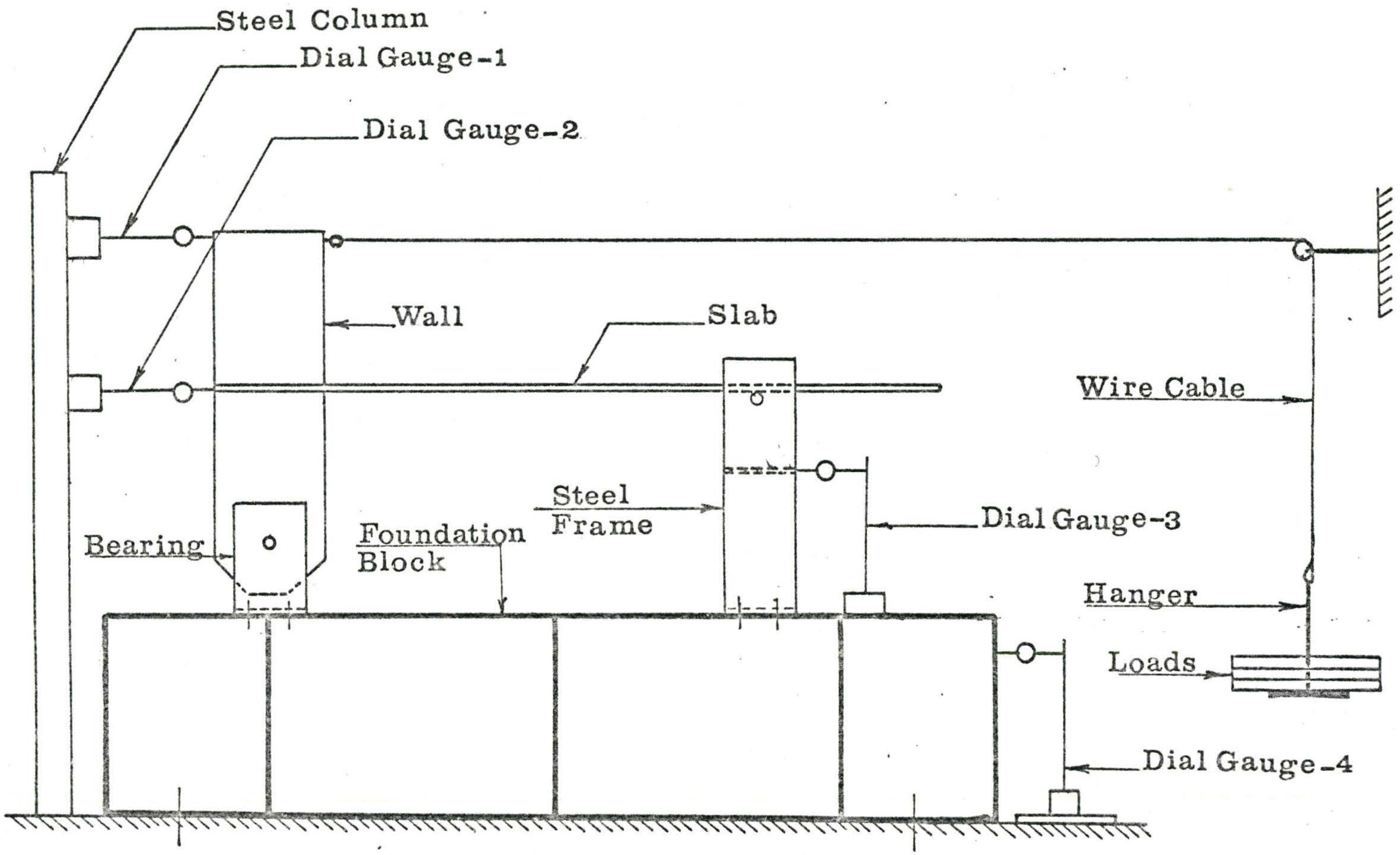

Figure (4.5) Elevation for the Model with the Positions of Dial Gauges.

shown in Figure (4.6). The slab is welded to the wall, and the excess weld is machined off. The distance ℓ between the two walls can be adjusted by moving the roller support. The roller support is lubricated to allow the free movement of the slab with a minimum of friction. The shear wall is loaded horizontally through a wire cable connected at the top of the wall and passes horizontally through a smooth pulley system. At the end of the cable, there is a hanger where the loads can be added. Two dial gauges are used to measure the deflections at the top and the mid-height of the wall respectively. The other two dial gauges are used to measure the movement of the foundation block and the roller support steel frame to ensure their movements are negligible.

4.4 Test Procedure

Since the stiffness of the steel wall is very much larger than the stiffness of the thin slab, it may be assumed that the deformation of the former is negligible compared to the latter. Therefore, the measured deflection of the wall can be considered due to the deformation of the slab only. Seven values of wall openings are considered. The different values of the wall opening ℓ and the total spacing L are shown in Table (4.1). For each wall opening, the load is increased from zero to a maximum and the lateral deflections of the wall are recorded two minutes after each application of the load. At the same time, the movements of the roller support steel frame and the foundation block are

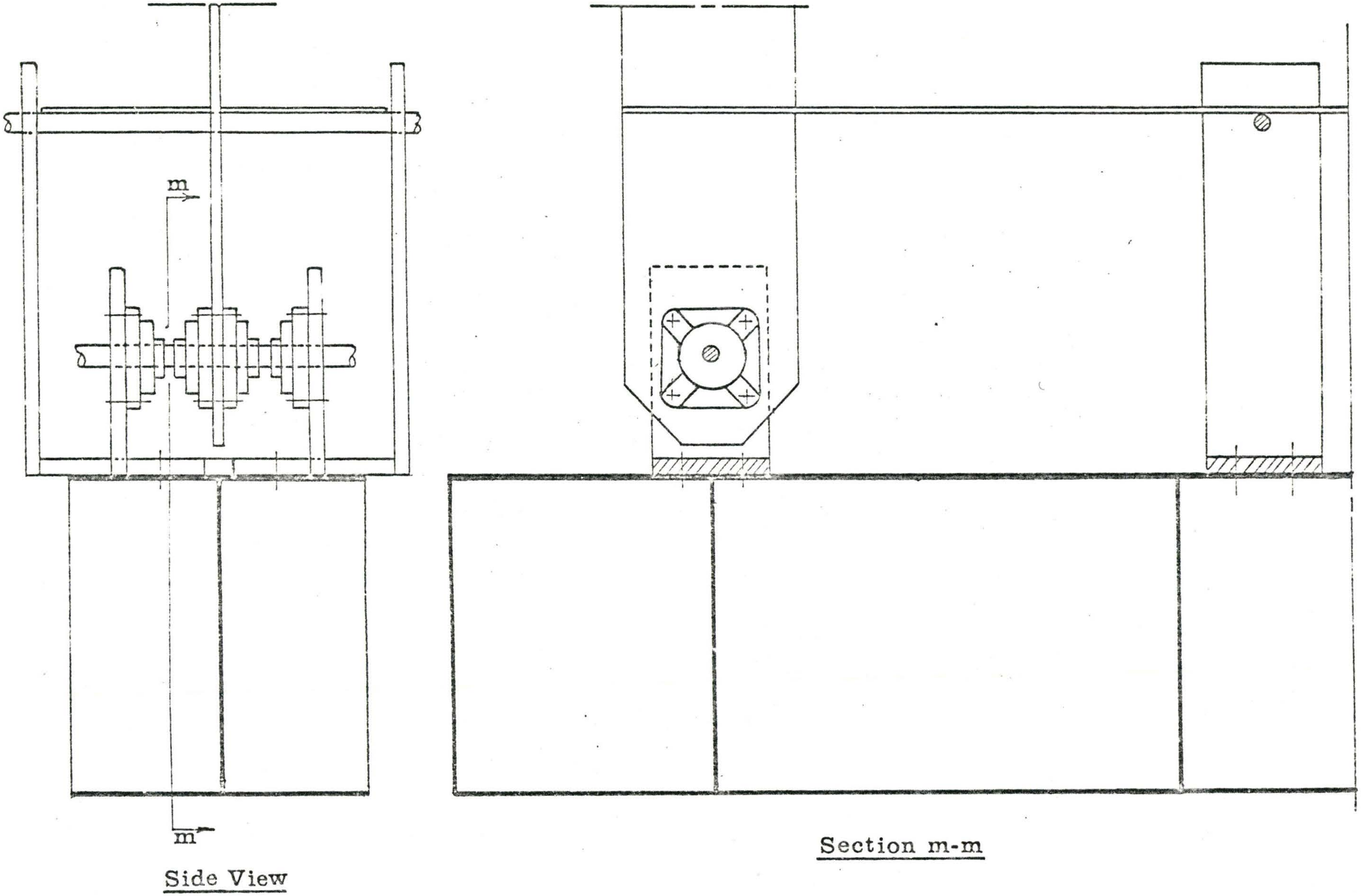

Figure (4.6) Connection Between the Wall and the Bearings.

Table (4.1) Wall Spacing for the Different Slabs.

Slab Configuration	ℓ in.	L in.	ℓ/L	Y/L
1	58	70	.83	.172
2	44.5	56.5	.79	.212
3	35	47	.745	.255
4	20	32	.625	.375
5	8	20	.4	.6
6	3.75	15.75	.24	.765
7	2	14	.143	.855

also recorded. For each wall opening, the experiment is carried out five times and the recorded values are the average over five readings. The load increments, the total loads, the corresponding average incremental lateral deflections and the total deflections are tabulated in Appendix C.

4.5 Results and Discussion

The recorded values for the movement of the roller support steel frame show negligible movement for this support. Also, the foundation steel block registers no movement. Figures (4.7) through (4.13) show the relationship between $\overline{P}$ and $\overline{\Delta}$ for the seven wall spacings tested as measured by both dial gauges on the wall. The values of $\overline{P}/\overline{\Delta}$ are obtained and the nondimensional rotational stiffness R and the normalized effective width of the slab Y_e/Y are calculated. The values of $\overline{a}$, E, ν, t, Y, w, used are as follows:

$$\overline{a} = 16.75''$$

$$t = 0.25''$$

$$w = 6''$$

$$\nu = 0.3$$

$$E = 3 \times 10^7 \text{ Ib/in}^2$$

Substituting into Equations (4.10) and (4.11) yields

$$R = 0.65 \times 10^{-2} \left(\frac{\overline{P}}{\Delta}\right)_{top} \tag{4.12}$$

or

$$R = 0.325 \times 10^{-2} \left(\frac{\overline{P}}{\overline{\Delta}}\right)_{mid} \tag{4.13}$$

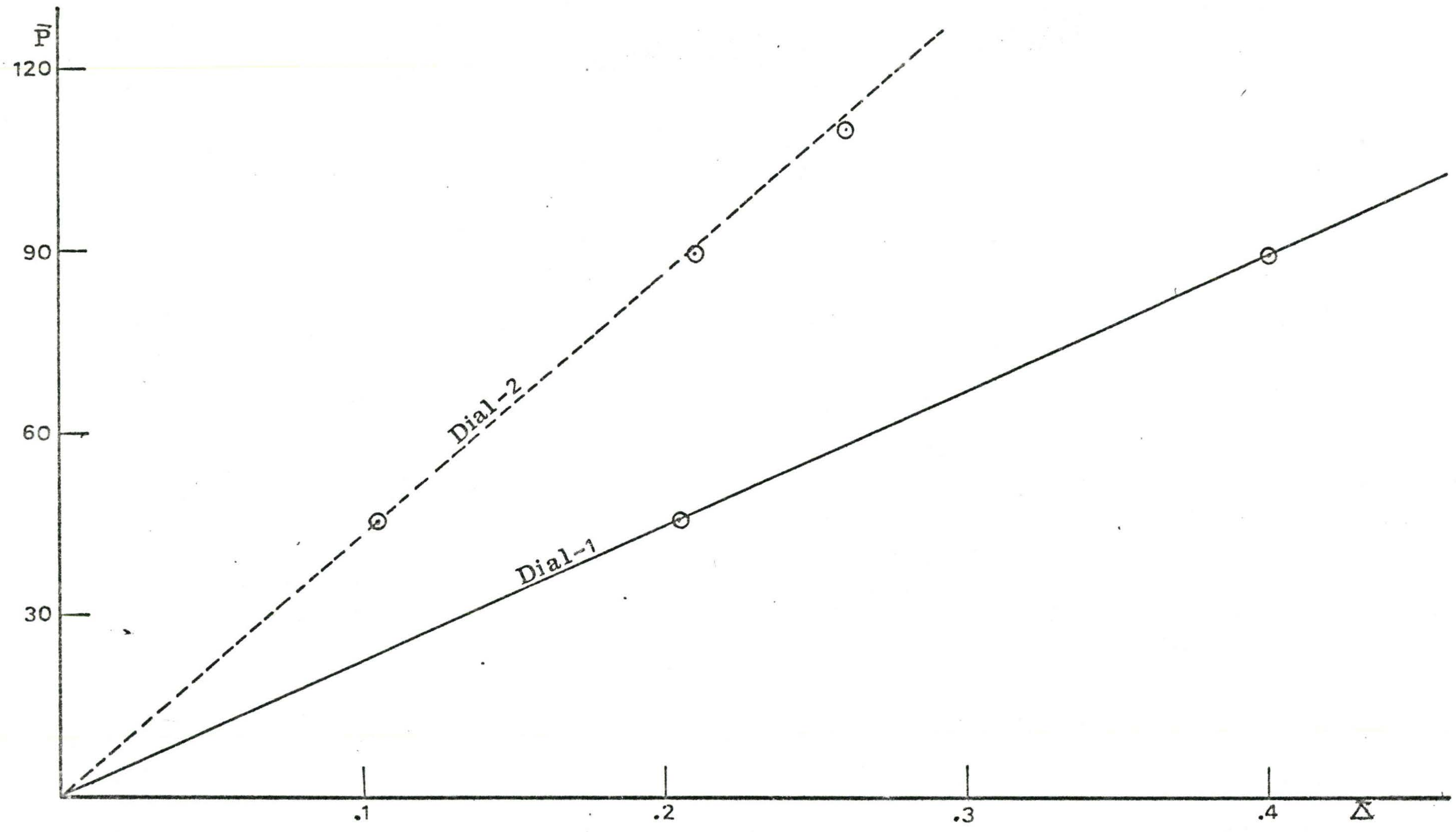

Figure (4.7) Slab Configuration 1.

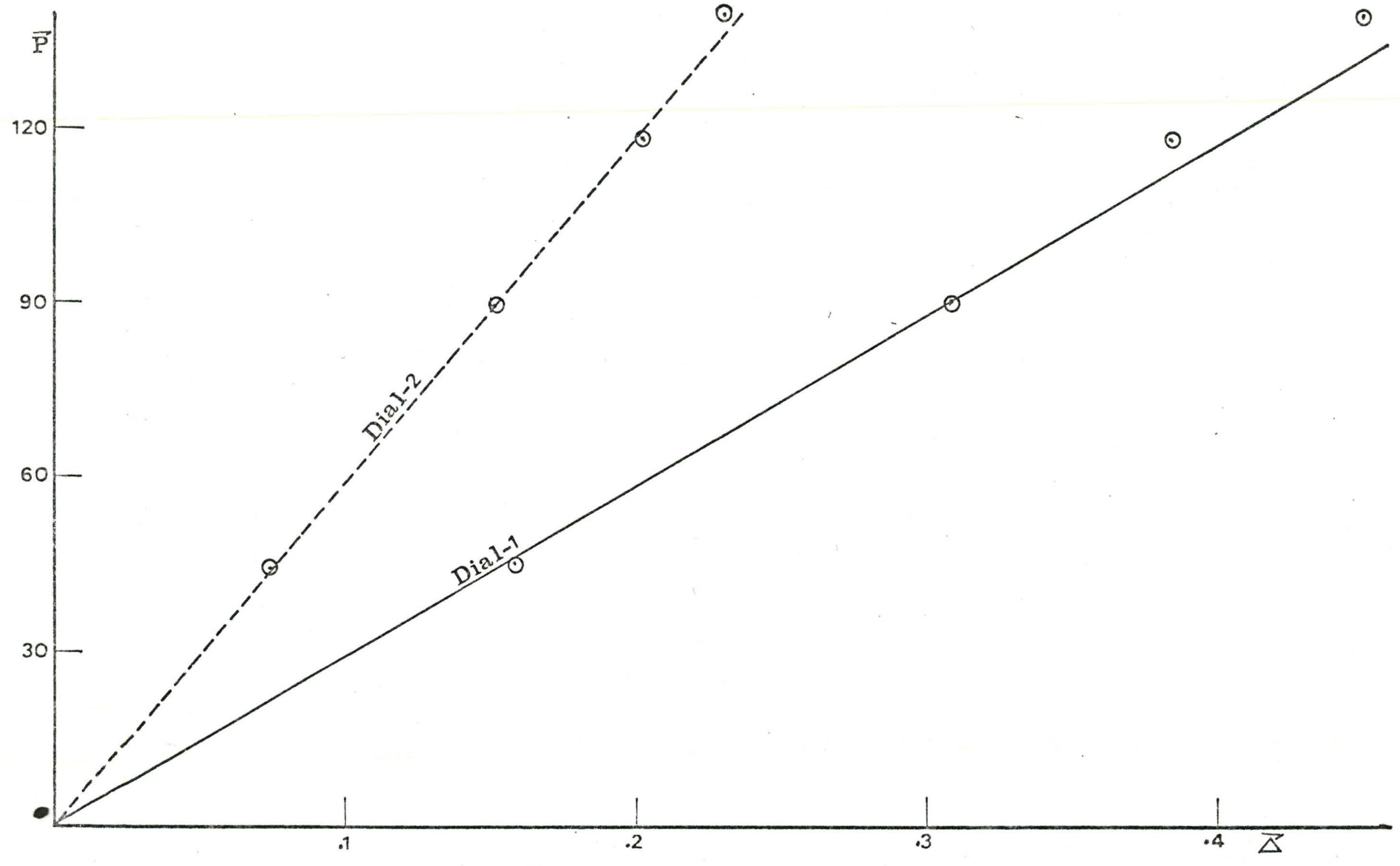

Figure (4.8) Slab Configuration 2.

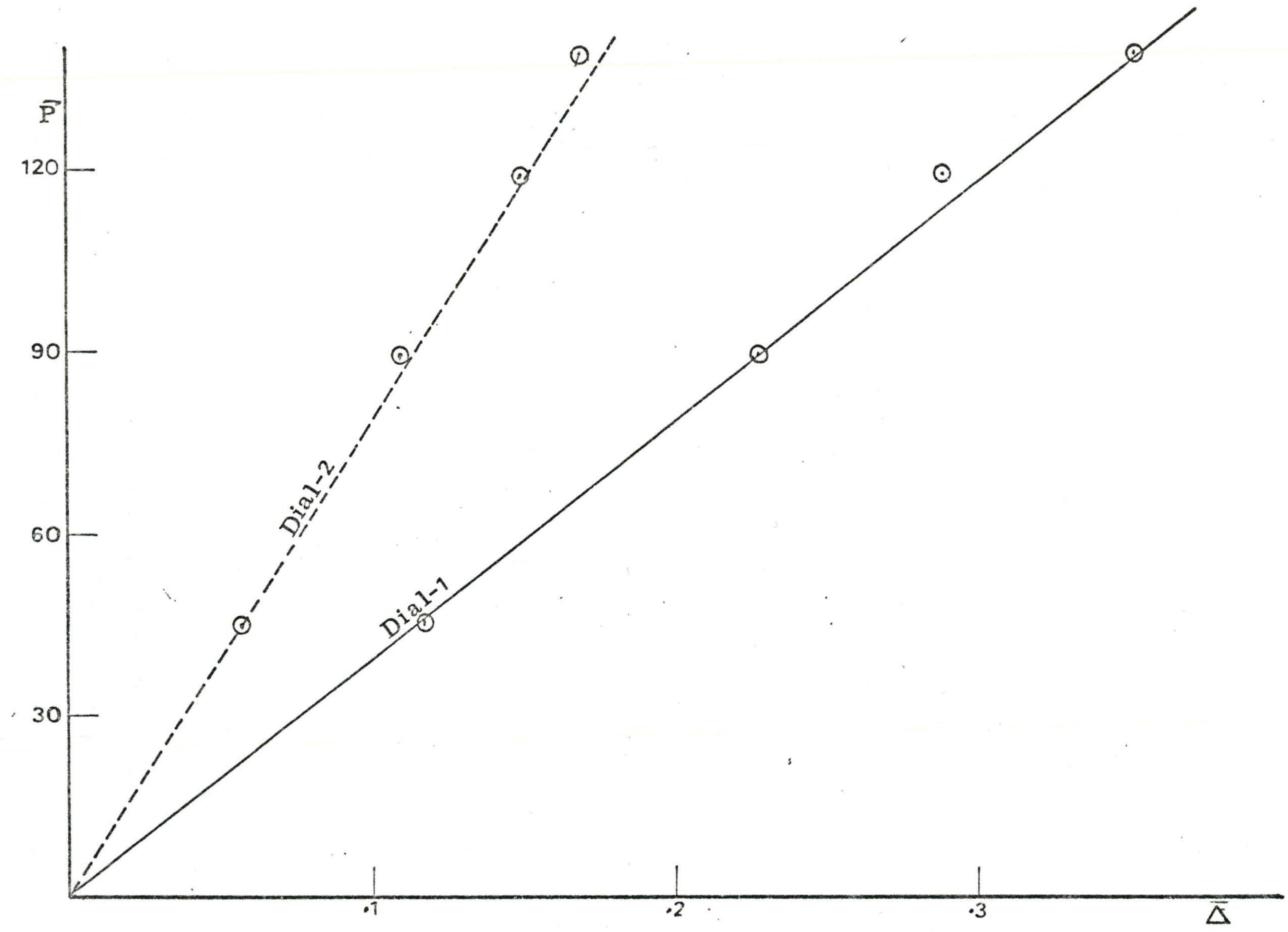

Figure (4.9) Slab Configuration 3.

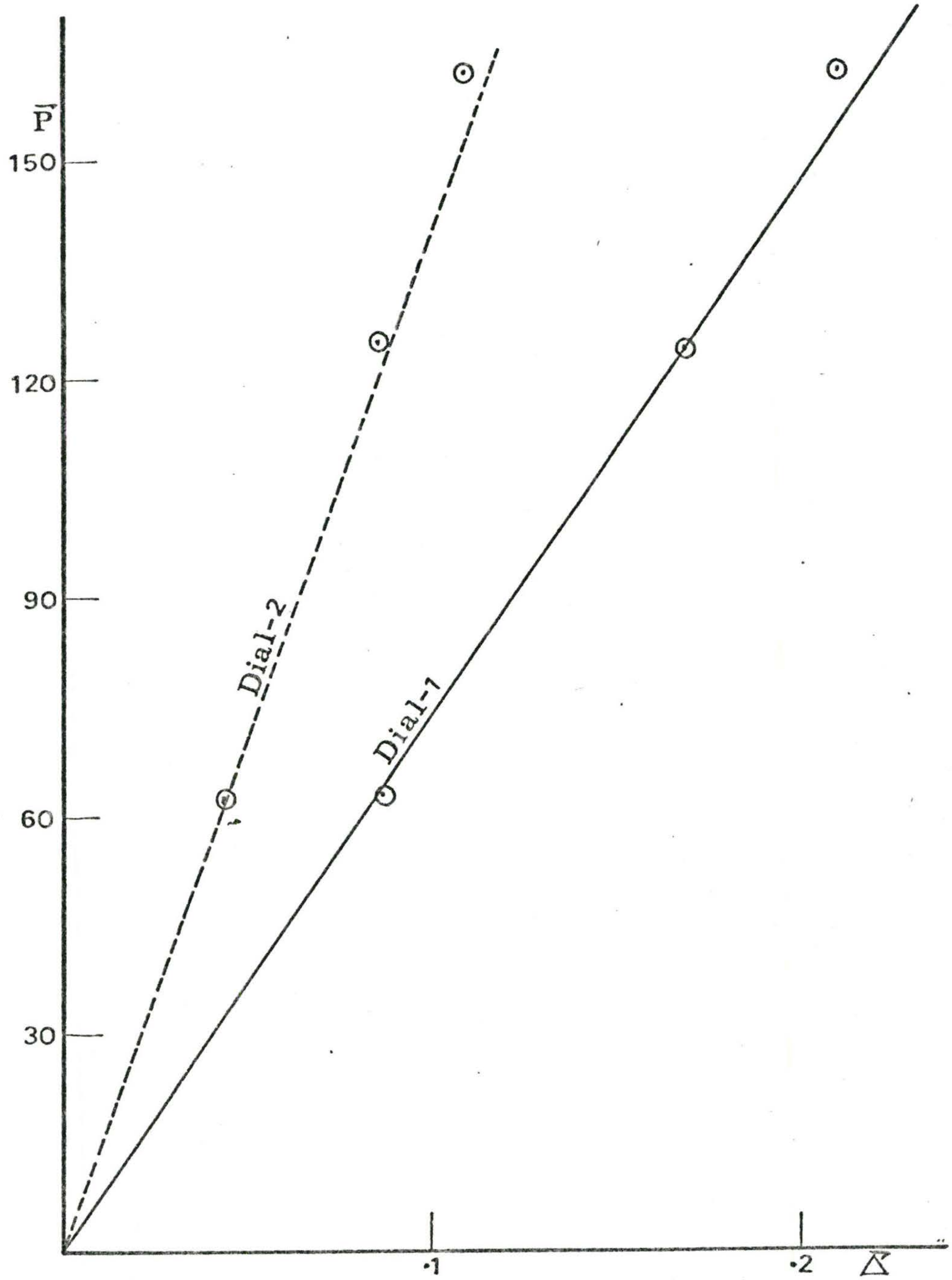

Figure (4.10) Slab Configuration 4.

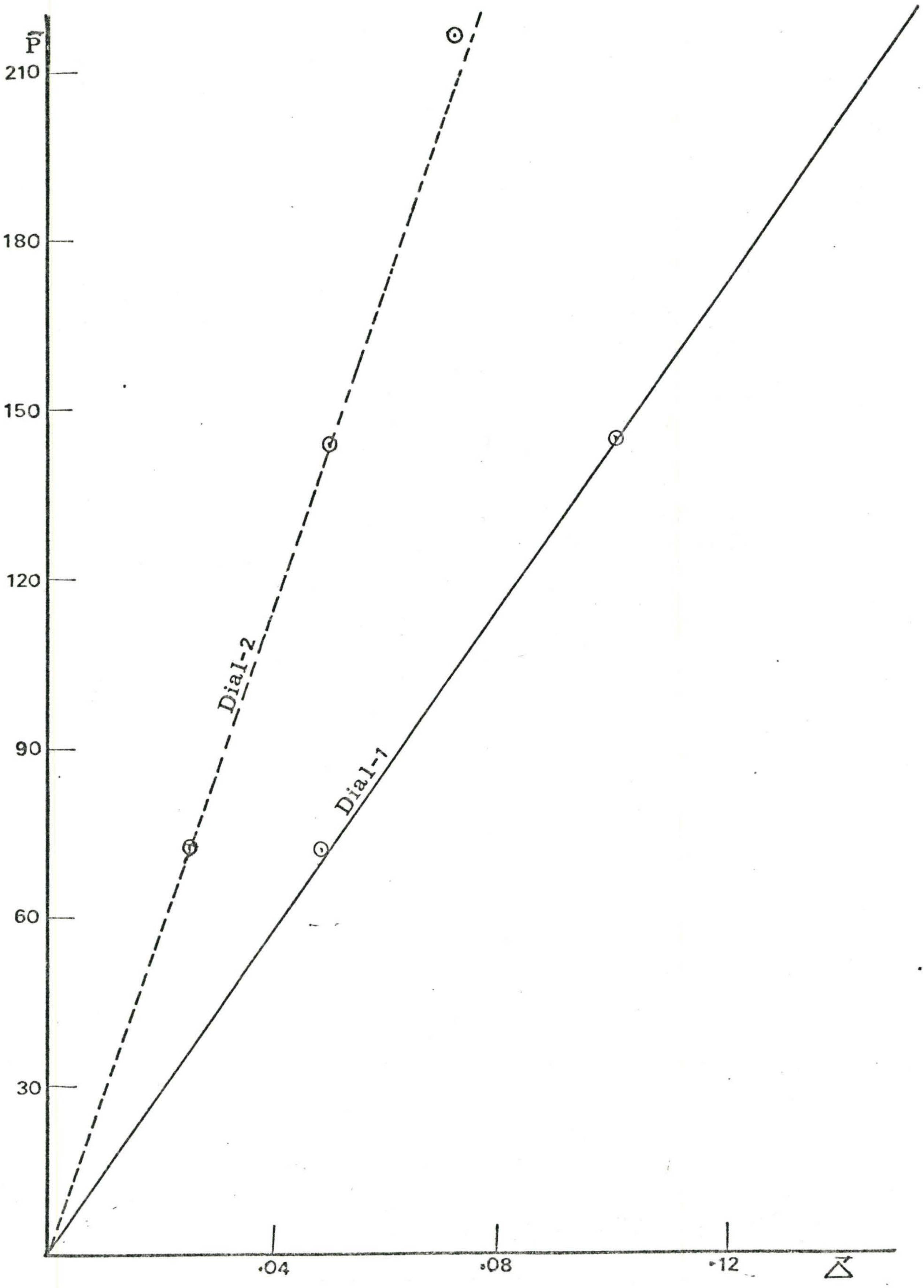

Figure (4.11) Slab Configuration 5.

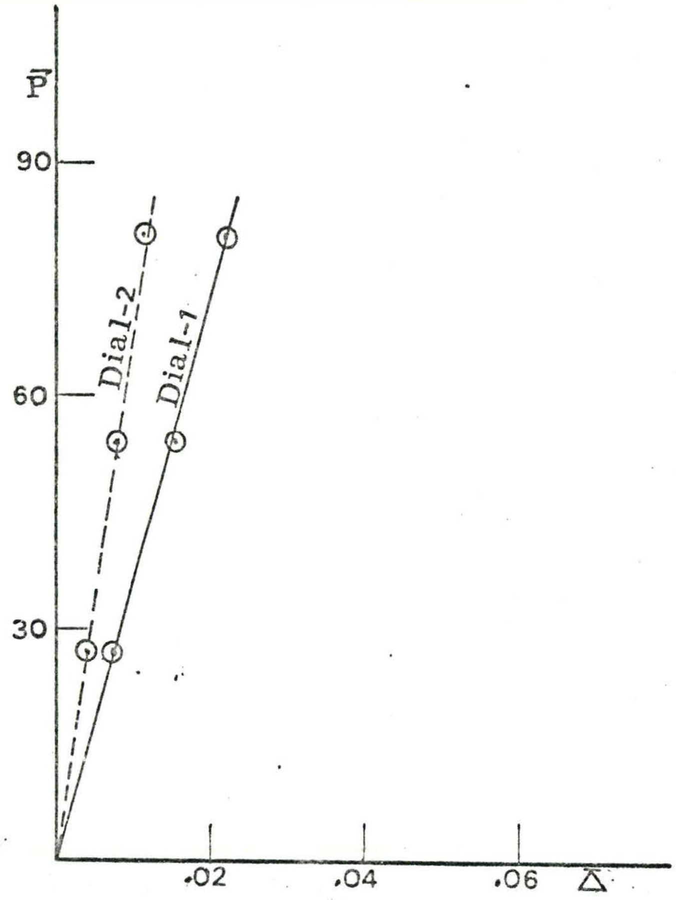

Figure (4.12) Slab Configuration 6.

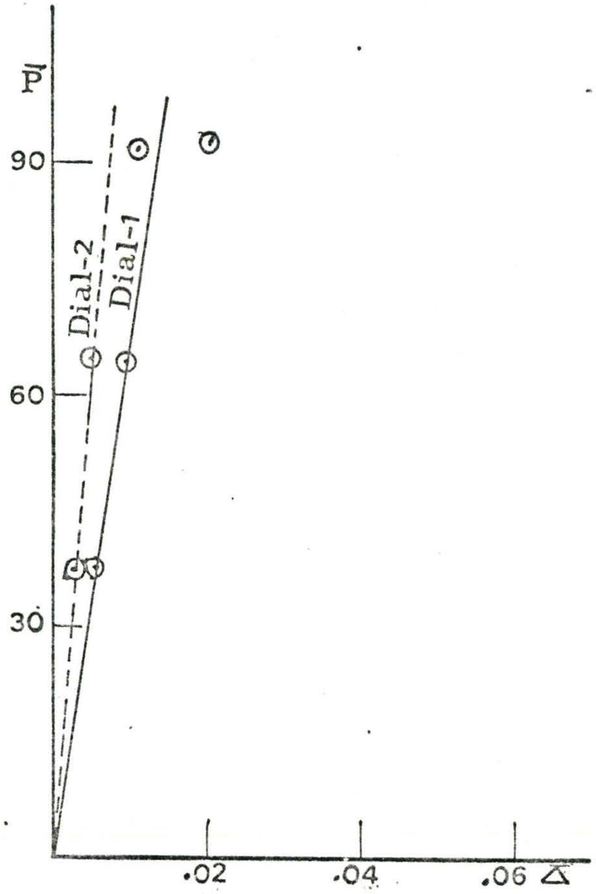

Figure (4.13) Slab Configuration 7.

and

$$\frac{Y_e}{Y} = 0.12 \times 10^{-2} \times \frac{1}{(Y/\ell)(1+ w/\ell)^2} \times (\frac{\bar{P}}{\bar{\Delta}})_{top} \qquad (4.14)$$

or

$$\frac{Y_e}{Y} = 0.06 \times 10^{-2} \times \frac{1}{(Y/\ell)(1+w/\ell)^2} (\frac{\bar{P}}{\bar{\Delta}})_{mid} \qquad (4.15)$$

Table (4.2) shows both the nondimensional rotational stiffness and the effective width of the slab for different wall openings, calculated for $\bar{P}/\bar{\Delta}$ measured at the top and at the mid-height of the wall.

A theoretical computation is carried out for the seven cases to obtain the effective width of the slab and its rotational stiffness. The theoretical results and the average of the two calculated experimental results are plotted in Figures (4.14) and (4.15) for the effective widths and the rotational stiffnesses, respectively.

The $\bar{P}$-$\bar{\Delta}$ curves provide a check on the linearity of the experimental set up. As shown in Figures (4.14) and (4.15), acceptable agreement is found between the experimental and the theoretical results. For ℓ/L equals 0.14, there is some difference in the value of the stiffness of the slab between the experimental and the theoretical results. At such small openings, the system becomes very stiff, resulting in a very small displacement for the loads applied. The inherent inaccuracy in displacement measurements will then have its biggest impact to cause the disagreement between the experimental and the theoretical results.

Table (4.2) Values of R and Y_e/Y for Different Wall Openings

Slab Configuration	Y/ℓ	w/ℓ	$(1+w/\ell)^2$	$(\frac{\bar{P}}{\Delta})_{top}$	$(\frac{\bar{P}}{\Delta})_{mid}$	$(\frac{Y_e}{Y})_{top}$	$(R)_{top}$	$(\frac{Y_e}{Y})_{mid}$	$(R)_{mid}$
1	0.21	0.105	1.23	220	430	1.02	1.43	0.995	1.4
2	0.27	0.135	1.285	282	582	0.96	1.83	0.99	1.9
3	0.344	0.172	1.375	387	770	0.965	2.52	0.96	2.5
4	0.6	0.3	1.69	730	1370	0.86	4.75	0.81	4.45
5	1.5	0.75	3.05	1470	2880	0.387	9.55	0.38	9.35
6	3.2	1.6	6.75	3800	7100	0.21	24.7	0.2	23
7	6	3.0	16	6650	12700	0.0835	43.4	0.08	41.5

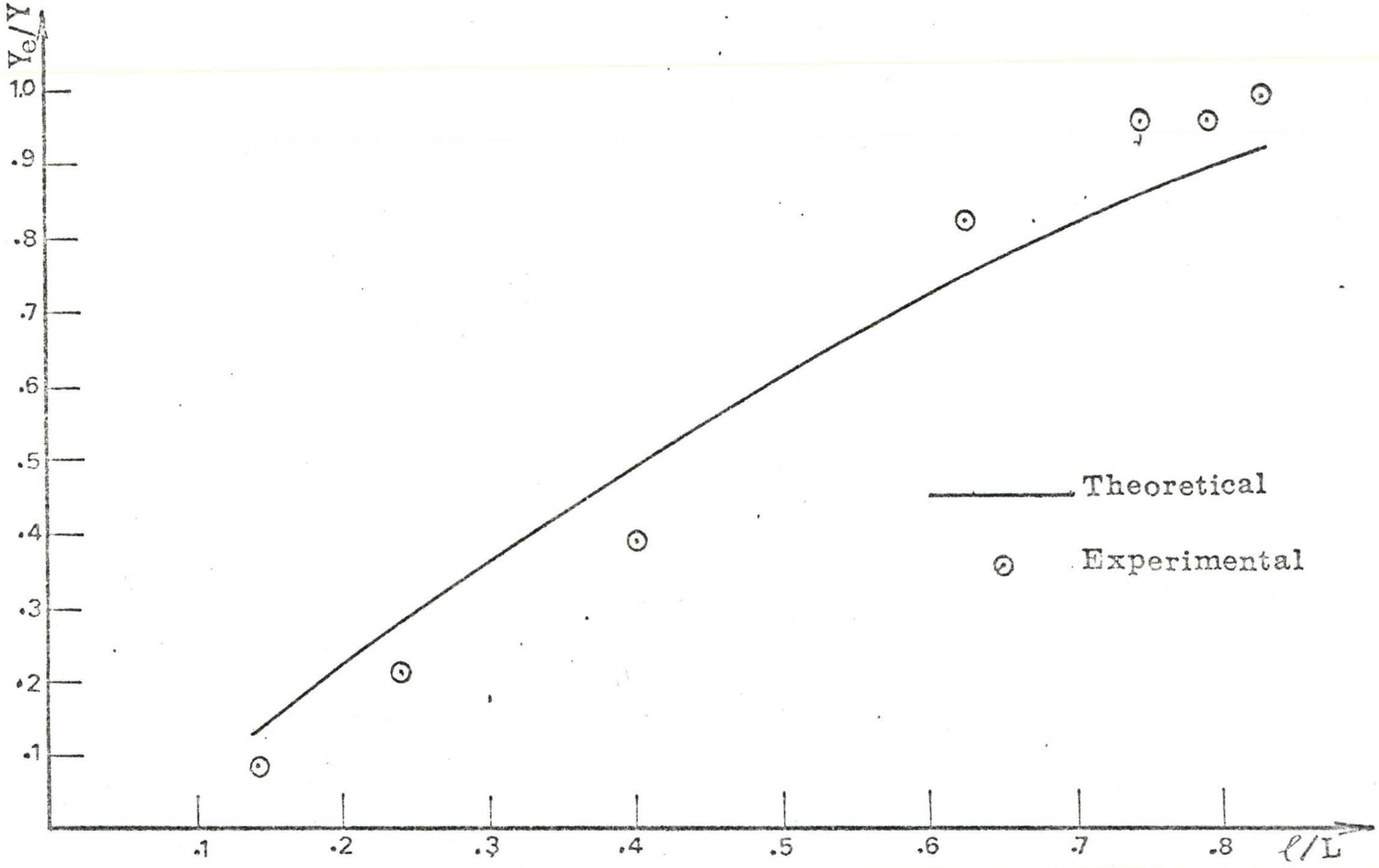

Figure (4.14) Experimental and the Finite Element Results (ℓ/L vs. Y_e/Y).

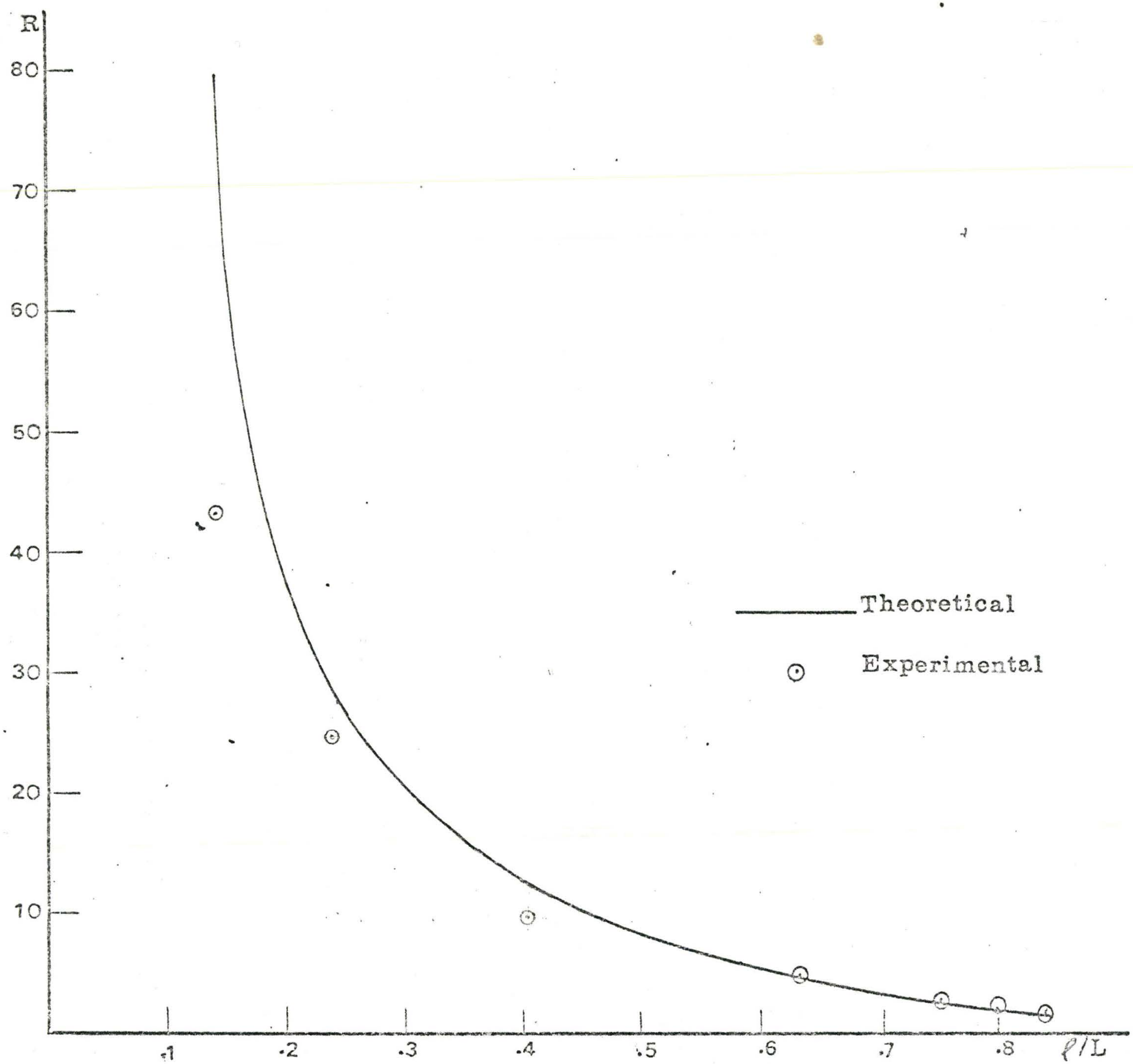

Figure (4.15) Experimental and the Finite Element Results (ℓ/L vs. R).

CHAPTER 5

DESIGN CURVES AND DISCUSSION OF RESULTS

5.1 General

In this chapter, the effect of taking the shear wall thickness into account on the slab stiffness is evaluated. In addition, the overhanging part of the slab beyond the walls, as defined in Figure (3.12) by the symbol d, is studied to evaluate its effect on the stiffness of the system. For each wall configuration shown in Figure (5.1), the coupling slab is analysed by using the computer program developed to obtain its stiffness. The effective width and the rotational stiffness of the equivalent beam are represented in sets of design curves. In order to use these curves it is necessary to know the geometry of the cross-sections of the walls, the width of the slab, Y, the opening between the walls, ℓ, the total length of the slab, L, and the thickness of the planar wall, h. Different examples are worked out to explain the use of these curves. The relations between the value "αH" in coupled shear wall analysis and the wall openings are also presented.

5.2 Effect of Shear Wall Thickness on the Slab Stiffness

Consider the configuration of two planar walls coupled by a slab. Three thicknesses of the walls are considered.

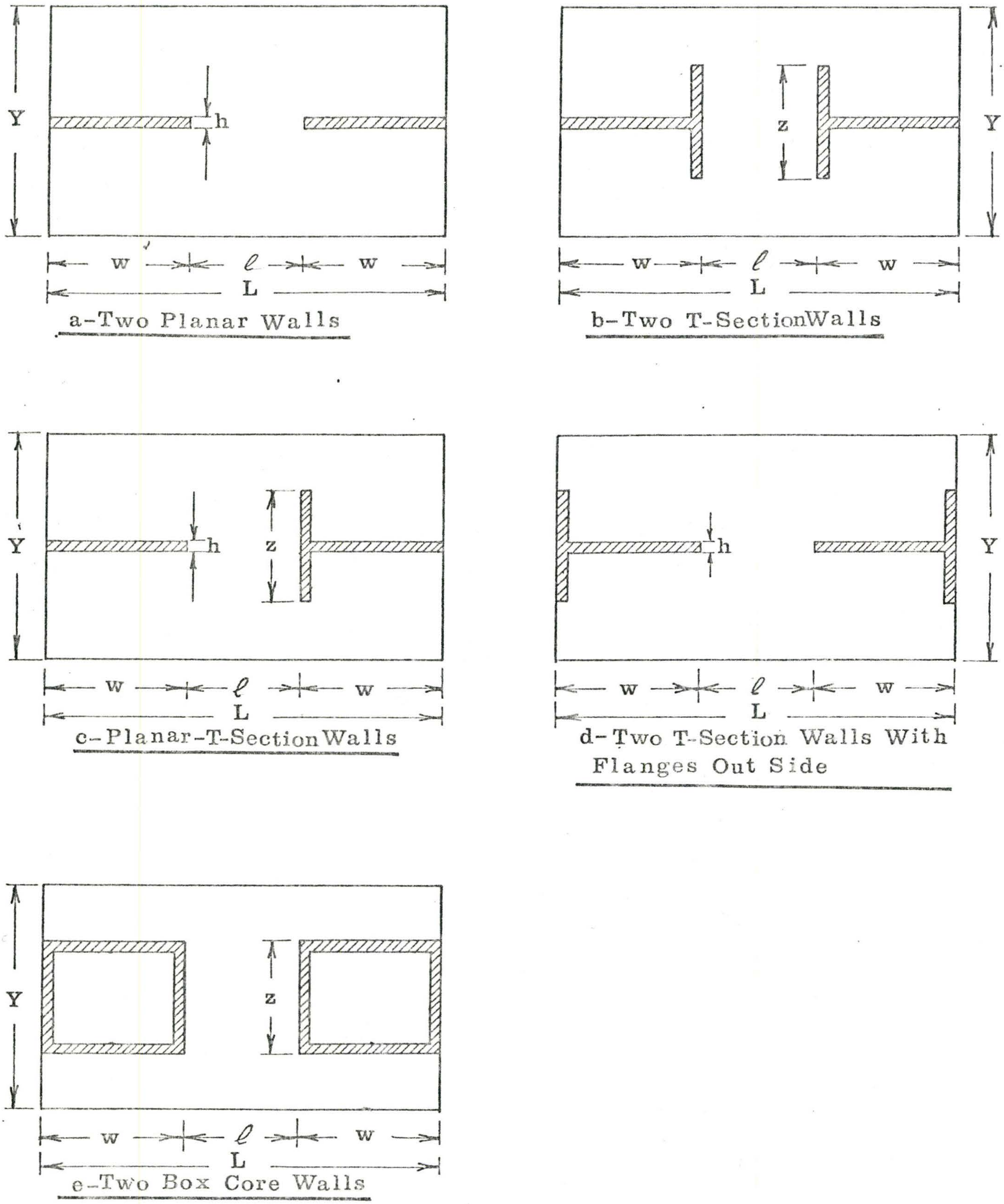

Figure (5.1) Wall Configurations Analysed.

These thicknesses are 12, 9 and 0 inches. The ratio Y/L is kept at a constant value of 0.25. For each wall thickness the value of Y_e/Y for different values of ℓ/L is obtained. Figure (5.2) shows the calculated equivalent beam width for the three thicknesses considered. In the same figure, the percentage error resulting from neglecting the wall thickness is plotted. The comparison of these curves shows that if the wall thickness is neglected, the analysis gives an effective width less than the actual width by a value ranging between 7% and 33%, calculated based on the value of a one foot thick wall. Within the practical range of ℓ/L (0.1-0.2) it is obvious that the thickness of the planar wall should be taken into consideration in estimating the slab stiffness.

It should be noted that the design curves presented by Qadeer and Smith [17] were obtained neglecting the shear wall thickness. Therefore their results will underestimate the slab stiffness.

5.3 Effect of the Overhanging Part of the Slab Beyond the Walls

Figure (3.12) shows a coupled shear wall with an overhanging part of the slab beyond the walls. To ensure that such overhanging has negligible effect on the stiffness of the system, within the range of the configurations studied, some preliminary analysis are carried out with different values of c

Consider the configuration of two planar walls coupled by a slab of Y/L equals 0.25 and ℓ/L equals 0.1. The overhanging part, normalized to the total length L, is varied

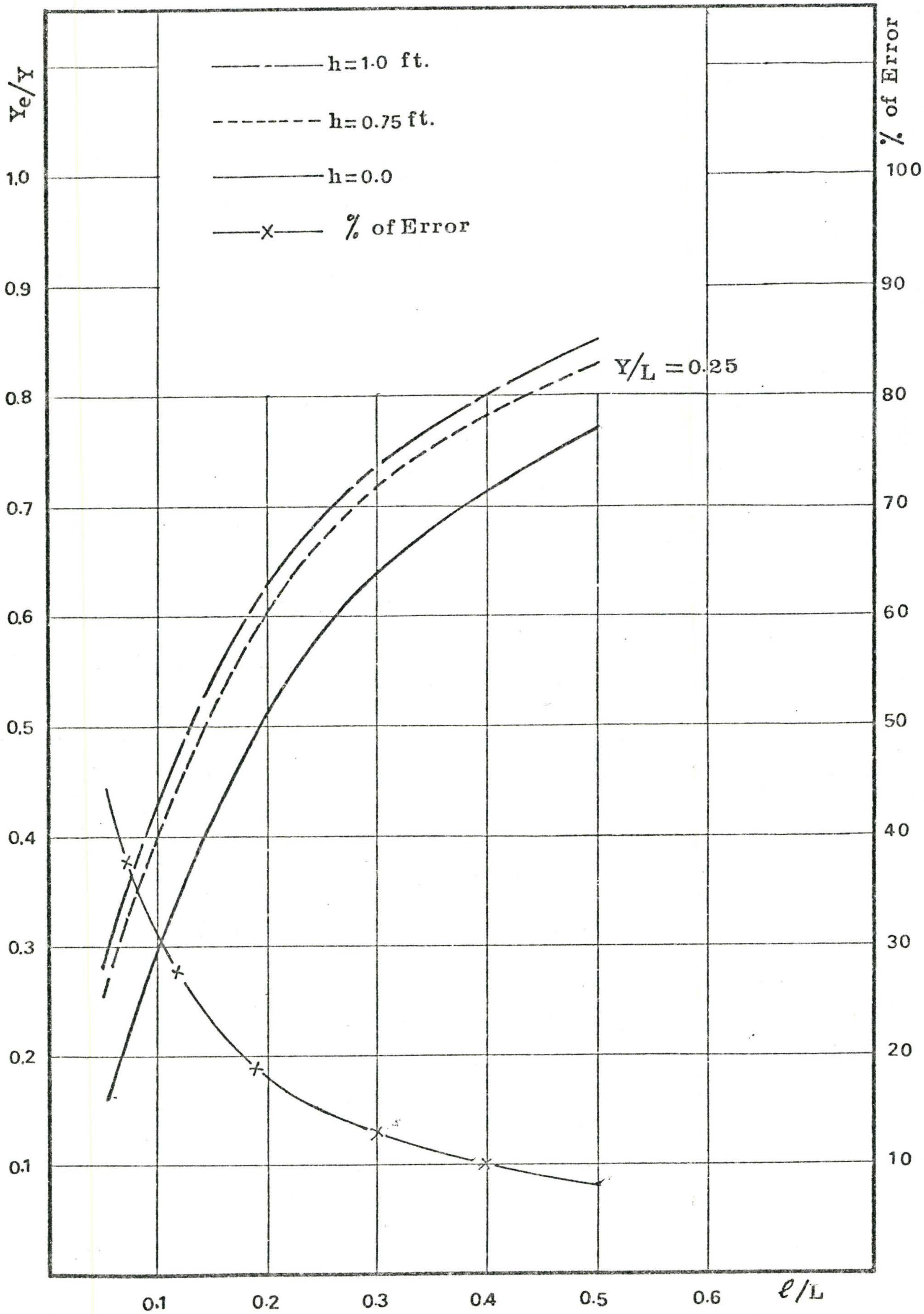

Figure (5.2) Effect of Wall Thickness on the Coupling Slab Stiffness.

between zero and 0.187. For each value of d/L the problem is solved and the effective width is obtained. The results are represented in Table (5.1). These results show that the stiffness of the system is insensitive to the overhanging part of the slab beyond the walls. Therefore, this effect will be neglected in all design curve calculations. All design curves will be obtained with no overhanging slab.

5.4 Presentation of the Design Curves

The design curves presented in this chapter will show the relations between the wall openings and both the effective width and the rotational stiffness of the different slab coupled shear wall configurations. Each curve is generated by five points, each point represents a specific wall opening value. For each wall opening, the slab is analysed by the finite-element method to obtain its stiffness. The total length thickness, Poisson's ratio, and the modulus of elasticity of the slabs are taken as 40 feet, 0.667 foot, 0.15 and 4.32×10^5 kip/ft^2, respectively. Three values of the slab's widths Y are considered, namely, 12 feet, 20 feet and 28 feet. The wall openings are changed as shown in Table (5.2). The shear wall thickness is taken as one foot.

5.4.1 Curves for Coupled Planar Walls

The first set of curves represent the stiffness of the slab coupled planar walls. The relations between the normalized values of ℓ/L and Y_e/Y for different values of Y/L are shown in Figure (5.3). The relations between the

Table (5.1) The Effective Width of the Slab for Different Values of Dimension d

d ft.	0.00	1	1.5	3	6
d/L	.00	.031	.047	.094	.187
Y_e/Y	0.311032	0.311032	0.311033	0.311054	0.311054

Table (5.2) Full Dimensions of Slabs and Walls

Y ft.	12					20					28				
ℓ ft.	2	4	8	12	20	2	4	8	12	20	2	4	8	12	20
w ft.	19	18	16	14	10	19	18	16	14	10	19	18	16	14	10

non-dimensional rotational stiffness R and the normalized wall openings ℓ/L for different values of Y/L are plotted in Figure (5.4). Figure (5.5) shows the relations between Y_e/Y and Y/L for different values of ℓ/L. This plot simplifies the interpolation between the curves in Figure (5.3).

For wall thicknesses less than one foot a reduction for the effective stiffness of the slab can be made. Curves representing the necessary correction are drawn in Figures (5.3) and (5.4). These correction curves are based on the results represented in Figure (5.2), using linear interpolation for the different wall thicknesses.

5.4.1.1 Example

The use of this set of design curves is illustrated by the following example. Let us choose a 40' x 20' slab connecting two planar walls of thickness 0.75 foot. The opening between the two walls is 8 feet. It is required to determine the equivalent width of the slab Y_e and its non-dimensional rotational stiffness.

The values of the relevant non-dimensional parameters are:

$$\ell/L = 0.2$$

$$Y/L = 0.5$$

Using these parameters, the normalized effective width Y_e/Y can be obtained from Figure (5.3),

$$Y_e/Y = 0.36$$

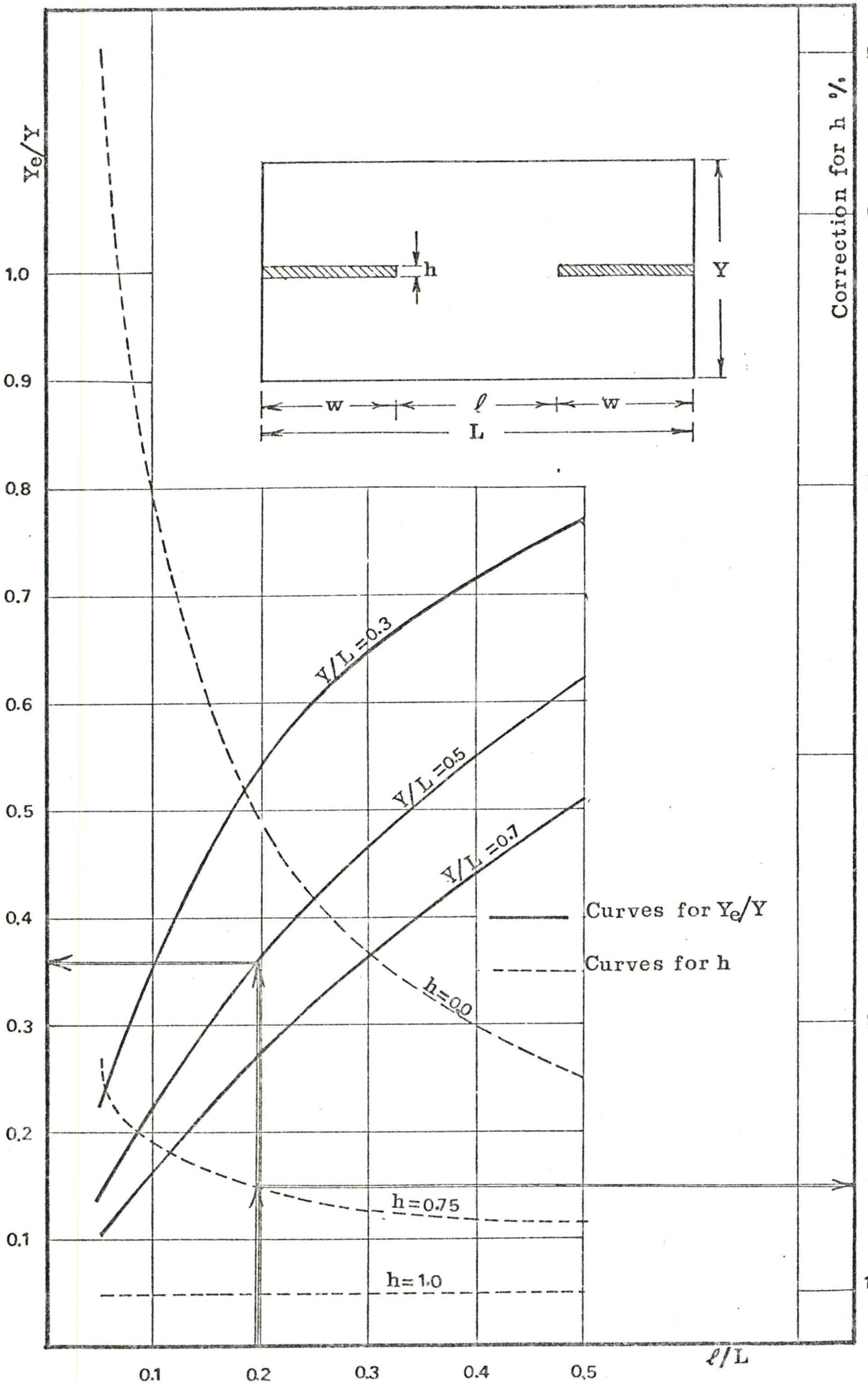

Figure (5.3) Variation of the Effective Width with Wall Opening for Planar Wall Configuration.

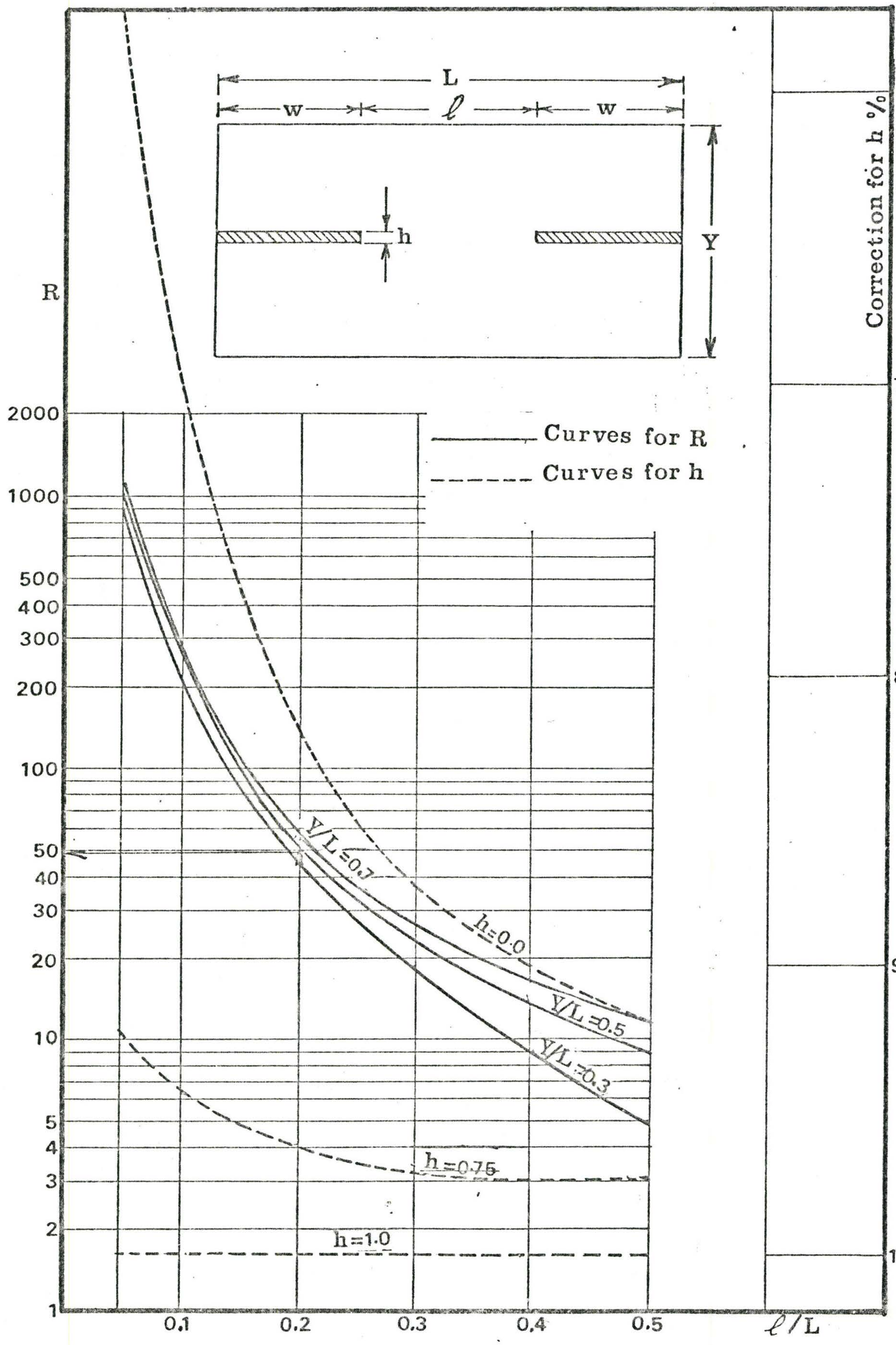

Figure (5.4) Variation of the Slab Stiffness with the Wall Opening for Planar Wall Configurations.

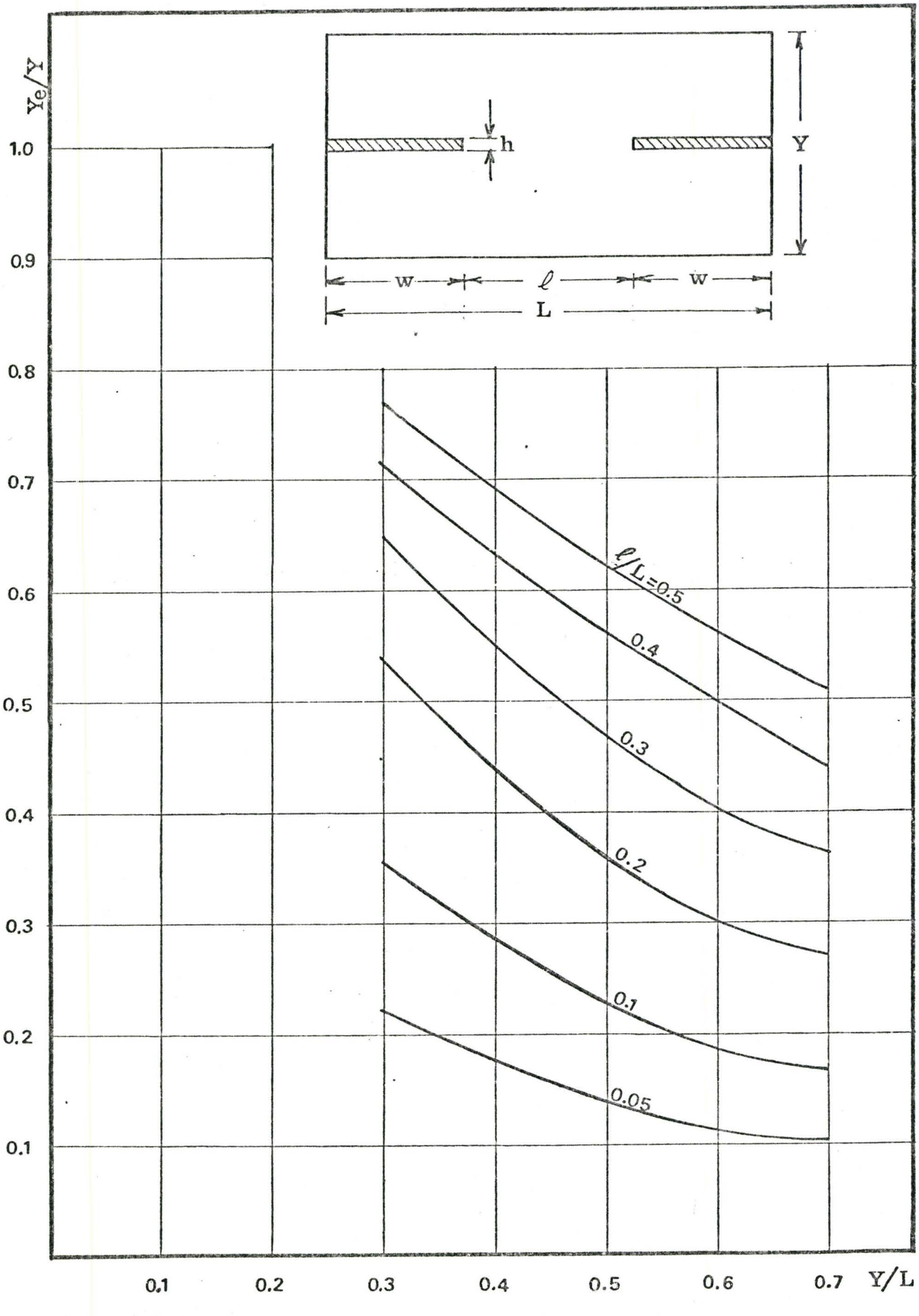

Figure (5.5) Variation of the Effective Width with Slab Width for Planar Wall Configurations.

The reduction factor for the wall thickness = 0.96.

The equivalent width of the slab is therefore

$$Y_e = 0.36 \times 0.96 \times 20$$

$$= 6.9 \text{ feet}$$

Similarly, using Figure (5.4), the non-dimensional rotational stiffness is

$$R = 49$$

After correction, the non-dimensional rotational stiffness is,

$$R = 49 \times 0.96$$

$$= 47$$

5.4.2 Curves for Coupled T-Section Wall Configurations

The second set of curves are those representing the stiffness of the slab coupling two T-section walls. The dimensions of the slabs and walls are those described in Section 5.4. The flange width z, are taken to be 10% and 20% of the total length, L. For z/L equals 0.1, the relations between ℓ/L and both the effective width Y_e/Y and the rotational stiffness are presented in Figures (5.6) and (5.7), respectively. The relation between Y/L and Y_e/Y is also represented in Figure (5.8). The corresponding relations are plotted in Figures (5.9), (5.10) and (5.11), respectively, for the case z/L equals 0.2. It should be noted that the thickness of the wall has no effect on the stiffness of the slab because it is essentially taken into account using finite

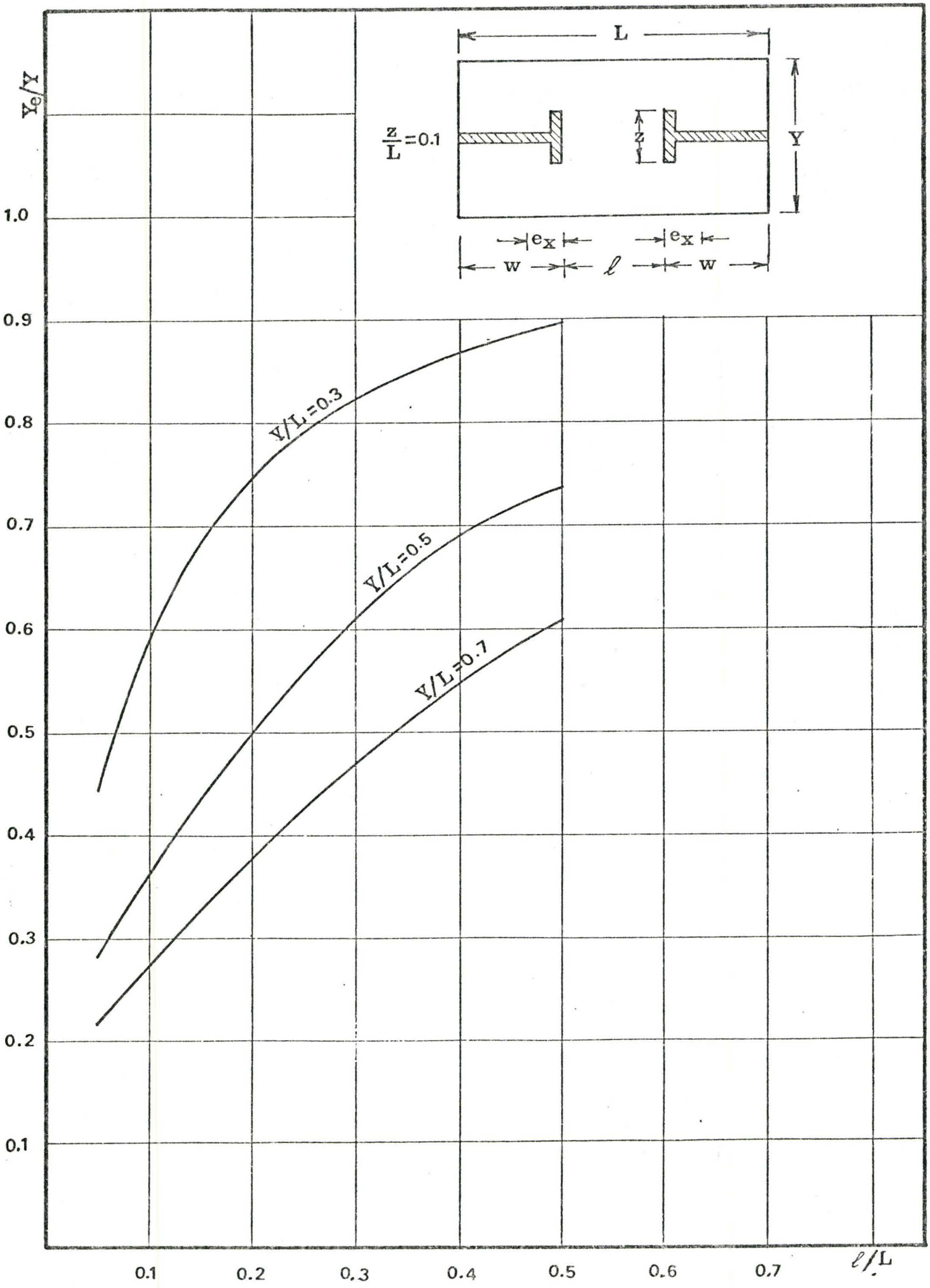

Figure (5.6) Variation of the Effective Width with Wall Opening for T-Section Wall Configurations.

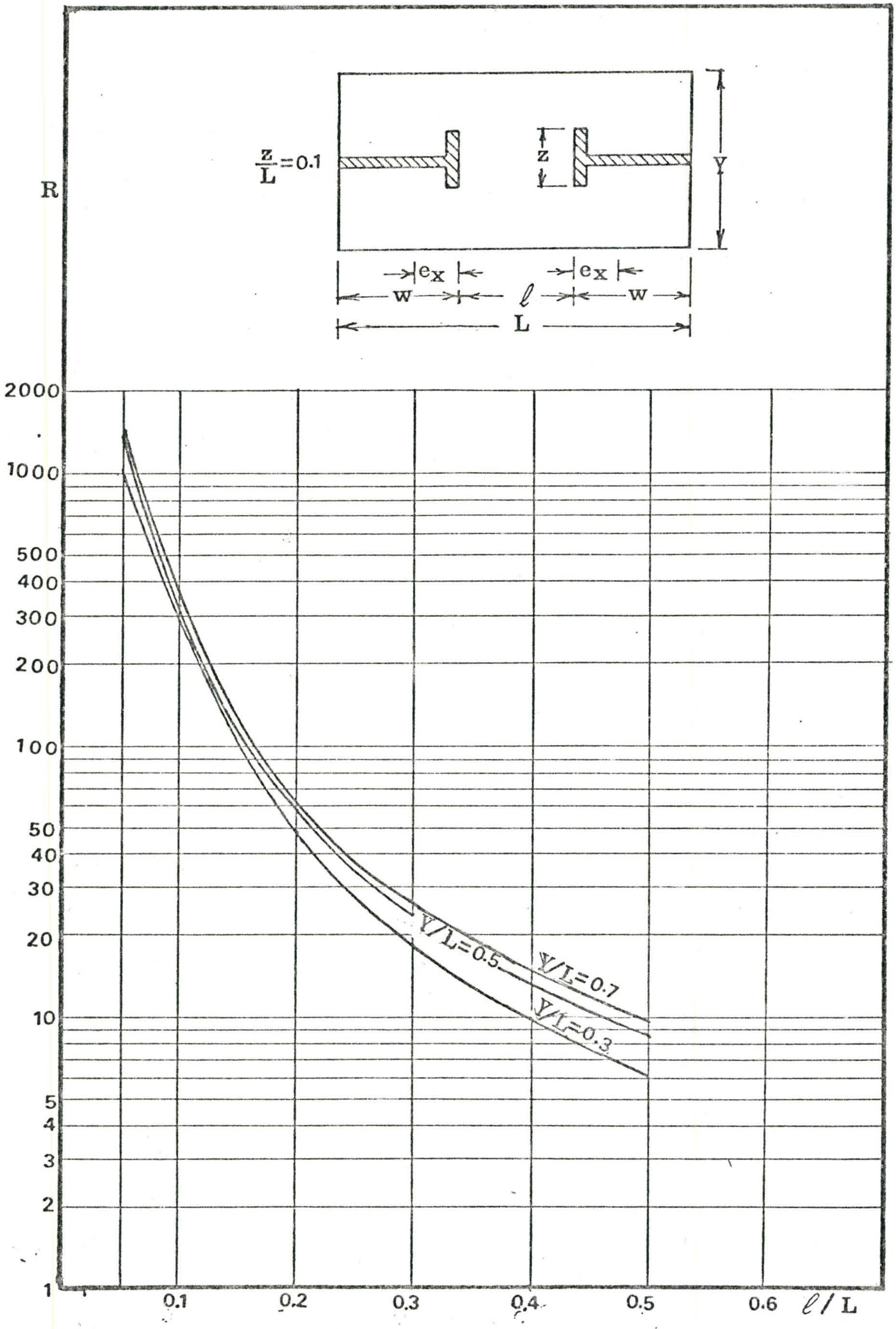

Figure (5.7) Variation of the Slab Stiffness with the Wall Opening for T-Section Wall Configurations.

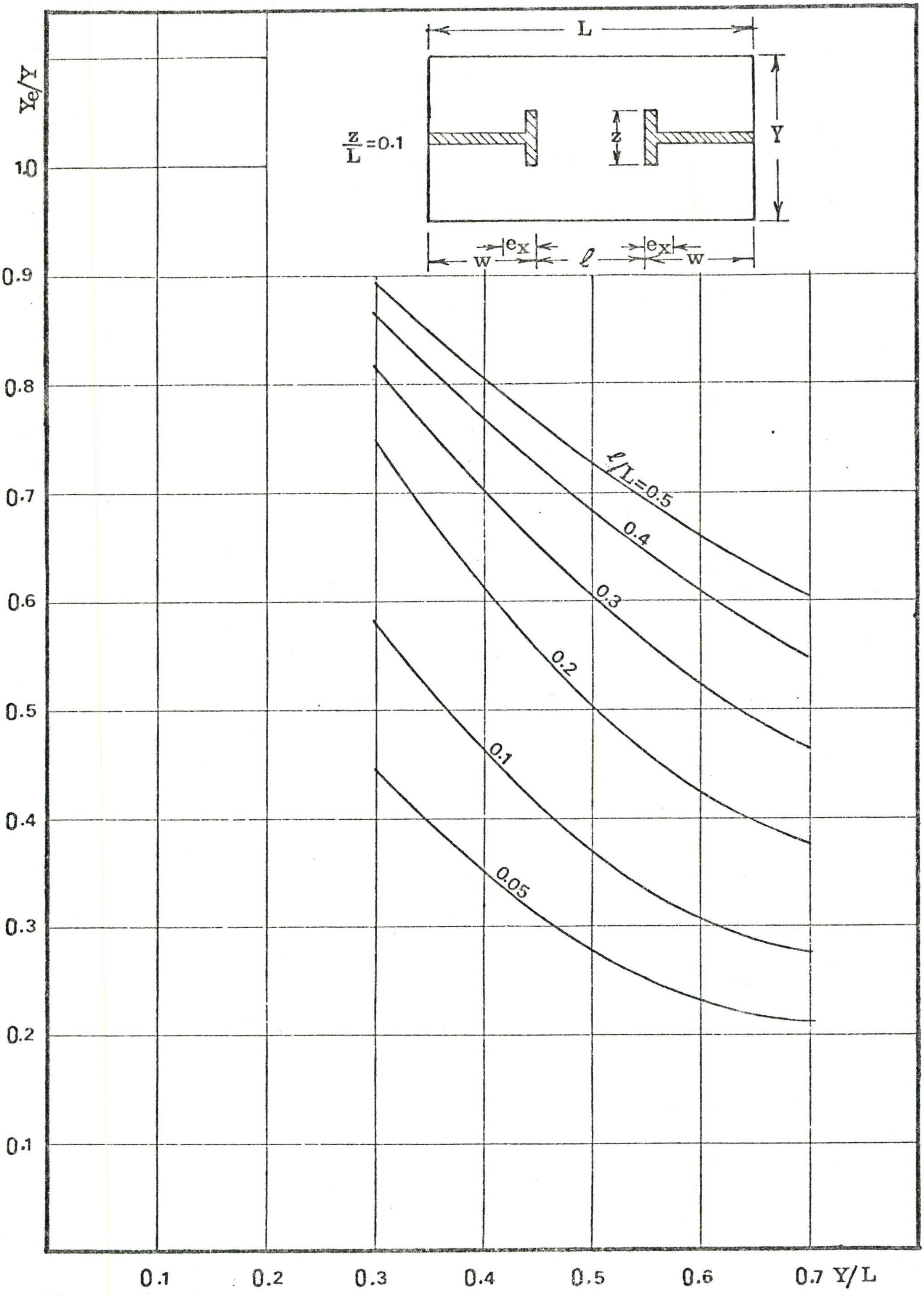

Figure (5.8) Variation of the Effective Width with Slab for T-Section Wall Configurations.

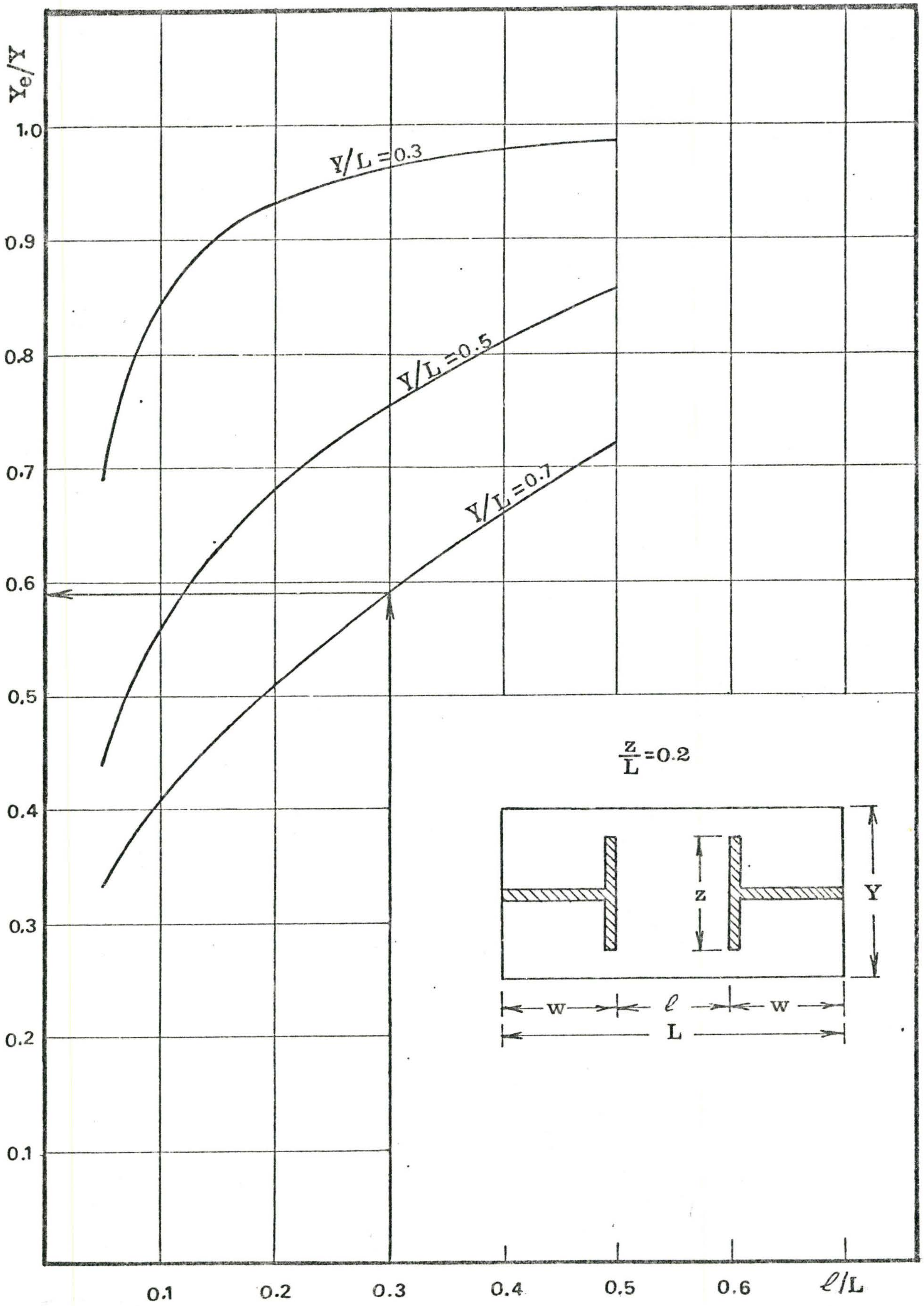

Figure (5.9) Variation of the Effective Width with Wall Opening for T-Section Wall Configurations.

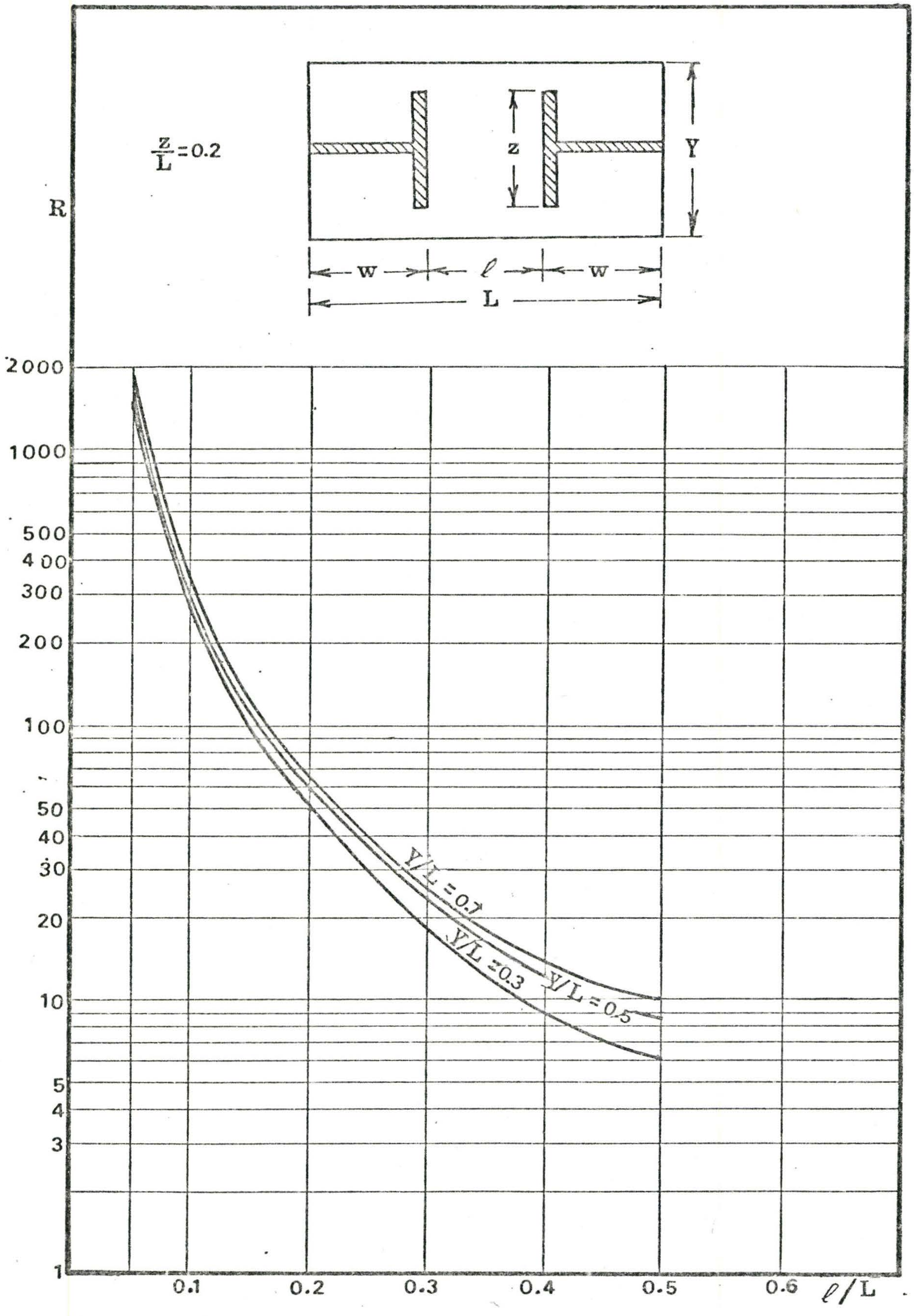

Figure (5.10) Variation of the Slab Stiffness with the Wall Opening for T-Section Wall Configurations.

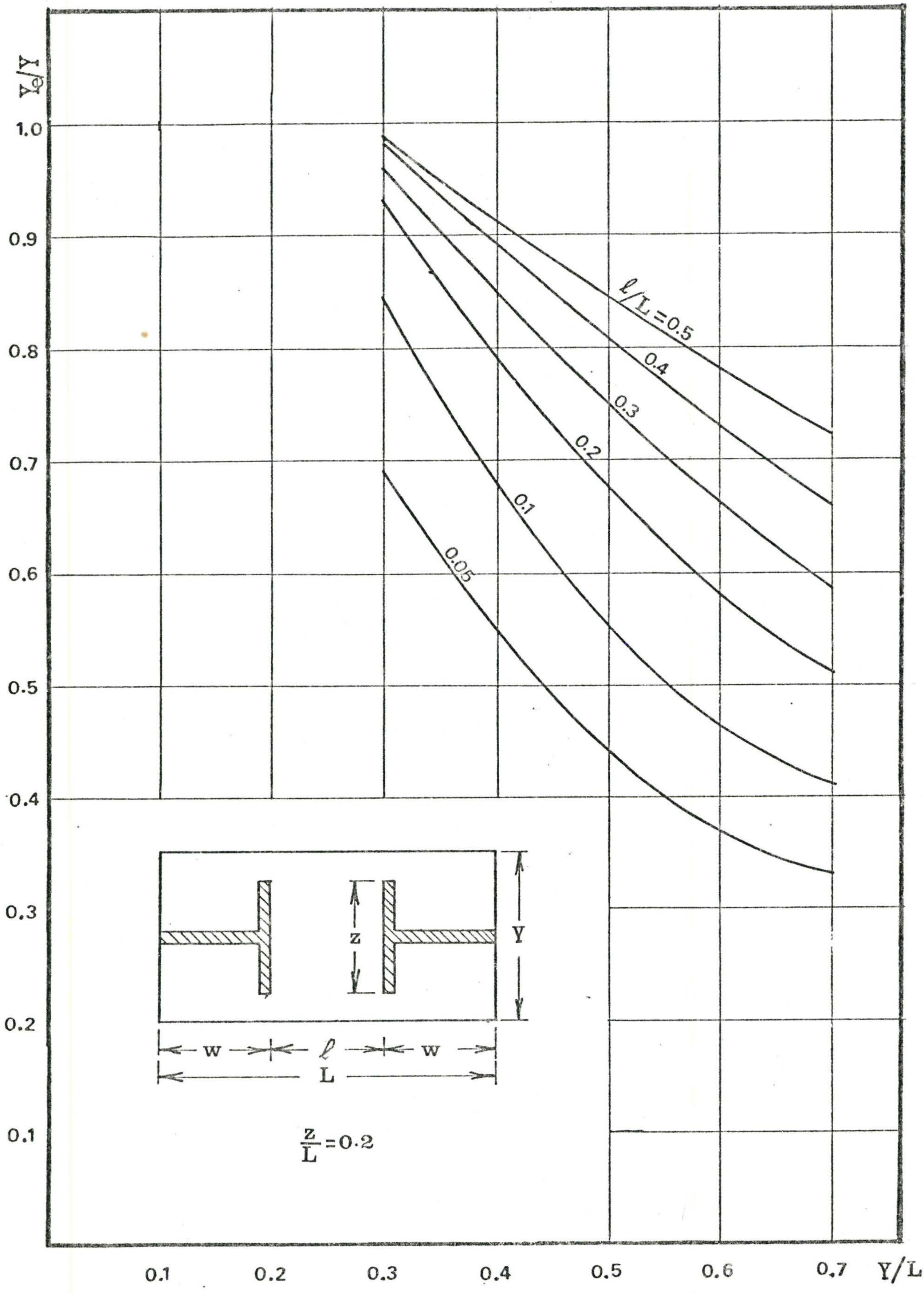

Figure (5.11) Variation of the Effective Width with Slab Width for T-Section Wall Configurations.

flange widths.

5.4.3 Curves for Coupled Planar and T-Section Wall Configurations

The configuration of the slab coupled planar wall with the T-section wall under lateral loading has one axis of symmetry (the X-X axis) only, as shown in Figure (3.6). The Y-Y axis is not the axis of antisymmetry in this case. Therefore, it is necessary to consider half of the slab instead of one quarter of the slab as in the previous two wall configurations. Due to the limitation of the computer storage, a coarser mesh has to be used. To obtain an idea for the error produced from the coarse mesh used, a slab coupled planar wall system is solved by two different ways. First, one quarter of the slab is solved and secondly, it is solved considering half of the slab using a coarser mesh. A comparison between the computational results of the two calculations will then provide an indication of the errors involved using a coarser mesh. Figure (5.12) shows the computed results. The error involved in using a coarser mesh as a function of ℓ/L is plotted in the same figure. The error ranges between 4% and 20% depending on the values of ℓ/L. Since the design curves for the slab coupled planar wall with the T-section wall are computed using a coarser mesh, the results may be modified according to the error curve as shown in Figure (5.12).

The flange width of the T-section wall is taken as 10% and 20% of the total length of the slab. The thickness of the planar wall is taken as one foot. Figure (5.13) shows

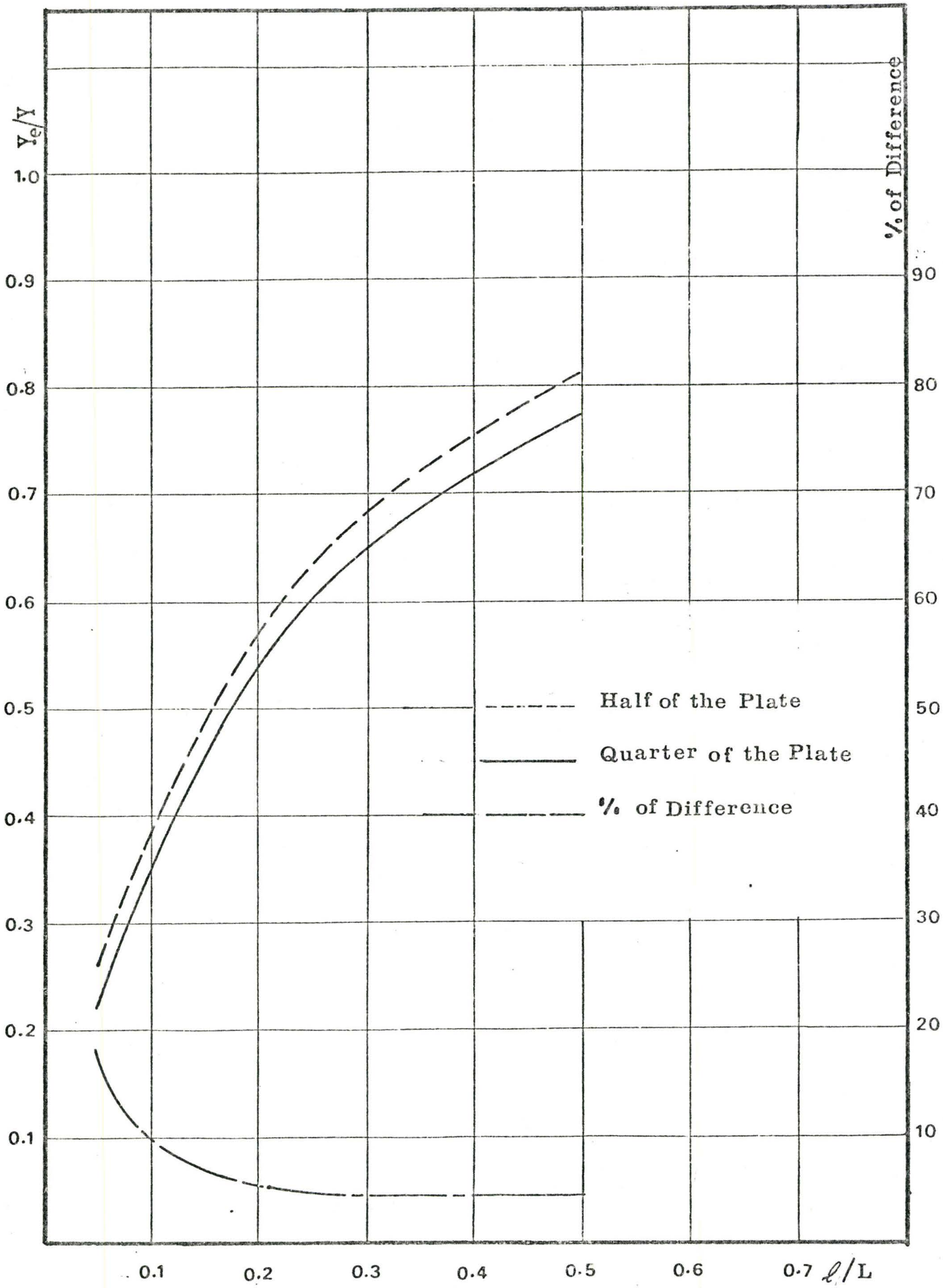

Figure (5.12) Effect of the Finite Element Mesh on the Slab Stiffness.

the relations between ℓ/L and Y_e/Y, while Figure (5.14) shows the relations between Y/L and Y_e/Y for z/L equals 0.1. The same relations are shown in Figures (5.15) and (5.16) for z/L equals 0.2.

5.5 Stiffness of the Slabs Coupled Box Core Walls or T-Section Walls with Flanges at the Outside Edges

The previous sets of curves represent the effective stiffness of the common slabs coupled shear wall configurations used in high-rise buildings. In addition to these configurations, the box core walls and the T-section walls with the flanges at the outside edges are used in high-rise buildings. The last two configurations are shown in Figures (5.18) and (5.17), respectively. Preliminary analysis for the slabs coupled box core walls or T-section walls with flanges at the outside edges was carried out. For simplicity we shall denote a T-section wall configuration with flange at the inner edge as a T-wall configuration and a T-section wall configuration with flange at the outside edge as an inverted T-wall configuration. Although the bending stiffness and correspondingly, the effective width of the slab coupled planar walls and the slab coupled inverted T-walls is the same, the rotational stiffness for these configurations is not the same. This is because the rotational stiffnesses are obtained at different points in the two cases. The same is true for the slab coupled box core walls and the slab coupled T-walls.

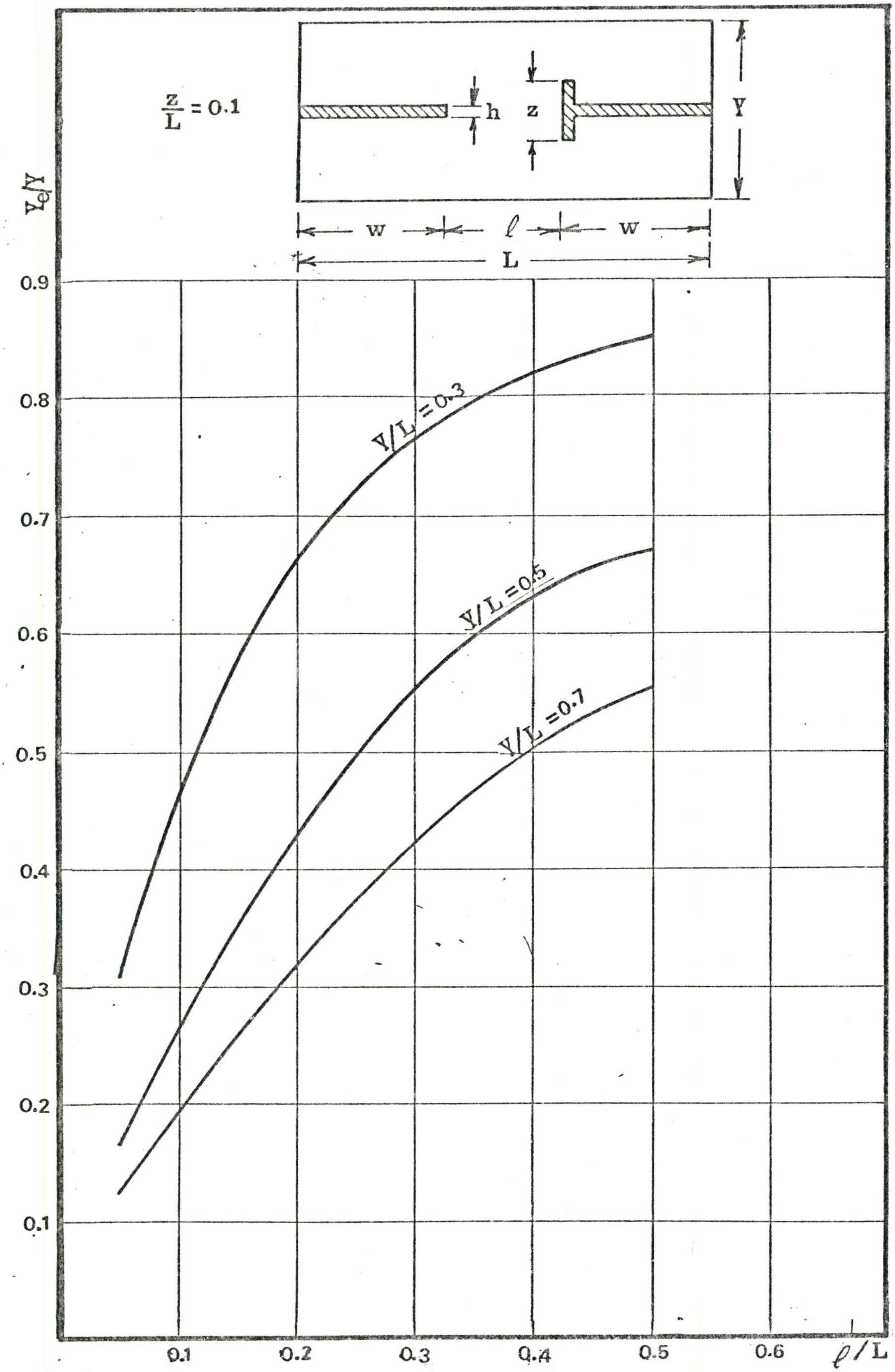

Figure (5.13) Variation of the Effective Width with the Wall Opening.

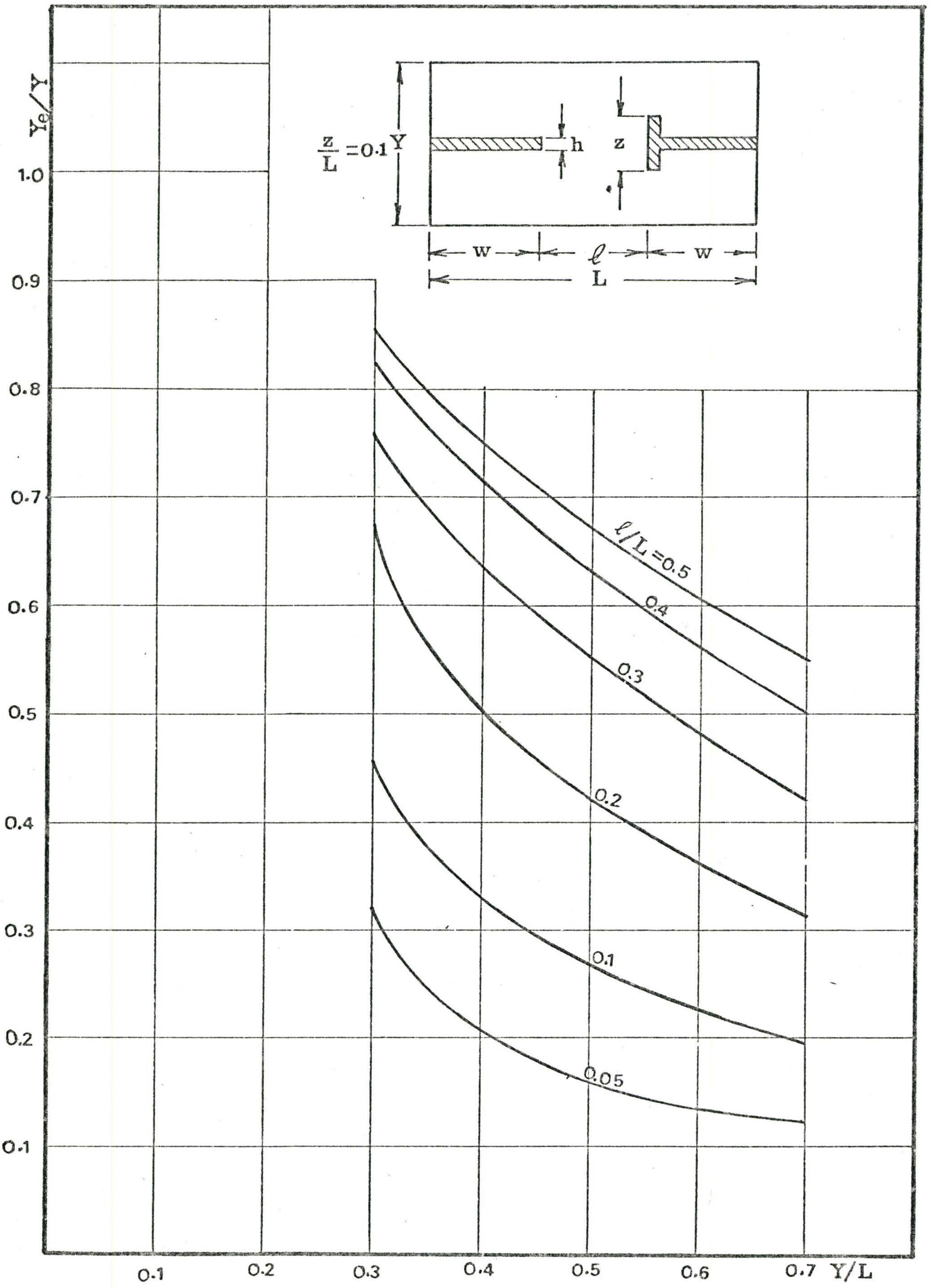

Figure (5.14) Variation of the Effective Width with the Slab Width.

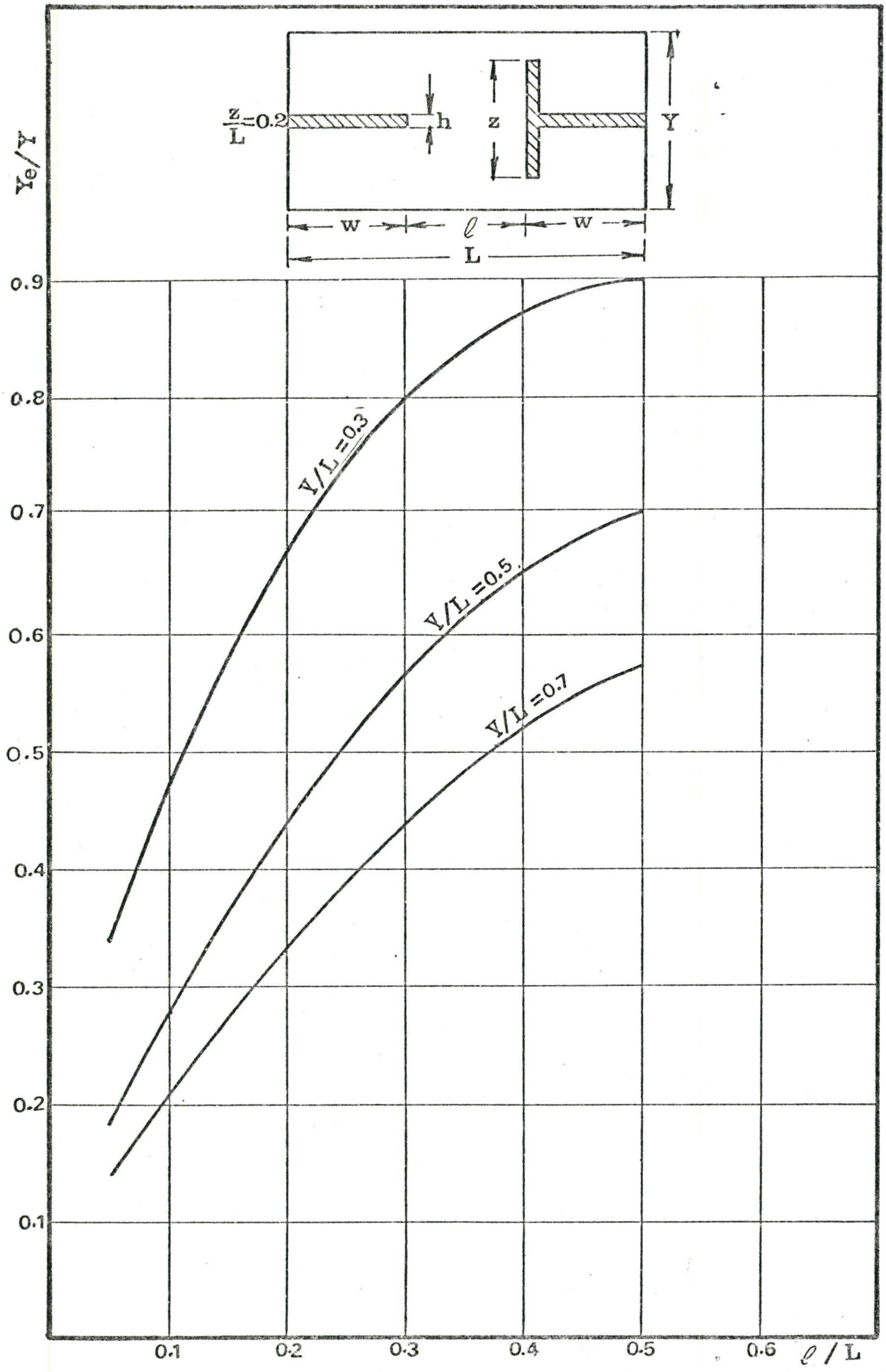

Figure (5.15) Variation of the Effective Width with the Wall Opening.

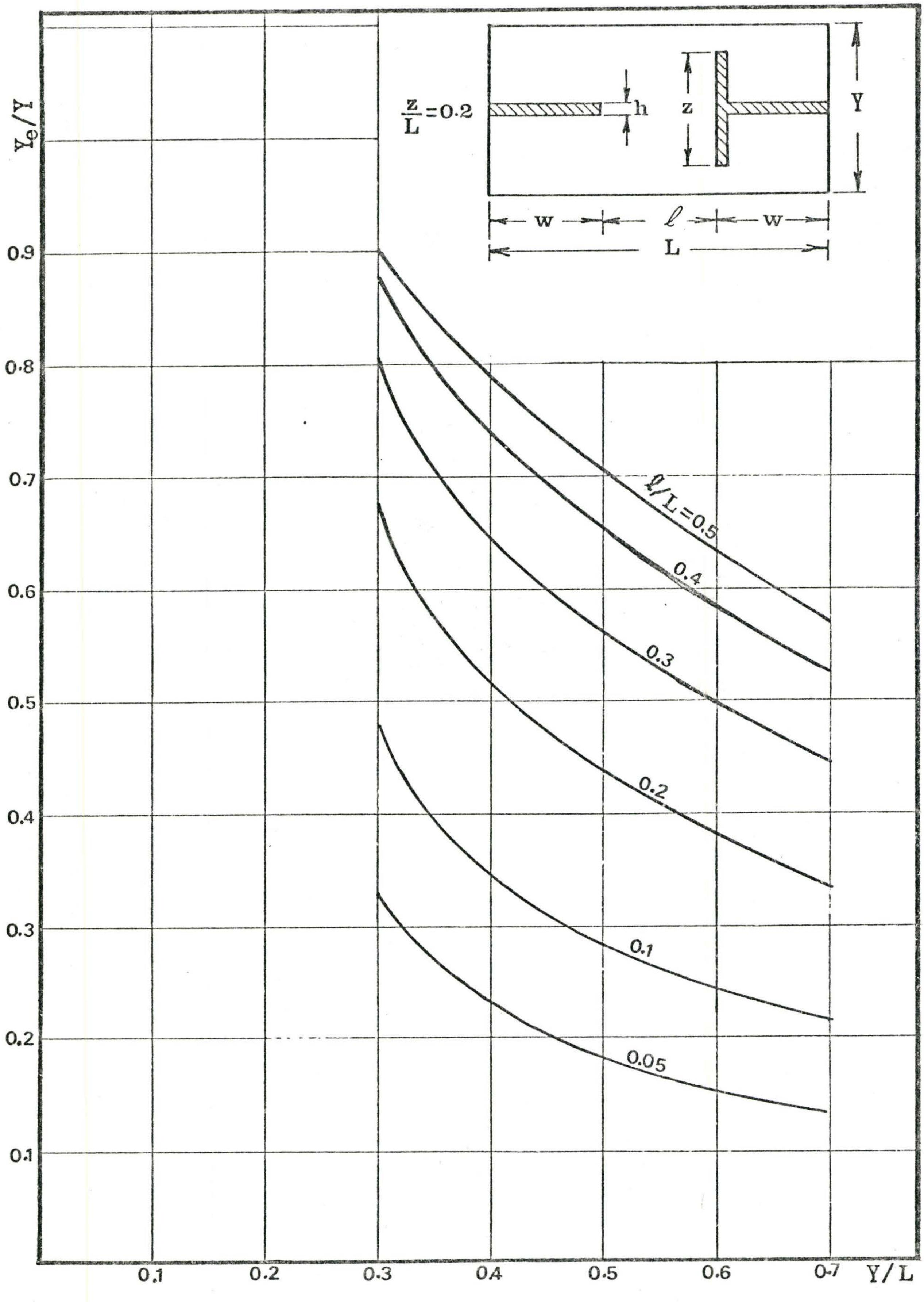

Figure (5.16) Variation of the Effective Width with the Slab Width.

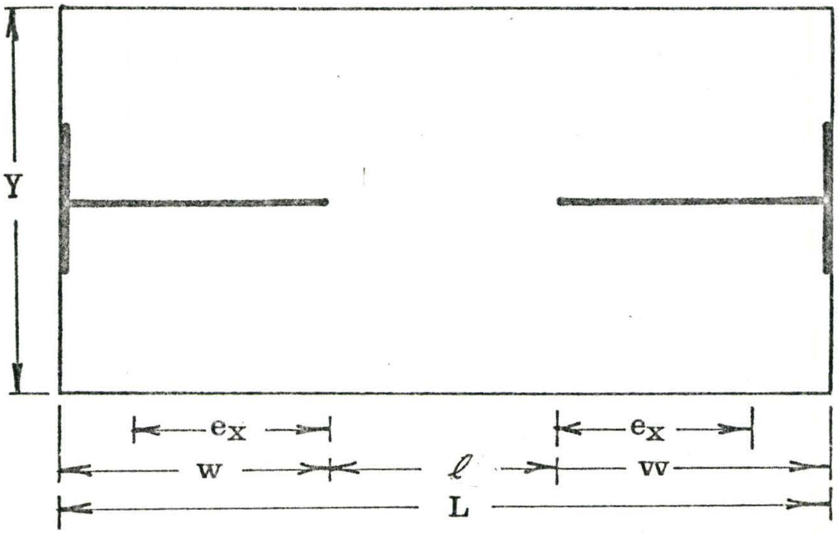

Figure (5.17) Slab Coupled T-Section Wall Configurations with Flanges at the Outside Edges.

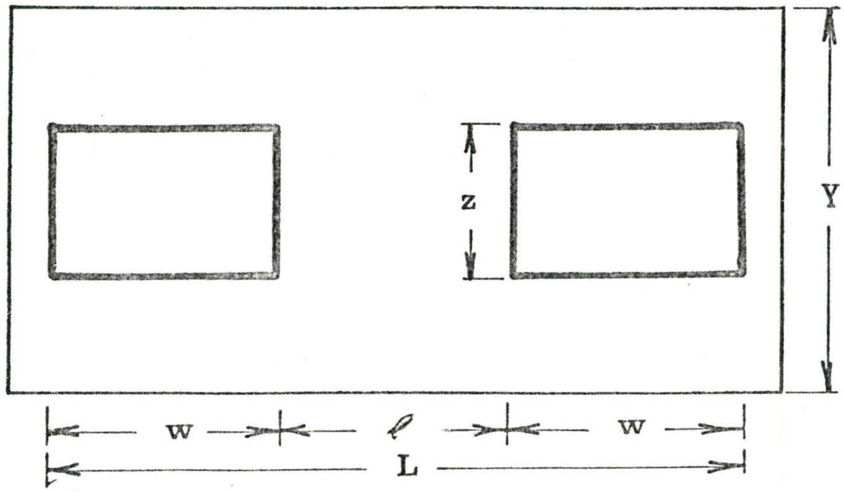

Figure (5.18) Slab Coupled Box Core Walls.

5.5.1 The Effective Width of the Slabs Coupled Inverted T-Wall and Box Core Wall Configurations

Two groups of slabs are analysed by the computer program developed. The first group represents the slabs coupled inverted T-walls with different openings, while the second group represents the slabs coupled planar walls with similar openings. Table (5.3) shows the effective width of each configuration for the different wall openings. The same procedure of analysis is carried out for the slab coupled box core walls and the slab coupled T-walls. Table (5.4) shows the effective width for each wall configuration.

From Tables (5.3) and (5.4) it is shown that the effective width of the slabs coupled inverted T-walls is the same as the effective width of the slabs coupled planar walls. Also, the effective width of the slab coupled box core walls is the same as the slab coupled T-walls. Therefore, the curves representing the effective width of the slabs coupled planar walls or T-walls can be used for the slabs coupled inverted T-walls or core walls, respectively.

5.5.2 The Rotational Stiffness of the Slab Coupled Inverted T-Wall and Box Core Wall Configurations

As mentioned in Chapter 3, the rotational stiffness of the slab coupled shear wall is calculated at the centroid of the cross-section of the wall. Since the centriod of a planar wall is at the mid-width point, while the centriod of an inverted T-wall will be further away from the mid-width of the wall, the rotational stiffness calculated for the planar

Table (5.3) The Effective Width of Slabs Coupled Planar Walls and Inverted T-Walls

ℓ/L		0.05	0.1	.2	.3	.5
Planar Wall	Y_e/Y	.22	.356	.535	.65	.77
Inverted T-Wall	Y_e/Y	.23	.363	.542	.659	.78

Table (5.4) The Effective Width of Slabs Coupled Core Walls and T-Walls

$\frac{W}{Y}$	$\frac{Z}{Y}$	$\frac{\ell}{L}$	Y_e/Y	
			Box Wall	T-Wall
0.3	0.3	0.25	0.467	0.461
		0.4	0.601	0.583
		0.5	0.699	0.671
0.5	0.5	0.25	0.731	0.739
		0.4	0.858	0.849
		0.5	0.915	0.894

wall will be different from that of the inverted T-wall although the effective width for the coupled planar walls and the inverted T-walls is the same.

In order to use the curves representing the rotational stiffness of the slab coupled planar walls to represent the rotational stiffness of the slabs coupled inverted T-walls, a relation between the rotational stiffnesses for both kinds of walls will be obtained.

Let R and R_T be the rotational non-dimensional stiffness of the slabs coupled planar walls and inverted T-walls respectively. From Equations (3.19) and (3.21), we have

$$R = \frac{6(Y_e/Y)(Y/\ell)(1-\nu^2)}{[\ell/(\ell + w)]^2} \tag{5.1}$$

and

$$R_T = \frac{6(Y_e/Y)(Y/\ell)(1-\nu^2)}{[\ell/(\ell + 2\,e_x)]^2} \tag{5.2}$$

Dividing Equation (5.2) by Equation (5.1) yields

$$\beta_T = \frac{R_T}{R}$$

$$= [\frac{\ell + 2\,e_x}{\ell + w}]^2 \tag{5.3}$$

where β_T is the correction factor for the effective stiffness for the inverted T-section wall. The value of e_x can be represented as a function of w, gives

$$e_x = \gamma w \tag{5.4}$$

where γ is a constant depending on the flange width of the

T-section wall. From Figure (5.1), we have

$$L = \ell + 2\,w \tag{5.5}$$

Thus, Equation (5.3) becomes

$$\beta_T = \left[\frac{(1-\gamma).\ell/L+\gamma}{\frac{1}{2}(1+\ell/L)}\right]^2 \tag{5.6}$$

Table (5.5) shows the relationship between β_T and ℓ/L for different values of γ.

The same procedure can be used to obtain the relation between the rotational stiffness of the slab coupled T-walls and that of the slab coupled box core walls. Let R and R_c be the non-dimensional rotational stiffness of the slab coupled T-wall and box core wall respectively. Referring to Equations (3.19) and (3.21), we have

$$R_c = \frac{6(Y_e/Y)(Y/\ell)(1-\nu^2)}{[\ell/(\ell+w)]^2} \tag{5.8}$$

$$R = \frac{6(Y_e/Y)(Y/\ell)(1-\nu^2)}{[\ell/(\ell+2\,e_x)]^2} \tag{5.9}$$

The correction factor for the rotational stiffness of the slab coupling box core walls is

$$\beta_c = \frac{R_c}{R}$$

$$= \left[\frac{\ell+w}{\ell+2\,e_x}\right]^2 \tag{5.10}$$

From Equation (5.5), we have

$$\frac{w}{L} = \frac{1}{2}\ (1-\ell/L) \tag{5.11}$$

Substituting into Equation (5.10) yields

$$\beta_c = \left[\frac{1+\ell/L}{\frac{2\ell}{L} + 4\ \frac{e_x}{L}}\right]^2 \tag{5.12}$$

Using

$$e_x = \frac{w^2-h^2+z.h}{2(z+w-h)} \tag{5.13}$$

where h is the thickness of the wall. Equation (5.13) can be written as

$$\frac{e_x}{L} = \frac{1}{2}\left[\left(\frac{w}{L}\right)^2 - \left(\frac{h}{L}\right)^2 + \left(\frac{z}{L}\right)\left(\frac{h}{L}\right)\right] / \left[\frac{z}{L}+\frac{w}{L}-\frac{h}{L}\right] \tag{5.14}$$

For a coupled wall of practical dimensions, the value of h/L is approximately 2.5%, and the maximum value of z/L used is 0.2. Hence, the product of z/L and h/L is about 0.5%. Thus one can neglect both h/L and (z/L x h/L) to simplify the expression to

$$\frac{e_x}{L} = \frac{1}{4}\ \left[\frac{(1-\ell/L)^2}{\frac{2z}{L} - \frac{\ell}{L} + 1}\right] \tag{5.15}$$

Substituting into Equation (5.12) yields

$$\beta_c = \left[\frac{(1+\ell/L)(2z/L-\ell/L+1)}{(2\ell/L)(2z/L-\ell/L+1) + (1-\ell/L)^2}\right]^2 \tag{5.16}$$

The values of β_c are calculated in Table (5.6) for different values of ℓ/L and z/L.

Table (5.5) Values of β_T for Different Values of γ and ℓ/L.

ℓ/L	β_T			
	γ = .6	γ = 0.7	γ = 0.8	γ = 0.9
0.05	1.4	1.86	2.4	3.0
0.1	1.36	1.76	2.22	2.75
0.2	1.28	1.62	1.96	2.34
0.3	1.23	1.48	1.75	2.04
0.5	1.14	1.29	1.44	1.61

Table (5.6) Values of β_c for Different Values of ℓ/L and Z/L

Z/L = 0.1		Z/L = 0.2	
ℓ/L	β_c	ℓ/L	β_c
0.05	1.42	0.05	1.88
0.1	1.38	0.1	1.79
0.2	1.33	0.2	1.65
0.3	1.29	0.3	1.55
0.4	1.26	0.4	1.46
0.5	1.21	0.5	1.38

5.5.3 Example

This example illustrates how to obtain the rotational non-dimensional stiffness of the slab coupled inverted T-section walls using the curves calculated for coupled planar walls. Let the slab dimensions be the same as that given in example (5.3.1), with a wall thickness of one foot. Then,

$$\ell/L = 0.2$$

$$Y/L = 0.5$$

$$\gamma = 0.8$$

Using Figure (5.4) the rotational stiffness R, with a wall thickness of one foot is

$$R = 49$$

From Table (5.5), the correction factor β_T is given by

$$\beta_T = 1.96$$

Therefore, the non-dimensional rotational stiffness of the slab for coupled inverted T-section walls becomes

$$R_T = 1.96 \times 49$$
$$= 96.2$$

5.6 Equivalent Beam Width of a Slab Connecting Two End Walls

Figure (5.19) shows the plan of a building in which both the intermediate and the end bays are shown. The tributary areas of the end bays have one half of the area of

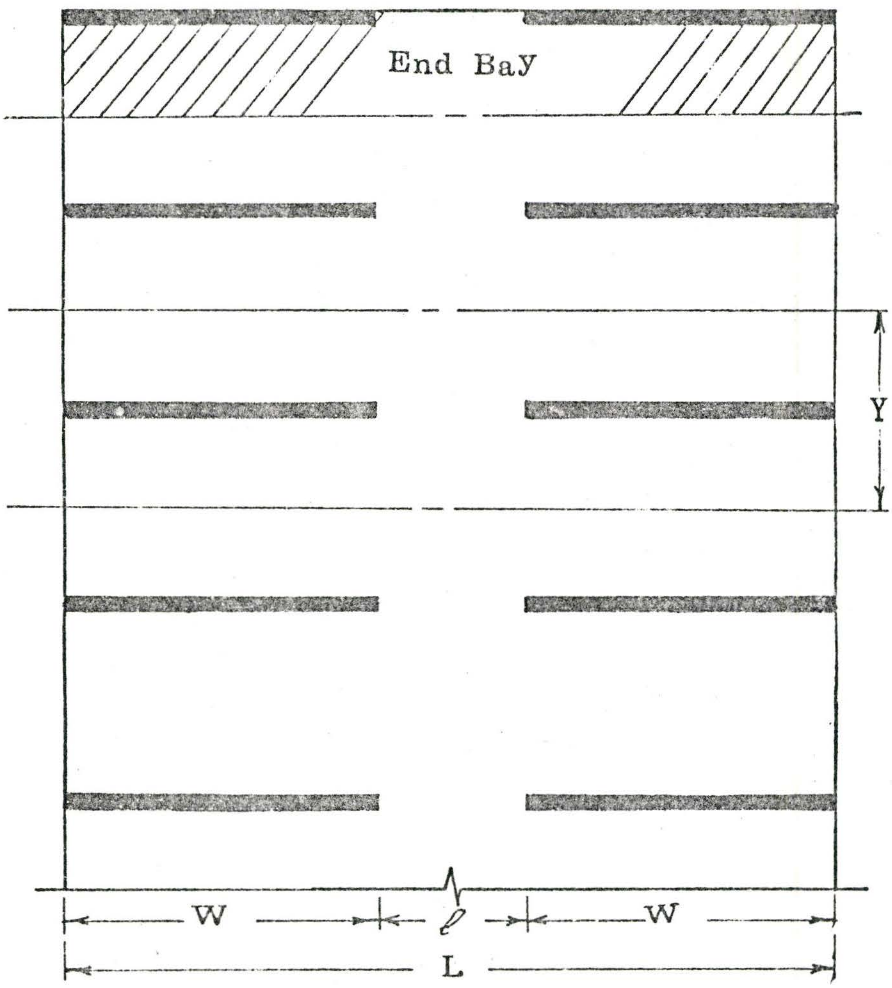

Figure (5.19) Plan Showing Interior and End Bays a typical interior bay, therefore the coupling effect of the slab will be different for an end shear wall. A relation between the stiffness of the end bay slab and the stiffness of the interior bay slab is obtained in this section. This relationship is obtained as a function of the end bay wall thickness and the slab width.

Two thicknesses of the end wall will be considered, namely, one foot and half a foot thick. As a comparison, an interior bay of Y/L equals 0.3 is analysed taking the wall thickness as one foot. Figure (5.20) shows the relations between ℓ/L and Y_e/Y for the interior and the end bays. In this figure, the two lower curves represent the equivalent beam width of the end bay slab normalized to the interior bay slab width. The cases of interior bays with Y/L equals 0.5 and 0.7 are also studied. The end bay and the interior bay comparison are shown in Figures (5.21) and (5.22).

To simplify the calculations of the end bay slab stiffness, the previous computed results are replotted in Figure (5.23). In this figure, the dotted lines represent the end bay slab stiffness as a percentage of the interior bay. These lines are obtained by dividing the effective width of the end bay slab by the corresponding effective width of the interior bay slab. The solid lines represent the reduction in the end bay slab stiffness, if the end wall thickness is taken to be different than one foot. Linear interpolation can be carried out for values of wall thickness between the two estimated values.

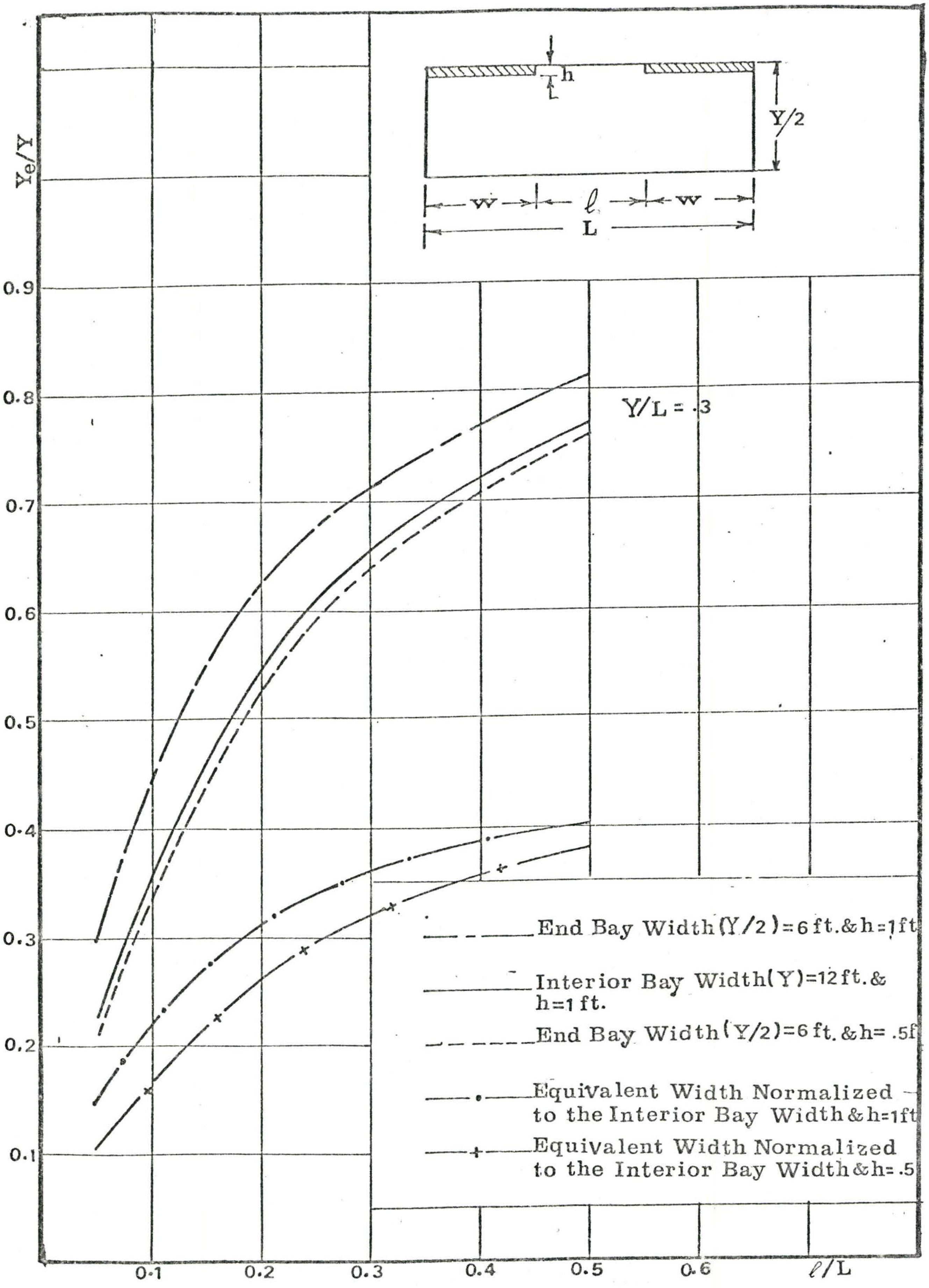

Figure (5.20) Variation of the Slab Effective Width with the Wall Opening for Interior and End Bays.

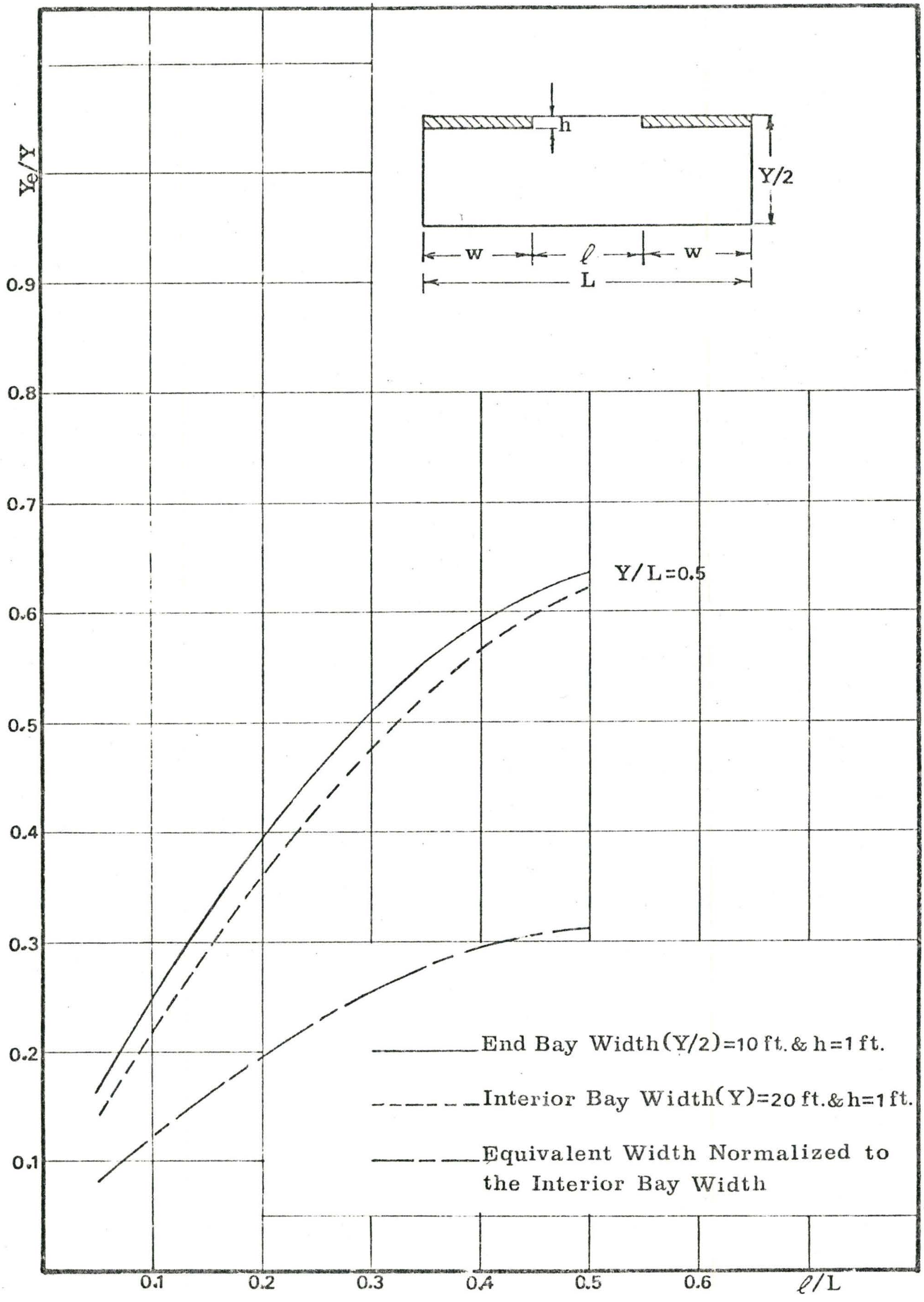

Figure (5.21) Variation of Slab Effective Width with Wall Openings for Interior and End Bay

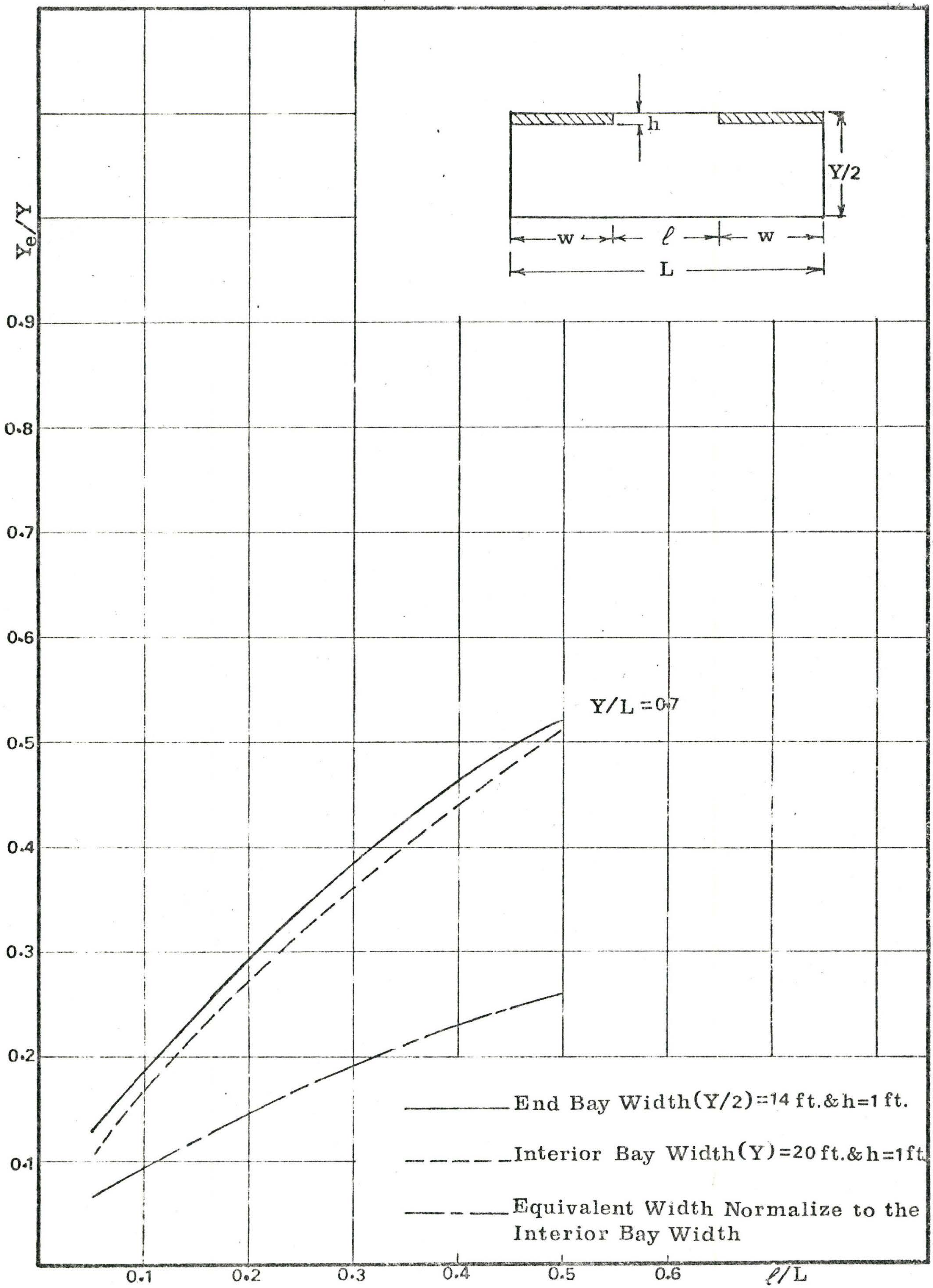

Figure (5.22) Variation of Slab Effective Width with Wall Opening for Interior and End Bays.

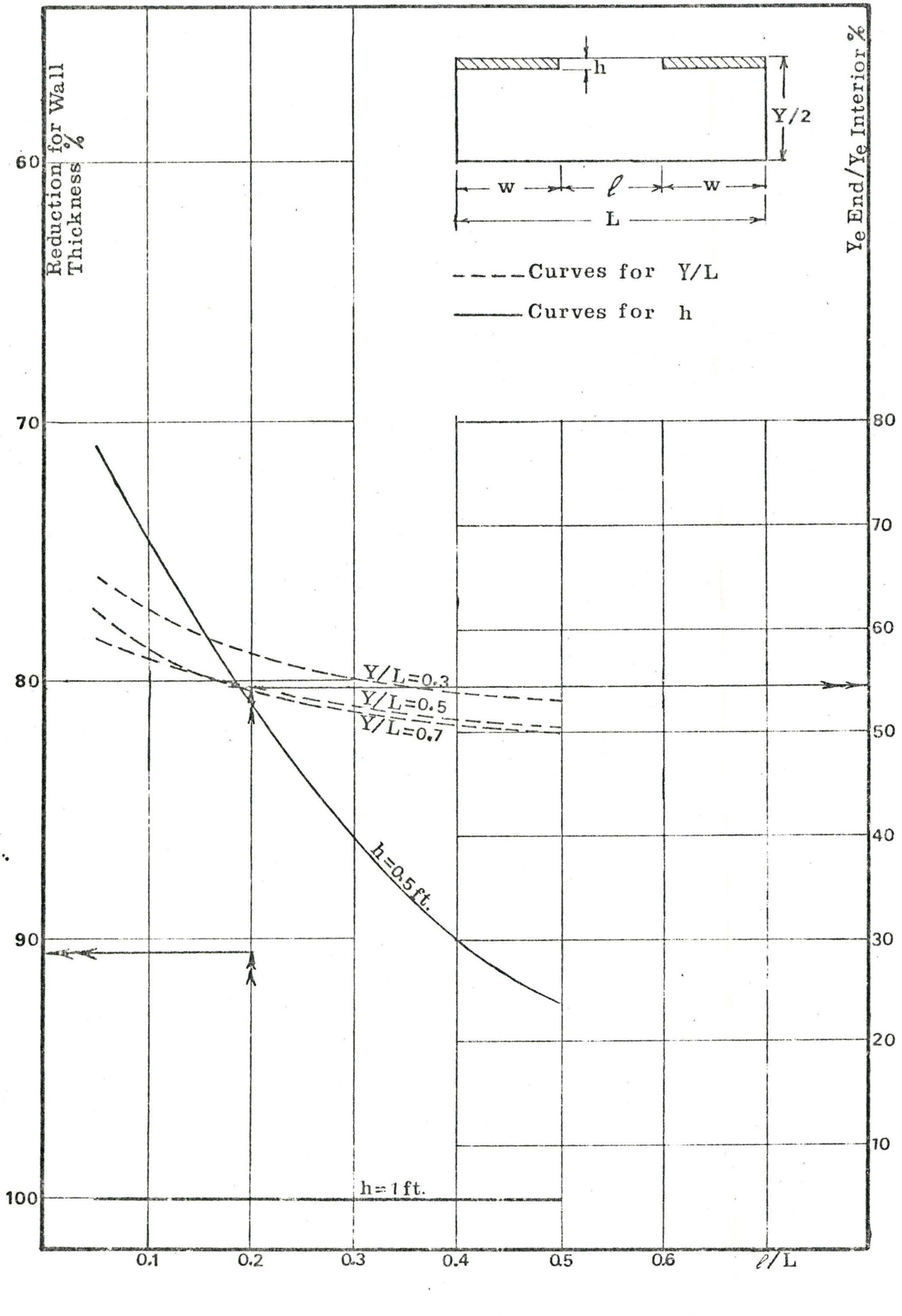

Figure (5.33) Reductions in End Bay Slab Stiffness.

It should be noted that the end bay slab stiffness as a percentage of the interior bay increases as the wall opening decreases. The continuity between the slab along the line of the walls is the main reason for this trend. If the end bay wall opening is small, most of the slab length is fixed in the walls and only a small part between the wall will be free. Therefore the effect for the discontinuity of the slab along the line of the walls is smaller. The effect of the wall thickness on the stiffness of the slab will be discussed at the end of this chapter. Qadeer and Smith [17] have suggested a values of 42 percent of the typical interior bay stiffness can be taken as a reasonably accurate approximation for the stiffness of end shear walls. Again, such underestimation of stiffness is due to the actual thickness of the wall is neglected in their analysis.

An example will be solved to show how these curves can be used to obtain the equivalent beam width and the rotational stiffness of the end bay slab.

5.6.1 Example

Consider a cross wall structure of plan shown in Figure (5.19). The total width of the structure is taken as 40 feet, with the wall opening being 8 feet and the wall spacing 20 feet apart. The intermediate and end bay wall thicknesses are taken as one foot and 0.75 foot, respectively. It is required to obtain the equivalent beam width coupling the end walls and its rotational stiffness.

From Figures (5.3) and (5.4) the effective width and the rotational stiffness of the interior slab are

$$Y_e/Y = 0.36$$

$$R = 49$$

From Figure (5.23), we have the reduction for the wall thickness = 0.906.

The reduction for the end bay = 0.545.

Therefore, the total reduction = 0.545 x 0.906

= 0.494

Thus, the rotational stiffness of the end bay slab is

= 0.494 x 49

= 24.2

The equivalent beam width of the end slab is

= 0.494 x 0.36 x 20

= 3.56 feet

5.7 Relation Between Coupled Shear Wall Openings and Overall Behaviour of Shear Wall Buildings

For coupled shear wall structures, the walls do not act as independent cantilevers due to the coupling action of the slabs or the connecting beams. The method of analysis of such shear wall structures are given in a large number of papers [1, 20]. In such an analysis, a factor denoted by "αH" is commonly used to denote the degree of coupling and is an important parameter to describe the behaviour of coupled shear wall structures. The relation between the wall opening and the factor "αH" will be obtained in this section.

Consider the coupled shear wall structure shown in Figure (5.24). The individual connecting beams of stiffness EI are replaced by an equivalent continuous connecting laminae of stiffness EI $/h_s$ per unit height, where h_s is the storey height. If it is assumed that the connecting beams do not deform axially under the action of the lateral loading, both walls will deflect equally with a point of contraflexure located at the mid-point of each connecting beam. The behaviour of the coupled wall is described by the equation [1, 20]

$$\frac{d^2 T(\bar{x})}{d\,\bar{x}^2} - \alpha^2 \cdot T(\bar{x}) = -\eta\, M_o\, (\bar{x}) \tag{5.17}$$

where

$$T = \int_0^{x_1} -q\,(\bar{x}).d\,\bar{x} \tag{5.18}$$

For two similar walls,

$$\alpha^2 = \eta\,\mu\,(\ell + 2\,e_x) \tag{5.19}$$

$$\eta = \frac{12\,I\,(\ell + 2\,e_x)}{2\,h_s\,\ell^3 \bar{I}} \tag{5.20}$$

$$\mu = 1 + \frac{4\,\bar{I}}{A(\ell + 2\,e_x)^2} \tag{5.21}$$

where

H is the total height of the structure

ℓ is the wall opening

e_x is the distance between the centriod of the cross-section of the wall and its inner edge

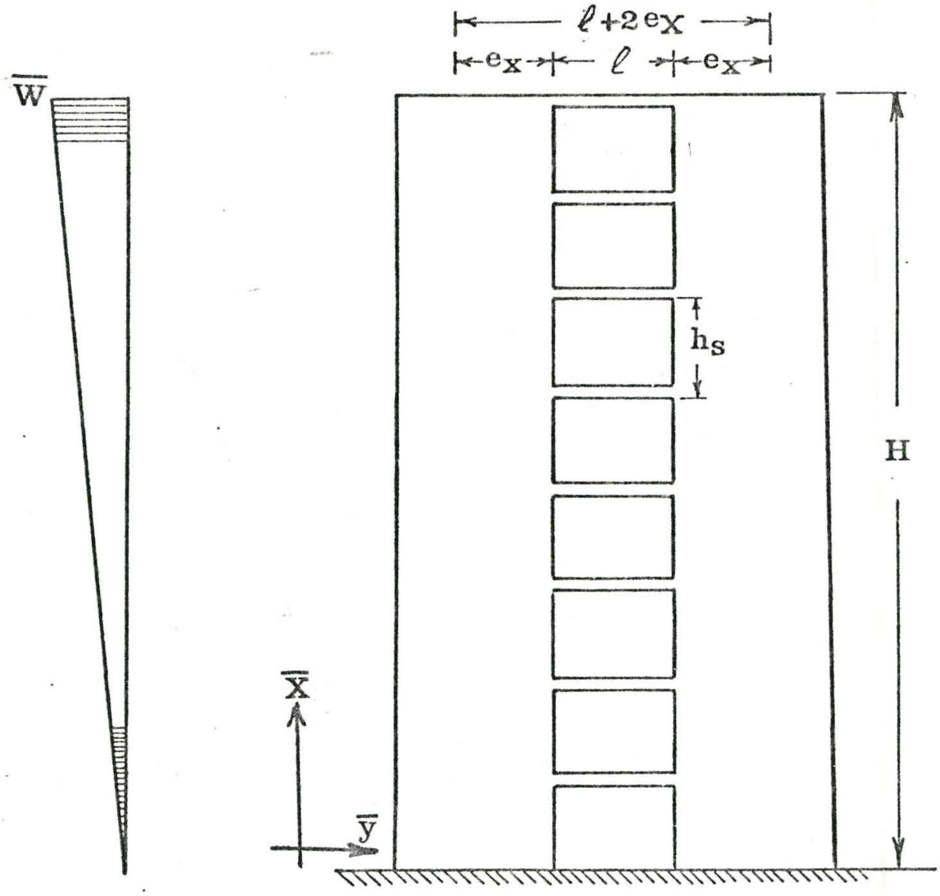

Figure (5.24) Coupled Shear Wall under Lateral Loading.

$\bar{I}$ is the moment of inertia of each wall

A is the cross-section area of each wall

$M_o(\bar{x})$ is the external moment at level $\bar{x}$

T is the integrated shear force in the connecting medium

Substituting Equations (5.20) and (5.21) into Equation (5.19) yields

$$\alpha^2 = \frac{6I\ (\ell+2\ e_x)^2}{h_s\ \ell^3 \bar{I}}\ [1 + \frac{4\bar{I}}{A(\ell+2\ e_x)^2}] \tag{5.22}$$

For the flat slab shear wall structure, the inertia of the connecting beams are

$$I = \frac{Y_e . t^3}{12} \tag{5.23}$$

It can be seen therefore that the factor α^2 is related to the wall opening and also the slab effective stiffness. Substituting Equation (5.23) into Equation (3.19), the non-dimensional rotational stiffness becomes,

$$R = \frac{72\ I\ \ (1-\nu^2)(\ell+\ 2\ e_x)}{t^3 . \ell^3} \tag{5.24}$$

From Equations (5.22) and (5.24) we can also express α^2 as a function of the rotational stiffness as

$$\alpha^2 = \frac{R . t^3}{12(1-\nu^2)} \cdot \frac{1}{h_s . \bar{I}}\ [1 + \frac{4\bar{I}}{A(\ell+2\ e_x)^2}] \tag{5.25}$$

5.7.1 The Parameter "αH" for Coupled Planar Walls

For coupled planar walls, we get

$$e_x = \frac{w}{2} \tag{5.26}$$

$$\bar{I} = \frac{h\ w^3}{12} \tag{5.27}$$

$$A = w.h \tag{5.28}$$

Substituting these values into Equation (5.25) yields

$$\alpha^2 = \frac{R.t^3}{h_s.h\ w^3(1-\nu^2)}\ [1 + \frac{1}{3(1+\ell/w)^2}] \tag{5.29}$$

If the values of t, h, h_s and ν are taken to be 0.667 foot, one foot, 10 feet and 0.15 , respectively, Equation (5.29) can be written as

$$\alpha^2 = V.R \tag{5.30}$$

where V is a variable which depends on the dimensions of the coupled walls and the storey height. Table (5.7) shows the relation between ℓ/L and α for different values of Y/L, while Table (5.8) shows the relations between ℓ/L and αH for different values of H. It should be noted that for the same value of H, the value of αH is insensitive to the change of the slab width Y. Hence, the relation between αH and ℓ/L will be represented by one curve for different slab widths. Figure (5.25) shows this relation for Y/L equals 0.3.

5.7.2 The Parameter "αH" for Coupled T-Section Wall Configurations

For the walls with equal web and flange thicknesses we have

Table (5.7) Relationship between ℓ/L and α for Coupled Planar Walls

ℓ/L	$V\times10^{-6}$	R			α		
		Y/L = .3	Y/L = .5	Y/L = .7	Y/L = .3	Y/L = .5	Y/L = .7
.05	5.5	860	900	1050	.069	.071	.076
.1	6.3	190	225	250	.0346	.0377	.0397
.2	8.3	43	49	52	.0189	.0202	.0208
.3	11.8	20	23	25	.0154	.0165	.0172
.5	30.6	5	9	11.2	.0124	.0166	.0185

Table (5.8) Relationship between ℓ/L and αH for Planar Walls

ℓ/L	αH														
	Y/L = .3					Y/L = .5					Y/L = .7				
	H=100	H=150	H=200	H=250	H=300	H=100	H=150	H=200	H=250	H=300	H=100	H=150	H=200	H=250	H=300
.05	6.9	10.3	13.8	17.2	20.7	7.1	10.6	14.2	17.7	21.3	7.6	11.4	15.2	19	22.8
.1	3.46	5.2	6.9	8.7	10.4	3.77	5.5	7.5	9.45	11.3	3.97	5.9	7.9	9.9	11.9
.2	1.89	2.85	3.7	4.7	5.7	2	3	4	5	6	2.1	3.15	4.2	5.25	6.3
.3	1.54	2.3	3.1	3.85	4.7	1.65	2.45	3.3	4.1	4.9	1.7	2.55	3.4	4.25	5.1
.5	1.24	1.86	2.5	3.1	3.7	1.66	2.5	3.3	4.15	5	1.8	2.7	3.6	4.5	5.4

$$e_x = \frac{w^2 - h^2 + zh}{2(z+w-h)} \quad (5.31)$$

and

$$\bar{I} = [\frac{h}{12}(w-h)^3 + h(w-h)(\frac{w+h}{2} - e_x)^2 + \frac{zh^3}{12} + zh(e_x - \frac{h}{2})^2] \quad (5.32)$$

For the same values of h, t, h_s and ν mentioned before, and using Equation (5.31), Equation (5.25) can be written as

$$\alpha^2 = \frac{V_1}{\bar{I}} .R \quad (5.33)$$

where V_1 is a variable which depends on the wall and the slab dimensions.

Table (5.9) shows the different values of α for each ℓ/L and Y/L. Table (5.10) shows the relationship between ℓ/L and αH for different values of z/L and H. It is also noticed that the parameter "αH" is insensitive to the change of the slab width. Figures (5.26) and (5.27) show the relations between "αH" and ℓ/L for a value of Y/L equals 0.3 and the flange width ratio z/L equals 0.1 and 0.2 respectively.

5.7.3 Corrections for h, t, and h_s

The previous curves of "αH" are obtained for the specific values of slab thickness, wall thickness and floor height. If other values for the slab thickness, wall thickness and floor height are used, the value of "αH" can be modified. The parameter α^2 is directly proportional to t^3 and inversely proportional to the storey height h_s. It is approximately inversely proportional to the wall thickness h. The parameter α can thus be written as

Table (5.9) Relations between ℓ/L and α for T-section Wall Configuration

ℓ/L	$\bar{I}$	V_1	R			α			$\frac{Z}{L}$
			Y/L = .3	Y/L = .5	Y/L = .7	Y/L = .3	Y/L = .5	Y/L = .7	
.05	779.53	1.404	1300	1370	1400	.077	.079	.08	.1
.1	668.3	1.336	260	300	330	.036	.0386	.0405	
.2	481.6	1.216	46	54	60	.0175	.0184	.0194	
.3	340.7	1.08	18	22.6	25	.0114	.0134	.0141	
.5	128.4	1.0254	6	8.2	9.6	.0117	.0127	.0127	
.05	985.17	1.58	1550	1640	1720	.079	.081	.083	.2
.1	851.67	1.46	280	301	320	.0348	.036	.0371	
.2	616.17	1.28	49	58.1	62	.016	.0174	.018	
.3	426.37	1.17	18.5	23.6	26	.0112	.0127	.0133	
.5	166.97	1.057	5.8	8.5	10	.0096	.0116	.0126	

Table (5.10) Relations between ℓ/L and αH for T-section Wall Configurations

ℓ/L	Z/L	αH														
		Y/L = .3					Y/L = .5					Y/L = .7				
		H=100	H=150	H=200	H=250	H=300	H=100	H=150	H=200	H=250	H=300	H=100	H=150	H=200	H=250	H=300
05 .01	.1	7.7	11.6	15.4	19.2	23.1	7.9	11.8	15.8	19.7	23.7	8	12	16	20	24
.1		3.6	5.4	7.2	9	10.8	3.86	5.8	7.72	9.6	11.58	4.05	6.1	8.1	10.1	12.15
.2		1.75	2.62	3.5	4.86	5.25	1.84	2.76	3.68	4.6	5.52	1.94	2.9	3.88	4.85	5.82
.3		1.14	1.71	2.28	2.85	3.42	1.34	2.	2.68	3.35	4.02	1.41	2.1	2.82	3.52	4.23
.5		1.17	1.76	2.34	2.92	3.51	1.27	1.9	2.54	3.17	3.81	1.27	1.9	2.54	3.17	3.88
.05	.2	7.9	11.8	15.8	19.7	23.7	8.1	12.2	16.2	20.2	24.3	8.3	12.4	16.6	20.7	24.9
.1		3.48	5.2	6.96	8.7	10.44	3.6	5.4	7.2	9	10.8	3.71	5.55	7.42	9.3	11.13
.2		1.6	2.4	3.2	4	4.8	1.74	2.6	3.48	4.35	5.22	1.8	2.7	3.6	4.5	5.4
.3		1.12	1.68	2.24	2.8	3.36	1.27	1.9	2.54	3.16	3.81	1.33	2	2.66	3.3	3.99
.5		.96	1.47	1.92	2.4	2.88	1.16	1.74	2.32	2.9	3.48	1.26	1.89	2.52	3.15	3.78

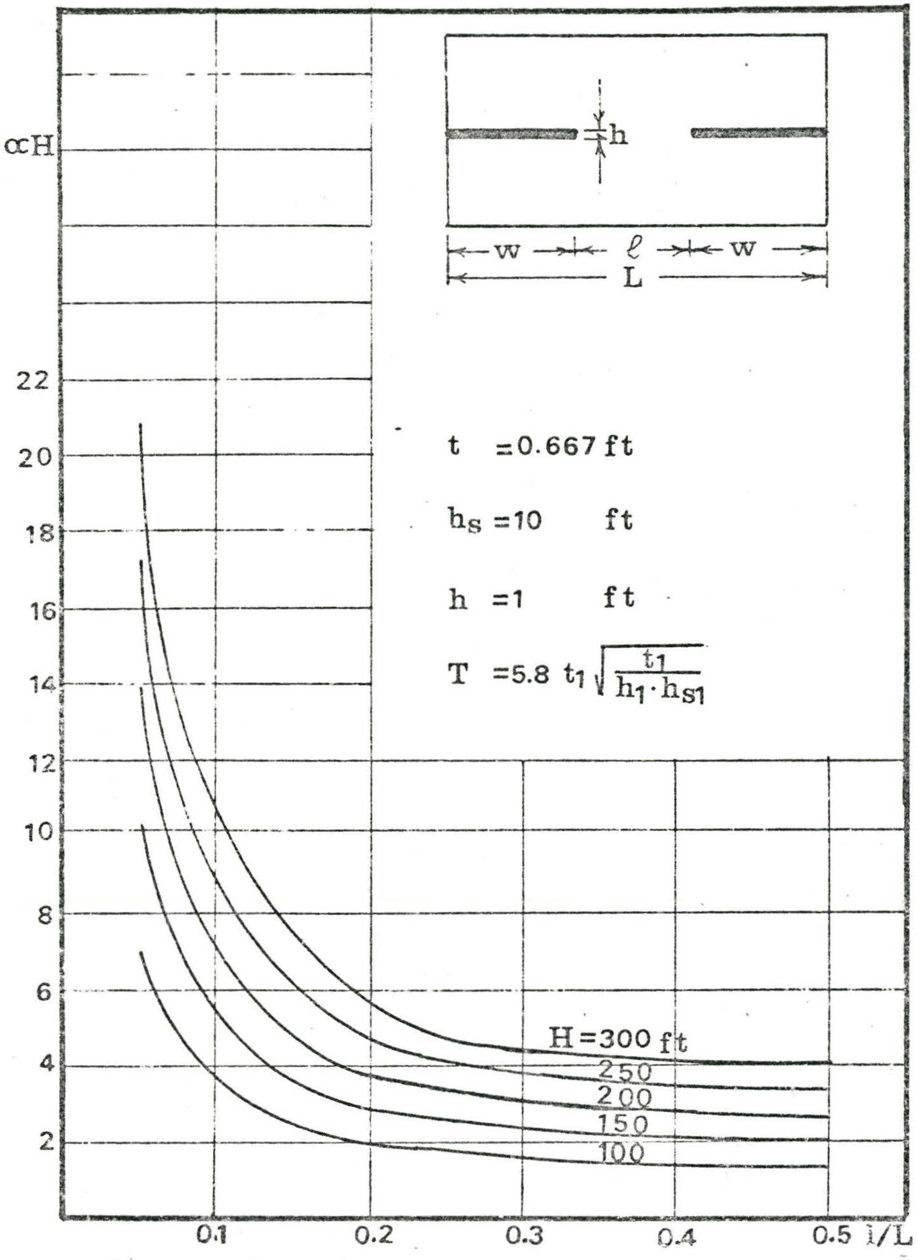

Figure (5.25) Variation of αH with Wall Openings.

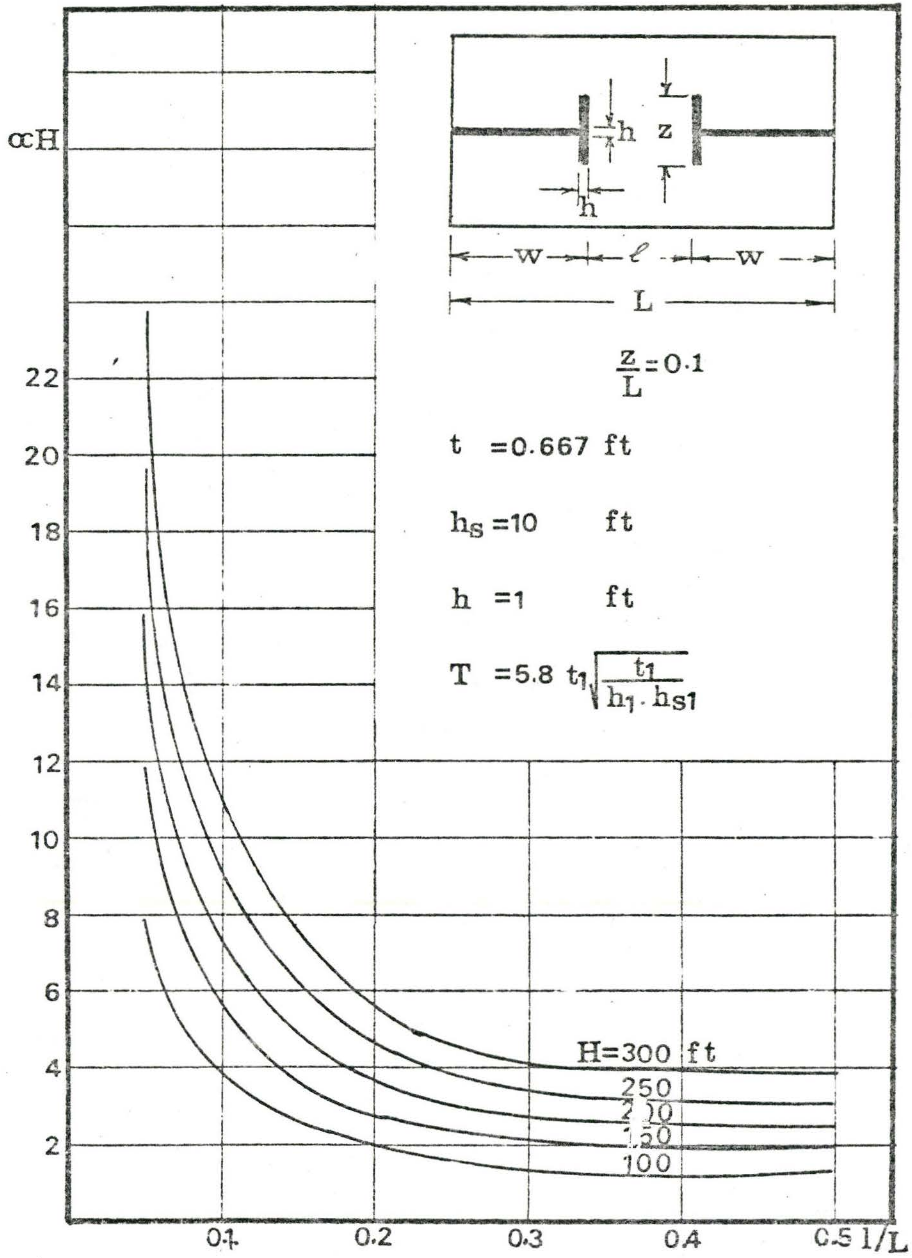

Figure (5.26) Variation of αH with Wall Opening.

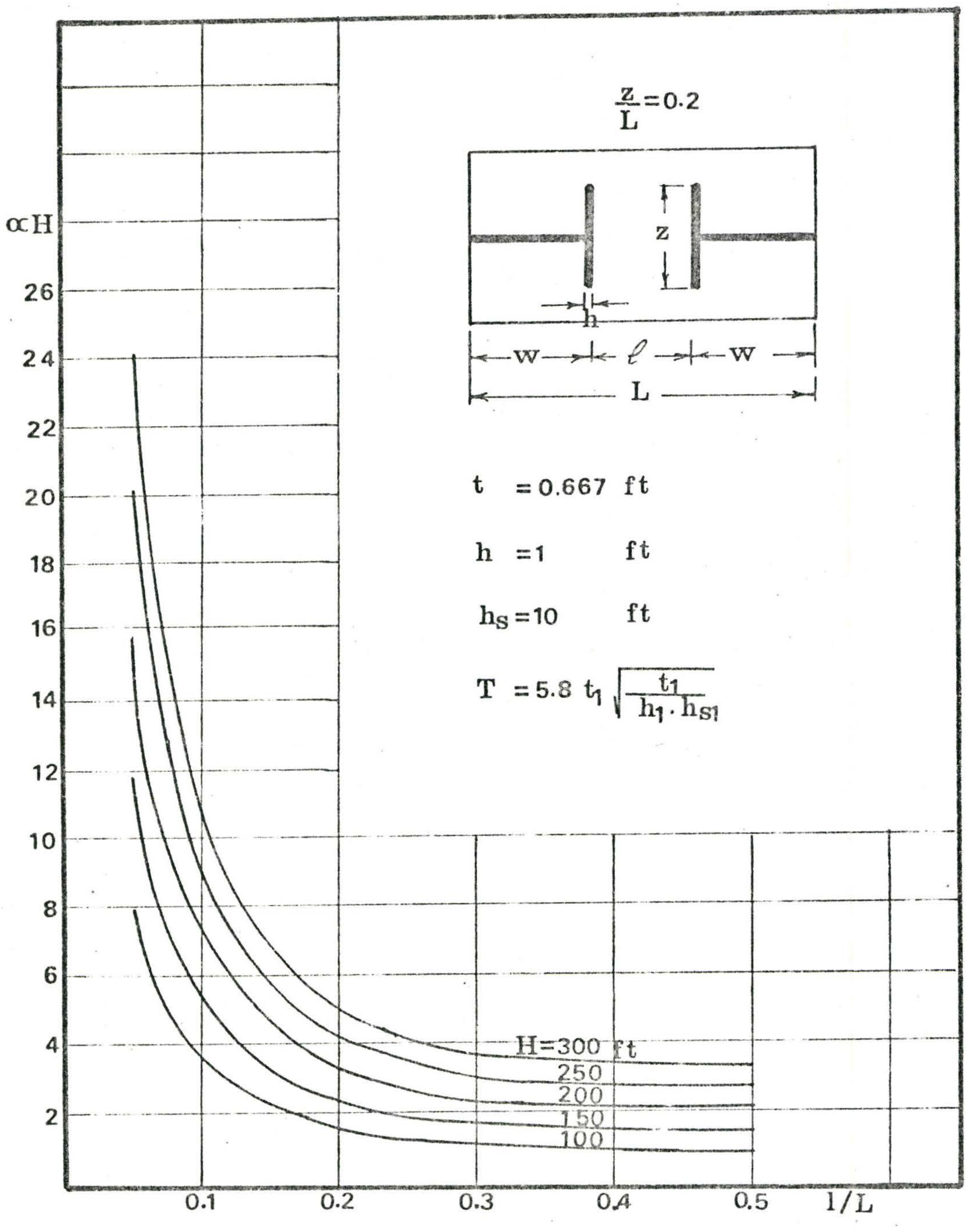

Figure (5.27) Variation of αH with Wall Openings.

$$\alpha = \psi . t \sqrt{\frac{t}{h_s \cdot h}} \tag{5.34}$$

where ψ is defined from Equation (5.25). If the values of t, h and h_s are changed to t_1, h_1 and h_{s1}, respectively, the value of α will be changed to α_1, where

$$\alpha_1 = \psi . \; t_1 \sqrt{\frac{t_1}{h_{s1} \cdot h_1}} \tag{5.35}$$

and

$$\frac{\alpha_1}{\alpha} = \frac{t_1}{t} \; . \; \sqrt{\frac{t_1 . h_s . h}{t . h_{s1} . h_1}} \tag{5.36}$$

Substituting for t, h and h_s with the previous values used, we have

$$\alpha_1 = 5.8 \; t_1 . \sqrt{\frac{t_1}{h_1 . h_{s1}}} . \alpha \tag{5.37}$$

Equation (5.37) gives the correction necessary if different values of wall thickness, slab thickness, or floor height are used.

5.8 Discussion of the Results

The aim of this study is to obtain a set of design curves to represent the effective width and the stiffness of the different slabs coupled shear walls. The finite element technique was used to obtain the design curves. It is useful to discuss the following points to gain further insight into the problem.

1. The effect of point of contraflexure location on the slab stiffness.

2. The slab reactions at shear wall support due to wall rotation.
3. The effect of wall thickness on the coupling slab stiffness.
4. The effect of the flange of the T-section wall on the slab stiffness, and the effect of local bending on the flange deformation.
5. The effect of the slab width on the slab stiffness.
6. The effect of the wall openings on the overall behaviour of the structure.

5.8.1 The Effect of Point of Contraflexure Location on the Slab Stiffness

If the two shear walls are of the same cross-section, the point of contraflexure will be located at the middle of the coupling beam. If the two walls have different moments of inertia, the point of contraflexure is no longer at the mid-point of the connecting beam. In section 3.4.2 the slab stiffness is obtained considering the point of contraflexure to be at its actual position. In this section the point of contraflexure location will be assumed at the mid-length of the connecting beam to calculate the slab stiffness. A comparison of the two cases will show the effect of shifting the position of the point of contraflexure on the slab stiffness.

As shown in Figure (5.28(a)), the point of contra-flexure is assumed to be at the middle of the connecting beam in the case of the planar wall coupled with the T-section wall

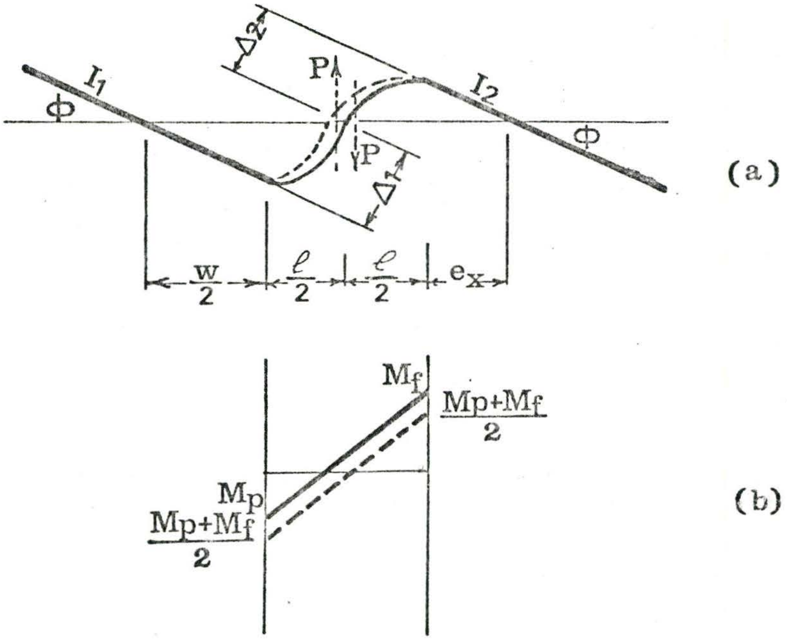

Figure (5.28) Exact and Approximate Positions of Point of Contraflexure.

configuration. The force P which causes relative displacement Δ between the two walls will appear if a cut is made at the assumed point of contraflexure. The rotational moment at the centroid of the cross-section of the planar wall M'_p, becomes

$$M'_p = P\left(\frac{\ell}{2} + \frac{W}{2}\right) \tag{5.38}$$

The moment acting at the centroid of the cross-section of the T-section wall M'_f , becomes

$$M'_f = P\left(\frac{\ell}{2} + e_x\right) \tag{5.39}$$

From Figure (5.28)

$$\frac{\Delta 1}{\Delta 2} = \frac{\ell + W}{\ell + 2\, e_x}$$

and

$$\phi = \frac{\Delta 2}{\ell/2 + e_x} \tag{5.40}$$

or

$$\phi = \frac{\Delta}{\ell + \frac{W}{2} + e_x} \tag{5.41}$$

Therefore, the non-dimensional approximate rotational stiffness of the slab at the centroid of the planar wall R'_p will be

$$R'_p = \frac{P}{2\bar{D}.\Delta}\,(\ell + W)\left(\ell + \frac{W}{2} + e_x\right) \tag{5.42}$$

From Equations (3.31) and (5.42), the ratio between the exact and the approximate rotational stiffness at the centroid of the planar wall becomes

$$\frac{R_p}{R'_p} = \frac{[2\ell/(1+I_2/I_1)]+w}{\ell+w} \tag{5.43}$$

In a similar way the ratio between the exact and the approximate non-dimensional rotational stiffness at the centroid of the T-section wall becomes

$$\frac{R_f}{R'_f} = \frac{[2\ell/(1+I_1/I_2)]+2\ e_x}{\ell + 2\ e_x} \tag{5.44}$$

Using Equations (5.4) and (5.11), Equations (5.43) and (5.44) can be written as

$$\frac{R_p}{R'_p} = \frac{(1+3\ell/L)+(1-\ell/L)(I_2/I_1)}{(1+\ell/L)(1+I_2/I_1)} \tag{5.45}$$

$$\frac{R_f}{R'_f} = \frac{(2\ell/L)+\gamma(1-\ell/L)(1+I_1/I_2)}{[\ell/L+\gamma(1-\ell/L)](1+I_1/I_2)} \tag{5.46}$$

Plotted in Figure (5.29) are the values of R_p/R'_p for the inertia ratio ranging between 1.0 and 2.0 and ℓ/L changing from 0.05 to 0.5. Also plotted in Figures (5.30(a)) through (5.30(d)), the relations between R_f/R'_f for the same range of I_2/I_1 and ℓ/L, and for the parameter γ changing from 0.2 to 0.8.

As shown in Figure (5.29), all the values of R_p/R'_p are less than unity. This indicates an over-estimation for the approximate stiffness of the slab at the centriod of the cross-section of the planar wall. However,

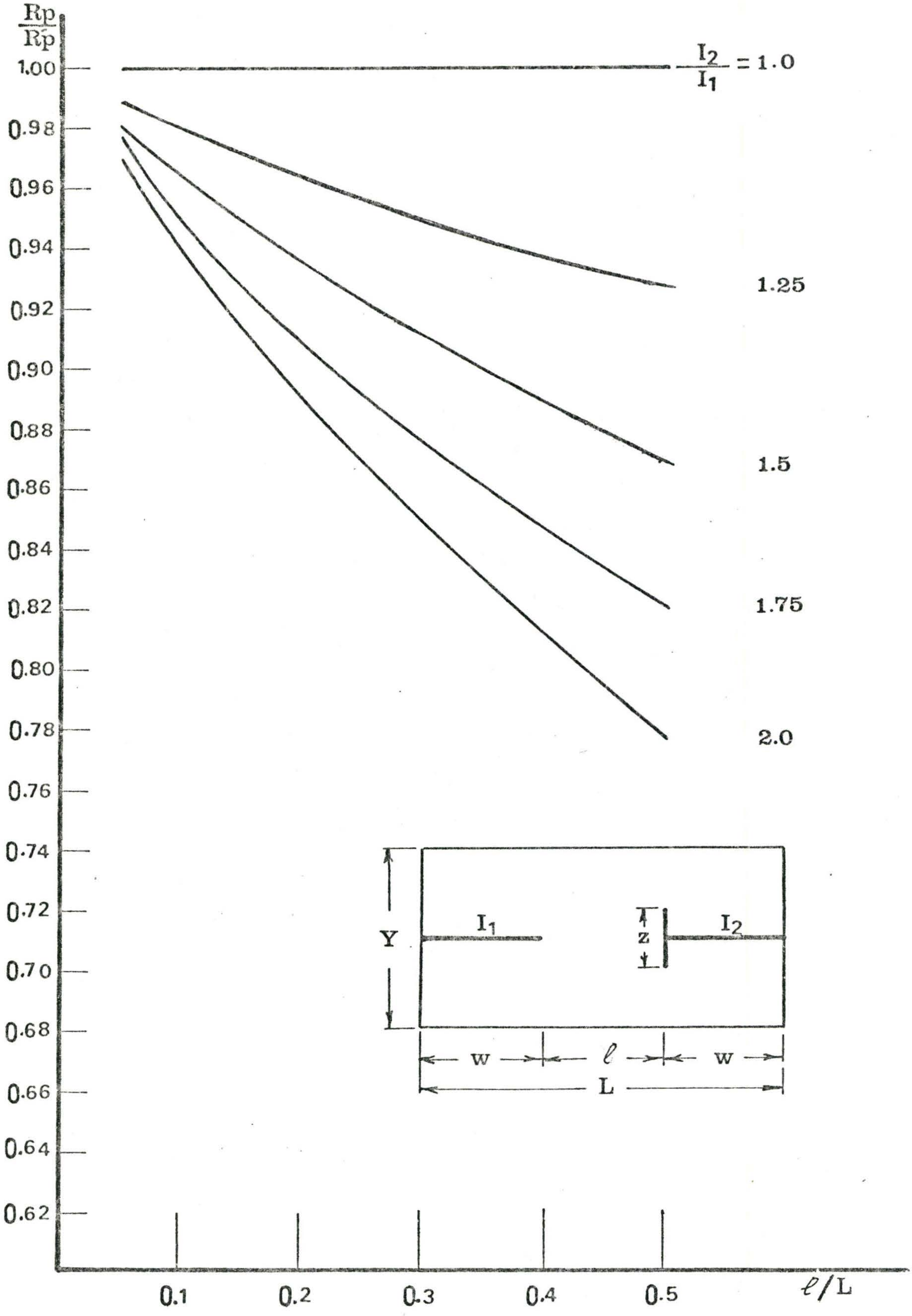

Figure (5.29) Variation of R_p/R'_p with the wall Opening and the Inertia Ratio.

for ℓ/L less than 0.2, the difference in the slab stiffness less than 9%. From the designer's point of view, such a difference is negligible.

From the previous discussion it is expected that the stiffness at the centroid of the T-section wall will be underestimated. Such an underestimation is shown in Figures (5.30(a)) through (5.30(d)). Again, for small wall openings, the error is sufficiently small to be neglected.

It is interesting to note that the effect of the relative inertias of the wall on the point of contraflexure location was discussed by MacLeod [15]. The variation of the stiffness of the connecting beam was not included in his analysis. It is concluded from the previous discussion that both the connecting beam stiffness and the relative inertias of the walls will affect the point of contraflexure location. For the small wall openings ($\ell/L \leq 0.2$) the variation of the point of contraflexure location can be neglected, and the assumption that it is located at mid-length of the connecting beam is sufficiently accurate.

5.8.2 The Slab Reaction at the Shear Wall Support

Figure (5.31) shows the distribution of the slab reaction along the walls due to an applied rotation of the walls. It is observed that the loads developed in the plane of the wall are concentrated at the inner edge. The concentration of the loads at the inner edge of the wall is rapidly decreased by increasing the wall opening. Local deformation

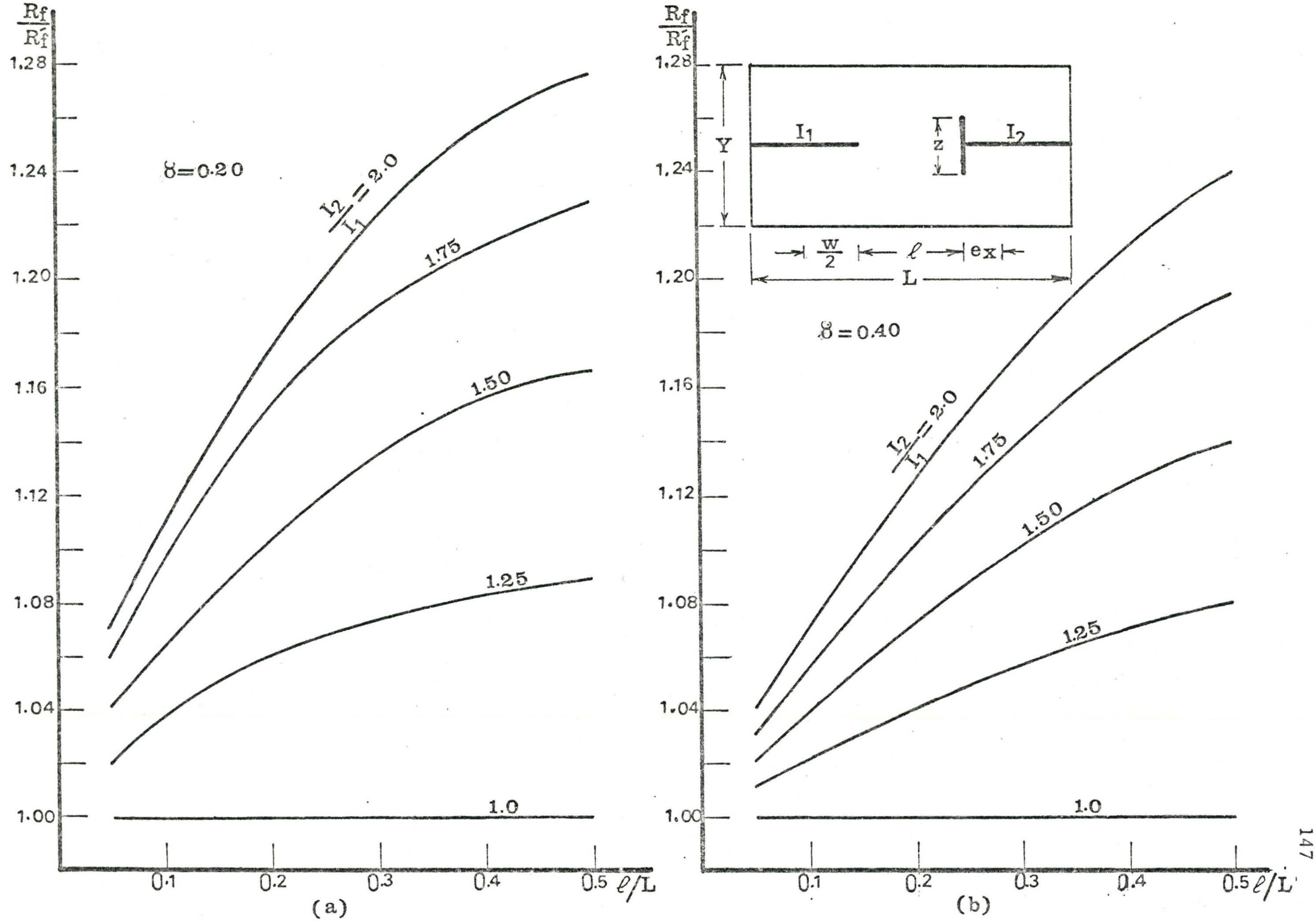

Figure (5.30) Variation of R_f/R'_f with Wall Opening and the Inertia Ratio.

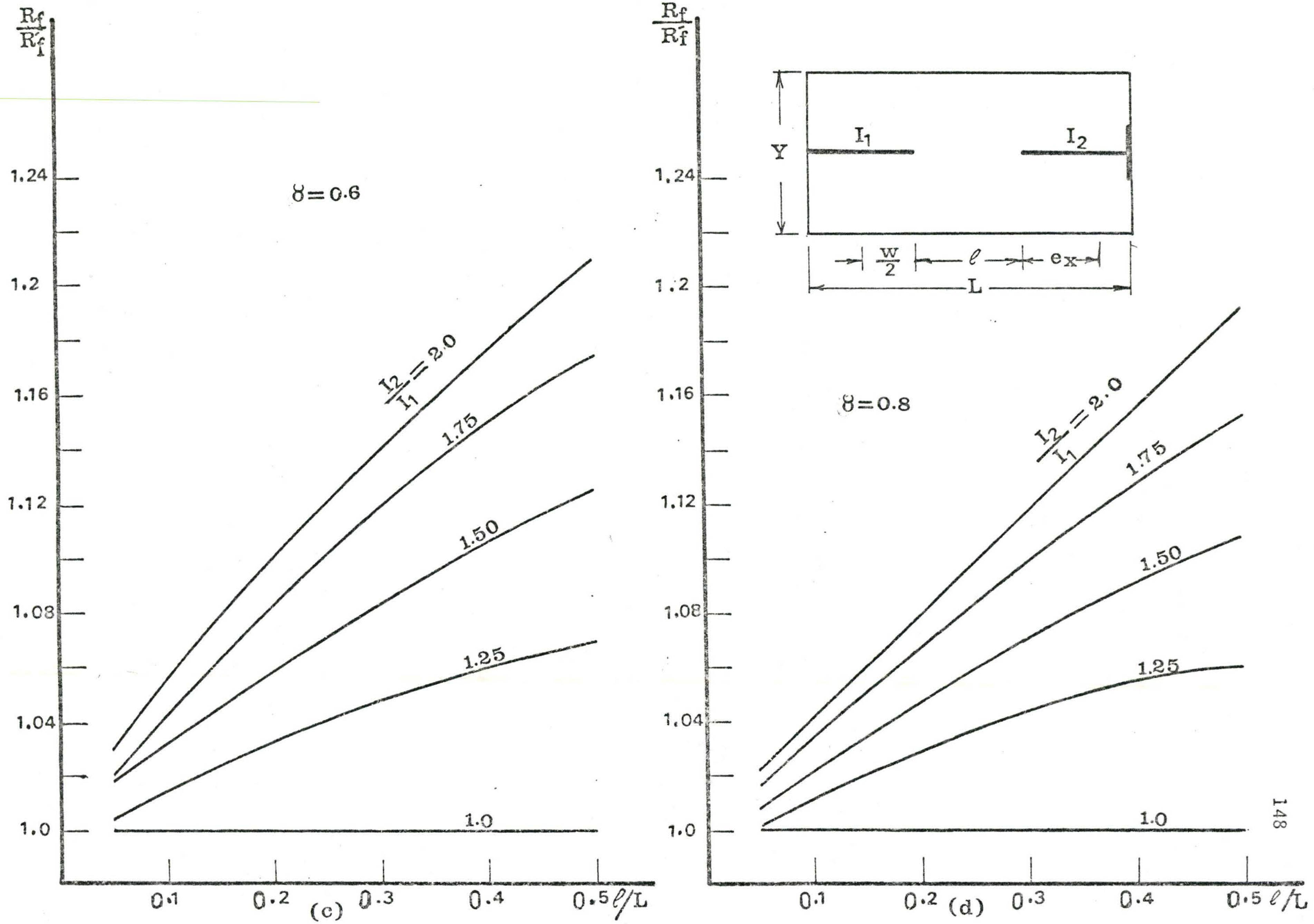

Figure (5.30) Variation of R_f/R'_f with Wall Opening and the Inertia Ratio.

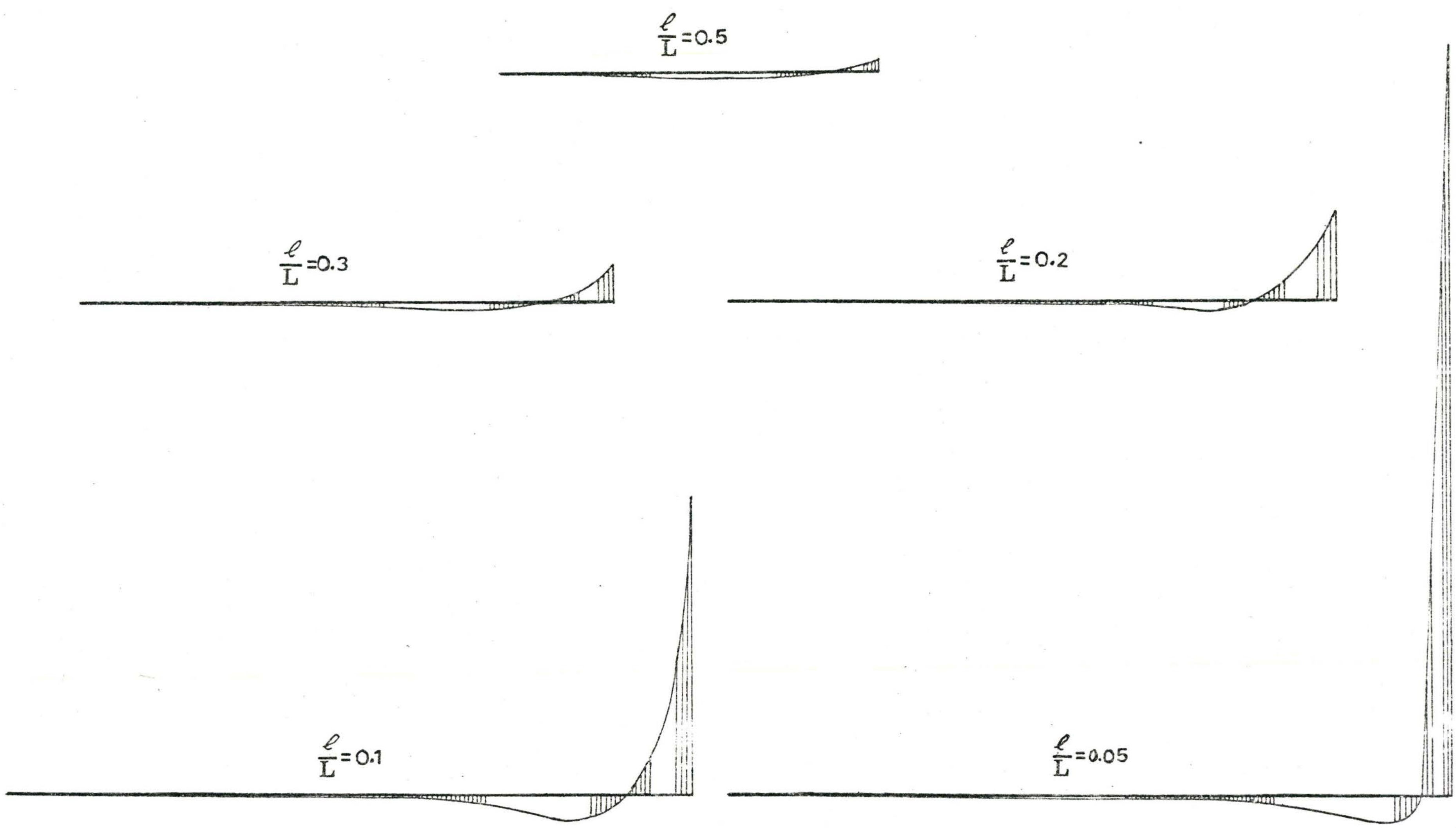

Figure (5.31) Slab Reaction at the Shear Wall Support for Different Wall Openings.

can be expected at the inner edges of the wall. Some more theoretical and experimental studies are needed to properly take into account such a force distribution in the walls.

5.8.3 The Effect of Planar Wall Thickness on the Slab Stiffness

Figure (5.32) shows the actual distribution of the moments along the slab in both directions due to an applied wall rotation [18]. Figure (5.33) shows a diagrammatic sketch for the stress distribution across the slab width for different wall openings. It is obvious that, for small wall openings ($\ell/L \leq 0.2$) the central width of the slab, which equals the wall thickness, is highly stressed while the stresses decrease rapidly away from the walls, as shown in Figure (5.33(a)). For larger wall openings, the stresses are approximately uniformly distributed across the slab width. If the wall thickness is neglected, the stress distribution will have the shapes as shown in Figures (5.33(e)) and (5.33(f)). The effective width of the beam Y_e can be considered a measure of the highly stressed area described in Figure (5.33). Comparing Figures (5.33(a)) and (5.33(e)), it is obvious that the area of the slab bounded by the walls is highly stressed and hence lends considerable stiffness to the system. Therefore, for small wall openings, the effect of the finite wall thickness is important and cannot be neglected. For larger wall openings, the stress is more uniformly distributed and hence, the effect of neglecting the wall thickness is less significant.

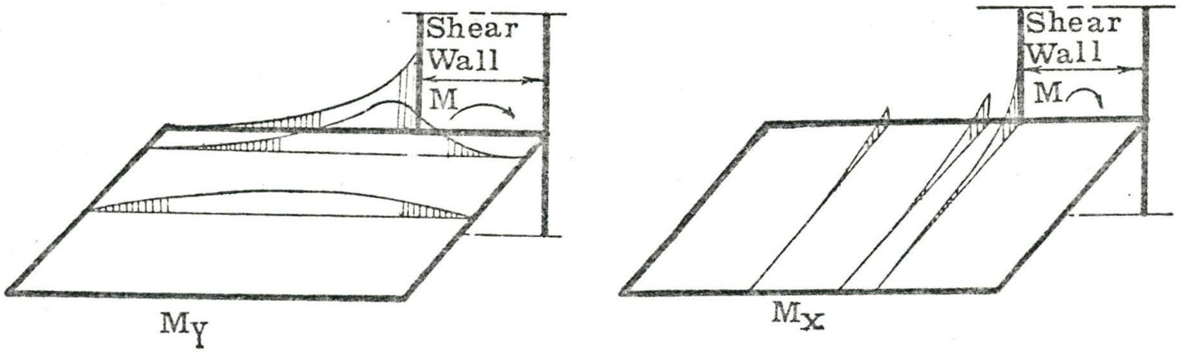

Figure (5.32) Distribution of Moments Along the Slab Due to Wall Rotation.

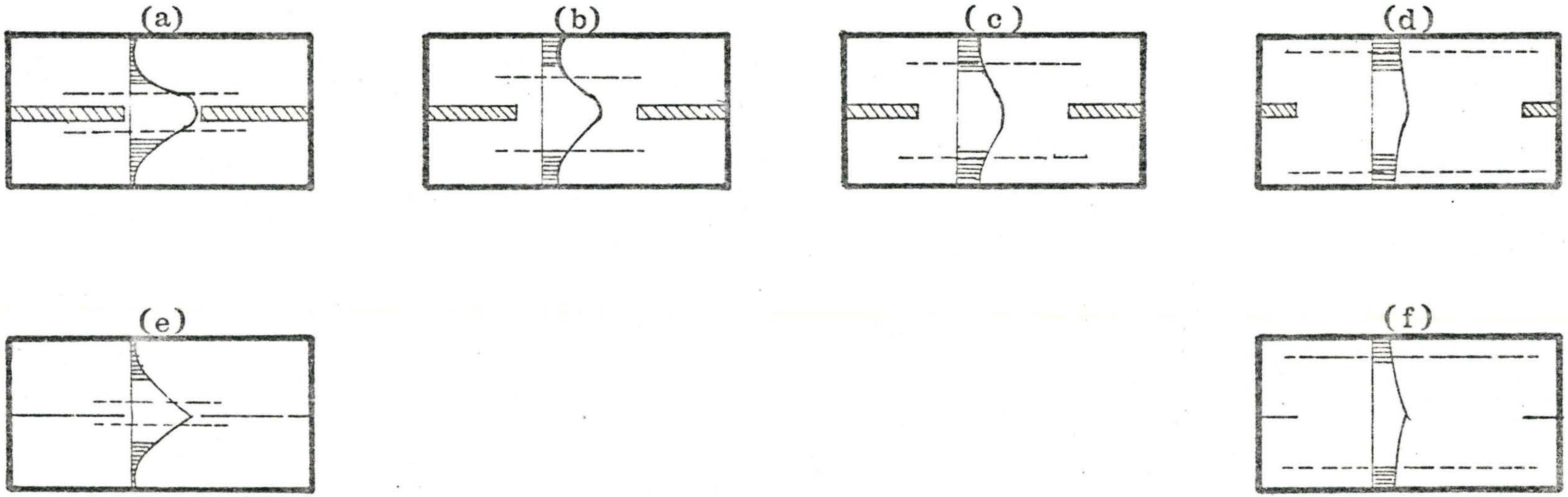

Figure (5.33) Distribution of Stress Across the Slab Width Due to Wall Rotation.

5.8.4 Flange Width of the T-Section Wall and Effect of Local Bending Deformation of Walls

A comparison between Figures (5.3), (5.6) and (5.9) indicates that the slab effective width is increased by using a T-section wall configuration instead of a planar wall configuration. At the same time, the effective slab width is increased by increasing the flange width for the same wall opening. However, it should be realized that if the flange width becomes too large, the end moments in the slab will induce local bending deformation at the flanges. Since the design curves are computed based on the assumption of negligible local deformation of the walls, the computed stiffness value will lead to an overestimated value and the effective width obtained should be reduced to reflect the possibility of local deformation of flanges. For small flange widths, the local bending deformation will be sufficiently small to be neglected. Therefore, the design curves obtained can be directly used. As the width of the flange is increased, the reduction in the stiffness due to local bending of the flange can be accounted for by using a reduced flange width for the T-section in computing the true stiffness of the system.

One way of obtaining this reduced section is to compare the available experimental results with the corresponding theoretical values. Coull and El-hag [9] carried out some tests for coupled T-section wall configurations. Table (5.11) shows the dimensions of the slab and the walls used in the test. The same wall and slab configurations are solved by the

Table (5.11) Dimensions of the Slabs and Walls Used by Coull and El-hag [9].

w/Y	Z/Y	ℓ/L	W	Z	ℓ	Y
.3	.5	.25	3.6	6	2.4	12
		.4			4.8	12
		.5			7.2	12
.5	.5	.1625	6	6	2.4	12
		.2875			4.84	12
		.375			7.2	12
.5	.3	.1625	6	3.6	2.4	12
		.2875			4.84	12
		.375			7.2	12
.3	.3	.25	3.6	3.6	2.4	12
		.4			4.8	12
		.5			7.2	12

finite element method. Two computations are carried out. In the first calculation, the full width of the flange is used, while only half the flange width is used in the second calculation. The results of the calculations together with the experimental results are plotted in Figures (5.34) through (5.37) for the two T-section wall configurations. Similar plots are presented in Figures (5.38) through (5.41) for the configuration consisting of a planar wall and a T-section wall.

From these figures it is clear that if the flange width is halved, good agreement between the theoretical and the experimental results can be obtained. Therefore, it is suggested that to allow for local bending of the flanges, a reduction of the flange width to half of its value may be used in conjunction with the design curves presented for the coupled T-section wall configurations and the coupled planar wall T-section wall configurations.

5.8.5 The Effect of the Slab Width on the Slab Stiffness

In order to study the effect of the slab width Y on the stiffness of the system, the equivalent beam width will be normalized to the total length instead of the width of the slab, i.e., we shall use the parameter Y_e/L instead of Y_e/Y as a variable.

$$Y_e/L = (Y_e/Y)(Y/L) \tag{5.47}$$

The values of Y_e/L are obtained for each value of Y/L and ℓ/L

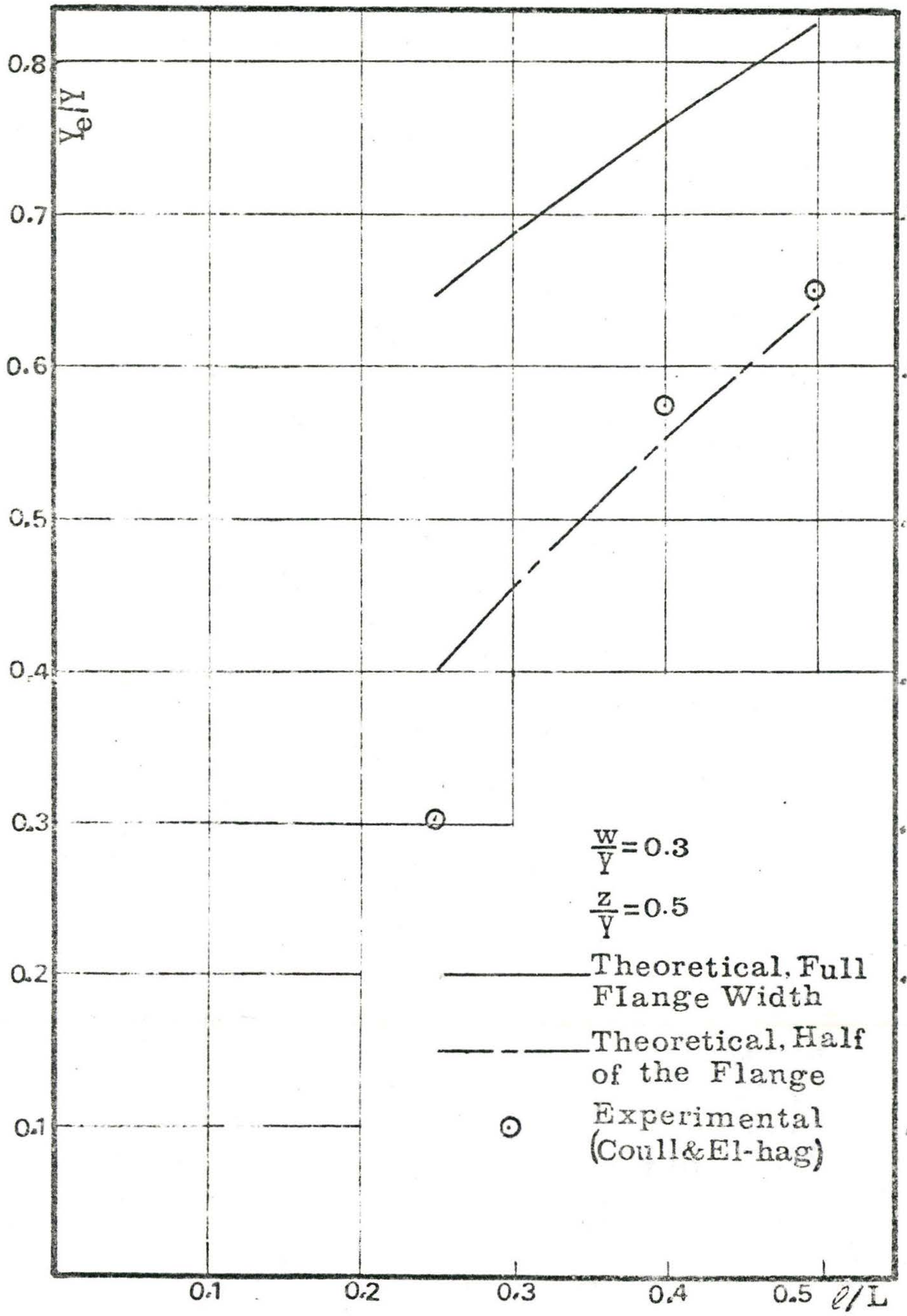

Figure (5.34)

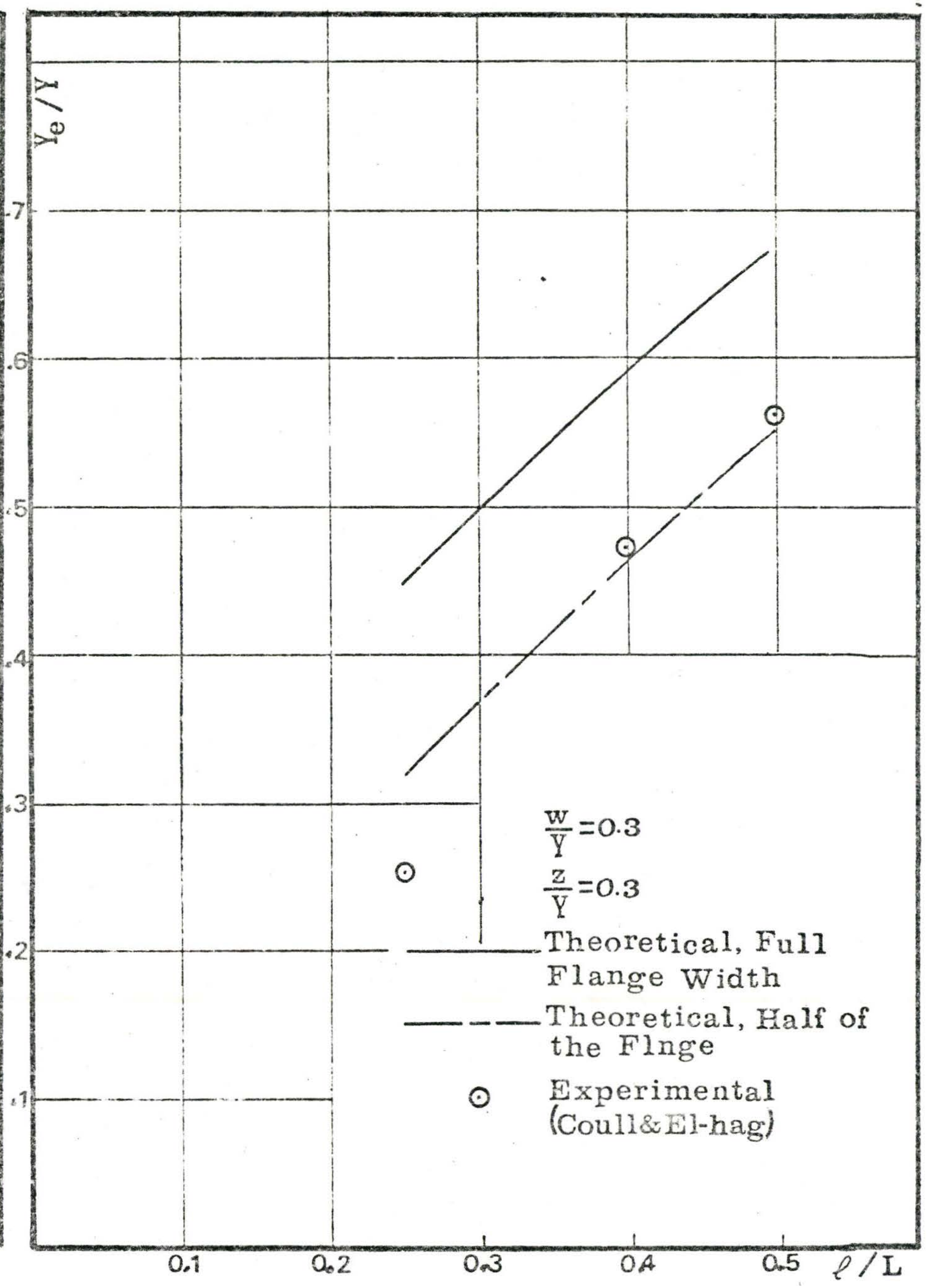

Figure (5.35)

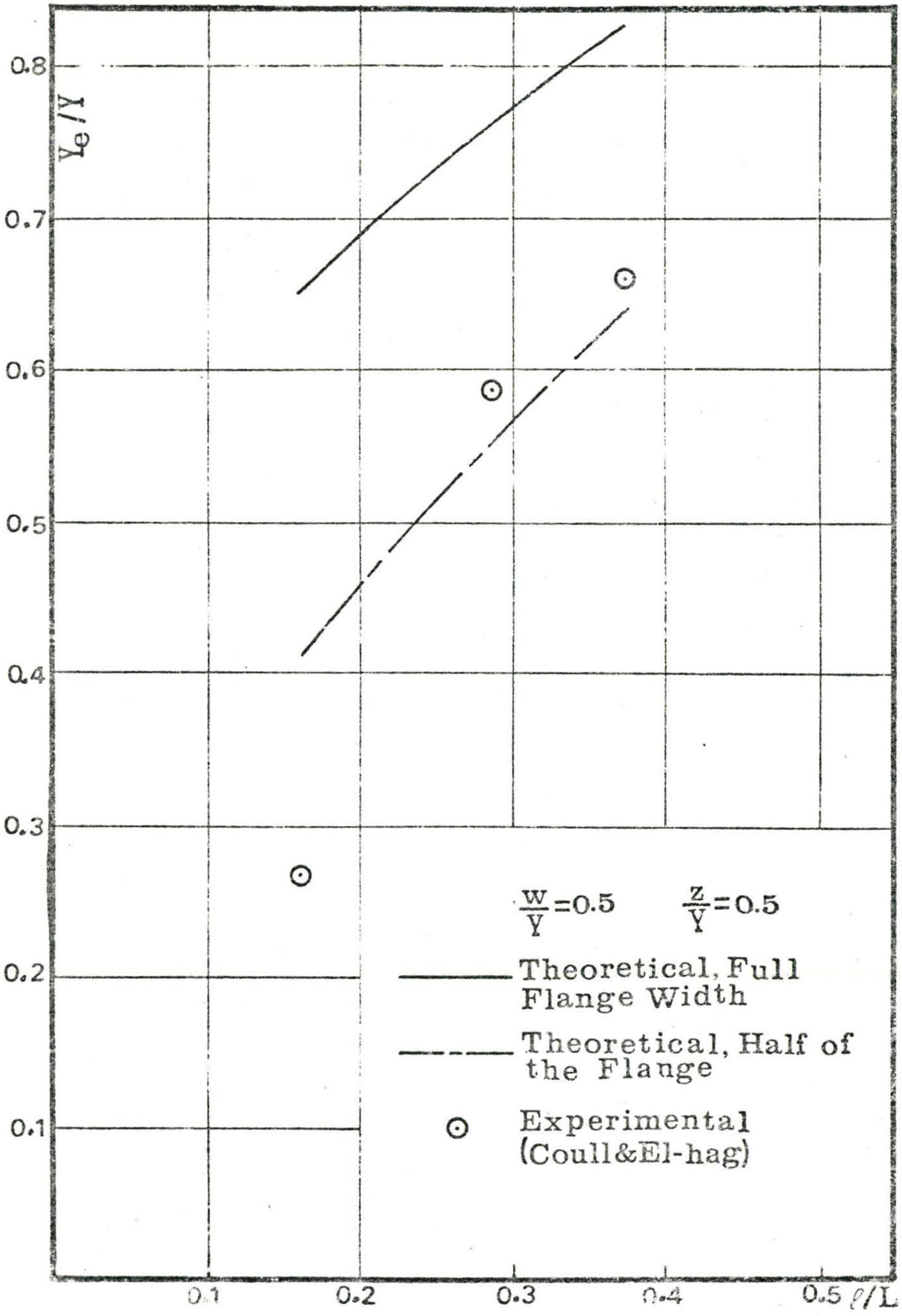

Figure (5.36)

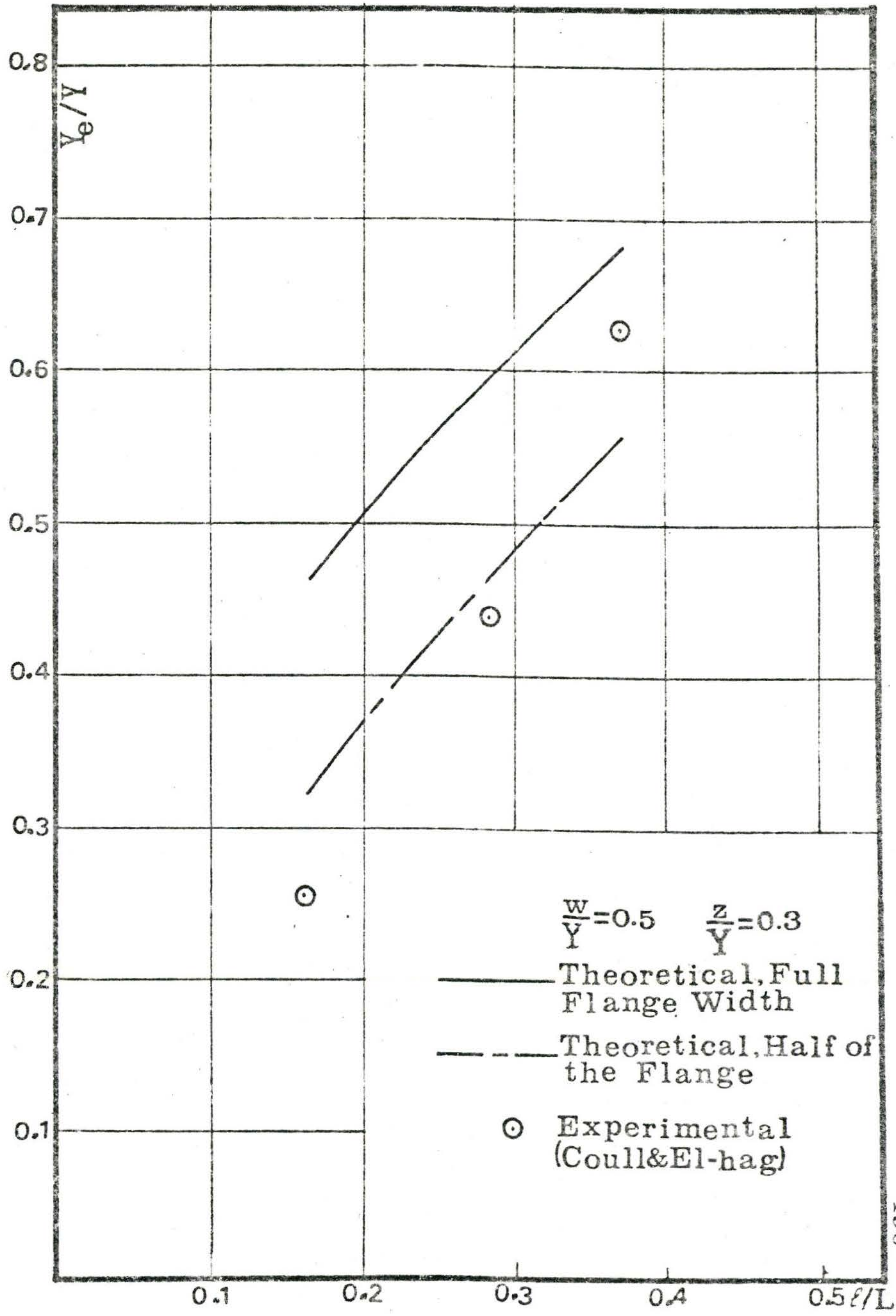

Figure (5.37)

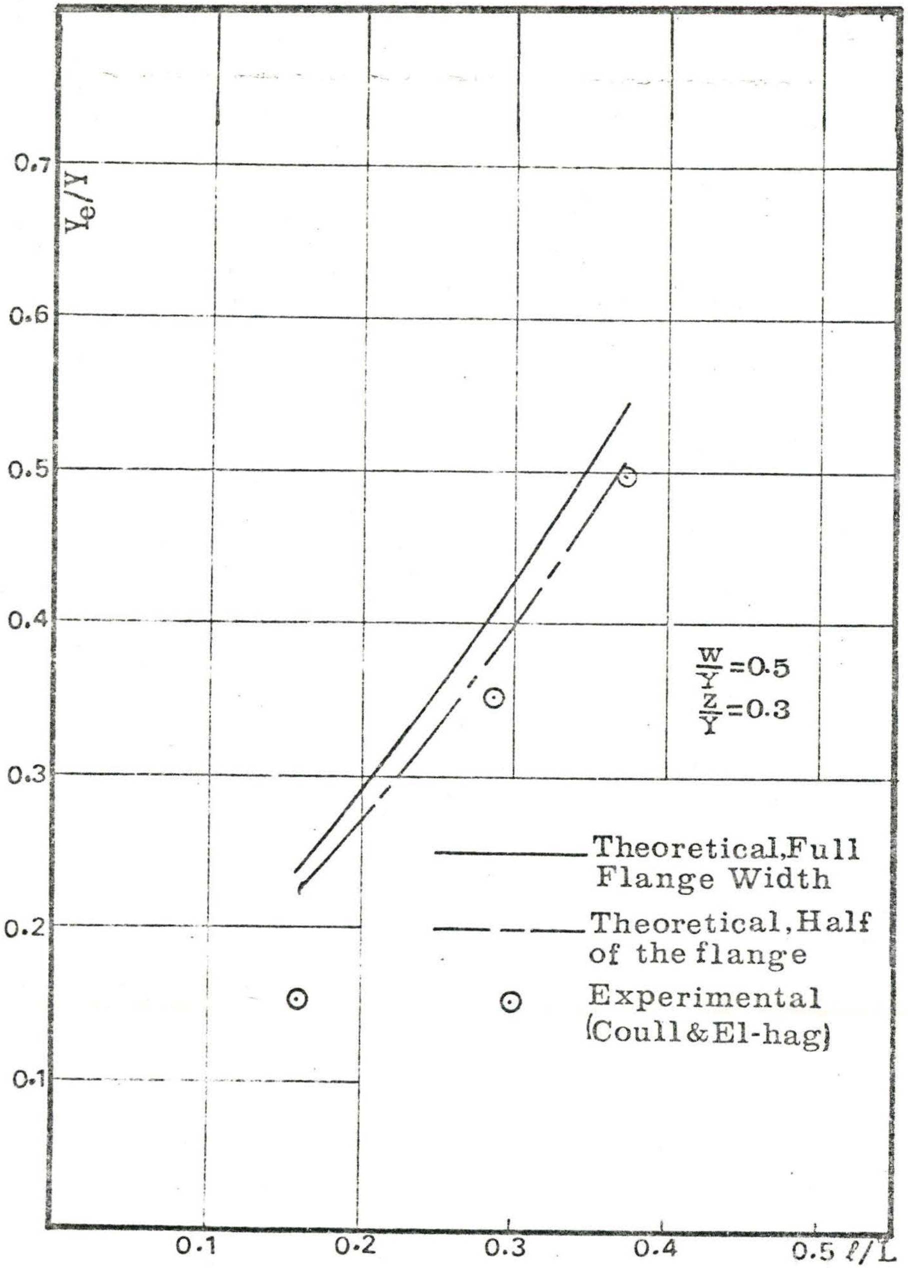

Figure (5.38)

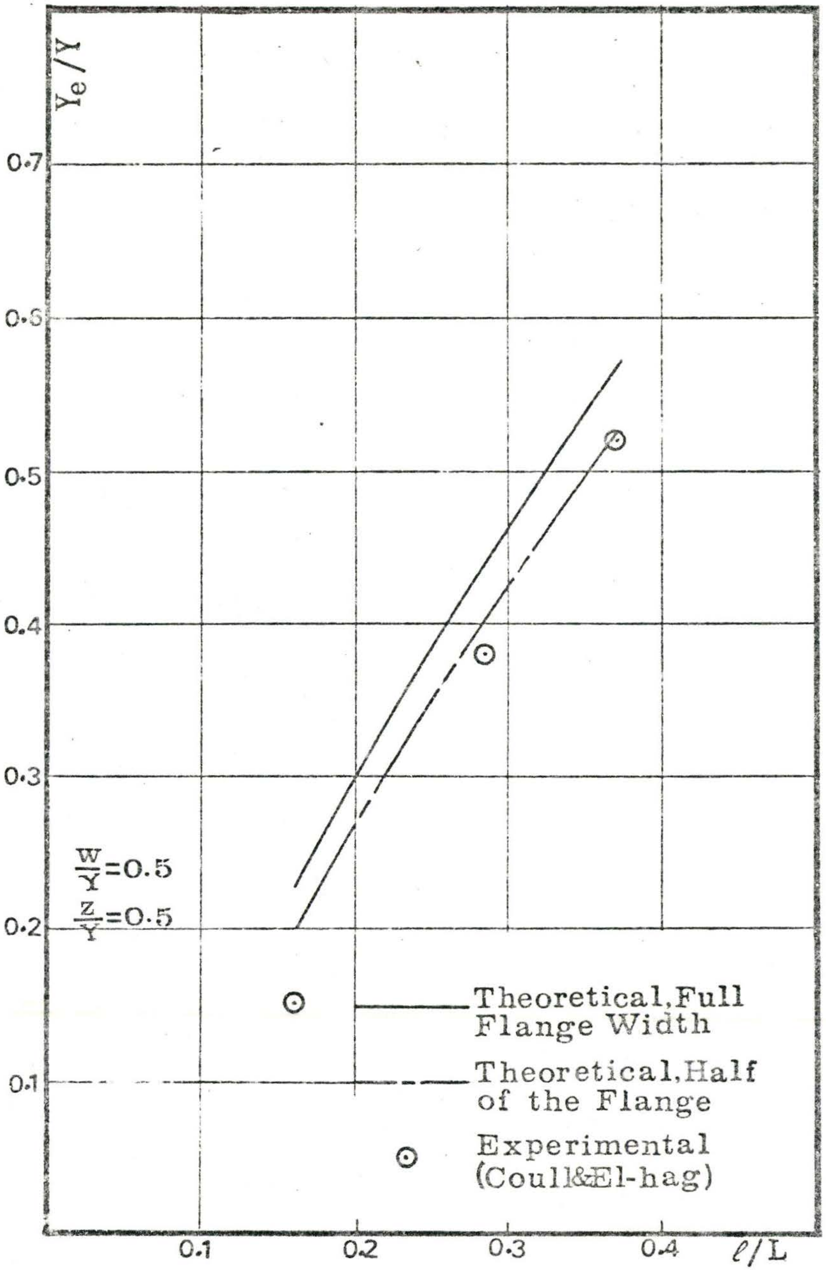

Figure (5.39)

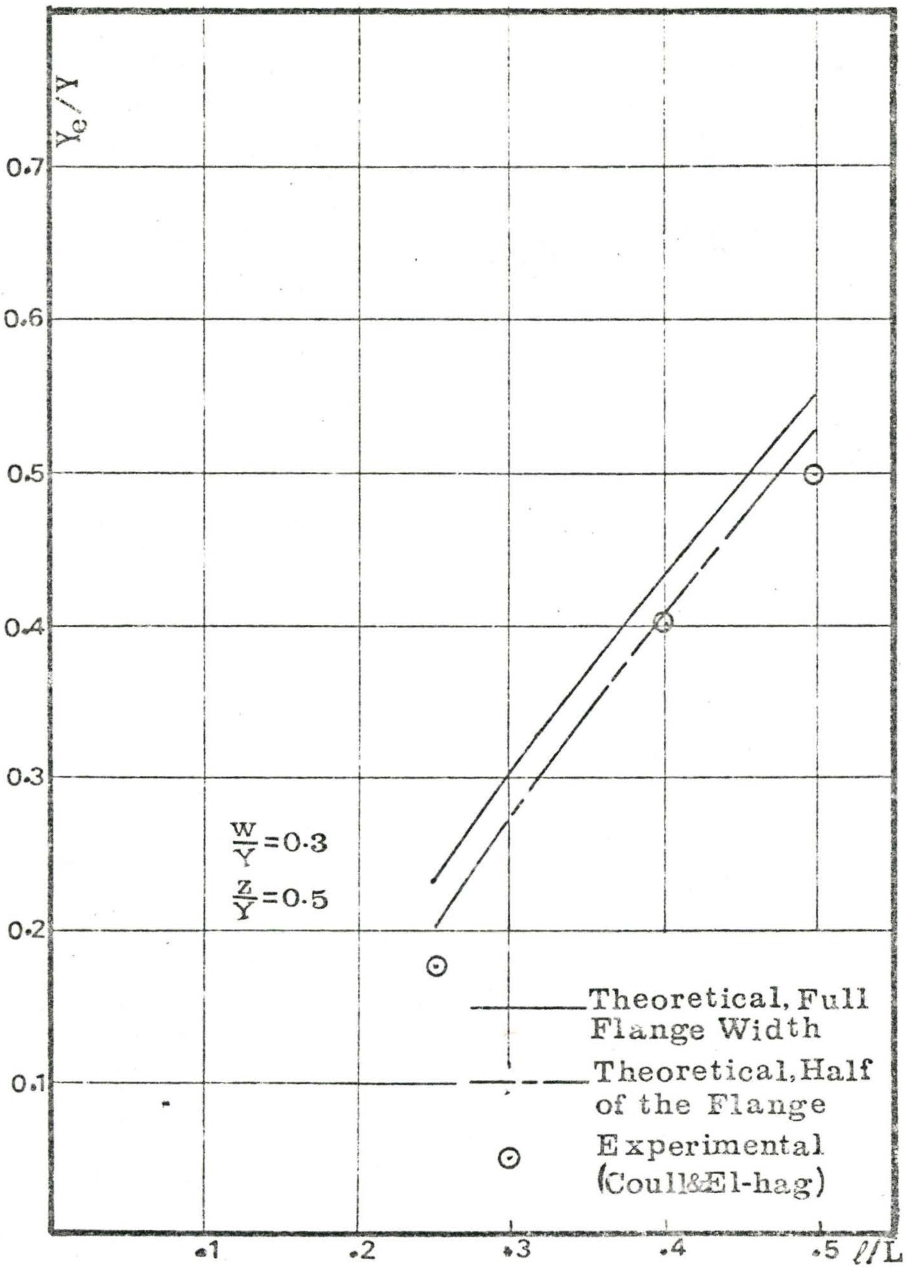

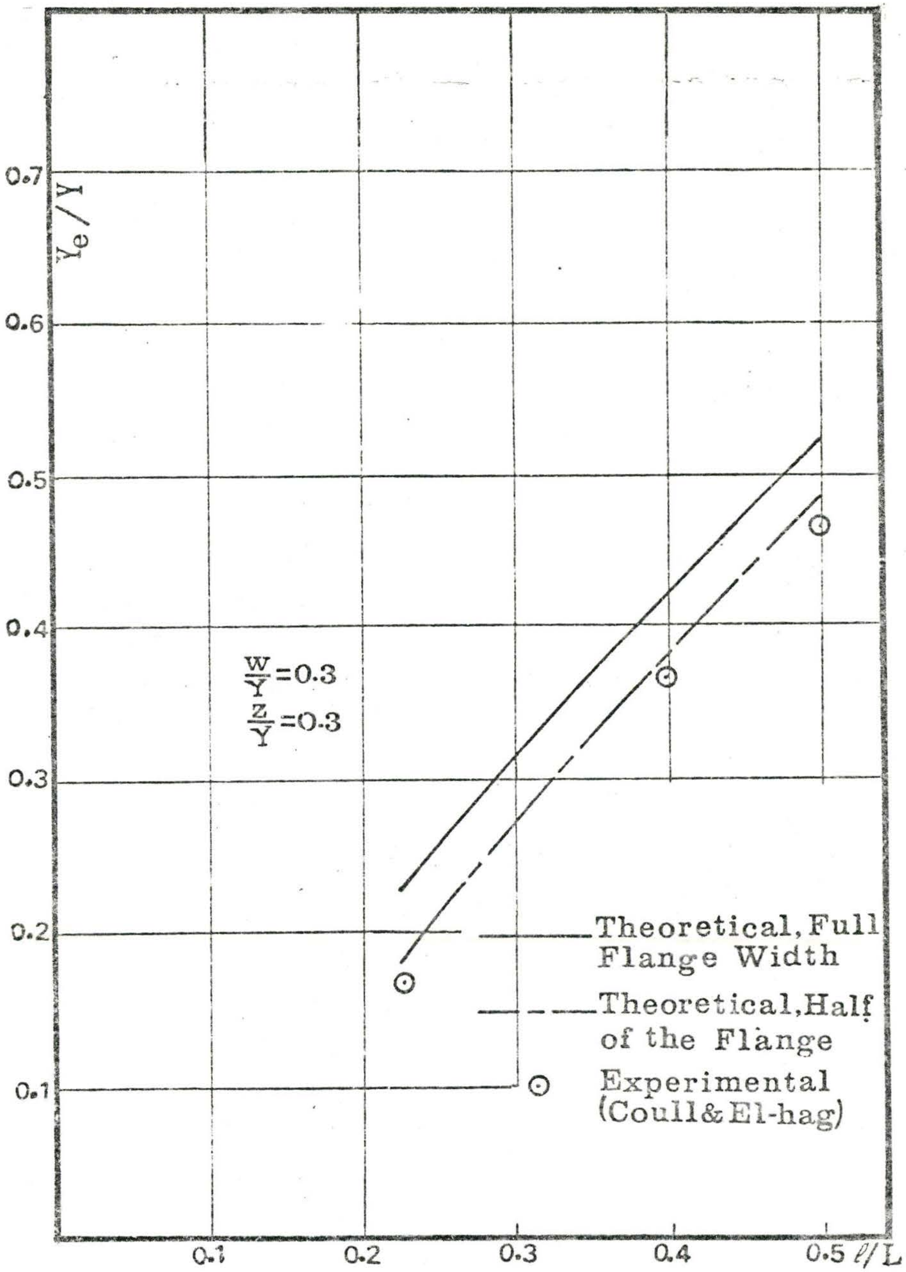

Figure (5.41)

158

given by the curves represented in Section 5.4. Table (5.12) shows the results of these calculations for the coupled planar walls, while Tables (5.13) through (5.16) show similar results for both the T-section wall configurations and the planar wall-T-section wall configurations. The results show that the equivalent beam width is increased by about 10%, when the normalized slab width Y/L is increased from 0.3 to 0.7 and the normalized wall openings are less than 0.2. In other words, the stiffness is insensitive to the slab width for small wall openings. However, the equivalent beam width is increased by values ranging between 50% and 70% for larger wall openings (ℓ/L of 0.5). Also, the T-section wall configurations are more sensitive to the change of the slab width than the planar walls.

To sum up, for small wall openings ($\ell/L \leq 0.2$) the equivalent beam width is insensitive to the change of the slab width, while it is greatly affected by the slab width for large wall openings ($\ell/L > 0.4$, say).

5.8.6 The Effect of Wall Openings on the Behaviour of the Structure

The deflection, the bending moments in the walls, and the shear in the connecting beams are functions of the parameter "αH" as defined before. They can be expressed in the form [4, 5, 6]

$$M = \frac{M_o}{200} \cdot k_1 \tag{5.48}$$

Table (5.12) Relations between ℓ/L and Y_e/L for Planar Walls.

ℓ/L	Y/L	Y_e/Y	Y_e/L	ℓ/L	Y/L	Y_e/Y	Y_e/L
0.05	0.3	0.22	.066	0.3	0.3	0.649	0.1947
	0.4	0.175	.07		0.4	0.55	0.22
	0.5	0.135	.0675		0.5	0.47	0.235
	0.6	0.115	.069		0.6	0.4	0.24
	0.7	0.1	.07		0.7	0.36	0.252
0.1	0.3	0.36	.108	0.4	0.3	0.715	0.2145
	0.4	0.275	.11		0.4	0.635	0.254
	0.5	0.225	.1125		0.5	0.565	0.2825
	0.6	0.19	.114		0.6	0.5	0.3
	0.7	0.17	.119		0.7	0.445	0.3115
0.2	0.3	0.54	.162	0.5	0.3	0.77	0.231
	0.4	0.44	.176		0.4	0.69	0.276
	0.5	0.36	.18		0.5	0.62	0.31
	0.6	0.3	.18		0.6	0.56	0.336
	0.7	0.27	.189		0.7	0.51	0.357

Table (5.13) Relations between ℓ/L and Y_e/L for T-section Walls Z/L = .1

ℓ/L	Y/L	Y_e/Y	Y_e/L	ℓ/L	Y/L	Y_e/Y	Y_e/L
.05	.3	.445	.1335	.3	.3	.82	.246
	.4	.34	.136		.4	.7	.28
	.5	.275	.1375		.5	.6	.3
	.6	.23	.138		.6	.52	.312
	.7	.21	.147		.7	.465	.325
.1	.3	.58	.174	.4	.3	.865	.2595
	.4	.45	.18		.4	.77	.308
	.5	.365	.1825		.5	.685	.3425
	.6	.305	.183		.6	.61	.366
	.7	.275	.1925		.7	.545	.3815
.2	.3	.75	.225	.5	.3	.895	.2685
	.4	.61	.244		.4	.805	.322
	.5	.5	.25		.5	.725	.3625
	.6	.42	.252		.6	.66	.396
	.7	.375	.2625		.7	.605	.4236

Table (5.14) Relations between ℓ/L and Y_e/L for T-section Walls $Z/L = .2$

ℓ/L	Y/L	Y_e/Y	Y_e/L	ℓ/L	Y/L	Y_e/Y	Y_e/L
.05	.3	.69	.207	.3	.3	.96	.288
	.4	.55	.22		.4	.85	.34
	.5	.45	.225		.5	.75	.375
	.6	.375	.225		.6	.66	.396
	.7	.331	.231		.7	.585	.4095
.1	.3	.84	.252	.4	.3	.98	.294
	.4	.675	.27		.4	.89	.356
	.5	.55	.275		.5	.81	.405
	.6	.46	.276		.6	.73	.438
	.7	.41	.287		.7	.651	.4557
.2	.3	.93	.279	.5	.3	.985	.295
	.4	.79	.316		.4	.915	.366
	.5	.675	.3375		.5	.845	.422
	.6	.575	.345		.6	.78	.468
	.7	.51	.357		.7	.72	.504

Table (5.15) Relations between ℓ/L and Y_e/L for Planar Wall with T-section Wall Z/L = .1.

ℓ/L	Y/L	Y_e/Y	Y_e/L	ℓ/L	Y/L	Y_e/Y	Y_e/L
.05	.3	.32	.096	.3	.3	.765	.2295
	.4	.205	.082		.4	.63	.252
	.5	.16	.080		.5	.55	.275
	.6	.135	.081		.6	.48	.288
	.7	.125	.0875		.7	.42	.294
.1	.3	.455	.1365	.4	.3	.82	.246
	.4	.33	.132		.4	.715	.286
	.5	.27	.135		.5	.63	.315
	.6	.225	.1350		.6	.56	.336
	.7	.195	.1365		.7	.5	.35
.2	.3	.675	.2025	.5	.3	.85	.255
	.4	.5	.2		.4	.75	.3
	.5	.425	.2125		.5	.675	.3375
	.6	.356	.2136		.6	.56	.336
	.7	.315	.2205		.7	.55	.385

Table (5.16) Relations between ℓ/L and Y_e/L for Planar Wall with T-section Wall $Z/L = 0.2$.

ℓ/L	Y/L	Y_e/Y	Y_e/L	ℓ/L	Y/L	Y_e/Y	Y_e/L
.05	.3	.33	.099	.3	.3	.8	.24
	.4	.23	.092		.4	.65	.26
	.5	.18	.090		.5	.56	.28
	.6	.15	.090		.6	.5	.3
	.7	.13	.091		.7	.44	.308
.1	.3	.475	.1425	.4	.3	.875	.2625
	.4	.35	.140		.4	.735	.294
	.5	.28	.140		.5	.65	.325
	.6	.24	.144		.6	.58	.348
	.7	.21	.147		.7	.525	.367
.2	.3	.675	.2025	.5	.3	.9	.27
	.4	.515	.2060		.4	.785	.314
	.5	.44	.22		.5	.7	.35
	.6	.38	.228		.6	.63	.378
	.7	.33	.231		.7	.57	.399

$$q \doteq \frac{\bar{w} \cdot H}{(\ell+2\ e_x)} \cdot \frac{1}{\mu} \cdot k_2 \tag{5.49}$$

$$y_{max} = \frac{11}{240} \cdot \frac{\bar{w}\ H4}{EI} \cdot k_3 \tag{5.50}$$

where

M is the moment carried by each wall

M_o is the external overturning moment

q is the shear intensity in the laminas

y_{max} is the maximum top deflection

$\bar{w}$ is the maximum intensity of the triangular load given in Figure (5.24)

The variables k_1, k_2, and k_3 are functions of the parameter "αH" and the external loading. Figure (5.42) shows the relationship between "αH" and each of k_1, k_2 and k_3. The shaded area in this figure with "αH" ranges between 3 and 8 represents the range where coupled shear walls of ordinary proportions usually falls in. The values of ℓ/L corresponding to these values of "αH" range between 0.1 and 0.2 as indicated in Figures (5.25) through (5.27). Therefore, if any significant coupling action is obtained in a coupled shear wall of ordinary proportion, the range of wall openings ℓ/L will be less than 0.2.

To evaluate the effect of the equivalent beam width on the behaviour of the structure, an example will be given. Let us consider a cross wall structure of height 150 feet, total width 40 feet, and wall spacing 20 feet. Let us

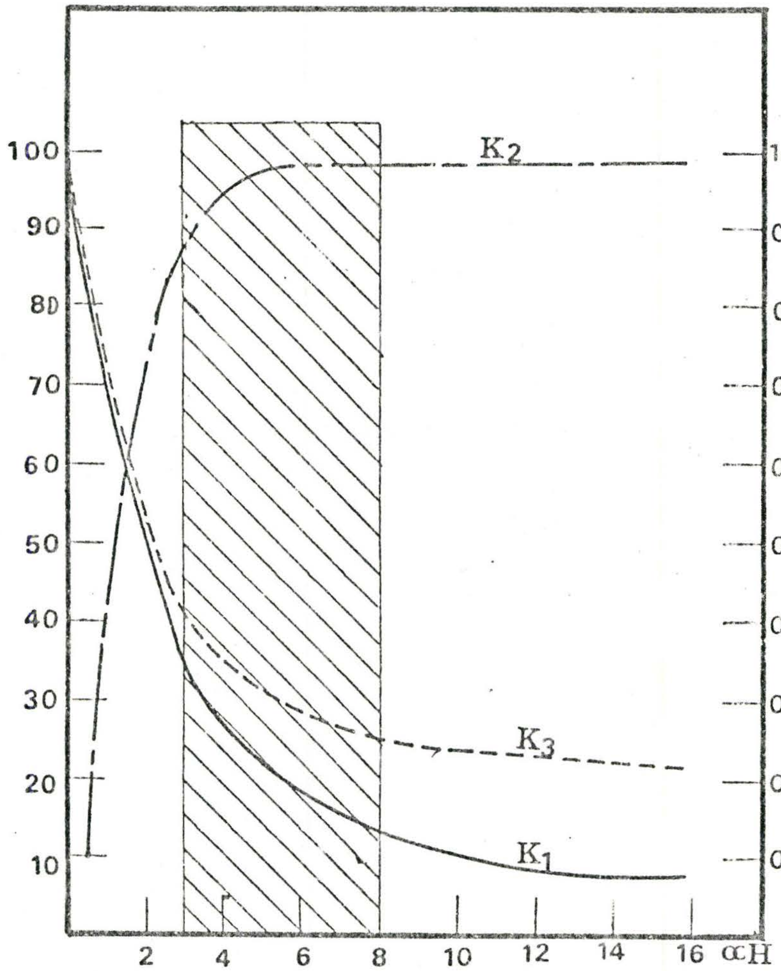

Figure (5.42) Variation of k_1, k_2, k_3 with αH
for Triangularly Distributed Load.

further assume that the equivalent beam width is over-estimated by 100% of the exact value. Referring to Equations (3.19) and (5.25), the corresponding value of "αH" will be increased by 40%. If the wall opening is 16 feet, which corresponds to ℓ/L equals 0.4, the actual value of "αH" is 2, and the overestimated value is 2.8. However, if the wall opening is 4 feet, the actual value of αH is 5.2 and the over-estimated value is 7.3. The behaviour of the coupled shear wall with "αH" is equal to 2 or 2.8 is comparable. However, the behaviour of a couple shear wall with "αH" values of 5.2 is different from one with a αH value of 7.3.

It is concluded that for large wall openings, ($\ell/L \geq 0.4$) the structure behaviour is relatively insensitive to the coupling effect with the floor slabs, while for small wall openings, ($\ell/L \leq 0.2$), the behaviour of the structure is greatly affected by the coupling action. Therefore, an accurate determination of the equivalent width for small wall openings is necessary.

CHAPTER 6

SUMMARY AND CONCLUSIONS

6.1 Summary

One of the methods to include the effect of the slabs in coupling the shear walls is to replace the slabs by beams having the same bending stiffness as the slabs. It is therefore necessary to evaluate the equivalent width of the slabs which represent the width of the beams for a vareity of shear wall configurations.

A method for the analysis of the slab coupled shear walls of different configuration has been developed in this thesis. The basic assumptions on which the analysis is based are that the slab is linearly elastic, homogeneous and its in-plane stiffness is infinite.

By using the finite element technique a computer program is developed to obtain the slab stiffness. The equivalent width and the rotational stiffness of the slab are also obtained.

To verify the method of analysis and the computer program, various examples are solved. The computed results are compared with existing analytical results. In addition, comparison is made between some experimental and the theoretical results for different wall configurations. Some of the experimental results were done by Coull and El-hag [9], while the other is done by the author. The results obtained by the computer program agreed well with the experimental results for the slabs coupled planar walls. There is some deviation between the theoretical and the experimental results for the slabs coupled core walls. This deviation is mainly due to the local deformation effect between the slab and the walls in the experimental model. Comparison between the theoretical and the experimental results for the slabs coupled T-section wall configurations is made to give an idea about the effect of local bending on the flanges of the walls.

A set of design curves is obtained to represent the relation between the wall opening and both the effective width and the rotational stiffness of the slab. These curves are provided for the following wall configurations: two planar walls, two T-section walls configuration with the flange at the inner edge. The relationship between the bending stiffness of the slab coupled box core walls and the slab coupled T-section wall configuration with the flanges at the inner edges is obtained. Such a relationship is also obtained between the slab coupled T-section walls configuration with flanges at the outside edges and the slab coupled planar walls.

Finally, a set of curves representing the relationship between the factor "αH" and the wall openings, for the three wall configurations studied, is presented.

6.2 Conclusions

As a conclusion from using the finite element method to the bending analysis of a slab coupled shear walls, we can state that:

1. The bending stiffness and the effective width of the slab are affected by, the planar wall thickness, the wall opening, the wall configuration, and the slab width.

2. It is shown that, for a given wall opening, the presence of a flange at the inner edge of the wall can increase considerably the effective coupling stiffness of a floor slab, and thus should be taken into account in the design of such systems. If the flange width becomes very large, the local bending and the highly concentrated forces at the inner edge of the wall will tend to reduce the bending stiffness of the slab. In such a case, reduced flange width should be used to correct for the effect of local bending deformations.

3. Due to the wall rotation, the slab reaction along the wall is highly concentrated at the inner edge and rapidly decreased across the wall length.

4. The slab coupled T-section wall configurations with flanges at the outside edges has the same equivalent beam width as the slab coupled planar walls. The same holds true for the slab coupled box core walls and the slab coupled T-section walls configuration with the flanges at the inner edges.

5. For small wall openings ($\ell/L \leq 0.2$) the equivalent beam width is insensitive to the change of the slab width.

For large wall openings ($\ell/L \geq 0.4$) the equivalent beam width is greatly affected by the slab width. At the same time the slab coupled T-section wall configurations with flanges at the inner edges is more sensitive to the change of the slab width than the slab coupled planar walls.

6. The stiffness of the end bay slab, which is one half the interior bay slab width, is not one half of the interior bay stiffness. Both the wall opening and the planar wall thickness affecting the coupled end wall stiffness.

7. The overhanging part of the slab beyond the walls has negligible effect on the slab effective width.

8. Once the effective width or stiffness of the slabs are known, the analysis of the complete coupled wall system may be carried out using the established techniques.

9. For large wall openings, the behaviour of the structure is insensitive to the coupling effect of the slab. Therefore, the accuracy to which the equivalent beam width should be known is relatively uncritical. For small wall openings, a small change in the value of equivalent beam width will have a strong effect on the coupling of the walls. Hence, it is in this range that the engineer should obtain as accurate an estimate of slab stiffness as possible.

APPENDIX A

STIFFNESS MATRIX FOR TRIANGULAR ISOTROPIC FINITE ELEMENT

APPENDIX A

STIFFNESS MATRIX FOR TRIANGULAR ISOTROPIC FINITE ELEMENT

The expression used in defining the triangular element stiffness is 9-term polynomial in X' and Y' due to Rawtani and Dokainish [19]. The vertical displacement w' is given by

$$w' = \alpha_1 + \alpha_2 X' + \alpha_3 Y' + \alpha_4 X'^2 + \alpha_5 X' Y' + \alpha_6 Y'^2 + \alpha_7 X'^3 + \alpha_8 X'^2 Y' + \alpha_9 Y'^3$$

The element stiffness matrix in the local coordinates becomes

$$[k'_e] = \frac{E\ t^3}{12(1-\nu^2)} [A^{-1}]^T\ [B][A^{-1}] \tag{A.1}$$

where

$$[B] = \iint [C_1]^T [D][C_1]\ dX'\ dY' \tag{A.2}$$

$$[C_1] = \begin{bmatrix} 0 & 0 & 0 & 2 & 0 & 0 & 6X' & 2Y' & 0 \\ 0 & 0 & 0 & 0 & 0 & 2 & 0 & 0 & 6Y' \\ 0 & 0 & 0 & 0 & 2 & 0 & 0 & 4X' & 0 \end{bmatrix} \tag{A.3}$$

and

$$[D] = \begin{bmatrix} 1 & \nu & 0 \\ \nu & 1 & 0 \\ 0 & 0 & \frac{1-\nu}{2} \end{bmatrix} \tag{A.4}$$

Premultiply [D] by $[C_1]^T$ and post multiply by $[C_1]$ we have

$$\therefore \quad \frac{d^2[B]}{dX'dY'} = \begin{bmatrix} 0 & 0 & 0 & 0 & 0 & 0 & 0 & 0 & 0 \\ 0 & 0 & 0 & 0 & 0 & 0 & 0 & 0 & 0 \\ 0 & 0 & 0 & 0 & 0 & 0 & 0 & 0 & 0 \\ 0 & 0 & 0 & 4 & 0 & 4\nu & 12X' & 4Y' & 12\nu Y' \\ 0 & 0 & 0 & 0 & 2(1-\nu) & 0 & 0 & 4(1-\nu)X' & 0 \\ 0 & 0 & 0 & 4\nu & 0 & 4 & 12\nu X' & 4\nu Y' & 12Y' \\ 0 & 0 & 0 & 12X' & 0 & 12\nu X' & 36X'^2 & 12X'Y' & 36\nu Y'X' \\ 0 & 0 & 0 & 4Y' & 4(1-\nu)X' & 4\nu Y' & 12X'Y' & 4Y'^2+8(1-\nu)X'^2 & 12\nu Y'^2 \\ 0 & 0 & 0 & 12\nu Y' & 0 & 12Y' & 36\nu X'Y' & 12\nu Y'^2 & 36Y'^2 \end{bmatrix} \tag{A.5}$$

Integrating each element of (A.5) over the area of the triangle i, j, k, as shown in the figure, we have

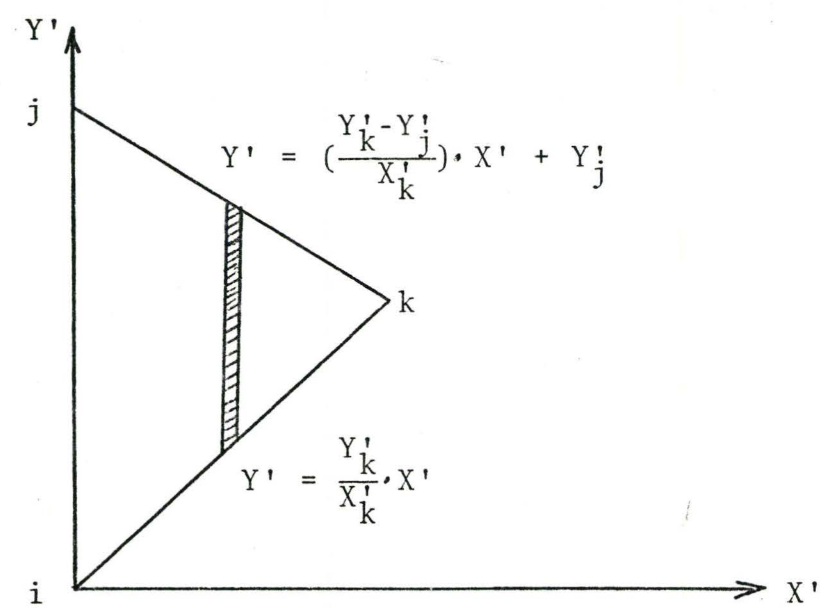

$$\ell_{11} = \int_{0}^{X_k'} \int_{Y_1'}^{Y_2'} dX'\, dY'$$

$$\ell_{11} = \int_{0}^{X_k'} [(\frac{Y_k'-Y_j'}{X_k'})\ X' + Y_j' - \frac{Y_k'}{X_k'}\ X']dX'$$

$$= [- \frac{Y_k'}{X_k'} + \frac{Y_k'-Y_j'}{X_k'}]\ \frac{X_k'^2}{2} + Y_j'\ X_k'$$

$$\therefore\ \underline{\ell_{11} = \frac{1}{2}\ Y_j'\ X_k'}$$

$$\ell_{21} = \int_{0}^{X_k'} \int_{Y_1'}^{Y_2'} X'\ dY'\ dX'$$

$$= \int_{0}^{X_k'} [\frac{Y_k'-Y_j'}{X_k'}\ X' + Y_j' - \frac{Y_k'}{X_k'}\ X']\ X'.dX'$$

$$= \frac{1}{3}\ [\frac{Y_k'-Y_j'-Y_k'}{X_k'}]\ X_k'^3 + \frac{Y_j'}{2}\ .\ X_k'^2$$

$$\therefore\ \underline{\ell_{21} = \frac{1}{6}\ Y_j'\ X_k'^2}$$

$$\ell_{12} = \int_{0}^{X_k'} \int_{Y_1'}^{Y_2'} Y'\ dY'\ dX'$$

$$= \int_{0}^{X_k'} [\frac{1}{2}\ (\frac{Y_k'-Y_j'}{X_k'})^2\ X'^2 + Y_j'^2 + 2Y_j'\ (\frac{Y_k'-Y_j'}{X_k'})\ X'^2 - (\frac{Y_k'}{X_k'})^2 X'^2]dX'$$

(continued)

$$= \frac{1}{2} \left[-\left(\frac{Y_j'}{X_k'}\right)\left(\frac{2Y_k' - Y_j'}{X_k'}\right)\left(\frac{X_k'^3}{3}\right) + \left(\frac{Y_k'Y_j' - Y_j'^2}{X_k'}\right) X_k'^2 + Y_j'^2 X_k' \right]$$

$$\therefore \quad \ell_{12} = \frac{1}{6} X_k' Y_j' [Y_k' + Y_j']$$

$$\ell_{31} = \int_0^{X_k'} \int_{Y_1'}^{Y_2'} X'^2 \, dY' \, dX'$$

$$= \int_0^{X_k'} \left[\left(-\frac{Y_j'}{X_k'}\right) X' + Y_j' \right] X'^2 \, dX'$$

$$= \frac{1}{4} \left(-\frac{Y_j'}{X_k'}\right) X_k'^4 + \frac{1}{3} Y_j' X_k'^3$$

$$\therefore \quad \ell_{31} = \frac{1}{12} Y_j' X_k'^3$$

$$\ell_{13} = \int_0^{X_k'} \int_{Y_1'}^{Y_2'} Y'^2 \, dY' \, dX'$$

$$= \frac{1}{3} \int_0^{X_k'} \left\{ \left[\left(\frac{Y_k' - Y_j'}{X_k'}\right)^3 - \left(\frac{Y_k'}{X_k'}\right)^3 \right] X'^3 + 3 \left[\left(\frac{Y_k' - Y_j'}{X_k'}\right)^2 (Y_j') \right] X'^2 \right.$$

$$\left. + 3 \left[\left(\frac{Y_k' - Y_j'}{X_k'}\right) (Y_j')^2 \right] X' + Y_j'^3 \right\} dX'$$

$$= \frac{1}{3} \left[-\frac{X_j'}{X_k'} \left(\frac{Y_k'^2 - 2Y_j'Y_k' + Y_j'^2}{X_k'^2} + \frac{Y_k'^2 - Y_k'Y_j'}{X_k'^2} + \frac{Y_k'^2}{X_k'^2} \right) \frac{X'^4}{4} \right.$$

(continued)

$$+ Y_j' \left(\frac{Y_k'^2 - 2Y_k'Y_j' + Y_j'^2}{X_k'^2}\right) X_k'^3 + \frac{3}{2} Y_j'^2 \left(\frac{Y_k' - Y_j'}{X_k'}\right) X_k'^2 + Y_j'^3 X_k']$$

$$\therefore \quad \underline{\ell_{13} = \frac{1}{12} X_k' Y_j' [Y_k'^2 + Y_k' Y_j' + Y_j'^2]}$$

$$\ell_{22} = \int_0^{X_k'} \int_{Y_1'}^{Y_2'} X'Y' \, dY' \, dX'$$

$$= \frac{1}{2} \int_0^{X_k'} [(-\frac{Y_j'}{X_k'})(\frac{2Y_k' - Y_j'}{X_k'}) X'^2 + 2Y_j' (\frac{Y_k' - Y_j'}{X_k'}) X' + Y_j'^2] X' \, dX'$$

$$= \frac{1}{2} Y_j' X_k'^2 [- \frac{1}{2} Y_k' + \frac{1}{4} Y_j' + \frac{2}{3} Y_k' - \frac{2}{3} Y_j' + \frac{1}{2} Y_j']$$

$$\therefore \quad \ell_{22} = \frac{1}{24} Y_j' X_k'^2 (2Y_k' + Y_j')$$

APPENDIX B

COMPUTER PROGRAM FOR SOLVING QUARTER OF THE SLAB IN ORDER TO OBTAIN ITS STIFFNESS

```
      PROGRAM TST(INPUT=1001,OUTPUT=1001,TAPE5=INPUT,TAPE6=OUTPUT,TAPE1=
     11001)
C
C     FINITE ELEMENT METHOD OF PLATE UNDER BENDING
C     THESIS PROJECT , BY A. MAHMOUD , GRADUATE STUDENT , DEPARTMENT OF
C     CIVIL ENGINEERING , MCMASTER UNIVERSITY , HAMILTON , ONTARIO.
C     THIS PROGRAM IS PREPARED TO SOLVE QUARTER OF THE PL2TE
C     THIS PROGRAM IS PREPARED TO SOLVE QUARTER OF THE PLATE.
C     THE NODES OUT OF AXES SHOULD BE NUMBERED AT FIRST.
C     NODES ALONG THE AXESYMMETRIC EDGE COMES THE SECOND.
C     THE NODES AT THE SYMMETRIC EDGE COMES THE THIRD.
C     FINALLY THE NODES AT THE BOUNDARY BETWEEN THE WALL AND THE SLAB.
C     UNITS SHOULD BE COMPATABLE==UNIS USED ARE KIP AND FEET.
C
C     DEFINITION OF VARIABLES GIVEN AS DATA
C
C     NN        NO. OF NODES
C     NE        NO. OF ELEMENTS
C     NF1       NO. OF NODES OFF THE AXES (NODES OF ZERO FORCES)
C     NF2       NO. OF NODES ALONG X-X AXIS
C     NF3       NO. OF NODES ALONG Y-Y AXIS
C     NF4       NO. OF NODES ON THE BOUNDARY BETWEEN THE SLAB AND THE WALL
C     SY        WIDTH OF THE SLAB
C     SL        OPENING WIDTH BETWEEN THE TWO WALLS
C     W         WIDTH OF THE WALL
C     TL        TOTAL WIDTH OF THE COUPLED SHEAR WALLS
C     EX        DISTANCE FROM THE INNER EDGE OF THE WALL TO ITS CENTRIOD
C     EMD       MODULUS OF ELASTICITY OF THE SLAB
C     EMU       PIOSSONS RATED
C     T         SLAB THICKNESS
C
C     DEFINITION OF THE VARIABLES CALCULATED THROUGH THE PROGRAM
C
C     NU        TOTAL NO. OF UNKNOWN DISPLACEMENTS
C     X(I)      X - COORDINATE OF NODE 1
C     Y(I)      Y - COORDINATE OF NODE 1
C     NI(N)     NUMBER OF NODE I IN ELEMENT N
C     NJ(N)     NUMBER OF NODE J IN ELEMENT N
C     NK(N)     NUMBER OF NODE K IN ELEMENT N
C     A1,A2,A3SQUARES OF SIDESLENGTH OF THE ELEMENT
C     YY(2)     Y - COORDINATE OF NODE J IN LOCAL AXES
C     XX(3)     X - COORDINATE OF NODE K IN LOCAL AXES
C     YY(3)     Y - COORDINATE OF NODE K IN LOCAL AXES
C     S:        TOTAL STIFFNESS MATRIX
C
      DIMENSION TITLE(18)
      DIMENSION XX(3), YY(3), ALMD(3,3), A(9,9)
      DIMENSION EKB(9,9), EKT(9,9)
      DIMENSION SM(18300), X(81), Y(81), Z(81)
      DIMENSION SMM(7300), NI(90), NJ(90), NK(90)
```

```
      DIMENSION S(66,66)
      DIMENSION E(160)
      COMMON NI,NJ,NK,X,Y,Z,XX,YY,ALHD,A,SM,EKB,EKT,SMM
      REWIND 1
      NNN=61
      MMM=3
      KKK=9
      READ (5,102) TITLE
      WRITE (6,73)
      WRITE (6,103) TITLE
C
C     READ NUMBER OF NODES , NO. OF ELEMENTS
C
      READ (5,71) NN,NE
C
C     READ FIOSSONS RATIO , MODULUS OF ELASTICITY , SLAB THICKNESS
C
      READ (5,72) EMU,EMD,T
C
C     READ NO. OF DIFFERENT TYPES OF NODES
C
      READ (5,85) NF1,NF2,NF3,NF4
C
C     READ WALL GEOMETRY
C
      READ (5,99) SY,SL
      READ (5,104) W,TL
      READ (5,108) EX
      WRITE (6,74) NN,NE
      WRITE (6,75) EMU,EMD,T
      WRITE (6,100) SY,SL
      WRITE (6,105) W,TL
      WRITE (6,109) EX
      NT=NF1+NF2+NF3+NF4
      IF (NT.NE.NN) WRITE (6,80)
      IF (NT.NE.NN) STOP
      TTL=SL+W+W
      IF (ABS(TTL-TL).GT.1.E-8) WRITE (6,107)
      IF (ABS(TTL-TL).GT.1.E-8) STOP
      NU=3*NN
      WRITE (6,95) NF1,NF2,NF3,NF4
      WRITE (6,76) NU
      NOF=3*NF1
      MAG=NU-NOF
C
C     CHECK PROBLEM DIMENSIONS AND DATA
C
      IF (NOF.GT.160) WRITE (6,94)
      IF (NOF.GT.160) STOP
      IF (MAG.GT.68) WRITE (6,96)
```

```
      IF (MAG.GT.66) STOP
      MUU=NU*(NU+1)/2
      IF (MUU.GT.16300) WRITE (6,88)
      IF (MUU.GT.16300) STOP
      IZ=MAG*NOF
      IF (IZ.GT.7800) WRITE (6,82)
      IF (IZ.GT.7800) STOP
      LHL=MAG*MAG
      MAH=NOF*(NOF+1)/2
      LML=MAH
      IF (LHL.GT.LML) WRITE (6,83)
      IF (LHL.GT.LML) STOP
      IF (LHL.GT.7800) WRITE (6,84)
      IF (LHL.GT.7800) STOP
      WRITE (6,73)
      WRITE (6,81)
C
C     READ COORDINATES OF NODES
C
      DO 1 KI=1,NN
      READ (5,78) X(KI),Y(KI)
      Z(KI)=0.0
1     CONTINUE
C
C     READ NODES NUMBER
C
      DO 2 N=1,NE
      READ (5,77) NI(N),NJ(N),NK(N)
      I=NI(N)
      J=NJ(N)
      K=NK(N)
      WRITE (6,79) N,I,J,K,X(I),Y(I),Z(I),X(J),Y(J),Z(J),X(K),Y(K),Z(K)
C
C     CALCULATE NODAL COORDINATES IN LOCAL AXES
C
      A1=(X(J)-X(I))**2+(Y(J)-Y(I))**2+(Z(J)-Z(I))**2
      A2=(X(K)-X(J))**2+(Y(K)-Y(J))**2+(Z(K)-Z(J))**2
      A3=(X(I)-X(K))**2+(Y(I)-Y(K))**2+(Z(I)-Z(K))**2
      YY(2)=SQRT(A1)
      YY(3)=(A3+A1-A2)/(2.*YY(2))
      XX(3)=SQRT(ABS(A3-YY(3)**2))
C
C     FORMULATION OF ELEMENT STIFFNESS MATRIX IN LOCAL AXES
C
      CALL LAMDA (X,Y,Z,NNN,MMM,I,J,K,ALMD)
C     INVERSION OF MATRIX IS OBTAINED
      CALL AINVRS (XX,YY,A)
C     THE ELEMENT STIFFNESS MATRIX NOW FORMED
      CALL BENDK (ENU,EMD,A,EKB,XX,YY,T)
      CALL TRANS (ALMD,EKB,EKT,KKK)
```

```
      WRITE (1) ((EKT(I,J),J=1,9),I=1,9)
    2 CONTINUE
C
C     FORMULATION OF TOTAL STIFFNESS MATRIX , HALF OF IT WILL STORED IN
C     A COLUMN VECTOR ROW BY ROW UP TO THE DIAGONAL ELEMENT
C
      DO 3 N=1,MUU
      SM(N)=0.0
    3 CONTINUE
      REWIND 1
      DO 7 LB=1,NE
      READ (1) ((EKT(KK,MM),MM=1,9),KK=1,9)
      I1=(NI(LB)-1)*3+1
      J1=(NJ(LB)-1)*3+1
      K1=(NK(LB)-1)*3+1
      I2=NI(LB)*3
      J2=NJ(LB)*3
      K2=NK(LB)*3
      M=0
      DO 4 II=I1,I2
      CALL ASSEMB (I1,I2,J1,J2,K1,K2,II,M,EKT,SM)
    4 CONTINUE
      DO 5 II=J1,J2
      CALL ASSEMB (I1,I2,J1,J2,K1,K2,II,M,EKT,SM)
    5 CONTINUE
      DO 6 II=K1,K2
      CALL ASSEMB (I1,I2,J1,J2,K1,K2,II,M,EKT,SM)
    6 CONTINUE
    7 CONTINUE
C
C     PARTION OF THE TOTAL STIFFNESS MATRIX
C
C
C     FIRST PART OF MATRIX SM IS INVERTED AND THE INVERSION CALLED KCC
C
      CALL INVSYM (SM,NCF,IERR)
      IF (IERR.NE.0) WRITE (6,110) IERR
      IF (IERR.NE.0) STOP
      LMM=0
C
C     MULTIPLICATION OF KCC BY KAB AND STORED AGAIN IN SMM ROW BY ROW
C
      DO 16 IA=1,NOF
      IF (IA.NE.1) GO TO 9
      DO 8 JA=1,NOF
      E(JA)=SM(JA*(JA-1)/2+IA)
    8 CONTINUE
      GO TO 13
    9 CONTINUE
      KA=IA-1
```

```
      KB=0
      DO 10 MAM=1,KA
      KB=KB+MAM
10    CONTINUE
      NAN=KB+1
      DO 12 JJJ=1,NUF
      IF (JJJ.GT.IA) GO TO 11
      E(JJJ)=SM(NAN+JJJ-1)
      NANN=NAN+JJJ-1
      GO TO 12
11    CONTINUE
      E(JJJ)=SM(NANN+JJJ-1)
      NANN=NANN+JJJ-1
12    CONTINUE
13    CONTINUE
      LKK=0
      DO 15 LLL=1,MAG
      SMM(LLL+LMM)=0.0
      DO 14 LKL=1,NUF
      MON=MAH+LKL+LKK+(LLL-1)*NUF
      SMM(LLL+LMM)=SMM(LLL+LMM)+E(LKL)*SM(MON)
14    CONTINUE
      LKK=LKK+LLL
15    CONTINUE
      LMM=LMM+MAG
16    CONTINUE
C
C     MULTIPLICATION OF KBA KCC KAB STORED IN FIRST PART OF SM COLUMN
C     BY COLUMN
C
      NSS=0
      DO 19 LLL=1,MAG
      LKK=0
      DO 18 NAH=1,MAG
      SM(NAH+NSS)=0.0
      LK1=0
      DO 17 LKL=1,NUF
      MON=MAH+LKL+LKK+(NAH-1)*NUF
      SM(NAH+NSS)=SM(NAH+NSS)+SM(MON)*SMM(LLL+LK1)
      LK1=LK1+MAG
17    CONTINUE
      LKK=LKK+NAH
18    CONTINUE
      NSS=NSS+MAG
19    CONTINUE
C
C     SUBTRACTION OF KBA KCC KAB FROM KAA AND THE RESULTANT MATRIX STOR-
C     ED COLUMN BY COLUMN IN THE FIRST PART OF SMM
C
      KOP=MAH+NCF+1
```

```
      MSS=0
      DO 27 IA=1,MAG
      IF (IA.NE.1) GO TO 21
      DO 20 JA=1,MAG
      E(JA)=SM(JA*(JA-1)/2+KOP+NOF*(JA-1))
20    CONTINUE
      GO TO 25
21    CONTINUE
      KA=IA-1
      KB=0
      DO 22 MAM=1,KA
      KB=KB+MAM
22    CONTINUE
      DO 24 JJJ=1,MAG
      IF (JJJ.GT.IA) GO TO 23
      E(JJJ)=SM(JJJ-1+KB+KOP+NOF*(IA-1))
      NANN=JJJ-1+KB+KOP+NOF*(IA-1)
      GO TO 24
23    CONTINUE
      E(JJJ)=SM(NANN+JJJ+NOF-1)
      NANN=NANN+JJJ-1+NOF
24    CONTINUE
25    CONTINUE
      DO 26 MER=1,MAG
      SMM(MER+MSS)=E(MER)-SM(MER+MSS)
26    CONTINUE
      MSS=MSS+MAG
27    CONTINUE
C
C     ARRANGEMENT OF STIFFNESS MATRIX ACCORDING TO THE BOUNDARY CONDISI-
C     ONS FOR SOLVING QUARTER OF THE SLAB
C
C     REPLACEMENT OF ROWS
C
      MSS=0
      DO 29 IB=1,MAG
      DO 28 JB=1,MAG
      S(JB,IB)=SMM(JB+MSS)
28    CONTINUE
      MSS=MSS+MAG
29    CONTINUE
      MAGG=MAG+MAG
      DO 30 IB=1,MAGG
      SM(IB)=0.0
30    CONTINUE
      NH1=3*NF2+3*NF3
      MSS=0
      DO 32 IB=3,NH1,3
      DO 31 JB=1,MAG
      SM(JB+MSS)=S(IB,JB)
```

```
   31 CONTINUE
      MSS=MSS+MAB
   32 CONTINUE
      IF (NF3.EQ.0) GO TO 39
      NH2=3*NF3
      DO 34 IB=1,NH2,3
      IIB=3*NF2+IB
      DO 33 JB=1,MAG
      SN(JB+MSS)=S(IIB,JB)
   33 CONTINUE
      MSS=MSS+MAG
   34 CONTINUE
   35 CONTINUE
      NH3=3*NF2
      DO 37 IB=1,NH3,3
      DO 36 JB=1,MAG
      SN(JB+MSS)=S(IB,JB)
   36 CONTINUE
      MSS=MSS+MAG
   37 CONTINUE
      DO 39 IB=2,NH1,3
      DO 38 JB=1,MAG
      SM(JB+MSS)=S(IB,JB)
   38 CONTINUE
      MSS=NSS+MAG
   39 CONTINUE
      MSS=0
      DO 41 IB=1,NH1
      DO 40 JB=1,MAG
      S(IB,JB)=SM(JB+MSS)
   40 CONTINUE
      MSS=MSS+MAG
   41 CONTINUE
      DO 42 IB=1,MAGG
      SM(IB)=0.0
   42 CONTINUE
C
C     REPLACEMENT OF COLUMNS
C
      MSS=0
      DO 44 IB=3,NH1,3
      DO 43 JB=1,MAG
      SM(JB+MSS)=S(JB,IB)
   43 CONTINUE
      MSS=MSS+MAG
   44 CONTINUE
      IF (NF3.EQ.0) GO TO 47
      DO 46 IB=1,NH2,3
      IIB=3*NF2+IB
      DO 45 JB=1,MAG
```

```
      SM(JB+MSS)=S(JB,IIB)
45    CONTINUE
      MSS=MSS+MAG
46    CONTINUE
47    CONTINUE
      DO 49 IB=1,NH3,3
      DO 48 JB=1,MAG
      SM(JB+MSS)=S(JB,IB)
48    CONTINUE
      MSS=MSS+MAG
49    CONTINUE
      DO 51 IB=2,NH1,3
      DO 50 JB=1,MAG
      SN(JB+MSS)=S(JB,IB)
50    CONTINUE
      MSS=MSS+MAG
51    CONTINUE
      MSS=0
      DO 53 IB=1,NH1
      DO 52 JB=1,MAG
      S(JB,IB)=SM(JB+MSS)
52    CONTINUE
      MSS=MSS+MAG
53    CONTINUE
C
C
C     AGAIN PARTION OF THE STIFFNESS MATRIX ACOORDING TO THE BOUNDARY C-
C     ONDITIONS
C
C     INVERSION OF FIRST PART OF S WHICH IS CALLED R11
C
      LH1=NF2+2*NF3
      MSS=0
      DO 54 IB=1,LH1
      DO 54 JB=1,IB
      MSS=MSS+1
      SMM(MSS)=S(IB,JB)
54    CONTINUE
      LAM=LH1*(LH1+1)/2
      CALL INVSYM (SMM,LH1,IERR)
      IF (IERR.NE.0) WRITE (6,110) IERR
      IF (IERR.NE.0) STOP
      MSS=0
      DO 55 IB=1,LH1
      DO 55 JB=1,IB
      MSS=MSS+1
      S(IB,JB)=SMM(MSS)
55    CONTINUE
      DO 56 IB=1,LH1
      DO 56 JB=1,LH1
      IF (IB.GE.JB) GO TO 56
```

```
      S(IB,JB)=S(JB,IB)
56    CONTINUE
C
C     MULTIPLICATION OF K21 AND K11 , THE RESULT STORED IN SM ROW BY ROW
C
      LH2=MAG-NF2-2*NF3
      MSS=0
      DO 58 IB=1,LH2
      IIB=LH1+IB
      DO 57 JB=1,LH1
      SM(JB+MSS)=0.0
      DO 57 KB=1,LH1
      SM(JB+MSS)=SM(JB+MSS)+S(IIB,KB)*S(KB,JB)
57    CONTINUE
      MSS=MSS+LH1
58    CONTINUE
C
C     MULTIPLICATIONK21 K11 AND K12 AND THE RESULT STORED IN SMM ROW BY
C
      LH3=LH2+LH1
      NSS=0
      MSS=0
      DO 61 IB=1,LH2
      DO 60 JB=1,LH2
      SMM(JB+NSS)=0.0
      JJB=JB+LH1
      DO 59 KB=1,LH1
      SMM(JB+NSS)=SMM(JB+MSS)+SM(KB+MSS)*S(KB,JJB)
59    CONTINUE
60    CONTINUE
      NSS=NSS+LH2
      MSS=MSS+LH1
61    CONTINUE
C
C     SUBTRACTION OF K21 K11 K12 FROM K22 STORED IN 4RTH CORNER OF S
C
      MSS=0
      DO 63 IB=1,LH2
      IIB=LH1+IB
      DO 62 JB=1,LH2
      JJB=LH1+JB
      S(IIB,JJB)=S(IIB,JJB)-SMM(JB+MSS)
62    CONTINUE
      MSS=MSS+LH2
63    CONTINUE
      LH3=3-NF4
      DO 64 IB=1,NF2
      Z(IB)=0.0
64    CONTINUE
      KKB=NF2+NF3
```

```
      DO 65 IB=1,KK3
      IIB=IB+NF2
      Z(IIB)=0.0
   65 CONTINUE
      DO 66 IB=1,LHS
      ILB=IB+IIB
C
C     READ NODAL DISPLACEMENTS OF THE NODES BETWEEN THE WALL AND THE SLA
C
      READ (5,91) Z(ILB)
   66 CONTINUE
      WRITE (6,73)
      WRITE (6,88)
      WRITE (6,87)
      WRITE (6,89) (Z(IB),IB=1,NF2)
      WRITE (6,90)
      DO 67 IB=1,KKS
      IIB=IB+NF2
      WRITE (6,88) Z(IIB)
   67 CONTINUE
      WRITE (8,93)
      DO 68 IB=1,LH3
      ILB=IB+IIB
      WRITE (6,89) Z(ILB)
   68 CONTINUE
C
C     MULTIPLICATION OF STIFFNESS MATRIX BY THE DISPLACEMENT VECTOR
C
      DO 69 IB=1,LH2
      IIB=LH1+IB
      SM(IB)=0.0
      DO 69 JB=1,LH2
      JJB=LH1+JB
      SM(IB)=SM(IB)+S(IIB,JJB)*Z(JB)
   69 CONTINUE
      WRITE (6,92)
      WRITE (6,98) (SM(IB),IB=1,LH2)
C
C     SLAB STIFFNESS
C
      S1=0.0
      DO 70 IB=1,LH3,3
      IIB=IB+2*NF2+NF3
      S1=S1+SN(IIB)
   70 CONTINUE
      WRITE (6,97)
      WRITE (6,89) S1
C
C     EQUIVALENT BEAM WIDTH
C
```

```
      S12=2*S1*SL*SL*SL
      S22=END*T*T*T*SY
      S13=S12/S22
      WRITE (6,101) S13
C
C     NONCIMENSICNAL ROTATIONAL STIFFNESS OF THE SLAB
C
      S14=6.*S13*(SY/SL)*(1.-EMU*EMU)
      S16=(SL/(SL+2.*EX))**2
      S15=S14/S16
      WRITE (6,106) S15
      STOP
C
71    FORMAT (I5,I5)
72    FORMAT (F5.2,E10.2,F10.5)
73    FORMAT (1F1)
74    FORMAT (5X,*NO. OF NODES    =*,I5,/,5X,*NO. OF ELEMENTS =*,I5//)
75    FORMAT (5X,*PIOSSONS RATIO              =*,F5.2,X,5X,*MODULUS OF ELASTIC
     1ITY =*,E11.4,2X,*KIP/FT.**2*,/,5X,*THICKNESS OF THE SLAB =*,F8.5,2
     2X,*FT.*,//)
76    FORMAT (5X,*NO. OF TOTAL DISPLACEMENTS                          =*, I5)
77    FORMAT (I5,I5,I5)
78    FORMAT (2F8.3)
79    FORMAT (6X,I4,6X,3(I4,2X),2X,3(F5.2,2X),3X,3(F5.2,3X),2X,3(F5.2,3X
     1))
80    FORMAT (X,5X,*ERROR IN DATA OF NO. OF NODES*)
81    FORMAT (5X,*PROPERTIES OF ELEMENTS*,XX,5X,*ELEMENT NO*,3X,*NI*,3X,
     1*NJ*,4X,*NK*,6X,*XI*,6X*YI*,6X*ZI*,6X,*XJ*,6X,*YJ*,6X,*ZJ*,6X,*XK*
     2,6X,*YK*,6X*ZK*)
82    FORMAT (6X,*FIRST SIZE GREATER THAN STORAGE OF SMM*)
83    FORMAT (5X,*SECOND SIZE GREATER THAN STORAGE OF SM*)
84    FORMAT (5X,*THIRD SIZE GREATER THAN STORAGE OF SM*)
85    FORMAT (4I5)
86    FORMAT (Xx,50X,*NODAL DISPLACEMENTS*,X)
87    FORMAT (5X,*VERTICAL DISPLACEMENT OF NODES OF AXISYMMETRIC EDGE OF
     1 SLAB*)
88    FORMAT (5X,*PROBLEM GREATER THAN THE STORAGE*)
89    FORMAT (5X,E10.4)
90    FORMAT (/,5X,*SLOPE ABOUT X AXIS FOR BOTH NODES OF AXISYMMETRIC AN
     1D SYMMETRIC EDGE OF SLAB*)
91    FORMAT (F6.3)
92    FORMAT (1H1,48X,*NODAL FORCES*)
93    FORMAT (/,5X,*DISPLACEMENTS OF NODES ON WALL*)
94    FORMAT (5X,*VECTOR E IS SMALL*)
95    FORMAT (5X,*NO. OF NODES OF ZERO FORCES                  =*,I5,/,5X,
     1*NO. OF NODES ON AXISYMMETRIC EDGE OF SLAB =*,I5,/,5X,*NO. OF NODE
     2S ON SYMMETRIC EDGE OF SLAB      ==*,I5,/,5X,*NO. OF NODES ON SYMMET
     3RC EDGE OF WALL      =*,I5,//)
96    FORMAT (5X,*MATRIX S IS SMALL*,//)
97    FORMAT (/,5X,*SLAB STIFFNESS*,/)
```

```
98    FORMAT (50X,E10.4)
99    FORMAT (2F6.3)
100   FORMAT (5X,*WIDTH OF THE SLAB          =*,F8.4,/,5X,*LENGTH OF CONNE
     1TING BEAM =*,F8.4)
101   FORMAT (/,5X,*RATIO OF EFFECTIVE WIDTH OF SLAB TO TOTAL WIDTH =*,F
     19.6,/)
102   FORMAT (13A6)
103   FORMAT (5X,13A6,////)
104   FORMAT (2F6.3)
105   FORMAT (5X,*LENGTH OF WALL             =*,F8.4,/,5X,*TOTAL LENGTH OF
     1 SLAB         =*,F8.4)
106   FORMAT (5X,*ROTATIONAL NONDIMENSIONAL STIFFNESS OF THE SLAB =*,E10
     1.4)
107   FORMAT (/,5X,*ERROR IN DIMENSION OF THE PROBLEM*)
108   FORMAT (F6.3)
109   FORMAT (5X,*DISTANCE EX                =*,F8.4,//)
110   FORMAT (5X,5HIERR=,I3)
      END
```

SUBROUTINE LAMDA (X,Y,Z,NNN,MMM,I,J,K,ALMD)

```
      SUBROUTINE LAMDA (X,Y,Z,NNN,MMM,I,J,K,ALMD)
C     THIS SUBROUTINE FINDS THE DIRECTION COSINES OF THE LOCAL COORDINAT
C     DESCRIPTION OF PARAMETERS
C     X,Y,Z........GLOBAL COORDINATES OF NODES
C     ALMD.........MATRIX OF DIRECTION COSINES
      DIMENSION X(NNN), Y(NNN), Z(NNN), ALMD(MMM,MMM)
      YJI=Y(J)-Y(I)
      YMI=Y(K)-Y(I)
      XJI=X(J)-X(I)
      XMI=X(K)-X(I)
      ZJI=Z(J)-Z(I)
      ZMI=Z(K)-Z(I)
      A=YJI*ZMI-YMI*ZJI
      B=-XJI*ZMI+XMI*ZJI
      C=XJI*YMI-XMI*YJI
      F=SQRT(XJI**2+YJI**2+ZJI**2)
      G=-SQRT(A**2+B**2+C**2)
      ALMD(2,1)=XJI/F
      ALMD(2,2)=YJI/F
      ALMD(2,3)=ZJI/F
      ALMD(3,1)=A/G
      ALMD(3,2)=B/G
      ALMD(3,3)=C/G
      ALMD(1,1)=ALMD(2,2)*ALMD(3,3)-ALMD(3,2)*ALMD(2,3)
      ALMD(1,2)=ALMD(3,1)*ALMD(2,3)-ALMD(3,3)*ALMD(2,1)
      ALMD(1,3)=ALMD(2,1)*ALMD(3,2)-ALMD(3,1)*ALMD(2,2)
      RETURN
      END
```

SUBROUTINE AINVRS (X,Y,A)

```
      SUBROUTINE AINVRS (X,Y,A)
C     THIS SUBROUTINE FINDS THE INVERSE OF MATRIX A
C     DESCRIPTION OF PARAMETERS
C     X,Y.....LOCAL COORDINATES OF THE NODES
C     A.......INVERSION OF MATRIX A
      DIMENSION X(3), Y(3), A(9,9), N(9)
      DO 1 IA=1,9
      DO 1 JA=1,9
      A(IA,JA)=0.0
1     CONTINUE
      I=1
      J=2
      K=3
      A(1,1)=1.
      A(4,1)=1.
```

```
      A(7,1)=1.
      A(3,2)=-1.
      A(6,2)=-1.
      A(7,2)=X(K)
      A(9,2)=-1.
      A(2,3)=1.
      A(4,3)=Y(J)
      A(5,3)=1.
      A(7,3)=Y(K)
      A(8,3)=1.
      A(7,4)=X(K)**2
      A(9,4)=-2.*X(K)
      A(6,5)=-Y(J)
      A(7,5)=X(K)*Y(K)
      A(8,5)=X(K)
      A(9,5)=-Y(K)
      A(4,6)=Y(J)**2
      A(5,6)=2.*Y(J)
      A(7,6)=Y(K)**2
      A(8,6)=2.*Y(K)
      A(7,7)=X(K)**3
      A(9,7)=-3.*X(K)**2
      A(7,8)=Y(K)*X(K)**2
      A(8,8)=X(K)**2
      A(9,8)=-2.*X(K)*Y(K)
      A(4,9)=Y(J)**3
      A(5,9)=3.*Y(J)**2
      A(7,9)=Y(K)**3
      A(8,9)=3.*Y(K)**2
C     MATRIX A IS NOW INVERTED,IF THE INVERSION FAILS  THE PROGRAM STOPS.
      CALL INVMAT (A,9,9,1.E-8,II,N)
      IF (II.NE.0) WRITE (8,2) II
      IF (II.NE.0) STOP
      RETURN
C
2     FORMAT (5X,5HIERR=,I3)
      END
```

SUBROUTINE MULTP (A,B,C,I,J,K,IT,NA,NB,NC)

```
      SUBROUTINE MULTP (A,B,C,I,J,K,IT,NA,NB,NC)
C     THIS SUBROUTINE GIVES THE PRODUCT OF TWO MATRICES
C     DESCRIPTION OF PARAMETERS
C     A,B,.........MATRECES TO BE MULTIPLIED,MATRIX A IS OF SIZE (I,K)IF
C                  IF IT IS NONZERO,A IS OF SIZE (K,I),MATRIX B IS OF SI
C     A*B..........IF IT =0
C     A (TRANSPOSE)*B     (IF IT IS NONZERO)
C     NA,NB,NC.....FIRST DIMENSION OF MATRICES A,B,C IN THE DIMENSION ST
```

```
      DIMENSION A(NA,1), B(NB,1), O(NO,1)
      DO 1 M=1,I
      DO 1 N=1,J
      C(M,N)=0.0
      DO 1 L=1,K
      IF (IT.EQ.0) C(N,N)=C(M,N)+A(M,L)*B(L,N)
      IF (IT.NE.0) C(N,N)=C(M,N)+A(L,N)*B(L,N)
    1 CONTINUE
      RETURN
      END
```

SUBROUTINE BENDK (EMU,EMD,A,EKB,X,Y,T)

```
      SUBROUTINE BENDK (EMU,EMD,A,EKB,X,Y,T)
C     THIS SUBROUTINE FINDS THE BENDING STIFFNESS MATRIX OF AN ELEMENT
C     DESCRIPTION OF PARAMETERS
C     EMU..........PIOSSONS RATIO
C     A............INVERTSON OF MATRIX A
C     XX, YY........LOCAL COORDINATES
C     EKB..........BENDING STIFFNESS MATRIX
      DIMENSION A(9,9), EKB(9,9), B(9,9), D1(9,9), X(3), Y(3)
      DO 1 I=1,9
      DO 1 J=1,9
      B(I,J)=0.0
    1 CONTINUE
      C11=.5*X(3)*Y(2)
      C21=Y(2)*(X(3)**2)/6.
      C31=Y(2)*(X(3)**3)/12.
      C12=Y(2)*X(3)*(Y(2)+Y(3))/6.
      C13=Y(2)*X(3)*(Y(2)**2+Y(3)**2+Y(2)*Y(3))/12.
      C22=Y(2)*(X(3)**2)*(Y(2)+2.*Y(3))/24.
      B(4,4)=4.*C11
      B(6,4)=4.*EMU*C11
      B(4,6)=B(6,4)
      B(7,4)=12.*C21
      B(4,7)=B(7,4)
      B(8,4)=4.*C12
      B(4,8)=B(8,4)
      B(9,4)=12.*EMU*C12
      B(4,9)=B(9,4)
      B(5,5)=2.*(1.-EMU)*C11
      B(6,5)=4.*(1.-EMU)*C21
      B(5,6)=B(6,5)
      B(6,6)=4.*C11
      B(7,6)=12.*EMU*C21
      B(6,7)=B(7,6)
      B(8,6)=4.*EMU*C12
      B(6,8)=B(8,6)
      B(9,6)=12.*C12
      B(6,9)=B(9,6)
      B(7,7)=36.*C31
```

```
      B(7,6)=12.*C22
      B(6,7)=B(7,8)
      B(9,7)=36.*EMU*C22
      B(7,9)=B(9,7)
      B(8,8)=4.*C13+8.*(1.-EMU)*C31
      B(9,8)=12.*EMU*C13
      B(8,9)=B(9,8)
      B(9,9)=36.*C13
      CALL MULTP (B,A,D1,9,9,9,0,9,9,9)
      CALL MULTP (A,D1,EKB,9,9,9,1,9,9,9)
      C=(EMD*T*T*T)/(12.*(1.-EMU*EMU))
      DO 2 I=1,9
      DO 2 J=1,9
      EKB(I,J)=EKB(I,J)*C
    2 CONTINUE
      RETURN
      END
```

SUBROUTINE TRANS (AA,BB,CC,KKK)

```
      SUBROUTINE TRANS (AA,BB,CC,KKK)
C     THIS SUBROUTINE TRANSFORM THE ELEMENT STIFFNESS MATRIX FROM LOCAL
C     ATES
C     DESCRIPION OF PARAMETERS
C     AA...........THE MATRIX OF CIRECTION COSINES OF AN ELEMENT
C     BB...........ELEMENT STIFFNESS MATRIX IN LOCAL COORDINATES
C     CC...........ELEMENT STIFFNESS MATRIX IN GLOBAL COORDINATES
C     D............TRANSFORMATION MATRIX
      DIMENSION AA(3,3), BB(KKK,1), CC(KKK,1), D(9,9), DT(9,9)
      DO 1 I=1,9
      DO 1 J=1,9
      D(I,J)=0.0
    1 CONTINUE
      D(1,1)=AA(3,3)
      DO 2 I=2,3
      DO 2 J=2,3
      D(I,J)=AA(I-1,J-1)
    2 CONTINUE
      DO 3 I=1,3
      DO 3 J=1,3
      D(I+3,J+3)=D(I,J)
      D(I+6,J+6)=D(I,J)
    3 CONTINUE
      CALL MULTP (BB,D,DT,9,9,9,0,9,9,9)
      CALL MULTP (D,DT,CC,9,9,9,1,9,9,9)
      RETURN
      END
```

SUBROUTINE ASSEMB (I1,I2,J1,J2,K1,K2,II,M,EKT,SM)

```
      SUBROUTINE ASSEMB (I1,I2,J1,J2,K1,K2,II,M,EKT,SM)
      DIMENSION SM(1), EKT(9,9)
      M=M+1
      N=0
      DO 1 JJ=I1,I2
      N=N+1
      IF (II.GE.JJ) L=II*(II-1)/2+JJ
      IF (II.LT.JJ) GO TO 1
      SM(L)=SM(L)+EKT(M,N)
1     CONTINUE
      DO 2 JJ=J1,J2
      N=N+1
      IF (II.GE.JJ) L=II*(II-1)/2+JJ
      IF (II.LT.JJ) GO TO 2
      SN(L)=SM(L)+EKT(M,N)
2     CONTINUE
      DO 3 JJ=K1,K2
      N=N+1
      IF (II.GE.JJ) L=II*(II-1)/2+JJ
      IF (II.LT.JJ) GO TO 3
      SM(L)=SM(L)+EKT(M,N)
3     CONTINUE
      RETURN
      END
```

APPENDIX C

EXPERIMENTAL DATA

Table (C.1) Results for Slab Configuration (1)

Load Ib.		Dial Gauge (1)		Dial Gauge (2)		Dial Gauge (3)	Dial Gauge (4)
$\Delta\bar{P}$	$\bar{P}$	Reading	$\bar{\Delta}$ Top	Reading	$\bar{\Delta}$ Middle		
0		.83		.611		.589	.546
	44.8		.219		.106		
44.8		.611		.505		.589	.546
	89.6		.404		.210		
44.8		.426		.401		.588	.546
	109.6		.502		.262		
20		.328		.349		.585	.546

Table (C.2) Results for Slab Configuration (2)

Load Ib.		Dial Gauge (1)		Dial Gauge (2)		Dial Gauge (3)	Dial Gauge (4)
$\Delta\overline{P}$	$\overline{P}$	Reading	$\overline{\Delta}$ Top	Reading	$\overline{\Delta}$ Middle		
0		.942		.617		.651	.546
	44.8		.159		.074		
44.8		.783		.543		.651	.546
	89.6		.31		.152		
44.8		.632		.465		.65	.546
	119.6		.386		.204		
30		.556		.413		.648	.546
	139.6		.452		.231		
20		.49		.386		.648	.546

Table (C.3) Results for Slab Configuration (3)

Load Ib.		Dial Gauge (1)		Dial Gauge (2)		Dial Gauge (3)	Dial Gauge (4)
$\Delta\overline{P}$	$\overline{P}$	Reading	$\overline{\Delta}$ Top	Reading	$\overline{\Delta}$ Middle		
0		.84		.623		.423	.763
	44.8		.117		.057		
44.8		.723		.566		.421	.763
	89.6		.224		.11		
44.8		.625		.513		.421	.763
	119.6		.29		.15		
30		.55		.473		.42	.763
	139.6		.352		.170		
20		.488		.453		.42	.763

Table (C.4) Results for Slab Configuration (4)

Load Ib.		Dial Gauge (1)		Dial Gauge (2)		Dial Gauge (3)	Dial Gauge (4)
$\Delta\overline{P}$	$\overline{P}$	Reading	$\overline{\Delta}$ Top	Reading	$\overline{\Delta}$ Middle		
0		.525		.239		.5	.763
	62.5		.087		.044		
62.5		.438		.195		.498	.763
	125		.169		.086		
62.5		.356		.153		.497	.763
	162		.211		.107		
37		.314		.132		.497	.763

Table (C.5) Results for Slab Configuration (5)

Load Ib.		Dial Gauge (1)		Dial Gauge (2)		Dial Gauge (3)	Dial Gauge (4)
$\Delta\bar{P}$	$\bar{P}$	Reading	$\bar{\Delta}$ Top	Reading	$\bar{\Delta}$ Middle		
0		.566		.234		.65	.6
	72		.048		.025		
72		.518		.209		.647	.6
	144		.101		.050		
72		.465		.184		.645	.6
	216		.167		.072		
32		.399		.162		.644	.6

Table (C-6) Results for Slab Configuration (6)

Load Ib.		Dial Gauge (1)		Dial Gauge (2)		Dial Gauge (3)	Dial Gauge (4)
$\Delta\overline{P}$	$\overline{P}$	Reading	$\overline{\Delta}$ Top	Reading	$\overline{\Delta}$ Middle		
0		.293		.484		.179	.65
	27		.007		.004		
27		.3		.488		.156	.65
	54		.016		.008		
27		.309		.492		.156	.65
	81		.022		.011		
27		.315		.495		.155	.65

Table (C.7) Results for Slab Configuration (7)

Load Ib.		Dial Gauge (1)		Dial Gauge (2)		Dial Gauge (3)	Dial Gauge (4)
$\Delta\bar{P}$	$\bar{P}$	Reading	$\bar{\Delta}$ Top	Reading	$\bar{\Delta}$ Middle		
0		.27		.45		.341	.65
	38		.006		.003		
38		.276		.453		.334	.65
	65		.011		.005		
27		.281		.455		.33	.65
	92		.022		.011		
27		.292		.461		.328	.65

BIBLIOGRAPHY

1. Beck, H., "Contribution to the Analysis of Coupled Shear Walls", Journal of Am. Conc. Inst., August, 1962.

2. Biswas, J. K. and Tso, W. K., "Three Dimensional Analysis of Shear Wall Buildings to Lateral Load", Journal of the Structural Division, May 1974.

3. Biswas, J. K., "Three Dimensional Analysis of Shear Wall Multi Storey Buildings", Ph.D Thesis, McMaster University, September 1974.

4. Coull, A. and Chaudhury, J. R., "Stress and Deformation in Coupled Shear Walls", Journal of Am. Conc. Inst., February 1967, pp. 65-72.

5. Coull, A. and Chaudhury, J. R., "Analysis of Coupled Shear Walls", Journal of Am. Conc. Inst., September 1967, pp. 553-593.

6. Coull, A. and Irwin, A. W., "Design of Connecting Beams in Coupled Shear Wall Structures", Journal of Am. Conc. Inst., March 1969.

7. Coull, A., "Interaction of Coupled Shear Walls with Elastic Foundations", Journal of Am. Conc. Inst., June 1971, pp. 456-461.

8. Coull, A. and Subedi, N. K., "Coupled Shear Walls with Two and Three Bands of Openings", Build. Sci., Vol. 7, 1972, pp. 81-86.

9. Coull, A. and El-hag., A., "Effective Coupling of Shear Walls by Floor Slabs", Journal of Am. Conc. Inst., August 1975, V. 72, No. 8.

10. Davis, J. D., "Analysis of Corner Supported Rectangular Slabs", The Structural Engineer, February 1970, No. 2, Vol. 48.

11. Desai, C. and Abel, J., "Introduction to the Finite Element Method", Van Nostrand Reinhold Company.

12. El Kholy, I. A. S. and Robinson, H., "Analysis of Multi-Bay Coupled Shear Walls", Build. Sci., Vol. 8, pp. 153-157, 1973.

13. Heidebrecht, A. C. and Swift, R. D., "Analysis of Asymmetrical Coupled Shear Walls", Journal of Structural Division, May 1971, pp. 1407-1422.

14. Hussein, W., "Analysis of Multi-Bay Shear Wall Structures by the Shear Connection Method", Build Sci., Vol. 7, 1972.

15. MacLeod, I. A., "Connected Shear Walls of Unequal Width", Journal of Am. Conc. Inst., May 1970, pp. 408-412.

16. Melosh, R. J., "Basis for Derivation of Matrices for the Direct Stiffness Method", AIAA Journal, Vol. 1, No. 7, July 1963.

17. Qadeer, A. and Smith, S., "The Bending Stiffness of Slabs Connecting Shear Walls", Journal of Am. Conc. Inst., June 1969, pp. 464-472.

18. Qadeer, A. and Smith, S., "Actions in Slabs Connecting Shear Walls", Proceedings of the Symposium on Tall Buildings, November 1974.

19. Rawtani, S., "Vibration Analysis of Rotating Low Aspect Ratio Blades", Ph.D Thesis, McMaster University, May 1970.

20. Rosman, R., "Approximate Analysis of Shear Walls Subjected to Lateral Loads", Journal of Am. Conc. Inst., June 1964, pp. 717-733.

21. Schwaighofer, J. and Microys, H. T., "Analysis of Shear Walls Using Standard Computer Programs", Journal of Am. Conc. Inst., December 1969, pp. 1005-1007.

22. Szilard, R. "Theory and Analysis of Plates, Classical and Numberical Methods", Prentice-Hall, Inc., Englwood Cliff, New Jersey.

23. Taranath, B. S., "The Torsional Behaviour of Open Section Shear Wall Structures", Ph.D Thesis, University of Southampton, 1968.

24. Timoshenko, S. and Woinowsky-Krieger, S., "Theory of Plates and Shells", McGraw Hill Book Company, New York.

25. Tso, W. K. and Chan, H. S., "Dynamic Analysis of Plane Coupled Shear Walls", Journal of Engineering Mechanics Division, February 1971.

26. Tso, W. K., "Stress in Coupled Shear Walls Induced by Foundation Deformation", Build. Sci., Vol. 7, pp. 197-2-3, 1972.

27. Tso, W. K. and Chan, P. C. K. "Flexible Foundation Effect on Coupled Shear Walls, Journal of Am. Conc. Inst. November 1972.

28. Tso, W. K. and Biswas, J. K., "General Analysis of Non-Planar Shear Walls", Journal of the Structural Division, March 1973.

29. Tso, W. K. and Biswas, J. K., "Analysis of Core Wall Structure Subjected to Applied Torque", Build. Sci., Vol. 8, pp. 251-257, 1973.

30. Zienkiewicz, O., "The Finite Element Method in Engineering Science", McGraw Hill Book Company, New York.